UNIVERSITY OF CALIFORNIA
IRVINE

Characterizing the Roles of Microglia in Disease and Repair in the CNS using a Viral Model of Multiple Sclerosis

DISSERTATION

submitted in partial satisfaction of the requirements
for the degree of

DOCTOR OF PHILOSOPHY

in Biological Sciences

by

Amber R. Syage

Dissertation Committee:
Professor Thomas E. Lane, Chair
Professor Kim N. Green
Professor Mathew M. Blurton-Jones
Associate Professor Munjal M. Acharya

2022

DEDICATION

To

my family

Elizabeth Syage, *Jack Syage*, and *George Syage*

and my partner

Wade Carden

for their constant love, encouragement, and steadfast support that made this research possible

TABLE OF CONTENTS

LIST OF ABBREVIATIONS

AD	Alzheimer's disease
APC	antigen-presenting cell
APOE	Apolipoprotein E
ASC	antibody secreting B cell
BBB	blood-brain barrier
CatC	Cathepsin C
CNS	Central nervous system
CPZ	Cuprizone
CSF	Cerebral spinal fluid
CSF1R	Colony stimulating factor-1 Receptor
Cst7, Cys F	Cystatin F
CXCL#	C-X-C motif chemokine ligand # (# = interchangeable number)
CXCR#	C-X-C motif chemokine receptor # (# = interchangeable number)
CX3CR1	C-X3-C motif chemokine receptor 1
DAM	disease-associated molecule
DC	dendritic cell
DEG	Differentially expressed gene
DMT	disease modifying therapies
DNA	Deoxyribonucleic acid
d.p.i	days post-infection
EAE	Experimental autoimmune (/allergic) encephalomyelitis
EBV	Ebstein-barr virus
FDA	food and drug administration
GFAP	hlial acidic fibrillary protein
H&E	hematoxylin and eosin
HBSS	Hanks balanced sterile solution
HHV-6	human herpervirus-6
HLA	human leukocyte antigen
IBA1	ionized calcium binding adaptor molecule 1
i.c.	intracranial
IFN	interferon
IGF-1, *Igf1*	insulin-like growth factor-1
IHC	Immunohistochemistry
IL-	Interleukin
ISH	*In situ* hybridization
JHMV	James Howard Mueller Virus, neurotropic strain of MHV
KO	Knock-out
LFB	Luxol fast blue
LPL, *Lpl*	Lipoprotein lipase
MHV	Mouse Hepatitis Virus
MOG	Major oligodendrocyte glycoprotein
MS	Multiple Sclerosis
NK	Natural killer cells

OL	oligodendrocyte
OPC	oligodendrocyte precursor cell
PFU	plaque forming units
p.i.	post-infection
PLP	Proteolipid protein
Plp4e/-	hemizygous proteolipid protein 1 transgenic mouse 4e
PLX5622	microglia-depleting drug
PPMS	Primary Progressive Multiple Sclerosis
RNA	ribonucleic acid
RRMS	Relapse-Remitting Multiple Sclerosis
scRNAseq	Single-cell RNA-sequencing
SEM	standard error of the mean
SPMS	Secondary progressive MS
SPP1, *Spp1*	Osteopontin
Th	T helper
TMEV	Theiler's Murine Encephalomyelitis virus
TNF	Tumor necrosis factor
TREM2	Triggering receptor expressed on myeloid cells 2
WT	Wild type
WNV	West Nile Virus

LIST OF FIGURES

ACKNOWLEDGMENTS

I would like to convey my deepest gratitude towards my thesis advisor and mentor Dr. Thomas E. Lane. The encouragement, support, and insight that Dr. Lane has provided these past few years has shaped me into the scientist that I am today, and I would like to thank him for all of the time and effort devoted to myself and the other graduate students in the lab. I would also like to thank my committee members Dr. Munjal Acharya, Dr. Kim Green, and Dr. Matt Blurton-Jones and the Department of Neurobiology and Behavior for the much-appreciated feedback and advice. I am incredibly grateful for the endless support, advice, and friendship that I have received from members of the Lane Lab family throughout the years. Lastly, I would like to thank my mother Elizabeth Syage, my father Jack Syage, and my brother George Syage for constantly inspiring me and for their love, support, and encouragement to strive to be the best version of myself and for reminding me to never sell myself short.

Chapter 2 of this dissertation is a reprint of the material as it appears in GLIA. The co-first author listed in this publication helped direct and supervise research which forms the basis for this dissertation. Chapter 3 of this dissertation is a reprint of the material as it appears in the Journal of Virology. The co-first author listed in this publication helped direct and supervise research which forms the basis for this dissertation. Chapter 4 of this dissertation is a reprint of the material as it appears in GLIA. The first author listed in this publication directed and supervised research which forms the basis for this dissertation.

VITA
Amber R. Syage

Education

Graduate Student – University of California, Irvine **2020 – 2022**
Biological Sciences Ph.D. Program (Advisor: Thomas E. Lane, Ph.D.) Irvine, CA
Department of Neurobiology and Behavior
(Transferred from the University of Utah – 2020)

Graduate Student – University of Utah School of Medicine **2017 – 2019**
Neuroscience Ph.D. Program (Advisor: Thomas E. Lane, Ph.D.) Salt Lake City, UT
Department of Pathology

BSc, California Polytechnic State University, Pomona **2009 – 2015**
Major – Biotechnology with Physiology Emphasis; Minor – Chemistry Pomona, CA

Research Experience

Neuroscience Graduate Student **2017 - 2022**
Graduate Advisor: Thomas E. Lane, Ph.D. - Professor
Department of Neurobiology and Behavior – University of California, Irvine 2020 – 2022
Department of Pathology – University of Utah School of Medicine 2017 –2019

- Characterizing the dynamic roles of microglia in demyelination and remyelination in a pre-clinical viral mouse model of multiple sclerosis.
- Pioneered the use of single cell RNA sequencing in our lab, along with downstream analysis using the R programming language.

Staff Research Associate I – Department of Radiation Oncology, UC Irvine **2015 – 2017**
Advisor: Charles Limoli, Ph.D. - Professor Irvine, CA

- Conducted research projects on therapeutic interventions to alleviate cancer therapy (chemo- or radiation) or cosmic radiation-induced CNS damage including the neurobiological and cognitive endpoints.
- Led a three-person team to NASA Space Radiation Laboratory at Brookhaven National Laboratory on two occasions to irradiate mice for several different NASA funded experiments.

Technician Volunteer – Department of Radiation Oncology, UC Irvine **2014 –2015**
Advisor: Charles Limoli, Ph.D. - Professor Irvine, CA

- Assisted in research projects on delineating the impact of cranial irradiation on neuron ultrastructure, spine density and receptor alterations following exosome transplantation using dual-immunofluorescence, confocal microscopy and 3D algorithm-based quantification (AutoQuant and Imaris) techniques.

Technician Volunteer – Department of Biological Sciences, Cal Poly Pomona **2013 –2014**
Advisor: Glenn Kageyama, Ph.D. - Professor Pomona, CA

- Investigated the relationship between oxidative metabolism and cellular function.

Clinical Experience

COPE Health Solutions: Clinical Care Extender Program **2014 –2015**
Citrus Valley Health Partners East San Gabriel Valley, CA

- Coordinated and assisted patients and patient care team in various departments within the three Citrus Valley Health Partner's hospital sites.
- Responsibilities with patients included bathing, feeding, repositioning, ambulation, vitalization, transfer, and discharge. As well as, sample delivery to lab, bed making, room cleaning, and preparing supplies for staff. Assisted staff within my scope of practice in procedures such as endotracheal intubation, nasogastric intubation, catheter insertion, sample collection, and electrocardiogram tests.
- Completed 300+ hours in Medical-Surgical Unit, Definitive Observational Unit, Surgical Intensive Care Unit, Coronary Intensive Care Unit, Emergency Department, and Mother Baby Care Unit.

Teaching and Leadership Experience

Teaching Assistant for Virtual N113 Neurobiology Lab – UC, Irvine **Winter 2021**

- Assisted Professor in grading, editing scientific writing assignments, answer student questions via email, and holding office hours.

Co-Chair of Snowbird Symposium Organizing Committee – University of Utah **2017 – 2019**

- Organized and ran the annual Snowbird Symposium on behalf of the Neuroscience Program.
- Tasks included choosing a theme, inviting guest speakers, crafting speaker profiles for the symposium website and abstract, creating the symposium schedule/speaker lineup, introducing speakers, and hosting the overall event.

Co-Chair of Neuroscience Program Recruitment Committee – University of Utah **2017 – 2019**

- Organize the Neuroscience Program's recruitment effort, coordinating airport pickups, interview schedules, ski trip, and student host responsibilities

Brain Bee Committee Member **2017 – 2019**

- Organize and host the U of Utah chapter of Brain Bee, the international high school level academic competition that consists of a neuroscience question-based competition, a graduate student panel session, and lab tours.

Brain Awareness Week Education Volunteer **2017 – 2019**

- Educate local elementary, middle, and high school students about neurobiology and neurological diseases.

Secretary and Scheduler of the Cancer Awareness Club – Cal Poly Pomona **2013 – 2015**

- General tasks included reserving rooms and university lots for meetings and fundraising/outreach events, managing the club's correspondence and social media, recording meeting minutes, and keeping track of members and meeting attendance logs.
- Helped organize and establish the BIO 302 – Biology of Cancer course, inviting guest professors to give lectures on different topics in cancer biology and coordinating student host responsibilities.
- Relay for Life team captain (2014).

Activities and Affiliations

American Society for Neurochemistry (2021-Present)
Society for Neuroscience (2020-Present)
Cancer Awareness Club – Cal Poly Pomona (2012 – 2015)
Tri-Beta Biological Honors Society– Cal Poly Pomona (2013 – 2015)
Ridge Runners Ski and Snowboard Club – Cal Poly Pomona (2012 – 2015)
Biological Sciences Club – Cal Poly Pomona (2010 – 2011)

Posters and Presentations

Poster: 52nd Annual American Society for Neurochemistry Meeting	Roanoke, VA – 2022
Presentation (Selected): 19th Annual UC Irvine Immunology Fair	Virtual – 2021
Presentation (Selected)/Poster: 2020 FASEB Conference: Translational Neuroimmunology	Virtual – 2020
Poster: ACTRIMS Young Scientist Summit	Austin, TX – 2020
Poster: Cell-Symposia: Neuro-Immune Axis	Long Beach, CA – 2019
Presentation (Selected): U of Utah, Annual Neuroscience Student Symposium	Salt Lake City, UT – 2019
Poster: 2018 FASEB Conference: Translational Neuroimmunology	Snowmass, CO – 2018
Poster: Cal Poly Pomona's 9th Annual Science Research Symposium	Pomona, CA – 2014

Publications

1. Skinner, D.S.*, **Syage, A.R.***, Olivarria, G., Stone, C., Hoglin, B., and Lane, T.L. (2022) Sustained infiltration of activated neutrophils into the CNS results in increased demyelination in a viral-induced model of multiple sclerosis. *Frontiers in Immunology, accepted August 2022*.
2. Hohsfield, L.A., Tsourmas, K.I., Ghorbanian, Y., **Syage, A.R.**, Kim, S.J., Cheng, Y., Furman, S., Inlay, M.A., Lane, T.E.*, and Green, K.N.* (2022) MAC2 is a long-lasting marker of peripheral cell infiltrates into the mouse CNS after bone marrow transplantation and coronavirus infection. *Glia*, 70(5):875-891.
3. Parihar, V.K., **Syage, A.R.**, Flores, L., Lilagan, A., Allen, B.D., Angulo, M.C., Smith, S.M., Arechavala, R.J., Song, J., Giedzinski, E., and Limoli, C.L. (2021) The cannabinoid receptor 1 reverse agonist AM251 ameliorates radiation-induced cognitive decrements. *Frontiers in Cellular Neuroscience*, 15:668286.
4. **Syage, A.R.,** Ekiz, H.A., Skinner, D.D., Stone, C., O'Connell, R.M., and Lane, T.E. (2020) Single cell RNA sequencing reveals the immunological landscape following CNS infection with a neurotropic virus. *Journal of Virology*, 94(24):e01295-20.
5. Parihar, V.K., Angulo, M.C., Allen, B.D., **Syage, A.R.**, Usmani, M.T., Passerat De La Chappelle, E., Nayan Amin, A., Flores, L., Lin, X., Giedzinski, E., and and Limoli, C.L. (2020) Sex specific cognitive deficits following space radiation exposure. *Frontiers in Behavioral Neuroscience*, 14:535885.
6. Mangale, V.*, **Syage, A.R.***, Ekiz, A.*, Cheng, Y., Stone, C., Skinner, D.D., O'Connell, R.M., and Lane, T.E. (2020) Microglia aid in host defense, disease, and repair following murine coronavirus infection of the central nervous system. *Glia*, 68(11):2345-2360. *Authors contributed equally to this work

7. Allen, B.D., **Syage, A.R.,** Maroso, M., Baddour, A.A., Luong, V., Minasyan, H., Giedzinski, E., West, B.L., Soltesz, I., Limoli, C.L., Baulch, J.E., and Acharya, M.M. (2019) Mitigation of 4He irradiation-induced brain injury by microglia depletion. *Journal of Neuroinflammation*, 17:159.

8. Allen, B.D., Apodaca, L.A., **Syage, A.R.,** Mineh, M., Baddour, A.A., Minasyan, H., Alikhani, L., Lu, C., West, B.L., Giedzinski, E., Baulch, J.E., and Acharya, M.M. (2019). Attenuation of neuroinflammation reverses Adriamycin-induced cognitive impairments. *Acta Neuropathologica Communications*, 7(1):186.

9. Montay-Gruel, P., Acharya, M.M., Petterson, K., Alikhani, L., Yakkala, C., Allen, B.D., Ollivier, J., Petit, B., Jorge, P.G., **Syage, A.,** Nguyen, T.A., Baddour, A.A., Lu, C., Singh, P., Moeckli, R., Bochud., F., Germond, J.F., Froidevaux, P., Bailet, C., Bourhis, J., Vozenin, M.C., and Limoli, C.L. (2019) Long-term neurocognitive benefits of FLASH radiotherapy driven by reduced reactive oxygen species. *PNAS,* 116(22):10943-10951.

10. Grist, J.J., Marro, B.S., Skinner, D.D., **Syage, A.R.,** Worne, C., Doty, D.J., Fujinami, R.S., and Lane, T.E. (2018) Induced CNS expression of CXCL1 augments neurological disease in a murine model of multiple sclerosis via enhanced neutrophil recruitment. *European Journal of Immunology*, 48(7):1199-1210.

11. Parihar, V.K., Maroso, M., **Syage, A.,** Allen, B.D., Angulo, M.C., Soltesz, I., and Limoli, C.L. (2018) Persistent nature of alterations in cognition and neuronal circuit excitability after exposure to simulated cosmic radiation in mice. *Experimental Neurology,* 305:44-55.

12. Acharya, M.M., Baddour, A.A., Kawashita, T., Allen, B.D., **Syage, A.R.,** Nguyen, T.H., Yoon, N., Giedzinski, E., Yu, L., Parihar, V.K., and Baulch, J.E. (2017) Epigenetic determinants of deep space radiation-induced cognitive dysfunction. *Scientific Reports,* 7:42885.

13. Acharya, M.M., Green, K.N., Allen, B.D., Najafi, A.R., **Syage, A.,** Minasyan, H., Le M.T., Kawashita, T., Giedzinski, E., Parihar, V.K., West, B.L., Baulch, J.E., and Limoli, C.L. (2016) Elimination of microglia improves cognitive function following cranial irradiation. *Scientific Reports*, 6:31545.

14. Baulch, J.E., Acharya, M.M., Allen, B.D., Ru, N., Chmielewski, N.N., Martirosian, V., Giedzinski, E., **Syage, A.,** Park, A.L., Benke, S.N., Parihar, V.K., and Limoli, C.L. (2015) Cranial grafting of stem cell-derived microvesicles improves cognition and reduces neuropathology in the irradiated brain. *PNAS,* 113(17):4836-4841.

ABSTRACT OF THE DISSERTATION

Characterizing the Roles of Microglia in Disease and Repair in the CNS using a Viral Model of Multiple Sclerosis

By

Amber R. Syage

Doctor of Philosophy in Biological Sciences

University of California, Irvine, 2022

Professor Thomas E. Lane, Chair

Multiple sclerosis (MS) leaves millions of people worldwide with impaired central nervous system (CNS) function. To make matters worse, a great deal is still unknown about the physiological landscape of MS pathogenesis and of what factors might exacerbate or ameliorate the severity of disease outcomes. As the resident immune cell of the CNS, microglia are considered active members of this pathogenic landscape, but whether their contributions are more destructive or protective remains controversial. Using the microglia-depleting drug PLX5622, an inhibitor of colony stimulating factor 1 receptor (CSF1R), it was demonstrated that upon depletion of microglia in mice infected with the neurotropic JHM strain of the mouse hepatitis virus (JHMV) results in an increase in viral load and severity of demyelination with a hindered capacity to remyelinate. Additionally, single-cell RNA sequencing (scRNAseq) revealed that microglia depletion prior to JHMV infection results in increased expression of transcripts associated with disease, including *Apoe*, *Trem2*, and *Spp1* (osteopontin), and reduced expression of remyelination associated transcripts *Igf1* (insulin-like growth factor-1), *Lpl* (lipoprotein lipase), and *Cst7* (cystatin F) in macrophage populations and remaining microglia. However, the mechanisms by

which microglia reduce the severity of demyelination and overall disease outcome is not yet understood. ScRNAseq was employed to apprehend the heterogeneous populations of cells at defined times post-infection in the pathogenic landscape following CNS infection with JHMV. Results exposed a subpopulation of microglia that have elevated expression of remyelination markers *Igf1*, *Lpl*, and *Cst7*, that are present at day 21 p.i., in chronic disease, when remyelination efforts are occurring. Cystatin F expression drastically increases in microglia when demyelination occurs and has been associated with remyelination in various pre-clinical models of demyelination and is even found overlapping with remyelinating areas of MS plaques in human post-mortem tissue. As microglia phagocytosis of compact myelin results in increased expression of Cst7, cystatin F may act as a signaling mediator to negatively regulate the inflammatory environment that causes demyelination. Therefore, we chose to investigate whether the effects of microglia on reducing demyelination and promoting remyelination were mediated through microglia expression and secretion of cystatin F. Using a cystatin F germline KO mouse (Cst7 KO), we demonstrated that JHMV infection of the CNS results in more severe clinical disease in mice lacking Cst7 when compared with infected wild-type littermates (WT), which correlated with a significant increase in demyelination in Cst7 KO mice at both day 14 and 21 p.i as well as impaired remyelination at day 21 p.i. Genetic ablation of cystatin F did not impact acute disease with no impairment in control of virus replication or effect on immune cell infiltration into the CNS at day 7 p.i. relative to WT littermates. However, at day 21 p.i., we found increased infiltration of CD8+, CD4+, and virus specific CD4+ T cells into spinal cords. Consistently, scRNAseq on CD45+ cells from spinal cords of uninfected and infected Cst7 KO and WT littermates revealed increased expression of T cell chemoattractant *Cxcl9* by microglia and macrophages and increased expression of activation markers for CD4+ T cells (*Icos*, *Ifng*, *Tnfrsf4*) and CD8+ T cells (*Gzmb*, *Prf1*, *Ifng*). Furthermore,

expression of disease-associated transcripts *Apoe* and *Trem2* were elevated in microglia and monocyte/macrophage populations. Together, these findings indicate that cystatin F plays a role in chronic JHMV-induced disease by restricting the severity of demyelination and promoting remyelination, potentially through negative regulation of T cell recruitment an activation. Results from this research provide further insight into the roles of microglia in disease and repair in a pre-clinical model of chronic MS and illuminate a potential mechanism for microglia in contributing to repair.

{This Page Intentionally Left Blank}

Chapter 1

BACKGROUND AND INTRODUCTION

1.1 Multiple Sclerosis

Multiple sclerosis (MS) is an autoimmune inflammatory disease that results in chronic demyelination and can lead to cognitive, visual, motor, and sensory impairments. More than 2.3 million worldwide live with MS, to which there is no known cure (www.nationalmssociety.org). Oligodendrocytes (OLs) are the myelin producers of the CNS and are rendered dysfunctional in MS patients. Histological characterization of CNS tissue from MS patients reveals demyelinating lesions that consist of inflammatory macrophages and activated lymphocytes, predominantly of the Th17 lineage[1–4]. Disruption of OL function is thought to occur as a result of perivascular infiltration of CD4+ T cells, CD8+ T cells, and macrophages acting with resident reactive microglia to release a milieu of damaging pro-inflammatory factors[2–4]. Accumulation of demyelinating lesions in white matter tracks progressively manifest clinically to a variety of symptoms such as cognitive decline, impaired motor abilities, and loss of vision [5,6].

During early disease, patients may experience focal attacks that are generally episodic and can last from 24 hours to several weeks followed by near complete recovery of symptoms[7]. This form of MS is called Relapse Remitting MS (RRMS)[7]. Remission in RRMS is thought to reflect reduced neuroinflammation and partial restoration of nerve conduction due to remyelination efforts[8,9]. Remyelination could be explained by the accumulation of oligodendrocyte precursor cells (OPCs) in the subacute lesions during the early stages of MS[10]. OPC maturation leads to patches of remyelinated white matter with thin myelin sheaths surrounding axons[5,11,12]. Approximately 85% of MS patients that are initially diagnosed with RRMS and will eventually develop Secondary Progressive MS (SPMS) within a decade of their initial diagnosis, while the remaining 15% are initially diagnosed with Primary Progressive MS (PPMS)[13]. PPMS is defined by unremitting clinical symptoms without periods of remission for more than 1 year. PPMS

patients experience significant neurologic degeneration and worsened motor capabilities due to increased accumulation of cortical white matter lesions[14]. Studies using postmortem tissue from progressive MS patients showed a reduction in immune cell infiltration in cortical lesions, but an increased number of apoptotic neurons with transected axons[15–17]. This suggests that demyelination and axonal damage are the primary contributors to the pathology of progressive MS patients and not the adaptive immune system. Additionally, while resident OPCs are found highly populated near chronic lesions, they fail to proliferate and differentiate to form mature myelin producing oligodendrocytes, leaving very little possibility of endogenous remyelination[10,18].

MS etiology remains enigmatic, but several factors have been associated with an increased risk of developing MS, including genetic predisposition, geography, gender, and microbial and viral infection[19–24]. For example, offspring of MS patients have a higher risk of developing the disease and twin studies have shown a significantly higher concordance in monozygotic twins compared to dizygotic twins, suggesting that certain risk alleles are associated with MS[25–28]. Additionally, genomic-wide association studies (GWAS) revealed the human leukocyte antigen (HLA) class II region of the HLA-DR-2 haplotype on chromosome 6p21 was also shown to be associated with MS and *HLADRB1*1501* is the major susceptibility allele in MS patients from North America or European Caucasians[21,29–31]. Women are also between 1.5 to 2.5 times more likely to develop MS compared to men, indicating that this predisposition could be hormonally related, as oral contraceptive pills are also considered a risk factor[32,33]. Another interesting factor associated with development of MS is geography, as individuals living further away from the equator have a higher risk of developing MS and people who move from low-risk to high-risk regions have a greater predisposition for becoming high-risk[34–36]. One potential reason that location may play a role is sunlight exposure, as low vitamin D levels due to reduced sun exposure

in the northern regions has been associated with an increase in MS risk and worsening of disease symptoms[35–40]. Another explanation for the differences in MS risk based on geographical location is exposure to pathogenic agents, particularly viruses. Two viruses that have been linked to MS are Epstein-Barr virus (EBV) and human herpervirus-6 (HHV-6)[24]. The risk of developing MS is ~15-fold higher in those infected with EBV early in life and ~30-fold higher with those infected with EBV in adulthood[24]. Additionally, viruses such as Varicella-zoster virus , have been found in the cerebral spinal fluid (CSF) in Relapse-Remitting MS, suggesting that virus can trigger relapse[41]. Effects of pathogen exposure in trigger an autoimmune response could potentially occur through molecular mimicry and/or bystander activation[42–44]. Additional factors that have been associated with onset of MS include smoking, sun exposure, and obesity[37–39,45–48].

Although there is currently no known cure for MS, there are ten approved preventative disease modifying therapies (DMTs) available to treat patients at the RRMS stages of MS by reducing the frequency and severity of attacks[49]. These therapies are aimed at reducing activated T and B lymphocyte infiltration into the CNS and at preventing new lesion formation. Some DMTs approved by the United States food and drug administration (FDA) include interferons (IFNs), glatiramer acetate, Mitoxantrone, Teriflunomide, Fingolimod, Dimethyl fumarate/BG-1 2, along with human monoclonal antibodies (HuMab) such as Natalizumab, Alemtuzumab and Ocrelizumab. Interferon beta (IFN-β) drugs and glatiramer acetate (GA) fall in the category of first-generation self-injectable DMTs. IFN-β modulates B and T cell cytokine function and reduces blood-brain-barrier (BBB) disruption, while GA is thought to stimulate regulatory T cell responses[50,51]. Both IFN-β and GA are attractive based upon long-term safety profiles and because they require less monitoring by medical professionals. However, over time patients develop IFN-β neutralizing antibodies that are associated with reduced efficacy of all IFN-β-type drugs[51–53].

There are currently only two agents approved to treat SPMS, the first being Mitoxantrone, which is a general immunosuppressant used for treatment in rapidly worsening RRMS and the second is Ocrelizumab[54]. However, long-term use of Mitoxantrone is associated with higher rates of cardiomyopathy, making it a less popularized treatment[55]. There are three oral DMTs that have been approved for RRMS: Fingolimod, Teriflunomide, and Dimethyl fumarate/BG-1 2. Fingolimod is a sphingosine-1-phosphate (S1P) agonist, interfering with lymphocyte exiting of the lymph nodes and therefore preventing entry into the CNS[56,57]. Teriflunomide functions by inhibiting the enzyme dihydroorotate dehydrogenase (DHODH) that is required for rapidly proliferating cells such as lymphocytes to meet their excessive metabolic needs[58]. The third oral DMT, Dimethyl fumarate/BG-I2, reduces oxidative stress through activation of the nuclear-related factor 2 transcription pathway, though the mechanism behind this is unclear[59,60]. The three humanized monoclonal antibodies Natalizumab, Alemtuzumab, and Ocrelizumab, act by either depleting lymphocytes or blocking CNS entry. Natalizumab targets the integrin subunit, $\alpha 4$, in the cell adhesion molecule, known as Very Late Antigen 4 (VLA-4) that is expressed by immune cells and allows for transmigration across the BBB into the CNS by way of its ligand, Vascular Cell Adhesion Molecule-1 (VCAM-1) located on brain vascular endothelium[61,62]. Alemtuzumab targets CD52 on immune cells and effectively depletes T cells, B cells, and NK cells[49,63]. Ocrelizumab is the second approved treatment for SPMS and functions by targeting CD20 to deplete B cells, but spares progenitor B cells and plasma cells[49,64]. With the exceptions of Mitoxantrone and Ocrelizumab, which was recently approved for treating progressive forms of MS, most of the FDA approved DMTs are for RRMS. Remyelination failure is the hallmark of progressive MS and results in the inability of endogenous OPCs to mature into myelin-producing oligodendrocytes.

1.2 Pre-Clinical Mouse Models of MS and Demyelination

Pre-clinical animal models that exhibit similar clinical symptoms and histopathology as MS patients are important to better understand mechanisms contributing to disease progression as well as repair of damaged tissue. Several toxin-based rodent models use cuprizone (CPZ), lysolecithin to induce demyelination by having a direct toxic effect on oligodendrocytes. Genetic models of demyelination are also used, including the hemizygous proteolipid protein 1 transgenic mouse strain 4e (Plp4/e) that develop spontaneous myelin degeneration from 2-to-6 months of age, where it then subsides and mice are left with chronic demyelination[65,66]. However, these models may not accurately represent stages of MS patients since they lack an immune cell mediated demyelination. Experimental autoimmune encephalitis (EAE) incorporates an autoimmune response against either defined encephalitogenic major oligodendrocyte glycoprotein (MOG) or proteolipid protein (PLP) peptides, depending upon mouse strain, and shares many pathological and clinical features with MS patients. EAE has provided a powerful model for identifying novel targets to dampen disease progression as well as potentially promote repair (REF). Nonetheless, in many cases EAE demyelination is reversed, and myelin integrity is eventually fully restored which does not occur MS patients[67]. Additionally, many therapeutic mechanisms have not been translatable from EAE model to humans, even though EAE still remains the most widely used model to study MS. Since viruses have been implicated as a possible environmental trigger for MS, viral models of MS present excellent tools to study the pathogenesis of MS[68,69]. The two main neurotropic viral models of MS that have provided important insights into the pathology of MS: Theiler's murine encephalomyelitis virus (TMEV) and John Howard Muller (JHM) strain of mouse hepatitis virus (MHV) (JHMV).

1.3 JHMV as a model for viral-induced demyelination

Mouse Hepatitis Virus (MHV) is an enveloped positive-strand RNA virus that is a member of the *Coronaviridae* family of viruses that can cause respiratory, gastro-intestinal, and neurologic disease in both humans and animals[70]. MHV is a natural pathogen of mice and pathogenesis is determined by factors including the strain of virus, inoculation route, and mouse background[71,72]. The JHM strain of MHV, referred to as JHMV, is a neuroadapted strain of the virus[73,74]. Intracranial inoculation (i.c.) of susceptible mice with JHMV results in acute encephalomyelitis characterized by viral replication in astrocytes, microglia, and oligodendrocytes with relative sparing of neurons[75–78]. MHV spike glycoprotein recognizes and binds to the host cell receptor Carcinoembryonic Antigen-Cell Adhesion Molecule (CEACAM-1)[71,79] that allows for virus entry into the cell and leads to resulting host immune response and disease pathogenesis[80–82]. Animals that survive the acute stage of disease develop a chronic demyelinating in which virus persists primarily in oligodendrocytes and astrocytes leading to chronic neuroinflammation consisting of both T cells and macrophages[78,83–85]. JHMV replication is controlled within astrocytes and microglia through CD8+ T cell perforin/granzyme-mediated cytolytic activity, while control in oligodendrocytes is mediated by IFN-γ[70,83–86]. JHMV is eventually cleared below detectable levels, but sterilizing immunity is not achieved and viral particles persist within oligodendrocytes[87]. Underlying reasons contributing to CNS persistence include CD8+ T cell exhaustion[88], muted expression of MHC class I and II on oligodendrocytes and antigen presenting cells (APCs)[89,90], and virus RNA evolution in the CNS producing viral quasispecies of spike deletion variants[91]. Early on in infection, MHV replicates within astrocytes and consequently these cells secrete macrophage chemoattractants chemokines CCL2 and CCl5 that bind to their corresponding receptors CCR2 and CCR5 on macrophages and allow for infiltration into CNS[92–96]. Astrocytes

also secrete the CXCL9 and CXCL10 that recruit virus-specific T cells and B cells into the CNS through the CXCR3 receptor[97–100]. CCR5 is also necessary for CD4+ T cell trafficking into the CNS, but not for CD8+ T[101,102]. However, effective CD8+ T cell activation and CNS infiltration is also dependent on CCL3[103]. Overall immune cell infiltration declines around 14 d.p.i, but virus-specific T cells and macrophages can reside within the CNS for as long as 3 months following infection[104–107]. Furthermore, demyelination is not associated with the apoptotic and necrotic death of myelinating OLs[108], but with the sustained presence of both viral antigen and inflammatory immune cells[109]. Both CD8+ and CD4+ T cells are necessary for effective viral clearance, and both contribute to increasing the severity of demyelination. CD4+ T cell secretion of IFN-γ upregulates MHC class II in microglia and MHC class I in oligodendrocytes and is important for CD8+ T cell function and survival[110–112]. IL-21 derived from CD4+ T cells was recently found to be important in enhancing anti- viral effector functions by CD8+ T cells following JHMV infection[113]. CD4+ T cells contribute to demyelination indirectly by secreting CCL5 and thus recruiting macrophages[96], while CD8+ T cells contribute more directly through cytolytic activity and IFN-γ secretion[114–116]. IFN-γ is directly damaging to OPCs and OLs[117–125], but also induces secretion of TNFα and ROS by microglia and macrophages, which can also trigger OL death[126–128]. Additionally, IFN-γ is associated with OL apoptosis at the leading edges of active MS lesions[118] and treatment of MS patients with IFN-γ neutralizing antibody reduces disease outcomes[129], while treatment with IFN-γ exacerbates disease[130]. However, IFN-γ is not the sole mediator of demyelination, as infection of mice with IFN-γR1 ablated on OLs had similar levels of demyelination[83]. Myelin laden macrophages have been found directly stripping and engulfing myelin from myelinated axons[131] and neutralization of the macrophage chemoattractant CCL5 resulted in reduced demyelination[95,96], as did genetic silencing of CCR5 in macrophages, even with impaired viral

clearance[94]. Interestingly, CCR5 expression on microglia is found in biopsy material taken from early remyelinating lesions in MS patients[132]. Though B cells do not contribute to viral clearance during acute infection[133,134], antibody secreting cells are detectable in CNS tissue by 5 days p.i. and in serum by day 10 p.i.[135], where virus-specific antibodies are essential in preventing viral reactivation in chronically infected mice[133,134,136].

1.4 Microglia in Demyelination and Remyelination in MS and Pre-Clinical Models of Demyelinating Disease

Microglia are the resident immune cells of the CNS and contribute a diverse array of functions that range from normal homeostatic maintenance to contributing to various disease-associated conditions[137–144]. Moreover, microglia are immunologically competent and capable of rapidly responding to infection and/or damage via specific expression of surface receptors culminating in morphologic changes accompanied by secretion of proinflammatory cytokines/chemokines that function in amplifying neuroinflammation. Research investigating the functional role of microglia in CNS infection and pathogenesis has been greatly aided by findings demonstrating that mice lacking of colony stimulating factor 1 receptor (CSF1R-/-) are microglia deficient, emphasizing the importance of the CSF1R signaling pathway in microglia development and homeostasis[145]. Further studies by Green and colleagues using a CSF1R antagonist to block signaling through CSF1R revealed its importance in the survival of microglia in adult mice[146]. Recent studies have employed treatment of mice with PLX5622, a brain penetrant and selective antagonist of the CSF1R that results in a dramatic reduction in microglia, to better understand functional roles of these cells in pre-clinical models of neurodegenerative disease[146–148]. However, whether microglia mediate or restrict the resulting pathologies of CNS degenerative diseases is

still heavily debated. One study showed that microglia depletion in EAE using a CSF1R inhibitor reduces clinical disease and demyelination, advocating that microglia contribute to MS pathology[149]. Others suggest a protective role for microglia in pre-clinical models of MS and neurodegenerative disease, showing that depletion of microglia results in worsened demyelination, impaired phagocytic function, and increased pro-inflammatory responses[147,150–153], while studies stimulating CSF1R signaling in CPZ and EAE models of MS showed reduced myelin loss and increased anti-inflammatory/pro-regenerative signaling and OPC migration[151,154]. Additionally, PLX5622-mediated depletion of microglia results in increased susceptibility to West Nile virus (WNV) [155,156], Japanese encephalitis virus (JEV)[155], Theiler's murine encephalomyelitis virus (TMEV)[157,158] and JHMV[152,153], arguing that microglia are protective against acute viral-induced encephalitis. These conflicting findings suggest that microglia function is highly dependent on situation and environmental ques. Interestingly, the small pool of surviving microglia following depletion with CSF1R inhibitor are a phenotypically regenerative population of microglia and thus proliferation and repopulation of these microglia may be the key to successful regeneration of myelin and neuronal integrity in degenerative disease[159]. One study even found that replacement of microglia in the aged brain through CSF1R inhibition and subsequent repopulation following removal of drug resulted in improved memory and reversal of tissue aging[160]. Though microglia replacement through repopulation may not be the best clinical solution, as the adult brain may only have the capacity for one complete repopulation event[161], knowledge of the extraordinary prolific and regenerative potential of microglia exposes future targets for therapeutic intervention.

Microglia contribute to successful remyelination through phagocytosis and recycling of myelin debris and by secreting growth factors that promote migration of OPCs to demyelinating lesions and maturation into myelinating OLs[140,162–164]. Over the past decade, the necessity of

microglia for remyelination following demyelination has grown more apparent. A common feature in MS is that there isn't a loss of OLs or OPCs, but an impaired ability to remyelinate. This could be due, in part, to a sustained inflammatory environment that is not conducive for OLs and OPCs to mature and remyelinate based on OPCs/OL state or receptiveness of damaged axons. Alternatively, it could be a result of impaired signaling for maturation and myelin production and an arrest in OPC progenitor status. In a lysolecithin model of demyelination, it was found that remyelination following demyelination was initiated by the polarization of both microglia and infiltrating peripheral macrophages from a pro-inflammatory state (iNOS+, TNFα+, CD16/32+) to an anti-inflammatory and regenerative state (Arg1+, IGF-1+, CD206+)[137]. Moreover, both microglia and macrophages contribute to this transition from pro-, to anti-inflammatory[137]. Though secreted factors from both pro-inflammatory and anti-inflammatory microglia, contribute to OPC proliferation and migration, only secreted factors from the latter promoted OPC differentiation into myelin producing OLs and also prevented OPC apoptosis[137]. Key secreted factors that have been found to elicit this transition to anti-inflammatory/pro-regenerative cells include IL-4, IL-13, IL-10, and fractalkine (CX3CL1)[137,140,165]. Microglia expression of CCR5 is also associated with early remyelination in MS[132]. This is believed to occur through OPC recruitment signaling, independent of phagocytosis of myelin debris[164]. Microglia phagocytosis of myelin debris in the demyelinating lesion is an essential component of remyelination. The mechanisms behind microglia phagocytosis are still poorly understood, but recent findings have indicated phagocytic dysfunction in Alzheimer's disease (AD) and most likely in other neurodegenerative disorders[166–168]. Additionally, whether contact with myelin debris and phagocytosis are associated with production of pro- or anti-inflammatory cytokines is still unclear[169,170]. One study investigating the role of microglia cystatin F in disease and remyelination found that microglia phagocytosis of compact

myelin triggers expression of *Cst7*, which has been shown to negatively regulate inflammatory activation states in target cells[66]. Another recent area of interest that appears to be associated with phagocytic dysfunction in microglia and macrophages are the presence of lipid droplets. They are lipid storing organelles that contain neutral lipids, including glycerolipids and cholesterylesters[171]. In both aging and in AD they appear to accumulate around lysosomes in microglia and appear to be more dominant on microglia with impaired phagocytic function[171]. One way of how this has been proposed to impact phagocytosis of myelin debris, is that lipid breakdown is important to occur so that microglia have the energy to complete functions like phagocytosis[171].

1.5 Cystatins and Cystatin F

Cystatins are a family of cysteine protease inhibitors that regulate several cellular functions including autophagy, apoptosis, cellular homeostasis, and antigen presentation, primarily through inhibition of their target cysteine protease, cathepsin, either extracellularly or within lysosomes and endosomes[172–180]. Cys F is normally expressed by immune cells and not in the CNS[181–184], but expression by microglia increases drastically in the CNS during acute demyelination and expression overlaps with areas of remyelination in EAE and *Plp*$^{4e/-}$ pre-clinical models of MS and in spinal cord tissue from MS patients[66,185,186]. Furthermore, cystatin F co-localizes with pro-regenerative microglia populations in both MOG-EAE and *Plp*$^{4e/-}$ models[67,185]. The main target of Cys F in the CNS is cathepsin C (catC), also known as dipeptidyl-peptidase 1 (DPP1)[181]. CatC is an aminopeptidase that functions by removing dipeptides from the amino terminal of the protein substrate. It is required for the activation of other serine proteases in immune cells and is involved in a range of functions, including granzyme release by effector immune cells, promoting pro-

inflammatory gene expression in microglia and macrophages, and stimulating secretion of immune cell chemoattractant CXCL2[187–192]. When Cys F was knocked down in the cuprizone and *Plp*$^{4e/-}$ model of demyelination, cathepsin C was no longer inhibited and this corresponded with increased demyelination[186]. Microglia-specific overexpression of catC in *Plp*$^{4e/-}$ mice also resulted in worsened demyelination[185]. The demyelinating effects from both Cys F knockdown and catC overexpression were reversed by the knockdown of catC[186]. Cys F is from the type II, secreted family of cystatins but is unique in that it is secreted as an inactive form and is only activated following a cleavage event when internalized by its target cell[193,194]. This suggests that it has the potential for signaling to other cells. Similar to a type I cystatin, it targets cathepsins inside lysosomes and endosomes[66]. Additionally, catC expressing immune cells were found to infiltrate into the CNS early in EAE induction, with no Cys F expression appearing until remyelination began within demyelinating lesions[67]. Interestingly, it was found that microglia phagocytosis of compact myelin and not neuronal debris or non-compact myelin, results in a drastic increase in expression and secretion of Cystatin F[66]. This further demonstrates that Cystatin F may act as a negative regulator of pro-inflammatory activation states in surrounding cells in response to severe demyelination.

1.6 Summary

Multiple Sclerosis is a devastating disease and etiology of chronic disease is still not clearly defined. As a result, availability of clinically approved drugs that can effectively reverse disease outcomes is nonexistent, leaving those with progressive forms of MS with little hope of recovery. Our goal is to better understand aspects of chronic disease so that we can expose potential targets

for therapeutic intervention that can prevent new lesion formation and promote sustained remyelination.

Chapter 2 describes a role for microglia in host defense in response to JHMV infection as well as in restricting the severity of demyelination and potentially promoting subsequent remyelination. Treatment of mice with PLX5622, a drug that efficiently depletes microglia, prior to JHMV infection, led to impaired control of virus replication, but increased infiltration of CD4+ and CD8+ T cells as well as virus specific CD4+ and CD8+ T cells, detected through flow cytometric analysis. Additionally, scRNAseq on CD45+ cells in brains and spinal cord tissue of infected mice showed elevated expression of transcripts encoding CD8+ T cell activation and MHC class I in macrophages. However, reduced expression of MHC class II and CD4+ T cell activation markers, including *Tbx21* (T-bet) was found in the microglia depleted group when compared to controls, indicating impaired priming of a Th1 response that resulted in persisting JHMV replication. Histological analysis of spinal cord tissue demonstrated increased severity of demyelination in the microglia depleted group compared to controls at both days 14 and 21 p.i. While EM analysis with g-ratio calculations showed impaired remyelination at day 21 p.i. Thus, microglia may contribute to reducing the severity of white matter pathology and may contribute to remyelination efforts in disease.

Chapter 3 describes a scRNAseq study conducted on CNS tissue from defined times post-infection using JHMV to gain better insight into the complicated interplay that occurs within a CNS disease where demyelination is immune mediated. This approach was chosen so that we could expose the various subpopulations of the different cell types present at specific points in disease progression and to gain insight into what aspects of disease they may be contributing to. In this study, we found a specific subpopulation of microglia that express transcripts associated

with remyelination in spinal cords during a chronic timepoint in disease, where remyelination efforts are occurring. This was an exciting finding to us, as a known substantial component to MS as well as other neurodegenerative diseases is the interplay between microglia and the pathogenic environment. Microglia are found to be both damaging and reparative, depending on their surroundings. Even more interesting is how fast they can change from one functional state to the other. Therefore, whether microglia contribute to some degree of demyelination, a fraction of them may also be taking on a pro-regenerative role in disease. If we can find what triggers a transition to this state, it may provide for an effective target for therapeutic drugs.

Chapter 4 reveals that galectin-3 (or MAC2) is a reliable marker to distinguish between infiltrating myeloid cell populations and microglia within the CNS. Within the scRNAseq dataset discussed in **Chapter 3**, elevated expression of *Lgals3* (encodes galectin-3) was confined to infiltrating myeloid cell populations, with very little expression in microglia. Additionally, immunostaining for galectin-3, also known as MAC2, in brains of JHMV infected mice as well as bone marrow chimeric mice displayed elevated levels of MAC2 protein in myeloid cells, with little to no MAC2 in microglia.

Chapter 5 demonstrates a role for Cystatin F in restricting the severity of demyelination and potentially promoting remyelination. In the study described in **Chapter 2**, we found that depletion of microglia results in reduced expression of *Cst7* (cystatin F) in macrophages, which is involved in remyelination in several models of demyelinating disease and is found in human MS tissue along the edge of plaques. Elevated expression of *Cst7* was also found in the remyelination associated microglia population found in our scRNAseq study described in **Chapter 3,** therefore we chose to investigate this suspect protein further. As microglia phagocytosis of compact myelin results in increased expression of *Cst7*, cystatin F may act as a signaling mediator to negatively

regulate the inflammatory environment that causes demyelination. In this study, we used a novel cystatin F knock-out (Cst7 KO) mouse model and infected Cst7 KO mice and wildtype littermates with JHMV. We showed increased severity of spinal cord demyelination at both day 14 and day 21 p.i. and impaired remyelination at day 21 p.i. No impairment in control of virus replication was found at day 7 p.i. and flow cytometric analysis of brains of infected Cst7 KO and WT littermates showed no change in infiltration of CD4+ and CD8+ T cells and macrophages at either day 7 or day 14 p.i. However, at day 21 p.i., Cst7 KO mice exhibited reduced infiltration of CD4+ and CD8+ T cells as well as virus specific CD4+ T cells. This result is consistent with the expression profile of cystatin F found in our previous study (**Chapter 3**), with expression highest at day 21 p.i. in microglia. ScRNAseq on CD45+ cells from spinal cords of uninfected and infected Cst7 KO and WT littermates showed an increase in expression of transcripts associated with CD4+ and CD8+ T cells as well as expression of transcripts encoding T cell chemoattractants CXCL9 and CXCL10 in microglia and macrophages. These findings indicated that cystatin F may negatively regulate granzyme-mediated cytolytic activity in T cells and chemoattractant signaling to recruit CD4+ and CD8+ T cells. Whether or not the sustained T cell infiltration and activation that occurrs in the absence of cystatin F is the reason for increased demyelination and impaired remyelination remains unclear and will be addressed in future studies.

REFERENCES

1. Lassmann, H., Brück, W. & Lucchinetti, C. F. The immunopathology of multiple sclerosis: An overview. *Brain Pathol.* **17**, 210–218 (2007).

2. Boyle, E. A. & McGeer, P. L. Cellular immune response in multiple sclerosis plaques. *Am. J. Pathol.* **137**, 575–584 (1990).

3. Traugott, U., Reinherz, E. L. & Raine, C. S. Multiple sclerosis. Distribution of T cells, T cell subsets and Ia-positive macrophages in lesions of different ages. *J. Neuroimmunol.* **4**, 201–221 (1983).

4. Traugott, U., Reinherz, E. L. & Raine, C. S. Multiple sclerosis: distribution of T cell subsets within active chronic lesions. *Science* **219**, 308–310 (1983).

5. Prineas, J. W. *et al.* Multiple sclerosis. Oligodendrocyte proliferation and differentiation in fresh lesions. *Lab. Invest.* **61**, 489–503 (1989).

6. Neumann, H., Medana, I. M., Bauer, J. & Lassmann, H. Cytotoxic T lymphocytes in autoimmune and degenerative CNS diseases. *Trends Neurosci.* **25**, 313–319 (2002).

7. Compston, A. & Coles, A. Multiple sclerosis. *Lancet (London, England)* **359**, 1221–1231 (2002).

8. Chang, A., Tourtellotte, W. W., Rudick, R. & Trapp, B. D. Premyelinating oligodendrocytes in chronic lesions of multiple sclerosis. *N. Engl. J. Med.* **346**, 165–173 (2002).

9. Kornek, B. *et al.* Multiple sclerosis and chronic autoimmune encephalomyelitis: a comparative quantitative study of axonal injury in active, inactive, and remyelinated lesions. *Am. J. Pathol.* **157**, 267–276 (2000).

10. Chang, A., Nishiyama, A., Peterson, J., Prineas, J. & Trapp, B. D. NG2-positive oligodendrocyte progenitor cells in adult human brain and multiple sclerosis lesions. *J. Neurosci.* **20**, 6404–6412 (2000).

11. Lucchinetti, C. *et al.* A quantitative analysis of oligodendrocytes in multiple sclerosis lesions. A study of 113 cases. *Brain* **122 (Pt 1**, 2279–2295 (1999).

12. Roy, N. S. *et al.* Identification, isolation, and promoter-defined separation of mitotic oligodendrocyte progenitor cells from the adult human subcortical white matter. *J. Neurosci.* **19**, 9986–9995 (1999).

13. Kremenchutzky, M., Rice, G. P. A., Baskerville, J., Wingerchuk, D. M. & Ebers, G. C. The natural history of multiple sclerosis: a geographically based study 9: observations on the progressive phase of the disease. *Brain* **129**, 584–594 (2006).

14. Lucchinetti, C. F. *et al.* Inflammatory cortical demyelination in early multiple sclerosis. *N.*

Engl. J. Med. **365**, 2188–2197 (2011).

15. Antel, J., Antel, S., Caramanos, Z., Arnold, D. L. & Kuhlmann, T. Primary progressive multiple sclerosis: part of the MS disease spectrum or separate disease entity? *Acta Neuropathol.* **123**, 627–638 (2012).

16. Trapp, B. D. *et al.* Axonal transection in the lesions of multiple sclerosis. *N. Engl. J. Med.* **338**, 278–285 (1998).

17. Peterson, J. W., Bö, L., Mörk, S., Chang, A. & Trapp, B. D. Transected neurites, apoptotic neurons, and reduced inflammation in cortical multiple sclerosis lesions. *Ann. Neurol.* **50**, 389–400 (2001).

18. Wolswijk, G. Chronic Stage Multiple Sclerosis Lesions Contain a Relatively Quiescent Population of Oligodendrocyte Precursor Cells. *J. Neurosci.* **18**, 601 LP – 609 (1998).

19. Sawcer, S. *et al.* Genetic risk and a primary role for cell-mediated immune mechanisms in multiple sclerosis. *Nature* **476**, 214–219 (2011).

20. Barcellos, L. F. *et al.* Heterogeneity at the HLA-DRB1 locus and risk for multiple sclerosis. *Hum. Mol. Genet.* **15**, 2813–2824 (2006).

21. Haines, J. L. *et al.* Linkage of the MHC to familial multiple sclerosis suggests genetic heterogeneity. *Hum. Mol. Genet.* **7**, 1229–1234 (1998).

22. Wtccc, C. C. *et al.* Genetic risk and a primary role for cell-mediated immune mechanisms in multiple sclerosis The. *Nature* **476**, 214–219 (2012).

23. Zipp, F. *et al.* Network-based multiple sclerosis pathway analysis with GWAS data from 15,000 cases and 30,000 controls. *Am. J. Hum. Genet.* **92**, 854–865 (2013).

24. Ascherio, A. & Munger, K. L. Environmental risk factors for multiple sclerosis. Part I: The role of infection. *Ann. Neurol.* **61**, 288–299 (2007).

25. Flores, J. *et al.* Absence of Multiple Sclerosis and Demyelinating Diseases among Lacandonians, a Pure Amerindian Ethnic Group in Mexico. *Mult. Scler. Int.* **2012**, 1–4 (2012).

26. Ebers, G. C., Yee, I. M., Sadovnick, A. D. & Duquette, P. Conjugal multiple sclerosis: population-based prevalence and recurrence risks in offspring. Canadian Collaborative Study Group. *Ann. Neurol.* **48**, 927–931 (2000).

27. Sadovnick, A. D. & Baird, P. A. The familial nature of multiple sclerosis: age-corrected empiric recurrence risks for children and siblings of patients. *Neurology* **38**, 990–991 (1988).

28. Sadovnick, A. D. *et al.* A population-based study of multiple sclerosis in twins: update. *Ann. Neurol.* **33**, 281–285 (1993).

29. Fernández, O. *et al.* DQB1*0602 allele shows a strong association with multiple sclerosis in patients in Malaga, Spain. *J. Neurol.* **251**, 440–444 (2004).

30. Olerup, O. & Hillert, J. HLA class II-associated genetic susceptibility in multiple sclerosis: a critical evaluation. *Tissue Antigens* **38**, 1–15 (1991).

31. Haegert, D. G. *et al.* HLA-DR beta, -DQ alpha, and -DQ beta restriction fragment length polymorphisms in multiple sclerosis. *J. Neurosci. Res.* **23**, 46–54 (1989).

32. Kotzamani, D. *et al.* Rising incidence of multiple sclerosis in females associated with urbanization. *Neurology* **78**, 1728–1735 (2012).

33. Ascherio, A. & Munger, K. L. Epidemiology of Multiple Sclerosis: From Risk Factors to Prevention-An Update. *Semin. Neurol.* **36**, 103–114 (2016).

34. Kurtzke, J. F. Epidemiology of multiple sclerosis. Does this really point toward an etiology? Lectio Doctoralis. *Neurol. Sci.* **21**, 383–403 (2000).

35. Dobson, R., Ramagopalan, S., Davis, A. & Giovannoni, G. Cerebrospinal fluid oligoclonal bands in multiple sclerosis and clinically isolated syndromes: a meta-analysis of prevalence, prognosis and effect of latitude. *J. Neurol. Neurosurg. Psychiatry* **84**, 909–914 (2013).

36. Koch-Henriksen, N. & Sørensen, P. S. The changing demographic pattern of multiple sclerosis epidemiology. *Lancet. Neurol.* **9**, 520–532 (2010).

37. Jelinek, G. A. *et al.* Latitude, sun exposure and vitamin D supplementation: Associations with quality of life and disease outcomes in a large international cohort of people with multiple sclerosis. *BMC Neurol.* **15**, 1 (2015).

38. van der Mei, I. A. F. *et al.* The high prevalence of vitamin D insufficiency across Australian populations is only partly explained by season and latitude. *Environ. Health Perspect.* **115**, 1132–1139 (2007).

39. Van Der Mei, I. A. F. *et al.* Past exposure to sun, skin phenotype, and risk of multiple sclerosis: Case-control study. *Bmj* **327**, 316 (2003).

40. Ascherio, A. *et al.* Vitamin D as an early predictor of multiple sclerosis activity and progression. *JAMA Neurol.* **71**, 306–314 (2014).

41. Sotelo, J. & Corona, T. Varicella Zoster Virus and Relapsing Remitting Multiple Sclerosis. *Mult. Scler. Int.* **2011**, 1–5 (2011).

42. Fujinami, R. S., Von Herrath, M. G., Christen, U. & Whitton, J. L. Molecular mimicry, bystander activation, or viral persistence: Infections and autoimmune disease. *Clin. Microbiol. Rev.* **19**, 80–94 (2006).

43. Fujinami, R. S. & Oldstone, M. B. Amino acid homology between the encephalitogenic

site of myelin basic protein and virus: mechanism for autoimmunity. *Science* **230**, 1043–1045 (1985).

44. O'Connor, K. C., Bar-Or, A. & Hafler, D. A. The neuroimmunology of multiple sclerosis: possible roles of T and B lymphocytes in immunopathogenesis. *J. Clin. Immunol.* **21**, 81–92 (2001).

45. Rosso, M. & Chitnis, T. Association Between Cigarette Smoking and Multiple Sclerosis: A Review. *JAMA Neurol.* **77**, 245–253 (2020).

46. Riise, T., Nortvedt, M. W. & Ascherio, A. Smoking is a risk factor for multiple sclerosis. *Neurology* **61**, 1122–1124 (2003).

47. Schreiner, T.-G. & Genes, T.-M. Obesity and Multiple Sclerosis-A Multifaceted Association. *J. Clin. Med.* **10**, (2021).

48. Tremlett, H., Zhu, F., Ascherio, A. & Munger, K. L. Sun exposure over the life course and associations with multiple sclerosis. *Neurology* **90**, e1191–e1199 (2018).

49. Wingerchuk, D. M. & Carter, J. L. Multiple Sclerosis: Current and Emerging Disease-Modifying Therapies and Treatment Strategies. *Mayo Clin. Proc.* **89**, 225–240 (2014).

50. Dhib-Jalbut, S. Mechanisms of action of interferons and glatiramer acetate in multiple sclerosis. *Neurology* **58**, S3-9 (2002).

51. Jacobs, L. D. *et al.* Intramuscular interferon beta-1a for disease progression in relapsing multiple sclerosis. The Multiple Sclerosis Collaborative Research Group (MSCRG). *Ann. Neurol.* **39**, 285–294 (1996).

52. Polman, C. H. *et al.* Recommendations for clinical use of data on neutralising antibodies to interferon-beta therapy in multiple sclerosis. *Lancet. Neurol.* **9**, 740–750 (2010).

53. Hegen, H. *et al.* Persistency of neutralizing antibodies depends on titer and interferon-beta preparation. *Mult. Scler.* **18**, 610–615 (2012).

54. Hartung, H.-P. *et al.* Mitoxantrone in progressive multiple sclerosis: a placebo-controlled, double-blind, randomised, multicentre trial. *Lancet (London, England)* **360**, 2018–2025 (2002).

55. Marriott, J. J., Miyasaki, J. M., Gronseth, G. & O'Connor, P. W. Evidence Report: The efficacy and safety of mitoxantrone (Novantrone) in the treatment of multiple sclerosis: Report of the Therapeutics and Technology Assessment Subcommittee of the American Academy of Neurology. *Neurology* **74**, 1463–1470 (2010).

56. Cohen, J. A. & Chun, J. Mechanisms of fingolimod's efficacy and adverse effects in multiple sclerosis. *Ann. Neurol.* **69**, 759–777 (2011).

57. Cohen, J. A. *et al.* Oral fingolimod or intramuscular interferon for relapsing multiple

sclerosis. *N. Engl. J. Med.* **362**, 402–415 (2010).

58. Claussen, M. C. & Korn, T. Immune mechanisms of new therapeutic strategies in MS: teriflunomide. *Clin. Immunol.* **142**, 49–56 (2012).

59. Linker, R. A. *et al.* Fumaric acid esters exert neuroprotective effects in neuroinflammation via activation of the Nrf2 antioxidant pathway. *Brain* **134**, 678–692 (2011).

60. Albrecht, P. *et al.* Effects of dimethyl fumarate on neuroprotection and immunomodulation. *J. Neuroinflammation* **9**, 163 (2012).

61. Ransohoff, R. M. Natalizumab for multiple sclerosis. *N. Engl. J. Med.* **356**, 2622–2629 (2007).

62. Butzkueven, H. *et al.* Efficacy and safety of natalizumab in multiple sclerosis: interim observational programme results. *J. Neurol. Neurosurg. Psychiatry* **85**, 1190–1197 (2014).

63. Coles, A. J. *et al.* Alemtuzumab CARE-MS II 5-year follow-up: Efficacy and safety findings. *Neurology* **89**, 1117–1126 (2017).

64. Frampton, J. E. Ocrelizumab: First Global Approval. *Drugs* **77**, 1035–1041 (2017).

65. Ma, J., Matsumoto, M., Tanaka, K. F., Takebayashi, H. & Ikenaka, K. An animal model for late onset chronic demyelination disease caused by failed terminal differentiation of oligodendrocytes. *Neuron Glia Biol.* **2**, 81–91 (2006).

66. Ma, J. *et al.* Microglial cystatin F expression is a sensitive indicator for ongoing demyelination with concurrent remyelination. *J. Neurosci. Res.* **89**, 639–649 (2011).

67. Durose, W. W. *et al.* Cathepsin C modulates myelin oligodendrocyte glycoprotein-induced experimental autoimmune encephalomyelitis. *J. Neurochem.* **148**, 413–425 (2019).

68. Mix, E., Meyer-Rienecker, H., Hartung, H. P. & Zettl, U. K. Animal models of multiple sclerosis-Potentials and limitations. *Prog. Neurobiol.* **92**, 386–404 (2010).

69. Tsunoda, I. & Fujinami, R. S. Two models for multiple sclerosis: experimental allergic encephalomyelitis and Theiler's murine encephalomyelitis virus. *J. Neuropathol. Exp. Neurol.* **55**, 673–686 (1996).

70. Bergmann, C. C., Lane, T. E. & Stohlman, S. A. Coronavirus infection of the central nervous system: Host-virus stand-off. *Nat. Rev. Microbiol.* **4**, 121–132 (2006).

71. Compton, S. R., Stephensen, C. B., Snyder, S. W., Weismiller, D. G. & Holmes, K. V. Coronavirus species specificity: murine coronavirus binds to a mouse-specific epitope on its carcinoembryonic antigen-related receptor glycoprotein. *J. Virol.* **66**, 7420–7428 (1992).

72. Das Sarma, J. *et al.* Demyelinating and Nondemyelinating Strains of Mouse Hepatitis Virus Differ in Their Neural Cell Tropism. *J. Virol.* **82**, 5519–5526 (2008).

73. Cheever, F. S., Daniels, J. B., Pappenheimer, A. M. & Bailey, O. T. A Murine Virus (JHM) Causing Disseminated Encephalomyelitis With Extensive Destruction of Myelin: I. Isolation and Biological Properties of the Virus. *J. Exp. Med.* **90**, 181–194 (1949).

74. Bailey, O. T., Pappenheimer, A. M., Cheever, F. S. & Daniels, J. B. A murine virus (jhm) causing disseminated encephalomyelitis with extensive destruction of myelin: II Pathology. *J. Exp. Med.* **90**, 195–212 (1949).

75. Buchmeier, M. J., Lewicki, H. A., Talbot, P. J. & Knobler, R. L. Murine hepatitis virus-4 (strain JHM)-induced neurologic disease is modulated in Vivo by monoclonal antibody. *Virology* **132**, 261–270 (1984).

76. Ireland, D. D. C., Stohlman, S. A., Hinton, D. R., Atkinson, R. & Bergmann, C. C. Type I Interferons Are Essential in Controlling Neurotropic Coronavirus Infection Irrespective of Functional CD8 T Cells. *J. Virol.* **82**, 300–310 (2008).

77. Fleming, J. O. *et al.* Antigenic relationships of murine coronaviruses: analysis using monoclonal antibodies to JHM (MHV-4) virus. **131**, 296–307 (1983).

78. Wang, F. I., Hinton, D. R., Gilmore, W., Trousdale, M. D. & Fleming, J. O. Sequential infection of glial cells by the murine hepatitis virus JHM strain (MHV-4) leads to a characteristic distribution of demyelination. *Lab. Invest.* **66**, 744–754 (1992).

79. Williams, R. K., Jiang, G. S., Snyder, S. W., Frana, M. F. & Holmes, K. V. Purification of the 110-kilodalton glycoprotein receptor for mouse hepatitis virus (MHV)-A59 from mouse liver and identification of a nonfunctional, homologous protein in MHV-resistant SJL/J mice. *J. Virol.* **64**, 3817–3823 (1990).

80. Ontiveros, E., Kim, T. S., Gallagher, T. M. & Perlman, S. Enhanced Virulence Mediated by the Murine Coronavirus, Mouse Hepatitis Virus Strain JHM, Is Associated with a Glycine at Residue 310 of the Spike Glycoprotein. *J. Virol.* **77**, 10260–10269 (2003).

81. Iacono, K. T., Kazi, L. & Weiss, S. R. Both Spike and Background Genes Contribute to Murine Coronavirus Neurovirulence. *J. Virol.* **80**, 6834–6843 (2006).

82. Phillips, J. J., Chua, M. M., Rall, G. F. & Weiss, S. R. Murine coronavirus spike glycoprotein mediates degree of viral spread, inflammation, and virus-induced immunopathology in the central nervous system. *Virology* **301**, 109–120 (2002).

83. González, J. M. *et al.* Inhibition of interferon-γ signaling in oligodendroglia delays coronavirus clearance without altering demyelination. *Am. J. Pathol.* **168**, 796–804 (2006).

84. Lin, M. T., Stohlman, S. A. & Hinton, D. R. Mouse hepatitis virus is cleared from the central nervous systems of mice lacking perforin-mediated cytolysis. *J. Virol.* **71**, 383–391

(1997).

85. Parra, B. *et al.* IFN-gamma is required for viral clearance from central nervous system oligodendroglia. *J. Immunol.* **162**, 1641–7 (1999).

86. Fleming, J. O., Trousdale, M. D., el-Zaatari, F. A., Stohlman, S. A. & Weiner, L. P. Pathogenicity of antigenic variants of murine coronavirus JHM selected with monoclonal antibodies. *J. Virol.* **58**, 869–875 (1986).

87. Lane, T. E. & Buchmeier, M. J. Murine coronavirus infection: A paradigm for virus-induced demyelinating disease. *Trends Microbiol.* **5**, 9–14 (1997).

88. Phares, T. W. *et al.* Target-Dependent B7-H1 Regulation Contributes to Clearance of Central Nervous Sysyem Infection and Dampens Morbidity. *J. Immunol.* **182**, 5430–5438 (2009).

89. Correale, J., Li, S., Weiner, L. P. & Gilmore, W. Effect of persistent mouse hepatitis virus infection on MHC class I expression in murine astrocytes. *J. Neurosci. Res.* **40**, 10–21 (1995).

90. Zuo, J. & Rowe, M. Herpesviruses placating the unwilling host: Manipulation of the MHC class II antigen presentation pathway. *Viruses* **4**, 1335–1353 (2012).

91. Rowe, C. L. *et al.* Generation of coronavirus spike deletion variants by high-frequency recombination at regions of predicted RNA secondary structure. *J. Virol.* **71**, 6183–6190 (1997).

92. Held, K. S., Chen, B. P., Kuziel, W. A., Rollins, B. J. & Lane, T. E. Differential roles of CCL2 and CCR2 in host defense to coronavirus infection. *Virology* **329**, 251–260 (2004).

93. Chen, B. P., Kuziel, W. A. & Lane, T. E. Lack of CCR2 Results in Increased Mortality and Impaired Leukocyte Activation and Trafficking Following Infection of the Central Nervous System with a Neurotropic Coronavirus. *J. Immunol.* **167**, 4585–4592 (2001).

94. Glass, W. G., Liu, M. T., Kuziel, W. A. & Lane, T. E. Reduced macrophage infiltration and demyelination in mice lacking the chemokine receptor CCR5 following infection with a neurotropic coronavirus. *Virology* **288**, 8–17 (2001).

95. Glass, W. G. *et al.* Antibody Targeting of the CC Chemokine Ligand 5 Results in Diminished Leukocyte Infiltration into the Central Nervous System and Reduced Neurologic Disease in a Viral Model of Multiple Sclerosis. *J. Immunol.* **172**, 4018–4025 (2004).

96. Lane, T. E. *et al.* A Central Role for CD4+ T Cells and RANTES in Virus-Induced Central Nervous System Inflammation and Demyelination. *J. Virol.* **74**, 1415–1424 (2000).

97. Stiles, L. N., Hardison, J. L., Schaumburg, C. S., Whitman, L. M. & Lane, T. E. T Cell

Antiviral Effector Function Is Not Dependent on CXCL10 Following Murine Coronavirus Infection. *J. Immunol.* **177**, 8372–8380 (2006).

98. Walsh, K. B. *et al.* Expression of CXC Chemokine Ligand 10 from the Mouse Hepatitis Virus Genome Results in Protection from Viral-Induced Neurological and Liver Disease. *J. Immunol.* **179**, 1155–1165 (2007).

99. Liu, M. T. *et al.* Cutting Edge: The T Cell Chemoattractant IFN-Inducible Protein 10 Is Essential in Host Defense Against Viral-Induced Neurologic Disease. *J. Immunol.* **165**, 2327–2330 (2000).

100. Liu, M. T., Armstrong, D., Hamilton, T. A. & Lane, T. E. Expression of Mig (Monokine Induced by Interferon-γ) Is Important in T Lymphocyte Recruitment and Host Defense Following Viral Infection of the Central Nervous System. *J. Immunol.* **166**, 1790–1795 (2001).

101. Glass, W. G. & Lane, T. E. Functional Expression of Chemokine Receptor CCR5 on CD4+ T Cells during Virus-Induced Central Nervous System Disease. *J. Virol.* **77**, 191–198 (2003).

102. Glass, W. G. & Lane, T. E. Functional analysis of the CC chemokine receptor 5 (CCR5) on virus-specific CD8+ T cells following coronavirus infection of the central nervous system. *Virology* **312**, 407–414 (2003).

103. Trifilo, M. J., Bergmann, C. C., Kuziel, W. A. & Lane, T. E. CC Chemokine Ligand 3 (CCL3) Regulates CD8+-T-Cell Effector Function and Migration following Viral Infection. *J. Virol.* **77**, 4004–4014 (2003).

104. Marten, N. W., Stohlman, S. A. & Bergmann, C. C. Role of Viral Persistence in Retaining CD8+ T Cells within the Central Nervous System. *J. Virol.* **74**, 7903–7910 (2000).

105. Ramakrishna, C., Stohlman, S. A., Atkinson, R. A., Hinton, D. R. & Bergmann, C. C. Differential Regulation of Primary and Secondary CD8 + T Cells in the Central Nervous System . *J. Immunol.* **173**, 6265–6273 (2004).

106. Liu, M. T., Keirstead, H. S. & Lane, T. E. Neutralization of the Chemokine CXCL10 Reduces Inflammatory Cell Invasion and Demyelination and Improves Neurological Function in a Viral Model of Multiple Sclerosis. *J. Immunol.* **167**, 4091–4097 (2001).

107. Castro, R. F., Evans, G. D., Jaszewski, A. & Perlman, S. Coronavirus-Induced Demyelination Occurs in the Presence of Virus-Specific Cytotoxic T Cells. *Virol. J.* **200**, 733–743 (1994).

108. Wu, G. F. & Perlman, S. Macrophage Infiltration, but Not Apoptosis, Is Correlated with Immune-Mediated Demyelination following Murine Infection with a Neurotropic Coronavirus. *J. Virol.* **73**, 8771–8780 (1999).

109. Stohlman, S. A. & Hinton, D. R. Viral induced demyelination. *Brain Pathol.* **11**, 92–106

(2001).

110. Bergmann, C. C. *et al.* Perforin-Mediated Effector Function Within the Central Nervous System Requires IFN-γ-Mediated MHC Up-Regulation. *J. Immunol.* **170**, 3204–3213 (2003).

111. Malone, K. E., Stohlman, S. A., Ramakrishna, C., Macklin, W. & Bergmann, C. C. Induction of class I antigen processing components in oligodendroglia and microglia during viral encephalomyelitis. *Glia* **56**, 426–435 (2008).

112. Pan, R. *et al.* Oligodendrocytes that survive acute coronavirus infection induce prolonged inflammatory responses in the CNS. *Proc. Natl. Acad. Sci. U. S. A.* **117**, 15902–15910 (2020).

113. Phares, T. W. *et al.* IL-21 optimizes T cell and humoral responses in the central nervous system during viral encephalitis. *J. Neuroimmunol.* **263**, 43–54 (2013).

114. Wu, G. F., Dandekar, A. A., Pewe, L. & Perlman, S. CD4 and CD8 T Cells Have Redundant But Not Identical Roles in Virus-Induced Demyelination. *J. Immunol.* **165**, 2278–2286 (2000).

115. Pewe, L., Haring, J. & Perlman, S. CD4 T-Cell-Mediated Demyelination Is Increased in the Absence of Gamma Interferon in Mice Infected with Mouse Hepatitis Virus. *J. Virol.* **76**, 7329–7333 (2002).

116. Pewe, L. & Perlman, S. Cutting Edge: CD8 T Cell-Mediated Demyelination Is IFN-γ Dependent in Mice Infected with a Neurotropic Coronavirus. *J. Immunol.* **168**, 1547–1551 (2002).

117. Lin, W., Harding, H. P., Ron, D. & Popko, B. Endoplasmic reticulum stress modulates the response of myelinating oligodendrocytes to the immune cytokine interferon-γ. *J. Cell Biol.* **169**, 603–612 (2005).

118. Vartanian, T., Li You, Zhao Meijuan & Stefansson, K. Interferon-gamma-induced oligodendrocyte cell death: Implications for the pathogenesis of multiple sclerosis. *Mol. Med.* **1**, 732–743 (1995).

119. Pouly, S., Becher, B., Blain, M. & Antel, J. P. Interferon-γ modulates human oligodendrocyte susceptibility to Fas- mediated apoptosis. *J. Neuropathol. Exp. Neurol.* **59**, 280–286 (2000).

120. Mann, S. A. *et al.* Corticosteroids reverse cytokine-induced block of survival and differentiation of oligodendrocyte progenitor cells from rats. *J. Neuroinflammation* **5**, 1–17 (2008).

121. Baerwald, K. D. & Popko, B. Developing and mature oligodendrocytes respond differently to the immune cytokine interferon-gamma. *J. Neurosci. Res.* **52**, 230–239 (1998).

122. Loughlin, A. J. *et al.* Myelination and remyelination of aggregate rat brain cell cultures enriched with macrophages. *J. Neurosci. Res.* **47**, 384–392 (1997).

123. Buntinx, M. *et al.* Cytokine-induced cell death in human oligodendroglial cell lines: I. Synergistic effects of IFN-gamma and TNF-alpha on apoptosis. *J. Neurosci. Res.* **76**, 834–845 (2004).

124. Molina-Holgado, E., Vela, J. M., Arévalo-Martín, A. & Guaza, C. LPS/IFN-gamma cytotoxicity in oligodendroglial cells: role of nitric oxide and protection by the anti-inflammatory cytokine IL-10. *Eur. J. Neurosci.* **13**, 493–502 (2001).

125. Zhang, X. *et al.* Cytokine toxicity to oligodendrocyte precursors is mediated by iron. *Glia* **52**, 199–208 (2005).

126. Yeo, Y. A. *et al.* CD137 ligand activated microglia induces oligodendrocyte apoptosis via reactive oxygen species. *J. Neuroinflammation* **9**, 1–9 (2012).

127. Merrill, J. E. & Zimmerman, R. P. Natural and induced cytotoxicity of oligodendrocytes by microglia is inhibitable by TGF beta. *Glia* **4**, 327–331 (1991).

128. Merrill, J. E., Ignarro, L. J., Sherman, M. P., Melinek, J. & Lane, T. E. Microglial cell cytotoxicity of oligodendrocytes is mediated through nitric oxide. *J. Immunol.* **151**, 2132–2141 (1993).

129. Skurkovich, S. *et al.* Randomized study of antibodies to IFN-gamma and TNF-alpha in secondary progressive multiple sclerosis. *Mult. Scler.* **7**, 277–284 (2001).

130. Panitch, H. S., Hirsch, R. L., Schindler, J. & Johnson, K. P. Treatment of multiple sclerosis with gamma interferon: exacerbations associated with activation of the immune system. *Neurology* **37**, 1097–1102 (1987).

131. Fleury, H. J. A., Sheppard, R. D., Bornstein, M. B. & Raine, C. S. Further ultrastructural observations of virus morphogenesis and myelin pathology in JHM virus encephalomyelitis. *Neuropathol. Appl. Neurobiol.* **6**, 165–179 (1980).

132. Trebst, C., König, F., Ransohoff, R. M., Brück, W. & Stangel, M. CCR5 expression on macrophages/microglia is associated with early remyelination in multiple sclerosis lesions. *Mult. Scler.* **14**, 728–733 (2008).

133. Ramakrishna, C., Bergmann, C. C., Atkinson, R. & Stohlman, S. A. Control of central nervous system viral persistence by neutralizing antibody. *J. Virol.* **77**, 4670–4678 (2003).

134. Ramakrishna, C., Stohlman, S. A., Atkinson, R. D., Shlomchik, M. J. & Bergmann, C. C. Mechanisms of central nervous system viral persistence: the critical role of antibody and B cells. *J. Immunol.* **168**, 1204–1211 (2002).

135. Tschen, S.-I. *et al.* Recruitment kinetics and composition of antibody-secreting cells within the central nervous system following viral encephalomyelitis. *J. Immunol.* **168**,

2922–2929 (2002).

136. Lin, M. T., Hinton, D. R., Bergmann, C. C., Stohlman, S. A. & Marten, N. W. Antibody prevents virus reactivation within the central nervous system. *J. Immunol.* **162**, 7358–7368 (1999).

137. Miron, V. E. *et al.* M2 microglia and macrophages drive oligodendrocyte differentiation during CNS remyelination. *Nat. Neurosci.* **16**, 1211–1218 (2013).

138. Salter, M. W. & Stevens, B. Microglia emerge as central players in brain disease. *Nat. Med.* **23**, 1018–1027 (2017).

139. Cash, E., Zhang, Y. & Rott, O. Microglia present myelin antigens to t cells after phagocytosis of oligodendrocytes. *Cellular Immunology* **147**, 129–138 (1993).

140. Edwards, J. P., Zhang, X., Frauwirth, K. A. & Mosser, D. M. Biochemical and functional characterization of three activated macrophage populations. *J. Leukoc. Biol.* **80**, 1298–1307 (2006).

141. Hammond, T. R., Robinton, D. & Stevens, B. Microglia and the Brain: Complementary Partners in Development and Disease. *Annu. Rev. Cell Dev. Biol.* **34**, 523–544 (2018).

142. Tejera, D. *et al.* Systemic inflammation impairs microglial Aβ clearance through NLRP 3 inflammasome . *EMBO J.* **38**, (2019).

143. Wolf, S. A., Boddeke, H. W. G. M. & Kettenmann, H. Microglia in Physiology and Disease. *Annu. Rev. Physiol.* **79**, 619–643 (2017).

144. Banati, R. B., Gehrmann, J., Schubert, P. & Kreutzberg, G. W. Cytotoxicity of microglia. *Glia* **7**, 111–118 (1993).

145. Ginhoux, F. *et al.* Fate Mapping Analysis Reveals That Adult Microglia Derive from Primitive Macrophages. *Science (80-.).* **330**, 841–845 (2010).

146. Elmore, M. R. P. *et al.* Colony-stimulating factor 1 receptor signaling is necessary for microglia viability, unmasking a microglia progenitor cell in the adult brain. *Neuron* **82**, 380–397 (2014).

147. Spangenberg, E. *et al.* Sustained microglial depletion with CSF1R inhibitor impairs parenchymal plaque development in an Alzheimer's disease model. *Nat. Commun.* **10**, 1–21 (2019).

148. Dagher, N. N. *et al.* Colony-stimulating factor 1 receptor inhibition prevents microglial plaque association and improves cognition in 3xTg-AD mice. *J. Neuroinflammation* **12**, 1–14 (2015).

149. Jillian C. Nissen, Kaitlyn K. Thompson, Brian L. West, S. E. T. Csf1R inhibition attenuates experimental autoimmune encephalomyelitis and promotes recovery. *Physiol.*

Behav. **176**, 139–148 (2016).

150. Mangale, V. *et al.* Microglia influence host defense, disease, and repair following murine coronavirus infection of the central nervous system. *Glia* 1–16 (2020). doi:10.1002/glia.23844

151. Laflamme, N. *et al.* mCSF-Induced Microglial Activation Prevents Myelin Loss and Promotes Its Repair in a Mouse Model of Multiple Sclerosis. *Front. Cell. Neurosci.* **12**, 1–15 (2018).

152. Sariol, A. *et al.* Microglia depletion exacerbates demyelination and impairs remyelination in a neurotropic coronavirus infection. *Proc. Natl. Acad. Sci. U. S. A.* **117**, 24464–24474 (2020).

153. Wheeler, D. L., Sariol, A., Meyerholz, D. K. & Perlman, S. Microglia are required for protection against lethal coronavirus encephalitis in mice. *J. Clin. Invest.* **128**, 931–943 (2018).

154. Wlodarczyk, A. *et al.* CSF1R Stimulation Promotes Increased Neuroprotection by CD11c+ Microglia in EAE. *Front. Cell. Neurosci.* **12**, (2019).

155. Seitz, S., Clarke, P. & Tyler, K. L. Pharmacologic Depletion of Microglia Increases Viral Load in the Brain and Enhances Mortality in Murine Models of Flavivirus-Induced Encephalitis. *J. Virol.* **92**, 1–10 (2018).

156. Funk, K. E. & Klein, R. S. CSF1R antagonism limits local restimulation of antiviral CD8+ T cells during viral encephalitis. *J. Neuroinflammation* **16**, 1–19 (2019).

157. Sanchez, J. M. S. *et al.* Microglial cell depletion is fatal with low level picornavirus infection of the central nervous system. *J. Neurovirol.* **25**, 415–421 (2019).

158. Inken Waltl *et al.* Microglia have a protective role in viral encephalitis-induced seizure development and hippocampal damage. *Brain. Behav. Immun.* **74**, 186–204 (2020).

159. Lloyd, A. F. *et al.* Central nervous system regeneration is driven by microglia necroptosis and repopulation. *Nat. Neurosci.* **22**, 1046–1052 (2019).

160. Elmore, M. R. P. *et al.* Replacement of microglia in the aged brain reverses cognitive, synaptic, and neuronal deficits in mice. *Aging Cell* **17**, (2018).

161. Najafi, A. R. *et al.* A limited capacity for microglial repopulation in the adult brain. *Glia* **66**, 2385–2396 (2018).

162. Kotter, M. R., Li, W. W., Zhao, C. & Franklin, R. J. M. Myelin impairs CNS remyelination by inhibiting oligodendrocyte precursor cell differentiation. *J. Neurosci.* **26**, 328–332 (2006).

163. Ruckh, J. M. *et al.* Rejuvenation of regeneration in the aging central nervous system. *Cell*

Stem Cell **10**, 96–103 (2012).

164. Kotter, M. R., Zhao, C., Van Rooijen, N. & Franklin, R. J. M. Macrophage-depletion induced impairment of experimental CNS remyelination is associated with a reduced oligodendrocyte progenitor cell response and altered growth factor expression. *Neurobiol. Dis.* **18**, 166–175 (2005).

165. Finneran, D. J. & Nash, K. R. Neuroinflammation and fractalkine signaling in Alzheimer's disease. *J. Neuroinflammation* **16**, 1–8 (2019).

166. Lucin, K. M. *et al.* Microglial Beclin 1 Regulates Retromer Trafficking and Phagocytosis and Is Impaired in Alzheimer's Disease. *Neuron* **79**, 873–886 (2013).

167. Han, J., Wang, M., Ren, M. & Lou, H. Contributions of triggering-receptor-expressed-on-myeloid-cells-2 to neurological diseases. *Int. J. Neurosci.* **127**, 368–375 (2017).

168. Krasemann, S. *et al.* The TREM2-APOE Pathway Drives the Transcriptional Phenotype of Dysfunctional Microglia in Neurodegenerative Diseases Article The TREM2-APOE Pathway Drives the Transcriptional Phenotype of Dysfunctional Microglia in Neurodegenerative Diseases. 566–581 (2017). doi:10.1016/j.immuni.2017.08.008

169. Takahashi, K., Rochford, C. D. P. & Neumann, H. Clearance of apoptotic neurons without inflammation by microglial triggering receptor expressed on myeloid cells-2. *J. Exp. Med.* **201**, 647–657 (2005).

170. Siddiqui, T. A., Lively, S. & Schlichter, L. C. Complex molecular and functional outcomes of single versus sequential cytokine stimulation of rat microglia. *J. Neuroinflammation* **13**, 66 (2016).

171. Marschallinger, J. *et al.* Lipid-droplet-accumulating microglia represent a dysfunctional and proinflammatory state in the aging brain. *Nat. Neurosci.* **23**, 194–208 (2020).

172. Honey, K. & Rudensky, A. Y. Lysosomal cysteine proteases regulate antigen presentation. *Nat. Rev. Immunol.* **3**, 472–482 (2003).

173. Zavasnik-Bergant, T. Differentiation- and maturation-dependent content, localization, and secretion of cystatin C in human dendritic cells. *J. Leukoc. Biol.* **78**, 122–134 (2005).

174. Kitamura, H. *et al.* IL-6-STAT3 controls intracellular MHC class II alphabeta dimer level through cathepsin S activity in dendritic cells. *Immunity* **23**, 491—502 (2005).

175. Pierre, P. & Mellman, I. Developmental regulation of invariant chain proteolysis controls MHC class II trafficking in mouse dendritic cells. *Cell* **93**, 1135–1145 (1998).

176. Hunt, D. F. *et al.* Peptides presented to the immune system by the murine class II major histocompatibility complex molecule I-Ad. *Science* **256**, 1817–1820 (1992).

177. Villadangos, J. A. *et al.* Proteases involved in MHC class II antigen presentation.

Immunol. Rev. **172**, 109–120 (1999).

178. Reinheckel, T., Deussing, J., Roth, W. & Peters, C. Towards specific functions of lysosomal cysteine peptidases: phenotypes of mice deficient for cathepsin B or cathepsin L. *Biol. Chem.* **382**, 735–741 (2001).

179. Nakagawa, T. Y. & Rudensky, A. Y. The role of lysosomal proteinases in MHC class II-mediated antigen processing and presentation. *Immunol. Rev.* **172**, 121–129 (1999).

180. Salvesen, G. S. A lysosomal protease enters the death scene. *J. Clin. Invest.* **107**, 21–22 (2001).

181. Hamilton, G., Colbert, J. D., Schuettelkopf, A. W. & Watts, C. Cystatin F is a cathepsin C-directed protease inhibitor regulated by proteolysis. *EMBO J.* **27**, 499–508 (2008).

182. Halfon, S. *et al.* Leukocystatin, a new Class II cystatin expressed selectively by hematopoietic cells. *J. Biol. Chem.* **273**, 16400–16408 (1998).

183. Hashimoto, S. I. *et al.* Identification of genes specifically expressed in human activated and mature dendritic cells through serial analysis of gene expression. *Blood* **96**, 2206–2214 (2000).

184. Obata-Onai, A. *et al.* Comprehensive gene expression analysis of human NK cells and CD8(+) T lymphocytes. *Int. Immunol.* **14**, 1085–1098 (2002).

185. Shimizu, T. *et al.* The balance between cathepsin C and cystatin F controls remyelination in the brain of Plp1-overexpressing mouse, a chronic demyelinating disease model. *Glia* **65**, 917–930 (2017).

186. Liang, J. *et al.* Disinhibition of cathepsin C caused by cystatin F deficiency aggravates the demyelination in a cuprizone model. *Front. Mol. Neurosci.* **9**, 1–12 (2016).

187. Liu, Q. *et al.* Cathepsin C promotes microglia M1 polarization and aggravates neuroinflammation via activation of Ca 2+ -dependent PKC/p38MAPK/NF-κB pathway. *J. Neuroinflammation* **16**, 1–18 (2019).

188. Prunk, M., Nanut, M. P., Sabotic, J., Svajger, U. & Kos, J. Increased cystatin F levels correlate with decreased cytotoxicity of cytotoxic T cells. *Radiol. Oncol.* **53**, 57–68 (2019).

189. Kos, J. *et al.* Cystatin F as a regulator of immune cell cytotoxicity. *Cancer Immunology, Immunotherapy* **67**, 1931–1938 (2018).

190. De, I. *et al.* CSF1 overexpression has pleiotropic effects on microglia in vivo. *Glia* **62**, 1955–1967 (2014).

191. Fan, K. *et al.* Up-regulation of microglial cathepsin C expression and activity in lipopolysaccharide-induced neuroinflammation. *J. Neuroinflammation* **9**, 1–13 (2012).

192. Nakanishi, H. Cathepsin regulation on microglial function. *Biochim. Biophys. Acta - Proteins Proteomics* **1868**, 140465 (2020).

193. Colbert, J. D., Plechanovová, A. & Watts, C. Glycosylation directs targeting and activation of cystatin F from intracellular and extracellular sources. *Traffic* **10**, 425–437 (2009).

194. Nathanson, C. M., Wassélius, J., Wallin, H. & Abrahamson, M. Regulated expression and intracellular localization of cystatin F in human U937 cells. *Eur. J. Biochem.* **269**, 5502–5511 (2002).

Chapter 2

MICROGLIA INFLUENCE HOST DEFENSE, DISEASE, AND REPAIR FOLLOWING MURINE CORONAVIRUS INFECTION OF THE CENTRAL NERVOUS SYSTEM

Glia, 2020:1-16

Microglia influence host defense, disease, and repair following coronavirus infection of the central nervous system

Vrushali Mangale[*1], Amber R. Syage[*3], H. Atakan Ekiz[*1], Dominic D. Skinner[1], Yuting Cheng[3], Colleen L. Stone[1], R. Marshall Brown[1], Ryan M. O'Connell[1], Kim N. Green[2], and Thomas E. Lane[3]

[*]These authors equally contributed to this work

[1]Division of Microbiology & Immunology, Department of Pathology, University of Utah School of Medicine, Salt Lake City, Utah 84112

[2]Department of Neurobiology & Behavior, 2205 McGaugh Hall, School of Biological Sciences, University of California, Irvine 92697

[3]Department of Neurobiology & Behavior, 2205 McGaugh Hall, School of Biological Sciences, University of California, Irvine 92697

Correspondence

Thomas E. Lane, Ph.D.

Department of Neurobiology & Behavior

2205 McGaugh Hall, University of California, Irvine 92697

Email: tlane@uci.edu

ABSTRACT

The present study examines functional contributions of microglia in host defense, demyelination, and remyelination following infection of susceptible mice with a neurotropic coronavirus. Treatment with PLX5622, an inhibitor of colony stimulating factor 1 receptor (CSF1R) that efficiently depletes microglia, prior to infection of the central nervous system (CNS) with the neurotropic JHM strain of mouse hepatitis virus (JHMV) resulted in increased mortality compared to control mice that correlated with impaired control of viral replication. Single cell RNA sequencing (scRNAseq) of CD45+ cells isolated from the CNS revealed that PLX5622 treatment resulted in muted CD4+ T cell activation profile that was associated with decreased expression of transcripts encoding MHC class II and CD86 in macrophages but not dendritic cells. Evaluation of spinal cord demyelination revealed a marked increase in white matter damage in PLX5622-treated mice that corresponded with elevated expression of transcripts encoding disease-associated proteins Osteopontin (*Spp1*), Apolipoprotein E (*Apoe*), and Triggering receptor expressed on myeloid cells 2 (*Trem2*) that were enriched within macrophages. In addition, PLX5622 treatment dampened expression of Cystatin F (*Cst7*), Insulin growth factor 1 (*Igf1*), and lipoprotein lipase (*Lpl*) within macrophage populations which have been implicated in promoting repair of damaged nerve tissue and this was associated with impaired remyelination. Collectively, these findings argue that microglia tailor the CNS microenvironment to enhance control of coronavirus replication as well as dampen the severity of demyelination and influence repair.

Keywords: Coronavirus, microglia, host defense, demyelination, remyelination

Main Points

Microglia are the resident immune cells of the CNS and recent studies have emphasized the importance of this population of cells in both health and disease. To better understand the role of microglia in host defense and disease, we pharmacologically (PLX5622, an inhibitor of colony stimulator factor 1 receptor) depleted microglia and infected PLX5622-treated and control mice with a neurotropic coronavirus. Our findings support an important role for microglia aiding in control of viral replication as well as restricting the severity of demyelination and influencing remyelination. Single cell RNA sequencing on CD45+ cells enriched from the CNS of experimental mice revealed the heterogeneity of immune cells infiltrating into the CNS that is dictated by disease stage. Moreover, our findings reveal an important role for microglia in tailoring the CNS microenvironment in response to CNS viral infection that subsequently influences disease progression and repair.

INTRODUCTION

Intracranial inoculation of C57BL/6 mice with the neurotropic JHM strain of mouse hepatitis virus (JHMV), a member of the *Coronaviridae* family, leads to an acute encephalomyelitis in which virus infects and replicates within glial cells with relative sparing of neurons (1-4). Expression of type I interferon (IFN-I) is critical in helping control viral replication as mice lacking IFN-I receptor exhibit increased mortality associated with enhanced viral replication (5). In addition, localized expression of T cell chemotactic chemokines including CCL5, CXCL9 and CXCL10 within the CNS contribute to host defense by attracting virus-specific CD4+ and CD8+ T cells into the CNS that further control viral replication through secretion of interferon-γ (IFN-γ) and cytolytic activity (6-13). Antibody-secreting cells (ASCs) are also capable of responding to CXCL9 and CXCL10 and aid in host defense (14, 15). Nonetheless, sterile immunity is not achieved and the majority of animals that survive the acute stage of disease develop immune-mediated demyelination in which both virus-specific T cells and macrophages amplify the severity of white matter damage associated with hind-limb paralysis (1, 3, 16, 17).

While the functional roles of T cells and B cells in both host defense and disease in JHMV-infected mice have been extensively studied, there is increasing interest in better understanding how resident cells of the CNS contribute to these events. Microglia are considered the resident immune cells of the CNS and aid in a diverse array of functions including maintaining CNS homeostasis as well as contributing to various disease-associated conditions (18-21). Moreover, microglia are immunologically competent and capable of rapidly responding to infection and/or damage via specific expression of surface receptors culminating in morphologic changes accompanied by secretion of proinflammatory cytokines/chemokines that

function in amplifying neuroinflammation. Recently, the functional role of microglia in contributing to host defense in response to CNS infection with neurotropic viruses has been examined. These studies have been greatly aided by findings demonstrating that mice lacking colony stimulating factor 1 receptor (CSF1R-/-) lack microglia emphasizing the importance of this signaling pathway in microglia development (22). Subsequent studies by Green and colleagues (23) showed that blocking CSF1R signaling in adult mice through administration of CSF1R antagonists is also important in survival of microglia in adult mice . Recent studies have employed treatment of mice with PLX5622, a brain penetrant and selective antagonist of the CSF1R that results in a dramatic reduction in microglia, to better understand functional roles of these cells in pre-clinical models of neurodegenerative disease (23-26). In addition, PLX5622-mediated targeting of microglia results in increased susceptibility to West Nile virus (27, 28), Japanese encephalitis virus (JEV) (28), Theiler's murine encephalomyelitis virus (TMEV) (29, 30) and JHMV (31) arguing for a protective role for microglia against acute viral-induced encephalitis.

The current study was undertaken to better understand how microglia tailor the immunological landscape in response to JHMV infection with regards to both host defense and neuropathology. To address these, we used a comprehensive set of analytical approaches including single cell RNA sequencing (scRNAseq), flow cytometry and histopathological techniques to assess disease outcome in JHMV-infected mice treated with PLX5622 at defined times post-infection. Our findings emphasize an important role for microglia in aiding in host defense as well as influencing both the severity of spinal cord demyelination and remyelination in a model of coronavirus-induced neurologic disease.

MATERIALS AND METHODS

Mice and viral infection. Five-week old C57BL/6 male mice were purchased from The Jackson Laboratory. Mice were infected intracranially (i.c.) with 250 plaque forming units (PFU) of JHMV strain J2.2v-1 in 30μL of sterile Hanks balanced sterile solution (HBSS) and animals were euthanized at days 3, 7, 12 and 21 post-infection (p.i). Clinical disease in JHMV-infected mice was evaluated using a previously described scale (32). To determine viral titers within brains, experimental animals were sacrificed at defined times p.i, brains isolated, homogenized and plaque assay were performed on the DBT astrocytoma cell line as described previously (33). All animal studies were reviewed and approved by the University of Utah Animal Care and Use Committee.

PLX5622 treatment. AIN-76A (Research Diets, NJ) rodent chow formulated with CSF1R inhibitor- PLX5622 at a dose of 1,200 mg/kg of chow was kindly provided by Plexxikon, Inc (Berkeley, CA). Mice were fed with either PLX5622 chow or control chow 7 days prior to viral infection and chow was continued until the mice were sacrificed to harvest tissues at defined times p.i.

Cell isolation and flow cytometry. Flow cytometry was performed to identify inflammatory cells entering the CNS using established protocols (34, 35). In brief, single cell suspensions were generated from tissue samples by grinding with frosted microscope slides. Immune cells were enriched via a 2-step Percoll cushion (90% and 63%) and cells were collected at the interface of the two Percoll layers. Before staining with fluorescent antibodies, isolated cells were incubated with anti-CD16/32 Fc block (BD Biosciences, San Jose, CA) at a 1:200 dilution.

Immunophenotyping was performed using commercially available antibodies specific for the following cell surface markers: CD4, CD8, CD11b (BD Biosciences, San Jose, CA) and CD45 (eBioscience, San Diego, CA). The following flow cytometric gating strategies were employed for inflammatory cells isolated from the CNS: macrophages ($CD45^{hi}CD11b+$) and microglia ($CD45^{lo}$ CD11b+). APC-conjugated rat anti-mouse CD4 and a PE-conjugated tetramer specific for the CD4 immunodominant epitope present within the JHMV matrix (M) glycoprotein spanning amino acids 133-147 (M133-147 tetramer) to determine total and virus-specific $CD4^+$ cells, respectively (35, 36); APC-conjugated rat anti-mouse CD8a and a PE-conjugated tetramer specific for the CD8 immunodominant epitope present in the spike (S) glycoprotein spanning amino acids 510-518 (S510-518) to identify total and virus-specific $CD8^+$ cells, respectively (35, 36). Data were collected using a BD LSR Fortessa X-20 flow cytometer and analyzed with FlowJo software (Tree Star Inc.).

Single cell RNA sequencing (scRNAseq). Immune cells were isolated as described above from brain (day 7 p.i) and spinal cord (day 14 p.i) and stained with DAPI and APC conjugated anti-CD45 for 20 minutes on ice in 1X PBS containing 0.5% bovine serum albumin (BSA). Live CD45+ cells were enriched through the use of BD FACS Aria flow sorter (University of Utah Health Science Center) and washed once with 0.04% BSA. Samples were then processed for single cell RNA sequencing via the 10X Genomics platform performed at the Huntsman Cancer Institute High Throughput Genomics Shared Resource Core Facility (https://uofuhealth.utah.edu/huntsman/ shared-resources/gba/). RNA sequencing was performed via Aligent Hiseq next generation sequencer. Sequencing data was processed using the 10X Genomics Cell Ranger pipeline and analyzed using the Seurat R package. Gene expression

signatures defining cell clusters were analyzed from PLX5622-treated and controls at day 7 p.i. (brains) and day 14 p.i. (spinal cords). Cells from each aggregated sample dataset were clustered into corresponding immune cell populations by a shared nearest neighbor modularity optimization-based clustering algorithm using the Seurat package. The resulting clusters were defined using an immune-cell scoring algorithm (https://aekiz.shinyapps.io/CIPR/) (37) that compares the gene signatures of each cluster in the experimental dataset with the microarray data available in the Immunological Genome (ImmGen) Project Database. Expression levels and distribution of population-specific immune cell markers were then analyzed to further refine the identified clusters and expose any subpopulations that should be separated as independent clusters. Once the clusters were established and identified, plots were generated using Seurat, ggpubr and fgsea R packages.

Histology. Mice were euthanized at defined times points according to IACUC-approved guidelines and the length of spinal cord extending from thoracic vertebrate 6-10 was cryoprotected in 30% sucrose, cut into 1-mm transverse blocks and processed so as to preserve the craniocaudal orientation and subsequently embedded in O.C.T. (VWR, Radnor, PA, USA). Eight micron (μm)-thick coronal sections were cut and sections were stained with hematoxylin/eosin (H&E) in combination with luxol fast blue (LFB) and between 4-8 sections/mouse analyzed. Areas of total white matter and demyelinated white matter were determined with Image J Software and demyelination was scored as a percentage of total demyelination from spinal cord sections analyzed (38-41).

Electron Microscopy and *g*-ratio analysis. For electron microscopy (EM) analysis of spinal cords, mice were sacrificed and underwent cardiac perfusion with 0.1 M cacodylate buffer containing 2% paraformaldehyde/2% glutaraldehyde. Serial ultrathin sections of spinal cords embedded in Epon epoxy resin were stained with uranyl acetate-lead citrate and analyzed as previously described (42). Images at 1200X magnification were analyzed for *g*-ratio using Image J software. In adult animals there is a relationship between axon circumference and myelin sheath thickness (number of lamellae) expressed by the g-ratio (axon diameter/total fiber diameter); in remyelination this relationship changes such that myelin sheaths are abnormally thin for the axons they surround (43). An abnormally thin myelin sheath, relative to axonal diameter, was used as the criterion for oligodendrocyte remyelination. Absence of a myelin sheath was used as the criterion for demyelination. For most axons, two measurements were conducted with a minimum of 400 axons analyzed per experimental group. In all cases, slides were blinded and read independently by two investigators.

Statistical analysis. GraphPad Prism was used to perform statistical analyses. Data for each experiment is presented as mean$\pm$standard error of mean (SEM). For flow cytometry analysis unpaired Student's *t* test was used to determine significance and a p value of < 0.05 was considered statistically significant. Wilcoxon test was used for analyzing gene expression in scRNAseq clusters and the resulting p values were corrected for multiple comparisons by Holm-Sidak method and a p value of < 0.05 was considered statistically significant.

RESULTS

PLX5622 treatment increases susceptibility to JHMV-induced neurologic disease.

To evaluate the contribution of microglia to disease progression in JHMV-infected mice, the CSF1R inhibitor PLX5622 was administered as previous studies have reported this pharmacologic approach effectively depletes >90% of microglia (24, 44). Mice were treated with PLX5622 (1,200 mg/kg) 7 days prior to infection and continued on the drug for the duration of the experiment. Treatment with PLX5622 resulted in an overall increase in mortality with ~25% of PLX5622-treated mice surviving to day 21 p.i. whereas ~75% of control-chow treated mice survived to this time (**Figure 1a**). The increase in mortality in PLX5622-treated mice correlated with increased viral titers within the brains and spinal cords at days 3, 7, and 12 p.i. compared to control animals; however, by day 21 p.i. viral titers were not detected (ND) in experimental groups (**Figure 1b**). We confirmed efficient microglia ($CD45^{lo}CD11b+$) depletion in PLX5622-treated mice within the brain at day 7 p.i. (**Figure 1c**) and spinal cord at day 14 p.i. (**Figure 1d**) using flow cytometry. PLX5622 treatment did not affect numbers of macrophages ($CD45^{hi}CD11b+$) within brains and spinal cords of experimental mice (**Figures 1c and d**). These findings support earlier work indicating that PLX5622-targeting of microglia impacts efficient immune-mediated control of viral replication following infection with neurotropic viruses (27-29, 31, 45).

PLX5622 treatment does not substantially alter immune cell infiltration into the CNS of JHMV-infected mice.

Our findings reveal that PLX5622 treatment of mice increases susceptibility to JHMV-induced neurologic disease associated with impaired ability to control viral replication. In order

to better understand the effects of PLX5622 treatment on influencing the immune cell composition of the CNS we employed 10x Genomics scRNAseq technology. Experimental mice were fed either control chow or chow containing PLX5622 for 7 days prior to infection and remained on chow until sacrifice at either day 7 p.i. or 14 p.i., at which point, live CD45+ cells were sorted from the brains or spinal cords, respectively. We aggregated data from cells taken from control and PLX5622-treated mice and performed unsupervised clustering analysis based on similarity of gene expression signatures using Seurat single cell genomics R package (37). This approach revealed 16 distinct cell clusters representative of both lymphoid and myeloid linages at day 7 p.i. (**Figure 2a**). To better understand the overlapping expression of marker genes and identification of cell clusters, we employed a recently described algorithm that compares the gene expression signatures of cell clusters with publicly available ImmGen database (37). As previously described (37), this algorithm calculates an aggregate identity score for each scRNAseq cell cluster as a measure of molecular similarity to the ImmGen subsets. Through combinations of these two approaches, we identified three CD8+ T cell subsets [naïve, effector(Eff.), and memory(Mem.)], two macrophage subsets (Mac 1 and Mac 2), four dendritic cell (DC) subsets [plasmacytoid, NADPH (*Nox2*), XCR1 (*Xcr1*), CCL22 (*Ccl22*)], and single subsets of CD4+ T cells, regulatory T cells (Treg), natural killer (NK) cells, B cells, microglia, neutrophils (neuts), and monocytes at day 7 p.i. (**Figure 2a**). In order to verify the algorithm-assisted identification of cell clusters, we examined expression of known cellular markers in our dataset; expression of these markers corresponded with the respective identities of the distinct clusters (**Figures 2b and c**).

We next analyzed differences in CD45+ cells between PLX5622-treated and control mice at day 7 p.i. following JHMV infection. When data from the cellular genotypes were plotted

side-by-side, treatment-dependent dynamics within the tissues started to emerge (**Figures 3a and b**). Importantly, we were able to show that PLX5622 treatment resulted in decreased expression of microglia-associated transcripts *Tmem119, P2ry12*, and *Sparc* compared to control mice (**Figure 3c**). Expression of IFN-α is critical in effective control of JHMV replication within the CNS (5, 46, 47). We examined IFN-α responses by both macrophages and DCs in order to gain better insight into potential mechanisms by which PLX5622 treatment led to impaired control of viral replication. When the global expression signatures of macrophages and DCs were examined, IFN-α response genes were found to be significantly enriched within the brains of PLX5622-treated mice compared to controls arguing that targeting microglia did not diminish IFN-I responses (**Figures 3d and e**).

PLX5622-treatment alters infiltration and activation phenotype of T cells.

Control of JHMV replication within the CNS is associated with infiltration of activated virus-specific CD4+ and CD8+ T cells (12, 48, 49). At day 7 p.i., PLX5622 treatment did not significantly alter CD4+ T cell infiltration yet there was an increase in CD8+ T cells ($p<0.05$) compared to control mice as determined by flow cytometric analysis (**Supplemental Figure 1a**). There were no differences in virus-specific CD4+ and CD8+ T cells specific for immunodominant epitopes present within the Matrix (M) (**Supplemental Figure 1b**) and Spike (S) glycoproteins (**Supplemental Figure 1c**) as determined by tetramer staining (39, 41).

Evaluation of defined factors associated with T cell activation at day 7 p.i. revealed reduced expression of the Th1-associated transcription factor Tbet (*Tbx21*) ($p<0.01$) and this was associated with reduced ($p<0.05$) expression of *Tnf* transcripts, but not *Ifng* transcripts, in PLX5622-treated mice compared to control mice (**Figure 4a**). We also determined reduced

expression of activation markers CD69 (*Cd69*) and CD44 (*Cd44*, $p<0.05$) in CD4+ T cells from the brains of PLX5622-treated mice compared to control mice at day 7 p.i. (**Figure 4a**). In addition, the CD4+ T cells subset from PLX5622-treated mice also expressed reduced transcripts for *Il2ra* ($p<0.05$)and *Il2rb* ($p<0.01$) that encode for components of the IL-2 receptor when compared to control-treated mice (**Figure 4a**). Previous work from Bergmann and colleagues (50) identified that IL-21 derived from CD4+ T cells is important in enhancing anti-viral effector functions by CD8+ T cells following JHMV infection. Comparison of *Il21* transcript levels in CD4+ T cells between PLX5622-treated mice compared to control mice indicated no significant difference at day 7 p.i. (**Figure 4c**). In contrast, CD8+ T cells isolated from brains of PLX5622-treated mice expressed increased transcripts specific for perforin (*Prf1*, $p<0.0001$), granzyme B (*Gzmb*, $p<0.001$) and programmed cell death 1, PD-1 (*Pdcd1*, $p<0.0001$) (**Figure 4b**). There was no difference in expression of *Ifng* transcripts between experimental groups (**Figure 4b**).

Correlating with muted CD4+ T cell activation was the demonstration of a reduction ($p<0.0001$) in transcripts associated with MHC class II as well as the co-stimulatory molecule CD86 in macrophages in PLX5622-treated mice compared controls (**Figure 4d**). Flow cytometric staining for MHC class II on cells isolated from the brains of PLX5622 and control mice at day 7 p.i. confirmed expression was reduced ($p<0.001$) on macrophages obtained from PLX5622-treated mice compared to controls (data not shown). Additionally, MHC class II expression on remaining microglia within the brains of PLX5622-treated mice was also reduced ($p<0.001$) compared to expression on microglia from control mice (data not shown). Dampened expression of MHC class II in PLX5622-treated mice was further confirmed through immunofluorescent staining in combination with Iba1 (data not shown). Expression of MHC class I-associated transcripts was increased ($p<0.0001$) in macrophages isolated from the brains

of PLX5622-treated mice compared to control animals in macrophages which was consistent with apparent increased CD8+ T cell activation (**Figure 4d**). With regards to dendritic cells at day 7 p.i., we did not detect changes in expression of transcripts associated with either MHC class II or MHC class I (**Figure 4e**) between PLX5622-treated mice and controls.

PLX5622 treatment and immune cell infiltration into spinal cords of JHMV-infected mice at day 14 p.i.

We next performed scRNAseq on CD45+ cells enriched from the spinal cords of JHMV-infected mice treated with either PLX5622 or control at day 14 p.i. Using the same approach as described above, we detected 18 cell clusters within spinal cords of experimental mice representing lymphoid and myeloid populations (**Figure 5a**). In brief, this included 3 DC subsets [plasmacytoid, NADPH (*Nox2*), XCR1 (*Xcr1*)], five macrophage subsets [CD40 (*Cd40*), [Interferon-induced proteins with Tetratricopeptide repeats IFIT (*Ifit1,Ifit2,Ifit3*)], Mac 1, Mac 2, and Mac 3), three populations of microglia that included Galectin+ microglia and Insulin growth factor 1-positive (*Igf1*+) microglia, two populations of CD8+ T cells [effector (Eff.) and effector cycling(Eff. Cyc.)], and single populations of neuts, Tregs, CD4+ T cells and B cells. Expression of known cellular markers in our dataset corresponded with respective identities of clusters (**Figures 5b and c**). Consistent with our spinal cord flow data (**Figure 1d**), PLX5622 treatment led to a reduction in microglia with a trend towards an increase in macrophage populations (**Figures 5d and e**). The presence of *Ifit*-positive macrophages argues for a role in contributing to anti-viral immune responses (51). Further, we also detected the presence of Galectin-positive microglia although there were no differences in frequency between experimental populations (**Figures 5d and e**). Finally, we did find a reduced frequency of *Igf-1*-positive microglia within

the spinal cords of PLX5622-treated mice compared to controls (**Figures 5d and e**).

CSF1R antagonism increases the severity of demyelination in JHMV-infected mice.

CNS inflammatory T cells augment demyelination in JHMV-infected mice presumably through recognition of viral antigens resulting in secretion of cytokines *e.g.* IFN-γ that activate both resident CNS cells and inflammatory macrophages/myeloid cells to secrete proinflammatory cytokines/chemokines as well as molecules damaging to oligodendrocyte function (3, 16). By day 14 p.i., we detected no difference in CD4+ T cells in the spinal cords of PLX5622-treated mice versus controls, though there was an increase ($p<0.05$) in CD8+ T cells (**Supplemental Figure 2a**) as well as virus-specific CD4+ (**Supplemental Figure 2b**) and CD8+ T cells (**Supplemental Figure 2c**) compared to controls. Similar to what we observed at day 7 p.i., we detected reduced expression of *Cd69* transcripts ($p<0.01$), *Il2rb* transcripts ($p<0.0001$), and *Tbx21* ($p<0.0001$) in CD4+ T cells isolated from spinal cords of PLX5622-treated mice compared to controls (**Figure 6a**). There were no differences in expression of *Cd44* or cytokines *Ifng* and *Tnf* within CD4+ T cells between experimental groups of mice (**Figure 6a**). However, *Il21* transcript levels were significantly ($p<0.0001$) reduced in CD4+ T cells isolated from PLX5622-treated mice compared to control mice at this time (**Figure 6c**). In addition, there was no difference in transcript levels for *Gzmb* or *Ifng* in CD8+ T cells isolated from spinal cords of PLX5622-treated mice compared to controls (**Figure 6b**). However, expression of both *Pdcd1* ($p<0.01$) and *Prf1* ($p<0.05$) were reduced in CD8+ T cells from PLX5622-treated mice versus controls (**Figure 6b**). PLX5622-treatment resulted in reduced expression of *Cd86* ($p<0.0001$), *H2_Aa* ($p<0.0001$), *H2_Ab1* ($p<0.001$), and *H2_DMb1* ($p<0.0001$) in spinal cord macrophages compared to control mice (**Figure 6d**). In contrast,

expression of MHC class I-associated transcripts *H2_K1* ($p<0.0001$), H2_M3 ($p<0.05$) remained elevated in spinal cord macrophages isolated from PLX5622-treated mice compared to controls yet there was no difference expression of *H2_Q7* transcripts (**Figure 6d**).

We next assessed how PLX5622 treatment affected the severity of demyelination in JHMV-infected mice. Using Luxol Fast Blue (LFB) staining of spinal cords from experimental mice, we determined that PLX5622 treatment resulted in an increase in the severity of demyelination at days 14 ($p<0.01$) and 21 p.i. ($p<0.05$) compared to control mice (**Figures 7a and b**). These findings indicate that targeting microglia via PLX5622 treatment results in increased demyelination arguing these cells exert a protective role in limiting the severity of white matter pathology in JHMV-infected mice. We also looked at expression of several genes associated with immune-mediated demyelinating diseases. Through scRNAseq analysis of CD45+-enriched cells from the spinal cords of JHMV-infected mice treated with either PLX5622 or control chow, we observed a dramatic increase in transcripts encoding for molecules associated with demyelination including Apoliprotein E (*Apoe*) (52), Osteopontin (*Spp1*) (53), and Triggering receptor expressed on myeloid cells (*Trem2*) (52, 54) in macrophage clusters within the spinal cords of PLX5622-treated mice compared to controls (**Figure 7c**). In addition, transcripts encoding proteins associated with remyelination including *Cst7* (Cystatin F), *Igf1* (insulin growth factor 1), and *Lpl* (Lipoprotein lipase) were decreased in spinal cord macrophages within the spinal cords of PLX5622-treated mice compared to controls (**Figure 7f**) (55-61). To determine whether remyelination was impacted in response to PLX5622 treatment, EM analysis of spinal cord sections was performed. Assessment of the *g*-ratio, the ratio of the inner axonal diameter to the total outer fiber diameter, is commonly employed as a structural index of remyelination; lower ratios indicate more extensive myelination (42, 62). High

magnification (1200X) images of the spinal cord ventral funiculus of PLX5622-treated and control mice were used to evaluate myelinated and demyelinated axons. PLX5622 treatment resulted in a significant ($p<0.05$) decrease in remyelination as determined by calculating *g*-ratio's (0.87 ± 0.004, minimum of 400 axons counted/mouse) compared to control treated mice (0.79 ± 0.003, minimum of 400 axons counted/mouse) (**Figures 7d**) as well as measuring myelin thickness (**Figure 7e**).

DISCUSSION

Viral infection of the central nervous system (CNS) presents unique challenges to the immune system with regard to controlling and eliminating the invading pathogen. The CNS is composed of a variety of highly specialized cells, many of which have limited renewal capacity, that represent potential targets of infection by numerous different viruses (63). A significant hurdle encountered by infiltrating antigen-specific lymphocytes is the elimination of virus from infected cells while limiting the damage that may have long-term detrimental consequences to the host. Therefore, characterizing the mechanisms involved in how viral infection of the CNS is controlled is an important question. It is becoming increasingly clear that CNS resident cells are critical in host defense through either secretion of anti-viral cytokines e.g. type I interferon (IFN-I) and/or presentation of antigen within the context of either MHC class I or II. Recently, an important role for microglia in aiding in host defense in response to CNS viral infection has been identified (27-31). Perlman and colleagues (31) have shown that microglia are required for optimal host defense in response to JHMV infection of the CNS. Targeted depletion of microglia through administration of PLX5622 revealed a role in limiting mortality that was associated with impaired control of JHMV replication. The increase in susceptibility to disease did not appear to be due to impaired expression of IFN-I but more likely a reflection of impaired antigen-presentation due to muted MHC class II expression by macrophages infiltrating the CNS of PLX5622-treated mice and this likely resulted in dampened T cell responses (31). Similarly, microglia depletion led to increased mortality in mice infected with West Nile Virus (WNV) associated with diminished activation of APCs and limited reactivation of virus-specific T cells that led to reduced viral clearance (27, 28). These findings clearly implicate microglia in

enhancing optimal host responses following CNS viral infection, in part, by influencing antigen-presentation that affects virus-specific T cell responses.

We undertook the present study to better understand how microglia contribute to host defense as well as demyelination and repair following JHMV infection of the CNS using sophisticated molecular, cellular and histologic approaches. Employing PLX5622 to deplete microglia, we found increased mortality associated with impaired control of CNS viral replication. CSF1R antagonism led to a selective decrease in microglia with sparing of macrophages as well dendritic cells indicating that resident APCs within the CNS were not affected. To better understand the functional contributions of microglia in aiding in host defense, we performed scRNAseq on CD45+ cells enriched from the brains of PLX5622 and control mice at day 7 p.i. Using a verified and unbiased bioinformatics approach (37), we were able to reliably identify clusters of cells associated with innate immune responses *e.g.* microglia, monocytes, macrophages, NK cells, and neutrophils as well as adaptive responses including T cell subsets and dendritic cells (**Figure 2a-c**). Moreover, this approach revealed the heterogeneity of both the innate and adaptive immune cell response by infiltrating cells as well as resident microglia with the identification of different subsets of DCs, macrophages, and T cells. These findings emphasize the complexity of both the innate and adaptive immune responses that occur in response to viral infection of the CNS and raises interesting questions with regards to functional roles for these populations of cells in either defense and/or disease progression. Surprisingly, scRNAseq demonstrated that PLX5622-mediated depletion of microglia did not dramatically alter the presence of the majority of immune cells identified including neutrophils, monocytes, DC and macrophage subsets, as well as Tregs and naïve and memory CD8+ T cells. This approach did indicate that PLX5622-treatment resulted in increased effector CD8+ T cells,

CD4+ T cells and, interestingly, B cells. These findings would argue that microglia may not impact either directly or indirectly the synthesis/secretion of proinflammatory cytokines/chemokines by other resident CNS cells *e.g.* astrocytes and/or inflammatory macrophages.

Expression of IFN-I is critical in host defense in response to JHMV infection of the CNS (5, 46, 47). PLX5622-mediated targeting of microglia did not affect IFN-I signaling as GSEA analysis revealed IFN-α response genes were significantly enriched in both macrophages and dendritic cells within the brains of PLX5622-treated mice at days 7 compared to controls (**Figures 3d and e**). These findings may reflect the increase in viral titers within the CNS of PLX5622-treated mice at these times but also argue that microglia are not solely responsible for production of IFN-I.

We detected altered T cell responses within the CNS following PLX5622 treatment as determined by both flow cytometry and scRNAseq. There were increased numbers of total CD8+ T cells ($p<0.05$) as well as virus-specific CD8+ T cells within the brains of JHMV-infected mice treated with PLX5622 compared to controls at day 7 p.i. We also found a trend towards increased total CD4+ T cells and virus-specific CD4+ T cells in PLX5622-treated mice compared to controls although these differences were not significant. In terms of T cell activation, we detected differential responses in T cell subsets at day 7 p.i. In CD4+ T cells, there was a reduction in transcripts associated with Th1-polarized activation *e.g.* T-bet (*Tbx21*) in PLX5622-treated mice compared to controls although there were no differences in *Ifng* transcripts in CD4+ T cells in experimental groups. PLX5622-treatment also resulted in reduced expression of CD4+ T cell surface activation markers including CD44, CD69, and components of IL-2 receptor in PLX5622-treated mice compared to controls whereas there was an overall

increased activation phenotype associated with CD8+ T cells compared to controls. A role for CD4+ T cell-derived IL-21 has previously been shown to enhance antiviral CD8+ T cell responses following JHMV infection of the CNS (50). While expression of *Il21* transcripts in CD4+ T cells was not affected at day 7 p.i. in PLX5622-treated mice, expression was significantly reduced by day 14 p.i. This reduction in *Il21* expression in CD4+ T cells in PLX5622-treated mice may have impacted virus-specific CD8+ T cell function and partially explain mechanisms associated with impaired control of JHMV replication within the CNS. In addition, the muted activation phenotype by CD4+ T cells was associated with reduced expression of MHC class II by macrophages, but not DCs, at day 7 p.i. in PLX5622-treated mice, demonstrating a selective effect in response to microglia depletion. This selective effect of reduced MHC class II expression by macrophages in PLX5622-treated mice was further emphasized in that expression of MHC class I transcripts was increased in macrophages, but not DCs, compared to control mice. Identifying the mechanisms by which microglia augment expression of MHC class II on macrophages will be a focus of ongoing studies.

Our results examining immune cell infiltration and activation in spinal cords of experimental mice at day 14 p.i. through scRNAseq were intriguing as we observed differences in both macrophage and microglial populations compared to the brain at day 7 p.i., regardless of the experimental groups. First, there were both *Ifit*+ and *CD40*+ macrophages present within the spinal cords of both PLX5622 and control mice, suggesting these cells may be responsible for host defense in response to viral infection (51). It is important to note that both populations of cells were present at a low frequency and there were no dramatic differences between experimental groups, although *CD40*+ macrophages were present at a much higher frequency compared to *Ifit*+ macrophages. Furthermore, there was a small population of Galectin+

microglia in spinal cords in control mice yet not in PLX5622-treated mice and previous studies argue for a role for certain isoforms of Galectin in potentially contributing to demyelination in patients with multiple sclerosis (MS) (64) while other isoforms are considered important in driving oligodendrocyte differentiation associated with remyelination (65). Our findings that spinal cord demyelination was significantly increased in PLX5622-treated mice supports an emerging role for microglia in restricting the severity of white matter and this is consistent with a recent study from our group indicating that microglia influence the severity of demyelination in JHMV-infected mice (66). While we are currently exploring the molecular and cellular mechanisms by which microglia may modulate the CNS microenvironment in mice persistently infected with JHMV, evidence presented in the current study indicates that PLX5622 treatment resulted in increased expression of transcripts encoding for Osteopontin, APOE, and TREM2 all of which have been implicated in contributing to demyelination (52-54). Interestingly, expression of all three transcripts were enriched within macrophage populations suggesting a specific effect by which microglia may suppress expression and limit myelin damage.

Emerging studies have pointed to a protective role for microglia in limiting neuropathology and promoting repair (67-69). In support of this concept are recent studies from Miron and colleagues (69) showing an important role for microglia in enhancing remyelination in a toxin-model of demyelination that is aided by microglial death and subsequent microglial repopulation; here, in this study, the absence of microglia prevents their further death and repopulation and is associated with increased white matter damage. Although mechanisms by which microglia may support remyelination have not been completely defined, it is though that these cells aid in clearance of myelin debris and/or secrete growth factors/cytokines that influence maturation of oligodendrocyte progenitor cells (OPCs) into mature myelin-producing

oligodendrocytes. What is also clear is that microglia are heterogenous in terms of transcriptome and protein expression which is likely regulated during the course of disease and this would influence the role of these cells in enhancing or muting disease progression and potential repair. In support of a protective role for microglia in restricting neuropathology and promoting repair is our data demonstrating that PLX5622 treatment of JHMV-infected mice results in an increase in white matter damage associated with impaired remyelination (**Figures 7a,b,d and e**). In addition, scRNAseq also shows reduced expression of genes encoding proteins previously associated with remyelination including Cystatin F (56, 58, 59), Insulin growth factor 1 (IGF1) (57, 60, 61) and Lipoprotein lipase (55) within macrophages isolated from the spinal cords of PLX5622-treated mice (**Figure 7f**). These findings further support the notion that microglia may either directly or indirectly influence remyelination within the spinal cord by contributing to controlling expression of genes encoding proteins that regulate OPC maturation. We are currently pursuing the functional contributions of Cystatin F, IGF1 and Lipoprotein lipase in contributing to remyelination in JHMV-infected mice.

We would caution that although demyelination was worsened and remyelination was impaired when microglia are depleted, this may reflect the model employed *i.e*. targeted depletion of microglia prior to JHMV infection of the CNS which may lead to increased neuropathology through altered macrophage biology and/or resident cells of the CNS including astrocytes and oligodendrocytes. We are currently determining if microglia depletion in mice persistently infected with JHMV in which demyelination is established affects either neuropathology and/or viral recrudescence as this is a more clinically-relevant question. Similarly, we are also determining if there is efficient repopulation of microglia in mice persistently infected with JHMV upon removal of PLX5622 treatment. Another important area

we are pursuing relates to whether depletion of microglia in mice with established demyelination impacts remyelination.

Acknowledgements

TEL was supported by funding from the National Institutes of Health (NIH) R01NS041249, R01NS091939, National Multiple Sclerosis Society (NMSS) Collaborative Research Center Grant CA-1607-25040 and The Ray and Tye Noorda Foundation. RMO was supported by NIH R01AG047956 and NMSS CA-1607-25040.

Conflict of interest

The authors declare no competing financial interests

REFERENCES

1. Bergmann CC, Lane TE, Stohlman SA. 2006. Coronavirus infection of the central nervous system: host-virus stand-off. Nat Rev Microbiol 4:121-32.

2. Lane TE, Hosking MP. 2010. The pathogenesis of murine coronavirus infection of the central nervous system. Crit Rev Immunol 30:119-30.

3. Templeton SP, Perlman S. 2007. Pathogenesis of acute and chronic central nervous system infection with variants of mouse hepatitis virus, strain JHM. Immunol Res 39:160-72.

4. Weiss SR, Leibowitz JL. 2011. Coronavirus pathogenesis. Adv Virus Res 81:85-164.

5. Ireland DD, Stohlman SA, Hinton DR, Atkinson R, Bergmann CC. 2008. Type I interferons are essential in controlling neurotropic coronavirus infection irrespective of functional CD8 T cells. J Virol 82:300-10.

6. Glass WG, Hickey MJ, Hardison JL, Liu MT, Manning JE, Lane TE. 2004. Antibody targeting of the CC chemokine ligand 5 results in diminished leukocyte infiltration into the central nervous system and reduced neurologic disease in a viral model of multiple sclerosis. J Immunol 172:4018-25.

7. Glass WG, Lane TE. 2003. Functional analysis of the CC chemokine receptor 5 (CCR5) on virus-specific CD8+ T cells following coronavirus infection of the central nervous system. Virology 312:407-14.

8. Glass WG, Lane TE. 2003. Functional expression of chemokine receptor CCR5 on CD4(+) T cells during virus-induced central nervous system disease. J Virol 77:191-8.

9. Liu MT, Armstrong D, Hamilton TA, Lane TE. 2001. Expression of Mig (monokine induced by interferon-gamma) is important in T lymphocyte recruitment and host defense following viral infection of the central nervous system. J Immunol 166:1790-5.

10. Liu MT, Chen BP, Oertel P, Buchmeier MJ, Armstrong D, Hamilton TA, Lane TE. 2000. The T cell chemoattractant IFN-inducible protein 10 is essential in host defense against viral-induced neurologic disease. J Immunol 165:2327-30.

11. Bergmann CC, Parra B, Hinton DR, Ramakrishna C, Dowdell KC, Stohlman SA. 2004. Perforin and gamma interferon-mediated control of coronavirus central nervous system infection by CD8 T cells in the absence of CD4 T cells. J Virol 78:1739-50.

12. Marten NW, Stohlman SA, Bergmann CC. 2001. MHV infection of the CNS: mechanisms of immune-mediated control. Viral Immunol 14:1-18.

13. Parra B, Hinton DR, Marten NW, Bergmann CC, Lin MT, Yang CS, Stohlman SA. 1999. IFN-gamma is required for viral clearance from central nervous system oligodendroglia. J Immunol 162:1641-7.

14. Phares TW, Marques CP, Stohlman SA, Hinton DR, Bergmann CC. 2011. Factors supporting intrathecal humoral responses following viral encephalomyelitis. J Virol 85:2589-98.

15. Phares TW, Stohlman SA, Hinton DR, Bergmann CC. 2013. Astrocyte-derived CXCL10 drives accumulation of antibody-secreting cells in the central nervous system during viral encephalomyelitis. J Virol 87:3382-92.

16. Hosking MP, Lane TE. 2009. The Biology of Persistent Infection: Inflammation and Demyelination following Murine Coronavirus Infection of the Central Nervous System. Curr Immunol Rev 5:267-276.

17. Hosking MP, Lane TE. 2010. The role of chemokines during viral infection of the CNS. PLoS Pathog 6:e1000937.

18. Hammond TR, Robinton D, Stevens B. 2018. Microglia and the Brain: Complementary Partners in Development and Disease. Annu Rev Cell Dev Biol 34:523-544.

19. Salter MW, Stevens B. 2017. Microglia emerge as central players in brain disease. Nat Med 23:1018-1027.

20. Tejera D, Heneka MT. 2019. Microglia in Neurodegenerative Disorders. Methods Mol Biol 2034:57-67.

21. Wolf SA, Boddeke HW, Kettenmann H. 2017. Microglia in Physiology and Disease. Annu Rev Physiol 79:619-643.

22. Ginhoux F, Greter M, Leboeuf M, Nandi S, See P, Gokhan S, Mehler MF, Conway SJ, Ng LG, Stanley ER, Samokhvalov IM, Merad M. 2010. Fate mapping analysis reveals that adult microglia derive from primitive macrophages. Science 330:841-5.

23. Elmore MR, Najafi AR, Koike MA, Dagher NN, Spangenberg EE, Rice RA, Kitazawa M, Matusow B, Nguyen H, West BL, Green KN. 2014. Colony-stimulating factor 1 receptor signaling is necessary for microglia viability, unmasking a microglia progenitor cell in the adult brain. Neuron 82:380-97.

24. Acharya MM, Green KN, Allen BD, Najafi AR, Syage A, Minasyan H, Le MT, Kawashita T, Giedzinski E, Parihar VK, West BL, Baulch JE, Limoli CL. 2016. Elimination of microglia improves cognitive function following cranial irradiation. Sci Rep 6:31545.

25. Dagher NN, Najafi AR, Kayala KM, Elmore MR, White TE, Medeiros R, West BL, Green KN. 2015. Colony-stimulating factor 1 receptor inhibition prevents microglial

plaque association and improves cognition in 3xTg-AD mice. J Neuroinflammation 12:139.

26. Spangenberg E, Severson PL, Hohsfield LA, Crapser J, Zhang J, Burton EA, Zhang Y, Spevak W, Lin J, Phan NY, Habets G, Rymar A, Tsang G, Walters J, Nespi M, Singh P, Broome S, Ibrahim P, Zhang C, Bollag G, West BL, Green KN. 2019. Sustained microglial depletion with CSF1R inhibitor impairs parenchymal plaque development in an Alzheimer's disease model. Nat Commun 10:3758.

27. Funk KE, Klein RS. 2019. CSF1R antagonism limits local restimulation of antiviral CD8(+) T cells during viral encephalitis. J Neuroinflammation 16:22.

28. Seitz S, Clarke P, Tyler KL. 2018. Pharmacologic Depletion of Microglia Increases Viral Load in the Brain and Enhances Mortality in Murine Models of Flavivirus-Induced Encephalitis. J Virol 92.

29. Waltl I, Kaufer C, Gerhauser I, Chhatbar C, Ghita L, Kalinke U, Loscher W. 2018. Microglia have a protective role in viral encephalitis-induced seizure development and hippocampal damage. Brain Behav Immun 74:186-204.

30. Sanchez JMS, DePaula-Silva AB, Doty DJ, Truong A, Libbey JE, Fujinami RS. 2019. Microglial cell depletion is fatal with low level picornavirus infection of the central nervous system. J Neurovirol 25:415-421.

31. Wheeler DL, Sariol A, Meyerholz DK, Perlman S. 2018. Microglia are required for protection against lethal coronavirus encephalitis in mice. J Clin Invest 128:931-943.

32. Lane TE, Liu MT, Chen BP, Asensio VC, Samawi RM, Paoletti AD, Campbell IL, Kunkel SL, Fox HS, Buchmeier MJ. 2000. A central role for CD4(+) T cells and RANTES in virus-induced central nervous system inflammation and demyelination. J Virol 74:1415-24.

33. Hirano N, Murakami T, Fujiwara K, Matsumoto M. 1978. Utility of mouse cell line DBT for propagation and assay of mouse hepatitis virus. Jpn J Exp Med 48:71-5.

34. Blanc CA, Rosen H, Lane TE. 2014. FTY720 (fingolimod) modulates the severity of viral-induced encephalomyelitis and demyelination. J Neuroinflammation 11:138.

35. Chen L, Coleman R, Leang R, Tran H, Kopf A, Walsh CM, Sears-Kraxberger I, Steward O, Macklin WB, Loring JF, Lane TE. 2014. Human neural precursor cells promote neurologic recovery in a viral model of multiple sclerosis. Stem Cell Reports 2:825-37.

36. Marro BS, Grist JJ, Lane TE. 2016. Inducible Expression of CXCL1 within the Central Nervous System Amplifies Viral-Induced Demyelination. J Immunol doi:10.4049/jimmunol.1501802.

37. Ekiz HA, Huffaker TB, Grossmann AH, Stephens WZ, Williams MA, Round JL, O'Connell RM. 2019. MicroRNA-155 coordinates the immunological landscape within murine melanoma and correlates with immunity in human cancers. JCI Insight 4.

38. Blanc CA, Grist JJ, Rosen H, Sears-Kraxberger I, Steward O, Lane TE. 2015. Sphingosine-1-phosphate receptor antagonism enhances proliferation and migration of engrafted neural progenitor cells in a model of viral-induced demyelination. Am J Pathol 185:2819-32.

39. Blanc CA, Rosen H, Lane TE. 2014. FTY720 (fingolimod) modulates the severity of viral-induced encephalomyelitis and demyelination. J Neuroinflammation 11:138.

40. Dickey LL, Worne CL, Glover JL, Lane TE, O'Connell RM. 2016. MicroRNA-155 enhances T cell trafficking and antiviral effector function in a model of coronavirus-induced neurologic disease. J Neuroinflammation 13:240.

41. Marro BS, Grist JJ, Lane TE. 2016. Inducible Expression of CXCL1 within the Central Nervous System Amplifies Viral-Induced Demyelination. J Immunol 196:1855-64.

42. Liu MT, Keirstead HS, Lane TE. 2001. Neutralization of the chemokine CXCL10 reduces inflammatory cell invasion and demyelination and improves neurological function in a viral model of multiple sclerosis. J Immunol 167:4091-7.

43. Smith KJ, Bostock H, Hall SM. 1982. Saltatory conduction precedes remyelination in axons demyelinated with lysophosphatidyl choline. J Neurol Sci 54:13-31.

44. Najafi AR, Crapser J, Jiang S, Ng W, Mortazavi A, West BL, Green KN. 2018. A limited capacity for microglial repopulation in the adult brain. Glia 66:2385-2396.

45. Sanchez JMS, DePaula-Silva AB, Doty DJ, Truong A, Libbey JE, Fujinami RS. 2019. Microglial cell depletion is fatal with low level picornavirus infection of the central nervous system. J Neurovirol doi:10.1007/s13365-019-00740-3.

46. Athmer J, Fehr AR, Grunewald ME, Qu W, Wheeler DL, Graepel KW, Channappanavar R, Sekine A, Aldabeeb DS, Gale M, Jr., Denison MR, Perlman S. 2018. Selective Packaging in Murine Coronavirus Promotes Virulence by Limiting Type I Interferon Responses. MBio 9.

47. Vijay R, Fehr AR, Janowski AM, Athmer J, Wheeler DL, Grunewald M, Sompallae R, Kurup SP, Meyerholz DK, Sutterwala FS, Narumiya S, Perlman S. 2017. Virus-induced inflammasome activation is suppressed by prostaglandin D2/DP1 signaling. Proc Natl Acad Sci U S A 114:E5444-E5453.

48. Williamson JS, Stohlman SA. 1990. Effective clearance of mouse hepatitis virus from the central nervous system requires both CD4+ and CD8+ T cells. J Virol 64:4589-92.

49. Pearce BD, Hobbs MV, McGraw TS, Buchmeier MJ. 1994. Cytokine induction during T-cell-mediated clearance of mouse hepatitis virus from neurons in vivo. J Virol 68:5483-95.

50. Phares TW, DiSano KD, Hinton DR, Hwang M, Zajac AJ, Stohlman SA, Bergmann CC. 2013. IL-21 optimizes T cell and humoral responses in the central nervous system during viral encephalitis. J Neuroimmunol 263:43-54.

51. Diamond MS, Farzan M. 2013. The broad-spectrum antiviral functions of IFIT and IFITM proteins. Nat Rev Immunol 13:46-57.

52. Krasemann S, Madore C, Cialic R, Baufeld C, Calcagno N, El Fatimy R, Beckers L, O'Loughlin E, Xu Y, Fanek Z, Greco DJ, Smith ST, Tweet G, Humulock Z, Zrzavy T, Conde-Sanroman P, Gacias M, Weng Z, Chen H, Tjon E, Mazaheri F, Hartmann K, Madi A, Ulrich JD, Glatzel M, Worthmann A, Heeren J, Budnik B, Lemere C, Ikezu T, Heppner FL, Litvak V, Holtzman DM, Lassmann H, Weiner HL, Ochando J, Haass C, Butovsky O. 2017. The TREM2-APOE Pathway Drives the Transcriptional Phenotype of Dysfunctional Microglia in Neurodegenerative Diseases. Immunity 47:566-581 e9.

53. Chabas D, Baranzini SE, Mitchell D, Bernard CC, Rittling SR, Denhardt DT, Sobel RA, Lock C, Karpuj M, Pedotti R, Heller R, Oksenberg JR, Steinman L. 2001. The influence of the proinflammatory cytokine, osteopontin, on autoimmune demyelinating disease. Science 294:1731-5.

54. Ulrich JD, Holtzman DM. 2016. TREM2 Function in Alzheimer's Disease and Neurodegeneration. ACS Chem Neurosci 7:420-7.

55. Bruce KD, Gorkhali S, Given K, Coates AM, Boyle KE, Macklin WB, Eckel RH. 2018. Lipoprotein Lipase Is a Feature of Alternatively-Activated Microglia and May Facilitate Lipid Uptake in the CNS During Demyelination. Front Mol Neurosci 11:57.

56. Durose WW, Shimizu T, Li J, Abe M, Sakimura K, Chetsawang B, Tanaka KF, Suzumura A, Tohyama K, Ikenaka K. 2019. Cathepsin C modulates myelin oligodendrocyte glycoprotein-induced experimental autoimmune encephalomyelitis. J Neurochem 148:413-425.

57. Hlavica M, Delparente A, Good A, Good N, Plattner PS, Seyedsadr MS, Schwab ME, Figlewicz DP, Ineichen BV. 2017. Intrathecal insulin-like growth factor 1 but not insulin enhances myelin repair in young and aged rats. Neurosci Lett 648:41-46.

58. Ma J, Tanaka KF, Shimizu T, Bernard CC, Kakita A, Takahashi H, Pfeiffer SE, Ikenaka K. 2011. Microglial cystatin F expression is a sensitive indicator for ongoing demyelination with concurrent remyelination. J Neurosci Res 89:639-49.

59. Shimizu T, Wisessmith W, Li J, Abe M, Sakimura K, Chetsawang B, Sahara Y, Tohyama K, Tanaka KF, Ikenaka K. 2017. The balance between cathepsin C and cystatin F controls remyelination in the brain of Plp1-overexpressing mouse, a chronic demyelinating disease model. Glia 65:917-930.

60. Wlodarczyk A, Holtman IR, Krueger M, Yogev N, Bruttger J, Khorooshi R, Benmamar-Badel A, de Boer-Bergsma JJ, Martin NA, Karram K, Kramer I, Boddeke EW, Waisman A, Eggen BJ, Owens T. 2017. A novel microglial subset plays a key role in myelinogenesis in developing brain. EMBO J 36:3292-3308.

61. Ye P, Li L, Richards RG, DiAugustine RP, D'Ercole AJ. 2002. Myelination is altered in insulin-like growth factor-I null mutant mice. J Neurosci 22:6041-51.

62. Moore S, Khalaj AJ, Yoon J, Patel R, Hannsun G, Yoo T, Sasidhar M, Martinez-Torres L, Hayardeny L, Tiwari-Woodruff SK. 2013. Therapeutic laquinimod treatment decreases inflammation, initiates axon remyelination, and improves motor deficit in a mouse model of multiple sclerosis. Brain Behav 3:664-82.

63. Klein RS, Garber C, Funk KE, Salimi H, Soung A, Kanmogne M, Manivasagam S, Agner S, Cain M. 2019. Neuroinflammation During RNA Viral Infections. Annu Rev Immunol 37:73-95.

64. de Jong C, Stancic M, Pinxterhuis TH, van Horssen J, van Dam AM, Gabius HJ, Baron W. 2018. Galectin-4, a Negative Regulator of Oligodendrocyte Differentiation, Is Persistently Present in Axons and Microglia/Macrophages in Multiple Sclerosis Lesions. J Neuropathol Exp Neurol 77:1024-1038.

65. Thomas L, Pasquini LA. 2018. Galectin-3-Mediated Glial Crosstalk Drives Oligodendrocyte Differentiation and (Re)myelination. Front Cell Neurosci 12:297.

66. Brown DG, Soto R, Yandamuri S, Stone C, Dickey L, Gomes-Neto JC, Pastuzyn ED, Bell R, Petersen C, Buhrke K, Fujinami RS, O'Connell RM, Stephens WZ, Shepherd JD, Lane TE, Round JL. 2019. The microbiota protects from viral-induced neurologic damage through microglia-intrinsic TLR signaling. Elife 8.

67. Baaklini CS, Rawji KS, Duncan GJ, Ho MFS, Plemel JR. 2019. Central Nervous System Remyelination: Roles of Glia and Innate Immune Cells. Front Mol Neurosci 12:225.

68. Lee J, Hamanaka G, Lo EH, Arai K. 2019. Heterogeneity of microglia and their differential roles in white matter pathology. CNS Neurosci Ther 25:1290-1298.

69. Lloyd AF, Miron VE. 2019. The pro-remyelination properties of microglia in the central nervous system. Nat Rev Neurol 15:447-458.

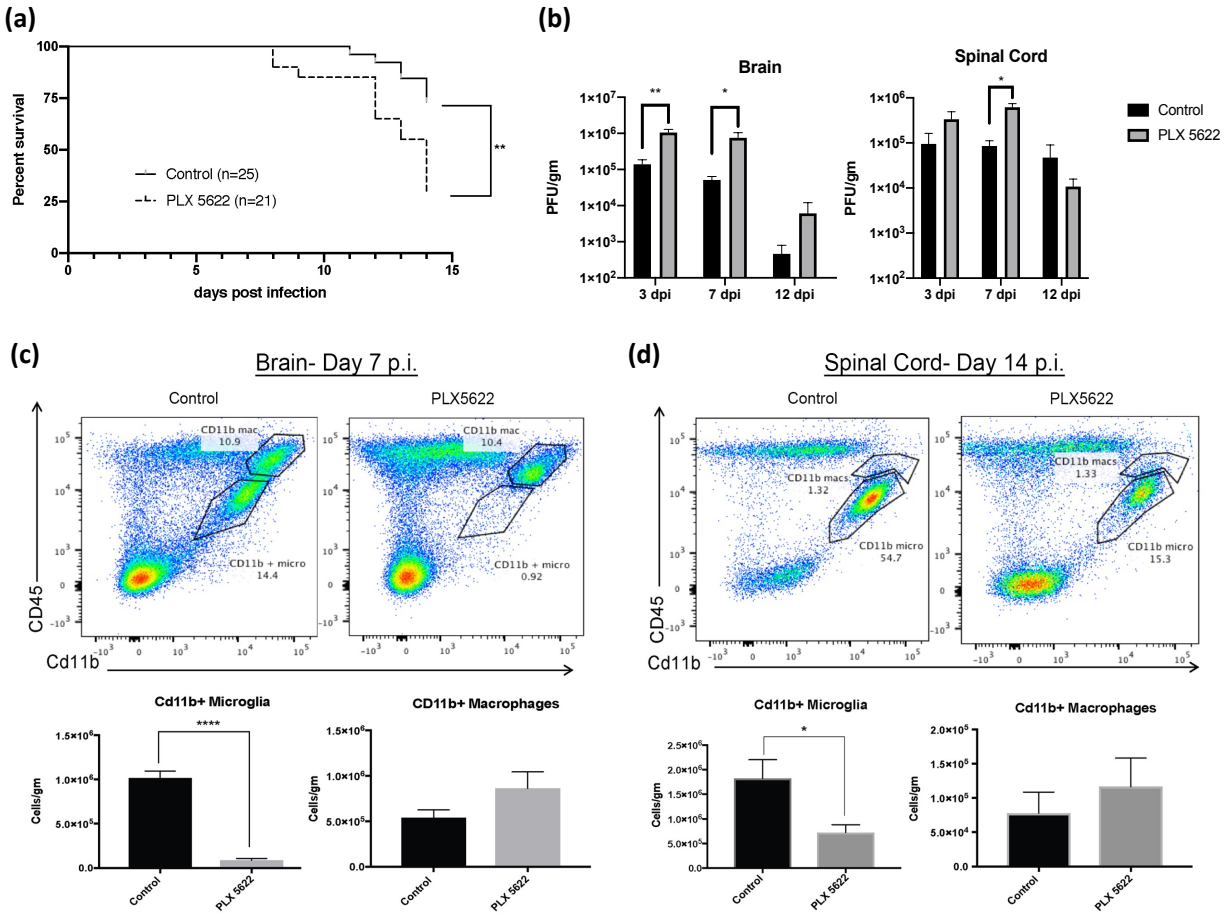

Figure 1: PLX5622 treatment increases susceptibility to JHMV-induced neurologic disease. Mice were fed either PLX5622 or control chow for 7 days prior to i.c. infection with JHMV (250 PFU) and subsequently remained specific chow for the duration of the experiment. PLX5622 treatment led to (**a**) increased mortality compared to control mice that was associated with an **(b)** impaired ability to control viral replication within the brains and spinal cords at days 3, 7, and 12 p.i. compared to control mice. Representative flow cytometric data from JHMV-infected mice treated with either PLX5622 or control chow and gating on microglia ($CD45^{lo}CD11b^{+}$ cells) or macrophages ($CD45^{hi}$ $CD11b^{+}$ cells) in (**c**) brains at day 7 p.i. and (**d**) spinal cords at day 14 p.i. PLX5622-treatment resulted in reduced numbers of microglia in brains and spinal cords compared to control mice. Data are derived from a minimum of 3 independent experiments with a minimum of 3 mice/time points. Data in *a*, *c*, and *d* are presented as average ± SEM. *p≤0.05; **p≤0.01; ***p≤0.001; ****p≤0.0001.

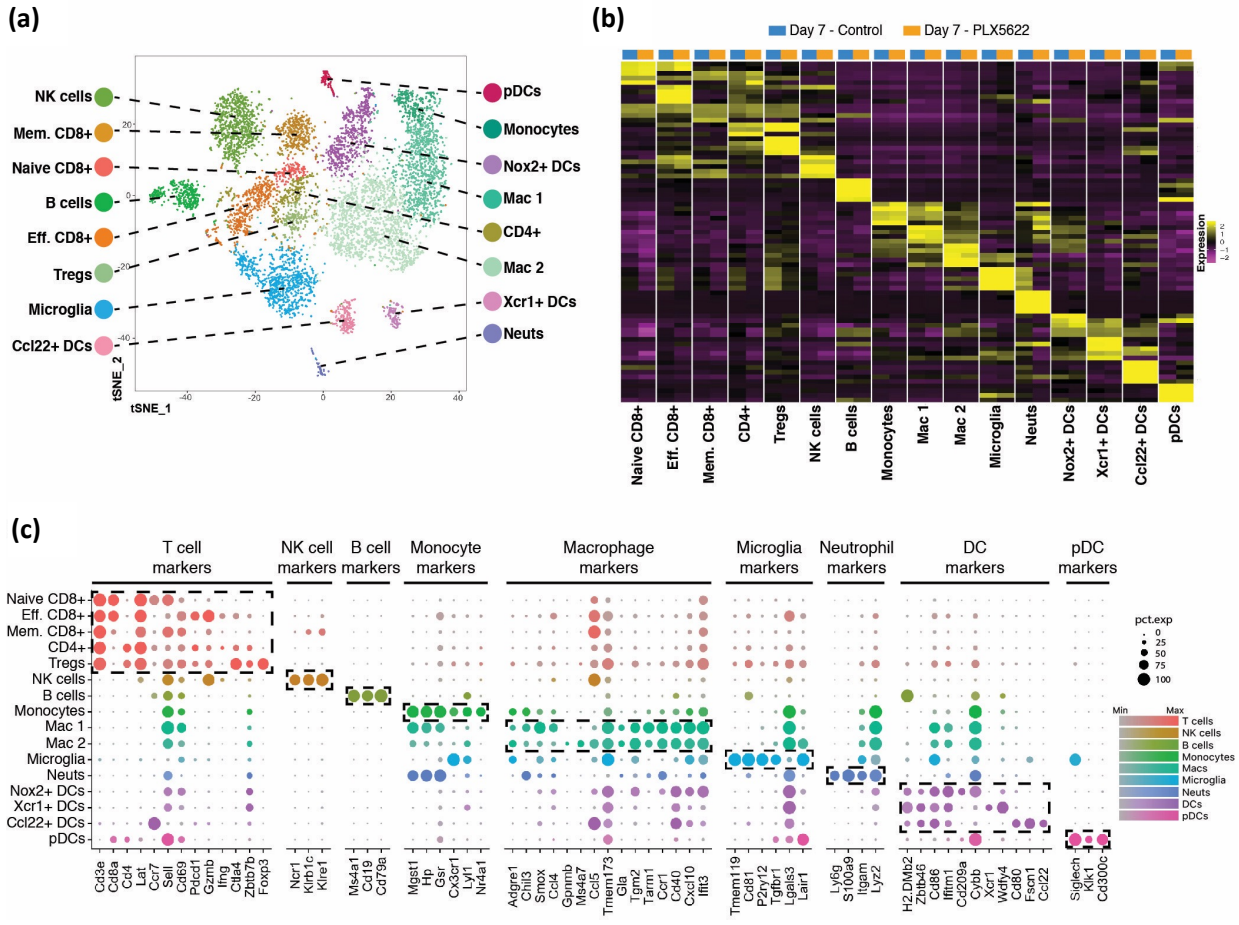

Figure 2: scRNAseq of CD45+ cells isolated from brains of JHMV-infected mice treated with PLX5622 at day 7 p.i. (a) T-distributed stochastic neighbor embedding (t-SNE) plot of scRNAseq data revealing 16 distinct cell clusters (aggregate data from PLX5622 and control treated animals at 7 days p.i). (**b**) Heat map showing the top 5 differentially expressed genes within each cluster. Columns represent the different clusters, with sub-columns displaying both control-treated (blue) and PLX5622-treated (orange) groups, and rows specify genes. **(c)** Dot plot presenting expression of selected genes within the 16 cell clusters. Size of the dot is representative of the frequency of cells within a cluster expressing the gene of interest, while the degree of color intensity is indicative of the level of expression of the gene. The dashed boxes highlight commonly and uniquely expressed genes of clusters within overarching cell types**.**

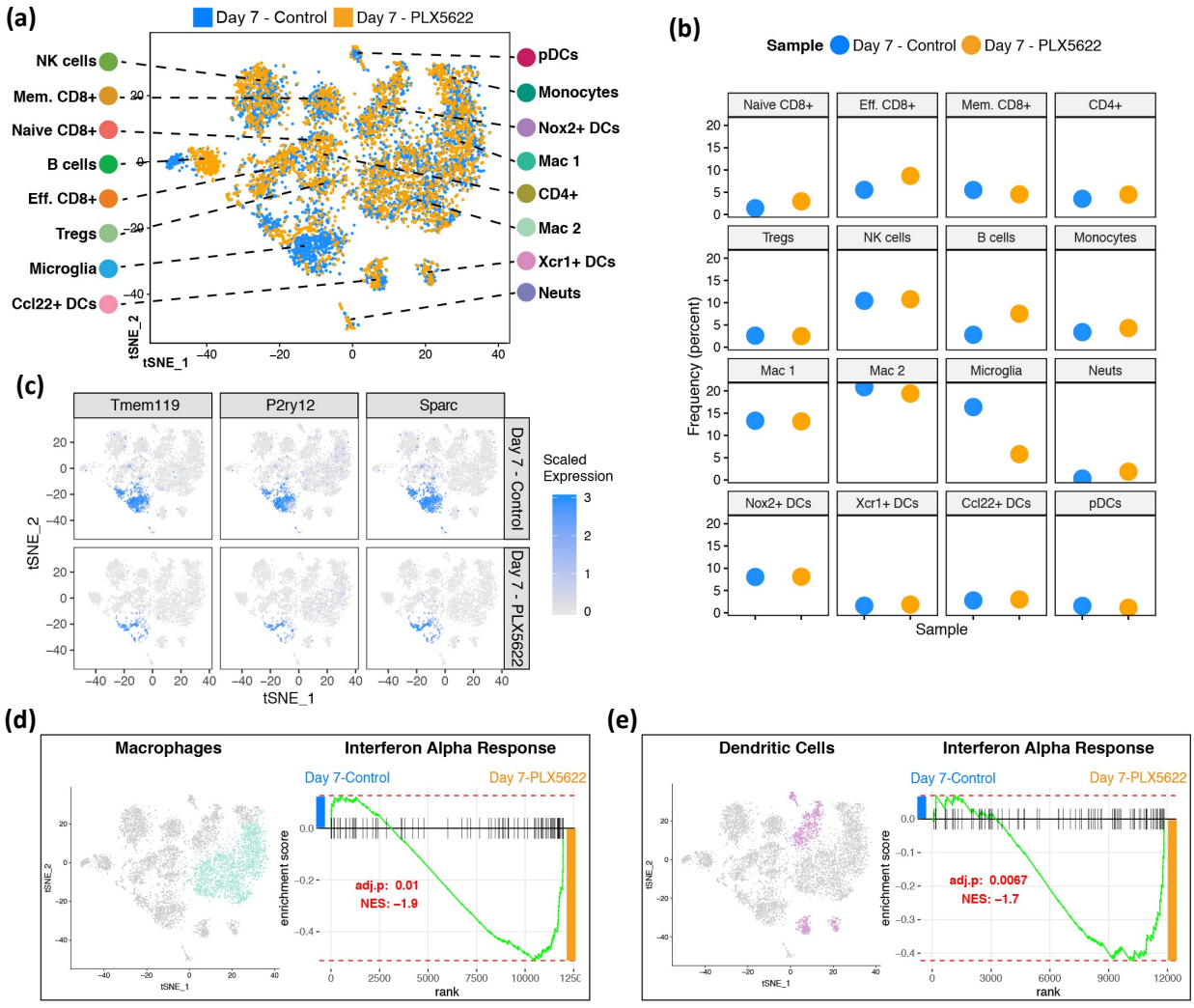

Figure 3: PLX5622 treatment and immune cell infiltration into the CNS at day 7 p.i. (a) t-SNE plot showing the immune landscape in brains of control- (blue) and PLX5622- (orange) treated animals at 7 days p.i. **(b)** Frequency of cell clusters in brains of control- and PLX5622-treated animals at 7 days post JHMV infection. **(c)** t-SNE plot showing decreased expression of microglia-associated transcripts *Tmem119*, *P2ry12*, and *Sparc* in PLX5622 mice compared to controls. Gene set enrichment analysis (GSEA) for IFN-α responses in combined (**d**) macrophage (teal) and (**e**) dendritic cell (purple) populations isolated at day 7 from brains of JHMV-infected mice treated with either PLX5622 or control chow, which are represented in t-SNE plots. Area under the curve represents enrichment of response genes. Responses to IFN-α were enriched in both macrophages and dendritic cells isolated from brains of PLX5622 mice compared to control animals at day 7 p.i. Normalized enrichment scores and *p* values are shown.

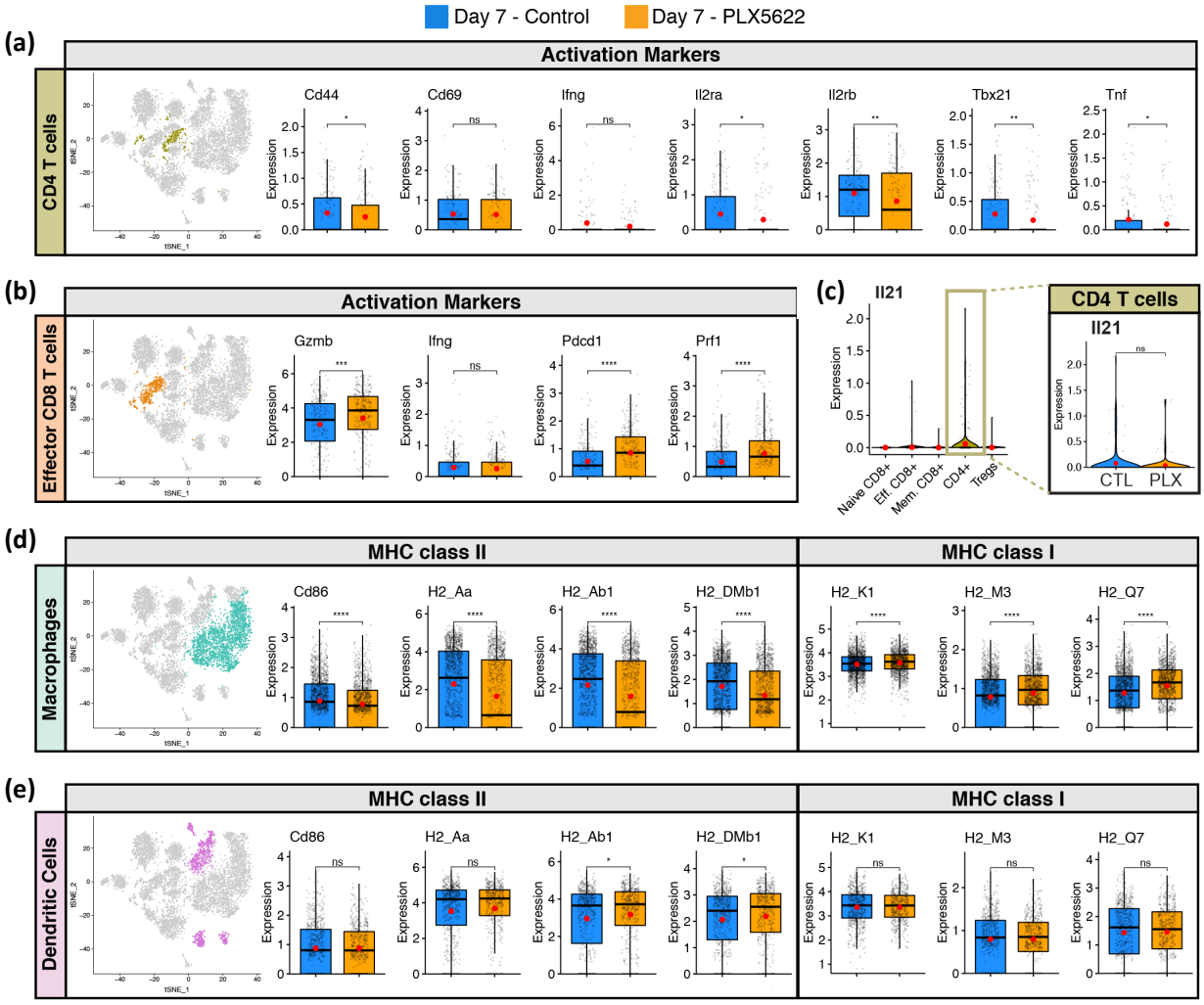

Figure 4: Altered T cell activation profiles in PLX5622-treated mice at day 7 p.i. t-SNE plot from brains of JHMV-infected mice treated with PLX5622 or control at day 7 p.i showing (**a**) CD4+ T cells (moss) from PLX5622-treated and control mice and box plots comparing expression of transcripts encoding for activation markers *Cd44* (CD44), *Cd69* (CD69), *Il2ra* (IL-2 receptor subunit alpha) *Il2rb* (IL-2 receptor subunit beta), *Tbx21* (Transcription factor T-bet) *Ifng* (interferon gamma), and *Tnf* (tumor necrosis factor alpha) between samples. (**b**) CD8+ T cells (orange) comparing the expression levels of transcripts encoding effector and activation markers in CD8+ T cells *Prf1* (Perforin), *Pdcd1* (Programmed cell death 1, PD1), *Gzmb* (Granzyme B) and *Ifng*. (**c**) Violin plots depicting expression of *Il21* transcripts within T cell populations isolated from the brains of experimental mice; there was no significant (ns) difference in expression of *Il21* in CD4+ T cells from control or PLX5622-treated mice. Expression of MHC class II-associated genes (*H2-Aa, H2-Ab1*, and *H-2DMb1*) and co-stimulatory molecule *Cd86*, as well as MHC class I-associated genes (*H2-K1, H2-M3,* and *H2-Q7*), are shown in combined (**d**) macrophage (teal) and (**e**) dendritic cell (purple) populations from experimental mice. In these plots, each dot represents a single cell. Normalized expression values were used and random noise was added to show the distribution of data points. The box

plots show interquartile range and the median value (bold horizontal bar). Average expression value per sample is indicated by the red dots. Wilcoxon's test was used for statistical analysis. ns, not significant; *p≤0.05; **p≤0.01; ***p≤0.001; ****p≤0.0001.

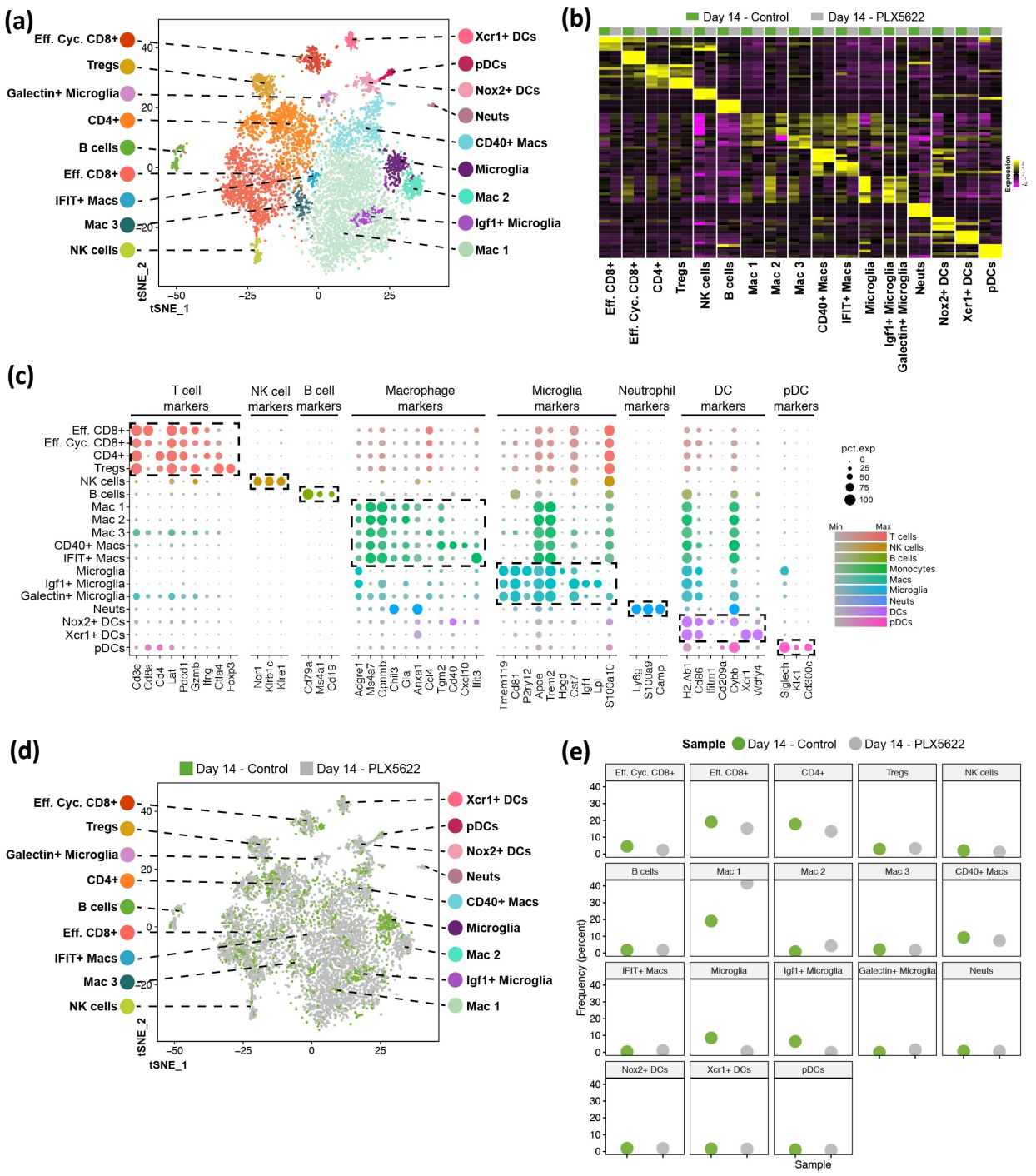

Figure 5: scRNAseq of CD45+ cells isolated from spinal cords of JHMV-infected mice treated with PLX5622 at day 14 p.i (a) t-SNE plots of scRNAseq data revealing 18 distinct cell clusters. Aggregate data are from spinal cords isolated from PLX5622- and control-treated animals at 14 days p.i. **(b)** Heat map showing the top 5 differentially expressed genes within each cluster. Columns represent the different clusters, with sub-columns displaying both control-treated (green) and PLX5622-treated (grey) groups, and rows specify genes. **(c)** Dot plot presenting expression of selected genes within the 18 cell clusters. Size of the dot is

representative of the frequency of cells within a cluster expressing the gene of interest, while the degree of color intensity is indicative of the level of expression of the gene. The dashed boxes highlight commonly and uniquely expressed genes of clusters within overarching cell types. **(d)** t-SNE plot showing the immune landscape in spinal cords of control- (green) and PLX5622- (grey) treated animals at day14 p.i. **(e)** Frequency of cell clusters in spinal cords of control- and PLX5622-treated animals at day 14 p.i.

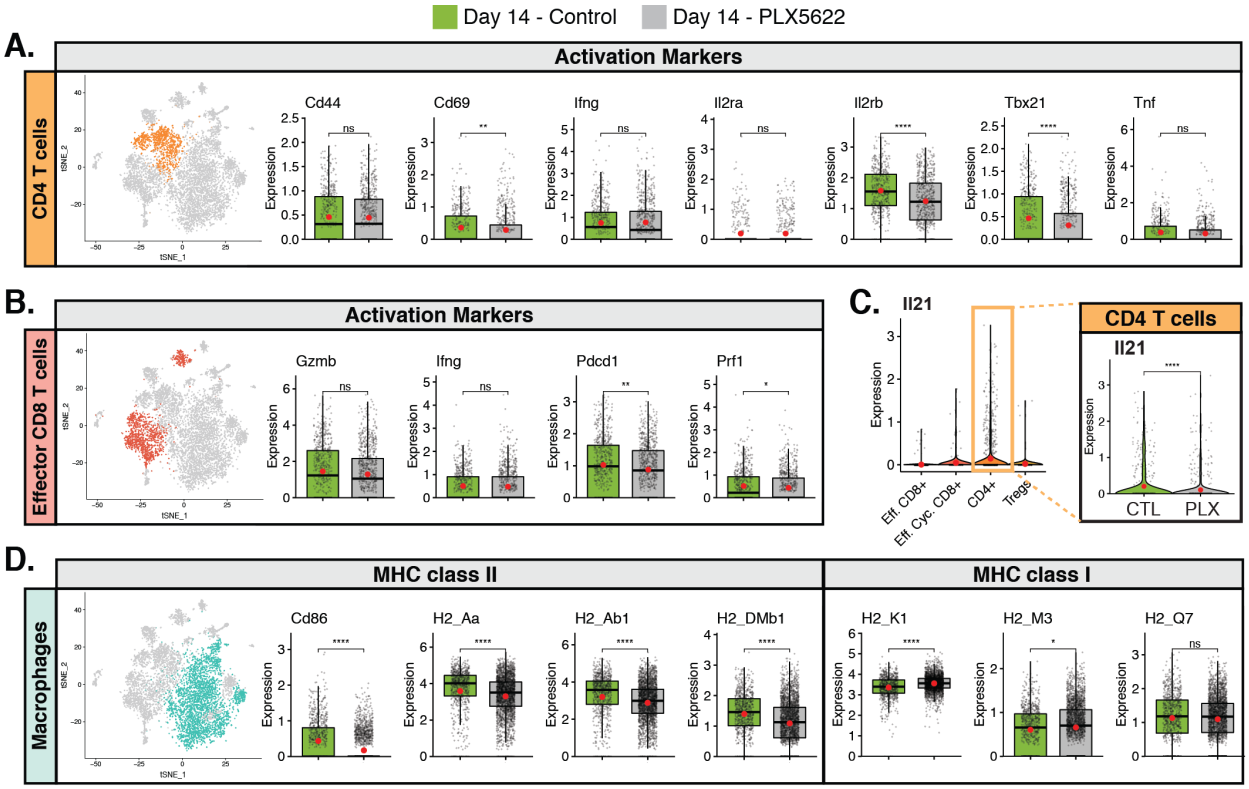

Figure 6: Muted activation profiles of spinal cord CD4+ T cells isolated from PLX5622-treated mice at day 14 p.i. JHMV-infected mice treated with either control chow or PLX5622 were sacrificed at day 14 p.i. and CD45+ cells sorted from spinal cords to evaluate mRNA expression profiles via scRNAseq. t-SNE plot showing (**a**) CD4+ T cells (orange) from spinal cords of mice treated with PLX5622-treated and control mice, comparing expression of transcripts encoding for activation markers *Cd44*, *Cd69*, *Il2ra*, *Il2rb*, *Tbx21*, *Ifng*, and *Tnf*. (**b**) Expression levels of transcripts encoding effector and activation markers in CD8+ T cells (salmon) *Prf1*, *Pdcd1*, *Gzmb* and *Ifng*. (**c**) Violin plots depicting expression of *Il21* transcripts within T cell populations isolated from the spinal cords of experimental mice; expression is reduced ($p<0.0001$) in CD4+ T cells from PLX5622-treated mice compared to controls. (**d**) Expression of MHC class II-associated genes (*H2-Aa, H2-Ab1*, and *H-2DMb1*) and co-stimulatory molecule *Cd86*, as well as MHC class I-associated genes (*H2-K1, H2-M3,* and *H2-Q7*), are shown in combined macrophage populations (teal) from experimental mice. In these plots, each dot represents a single cell. Normalized expression values were used and random noise was added to show the distribution of data points. The box plot shows interquartile range and the median value (bold horizontal bar). Average expression per sample is represented by the red dot. Wilcoxon test was used for statistical analysis. ns, not significant; *$p\leq 0.05$; ** $p\leq 0.01$; ****$p\leq 0.0001$.

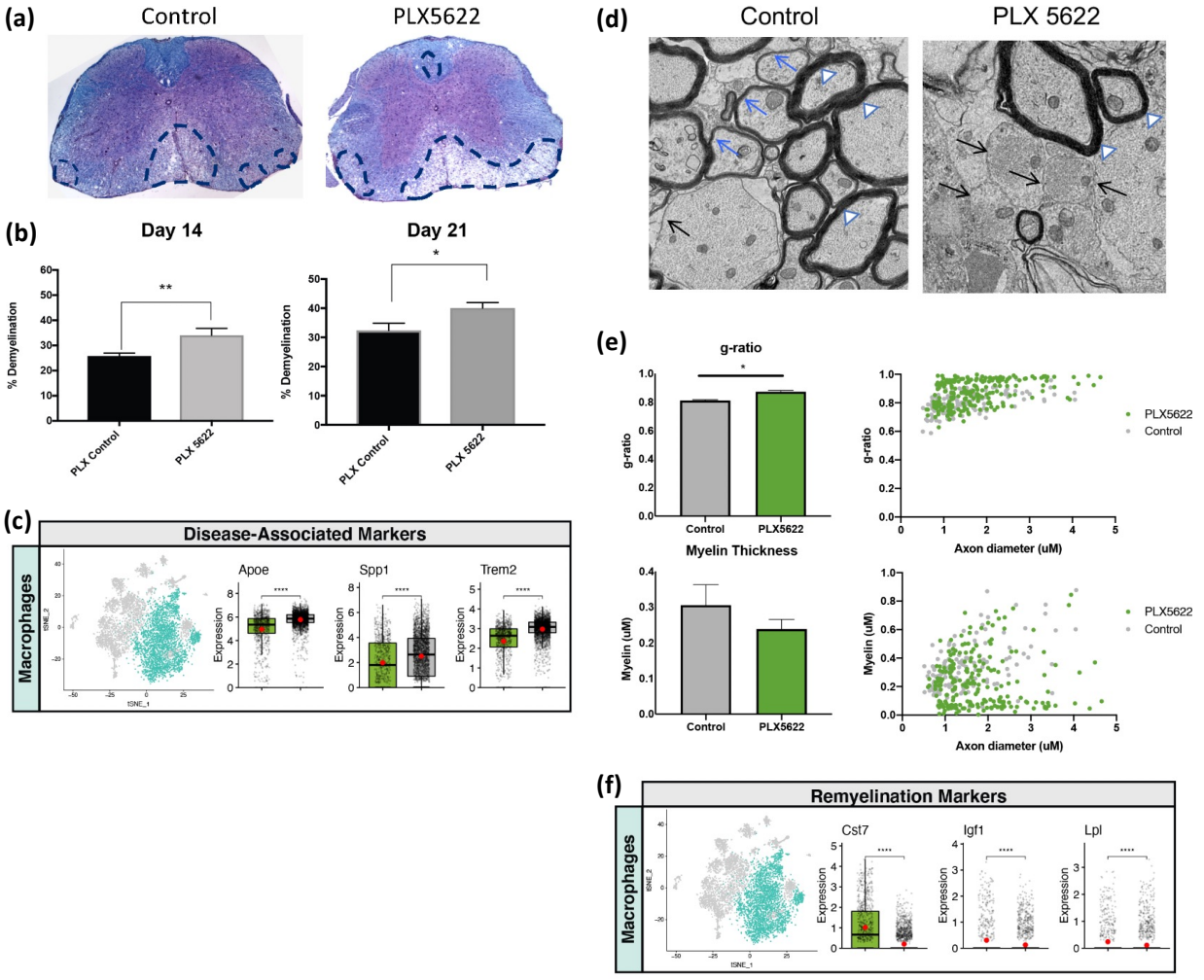

Figure 7: The severity of spinal cord demyelination is increased in PLX5622-treated mice compared to control mice. (**a**) Representative images of H&E/LFB-stained spinal cord sections showing an increase in severity of demyelination (dashed black lines) in JHMV-infected mice treated with PLX5622 compared to control treated mice at day 14 p.i. (**b**) Quantification of spinal cord demyelination reveals a significant increase after PLX5622 treatment compared to control-treated animals (minimum of 12 mice/experimental group) at days 14 and 21 p.i. (**c**) Box plots showing increased expression of transcripts encoding disease-associated factors APOE (*Apoe*), Osteopontin (*Spp1),* and TREM2 (*Trem2*) in spinal cords of PLX5622-treated mice compared to controls at day 14 p.i. in combined macrophage populations (teal), represented in the t-SNE plot. Normalized expression values were used, and random noise was added to show the distribution of data points. The box plots show interquartile range and the median value (bold horizontal bar). (**d**) Representative EM images (1200X) from spinal cords from control and PLX5622-treated mice showing normal myelinated axons (white arrowheads), demyelinated axons (black arrows) and remyelinated axons (blue arrows) at day 21 p.i. **(e)** Calculation of *g*-ratio of control and PLX5622; scatter plot depicting individual *g*-ratio's from lateral white matter columns of control (grey) and PLX5622 (green) treated mice as a function of axon diameter.

Data in panels *B* and *E* are presented as mean±SEM. Average expression value per sample is indicated by the red points. Wilcoxon's test was used for statistical comparisons. (**f**) Box plots showing decreased expression of transcripts encoding remyelination-associated markers Cystatin F (*Cst7*), Insulin growth factor 1 (*Igf1*), and Lipoprotein lipase (*Lpl*) in spinal cords of PLX5622-treated mice compared to controls at day 14 p.i. in combined macrophage populations (teal), represented in the t-SNE plot. *p≤0.05; **p≤0.01; ****p≤0.0001.

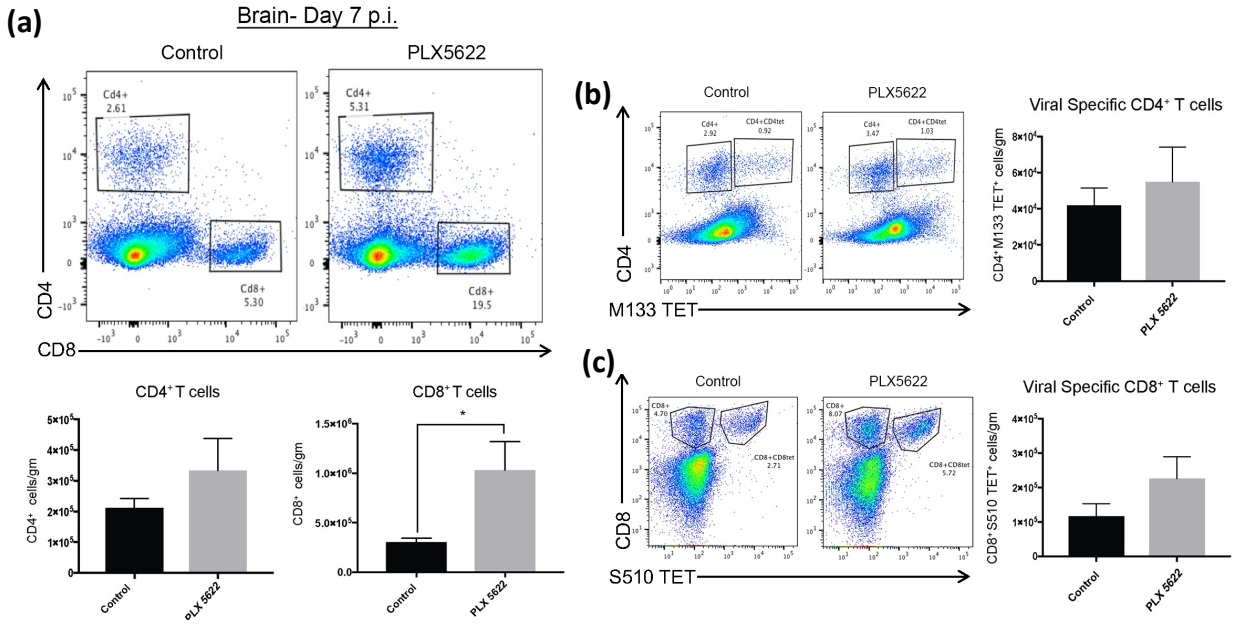

Supplemental Figure 1: PLX5622 treatment influences T cell infiltration and activation state within the CNS of JHMV-infected mice (a) Representative flow cytometric plots showing $CD4^+$ and $CD8^+$ T cells infiltrating into the brains of JHMV-infected mice treated with either PLX5622 or control at day 7 p.i. Quantification of flow data indicates increased infiltration of CD4+ T cells and CD8+ T cells ($p<0.05$) increase in brains of PLX5622-treated mice compared to controls, (n=6/group). Representative tetramer staining revealed increased infiltration of (**b**) virus-specific CD4+ T cells and (**c**) virus-specific CD8+ T cells within the brains of PLX5622-treated mice compared to controls at day 7 p.i., (n=6/group). Data are derived from 2 independent experiments and presented as mean±SEM. *p≤ 0.05.

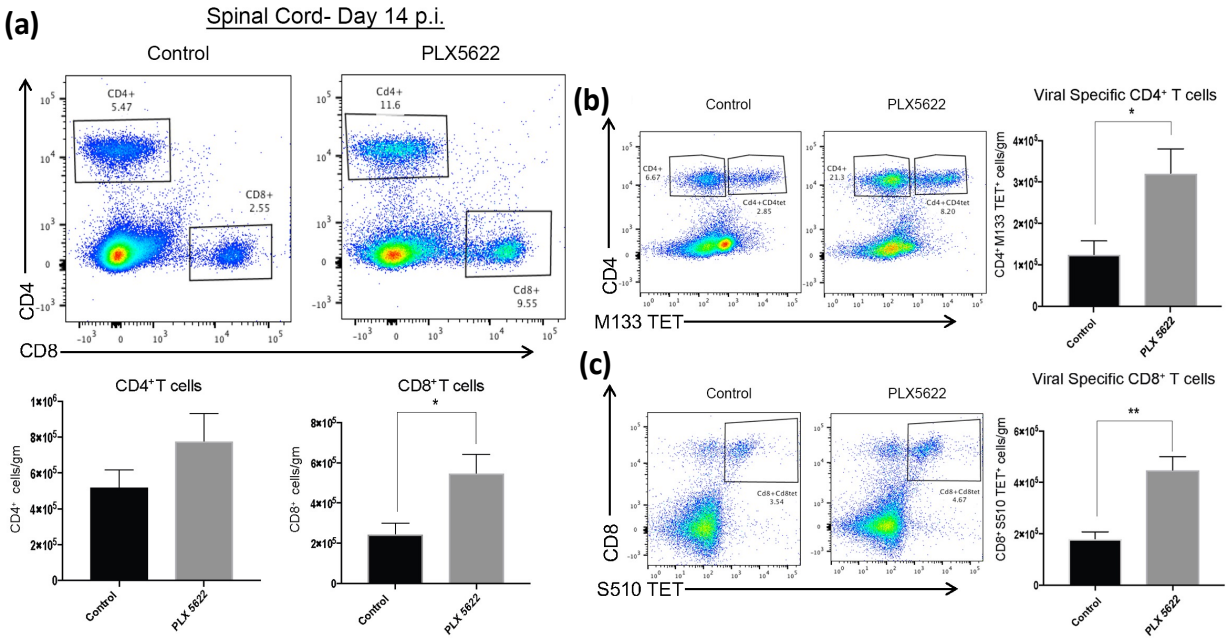

Supplemental Figure 2: PLX5622 modulates T cell infiltration into the spinal cord. (**a**) Flow analysis of spinal cords at day 14 p.i. from JHMV-infected mice indicate an increase in CD4+ T cells and CD8+ T cells ($p<0.05$) in PLX5622 compared to controls. PLX5622 treatment results in increased spinal cord infiltration of (**b**) virus-specific CD4+ T cells ($p<0.05$) and (**c**) virus-specific CD8+ T cells ($p<0.01$), (n=5/group). Data are derived from 2 independent experiments and presented as mean±SEM. *$p\leq 0.05$; ** $p\leq 0.01$.

Chapter 3

SINGLE-CELL RNA SEQUENCING REVEALS THE DIVERSITY OF THE IMMUNOLOGICAL LANDSCAPE FOLLOWING CNS INFECTION BY A MURINE CORONAVIRUS

Journal of Virology, 94(24): e01295-20

Single-cell RNA sequencing reveals the diversity of the immunological landscape following CNS infection by a murine coronavirus

Amber R. Syage,[1,3] H. Atakan Ekiz,[1,2] Dominic D. Skinner,[1,3] Colleen Stone,[1] Ryan M. O'Connell,[1,2] and Thomas E. Lane[1,3]

[1]Division of Microbiology & Immunology, Department of Pathology, University of Utah, School of Medicine, Salt Lake City, Utah, USA

[2]Huntsman Cancer Institute, University of Utah, Salt Lake City, Utah, USA.

[3]Department of Neurobiology & Behavior, School of Biological Sciences, University of California, Irvine, USA

Correspondence

Thomas E. Lane, Ph.D.

Department of Neurobiology & Behavior, School of Biological Sciences, University of California, Irvine, CA

Email: tlane@uci.edu

ABSTRACT

Intracranial (i.c.) infection of susceptible C57BL/6 mice with the neurotropic JHM strain of mouse hepatitis virus (JHMV) (a member of the *Coronaviridae* family) results in acute encephalomyelitis and viral persistence associated with an immune-mediated demyelinating disease. The present study was undertaken to better understand the molecular pathways evoked during innate and adaptive immune responses as well as the chronic demyelinating stage of disease in response to JHMV infection of the central nervous system (CNS). Using single cell RNA sequencing analysis (scRNAseq) on flow-sorted CD45-positive cells ($CD45^{+}$) enriched from brains and spinal cords of experimental mice, we demonstrate the heterogeneity of the immune response as determined by unique molecular signatures and pathways involved in effective anti-viral host defense. Furthermore, we identify potential genes involved in contributing to demyelination as well as remyelination being expressed by both microglia and macrophages. Collectively, these findings emphasize the diversity of the immune response and molecular networks at defined stages following viral infection of the CNS.

Keywords: Host defense, immunology, central nervous system, coronavirus

IMPORTANCE

Understanding the immunological mechanisms contributing to both host defense and disease following viral infection of the CNS is of critical importance given the increasing number of viruses that are capable of infecting and replicating within the nervous system. With this in mind, the present study was undertaken to evaluate the molecular signatures of immune cells within the CNS at defined times following infection with a neuroadapted murine coronavirus using scRNAseq. This approach has revealed that the immunological landscape is diverse with numerous immune cell subsets expressing distinct mRNA expression profiles that is, in part, dictated by the stage of infection. In addition, these findings reveal new insight into cellular pathways contributing to control of viral replication as well as to neurologic disease.

INTRODUCTION

Intracranial infection of susceptible mice with the neurotropic JHM strain of mouse hepatitis virus (JHMV) provides an excellent model in which to interrogate molecular and cellular mechanisms of host defense and disease in response to viral infection of the central nervous system (CNS) (1, 2). JHMV is a member of the betacoronavirus subfamily and is related to SARS-CoV, MERS-CoV and to the recently described SARS-CoV2, which rapidly spread to pandemic status in early 2020 (3). JHMV infection results in an acute encephalomyelitis characterized by viral replication in astrocytes, microglia, and oligodendrocytes with relative sparing of neurons (4). Following JHMV infection of the CNS, there is an orchestrated expression of cytokines and chemokines that results in targeted recruitment of cells of both the innate and adaptive immune response (5-20). Virus-specific $CD4^+$ and $CD8^+$ T cells infiltrate into the CNS and control the JHMV replication through IFN-γ secretion and perforin-mediated cytolytic activity (21, 22). Although a robust cell-mediated immune response occurs during acute disease, sterilizing immunity is not achieved, resulting in viral persistence in white matter tracts (23). Ultimately, virus-specific antibody is critical for additional control of viral replication and suppressing viral recrudescence (24). Histological features associated with viral persistence include the development of an immune-mediated demyelinating disease that is similar to the human demyelinating disease, multiple sclerosis (MS), with infiltrating T cells and macrophages amplifying white matter damage (25-27).

Although the previous studies on bulk cell populations have revealed important information on the mechanisms of disease and host defense in JHMV-infected mice, the characterization of molecular alterations at the single cell level is lacking. In this study, we have employed single cell RNA sequencing (scRNAseq) on enriched CD45-positive ($CD45^+$) cells

isolated from brains and spinal cords at defined times following JHMV infection to delineate mechanisms associated with effective host responses as well as those that contribute to both demyelination and remyelination within the CNS.

RESULTS

Intracranial infection of mice with JHMV.

Adult (5-6 week old) C57BL/6 mice were intracranially (i.c.) infected with 1,500 plaque forming units (PFU) of JHMV. Early following CNS infection, JHMV initiates replication within the brain and triggers a strong host immune response before ultimately spreading into the spinal cord, causing immune-mediated demyelination. Therefore, we chose to examine brains at days 3 and 7 post-infection (p.i.) to investigate the immune landscape during innate and adaptive responses, respectively and spinal cords at day 21 p.i. to evaluate immune cell responses during chronic demyelination. CD45-positive ($CD45^+$) cells were flow sorted from brains of JHMV-infected mice at days 3 and 7 p.i. and spinal cords at day 21 p.i. (**Figure 1A**). For controls, we flow sorted $CD45^+$ cells from brains of uninfected C57BL/6 mice. Assessment of disease phenotype out to day 21 p.i. showed that all experimental mice developed disease consistent with JHMV-induced neurologic disease (**Figure 1B**). Furthermore, plaque assays conducted using the brains of infected mice showed viral titers peaking at day 3 p.i. and subsequently declining at days 7 and 21 p.i. (**Figure 1C**). Viral titers within the spinal cords at day 21 p.i. are below the level of detection (~100 PFU/g tissue, **data not shown**) which is consistent with previous studies (23, 28). By day 21 p.i., there was extensive spinal cord demyelination compared to spinal cords from non-infected control animals (**Figure 1D**). As shown in **Figure 1E**, single cell RNA sequencing (scRNAseq) analysis was conducted on a total of 1,456 $CD45^+$ cells from the brains of uninfected mice (n=6, pooled), 3,863 $CD45^+$ cells at day 3 p.i. (n=5, pooled) and 2,573 $CD45^+$ cells at day 7 p.i. (n=5, pooled) from the brains of JHMV-infected mice, and 1,423 $CD45^+$ cells from spinal cords at day 21 p.i. (n=6, pooled) with JHMV.

scRNAseq and immune cell diversity within the CNS of JHMV-infected mice.

Downstream analysis of processed data was performed on a combined total of 9,315 cells from brains and spinal cords of experimental (both uninfected and infected) mice via principal correlation analysis (PCA) and uniform manifold approximation and projection (UMAP) dimensional reduction (29, 30). Unsupervised clustering revealed 7 different major populations with 22 different minor clusters (**Figure 2A**). We identified two different monocyte clusters, (Mono1, Mono2), three unique $CD8^+$ T cell clusters (Effector CD8, Memory CD8, and Effector Cycling CD8), four dendritic cell populations [$Cd209a^+$ (*Cd209a*), $Ccr7^+$ (*Ccr7*), $Xcr1^+$ (*Xcr1*), plasmacytoid (pDCs)], four microglia clusters (MG1, MG2, MG3, and Cycling MG), four macrophage populations (Mac1, Mac2, Mac3, Mac4), two B cell clusters which included plasma cells, and single CD4 T cell, NK cell, and neutrophil populations (**Figure 2A**). In order to verify the algorithm-assisted identification of cell clusters, we examined expression of known cellular markers in our dataset; expression of these markers corresponded with the respective identities of the distinct cell clusters (**Figure 2B**) (31, 32). When data from different timepoints were plotted side-by-side, the dynamic changes in the proportions of these cell populations following JHMV infection started to emerge (**Figure 2C**). For example, we detected a drop in the frequency of neutrophils at day 3 p.i. compared to uninfected mice and these levels remained reduced through the course of infection. NK cells peaked at day 7 p.i. and cells from this time p.i. predominate this cluster. With regards to cells involved in antigen presentation, we observed increases in the frequencies of all DC subsets by day 3 p.i. with levels peaking within the brain at day 7 p.i. A similar trend was found in macrophage subpopulations Mac3 and Mac4. In contrast, macrophage subsets Mac1, Mac2 and monocytes peaked at day 3 p.i. and subsequently declined at days 7 and 21 p.i. Microglia subsets MG1 and MG2 were detectable in uninfected brains (control) and at

day 3 p.i., but then were reduced at days 7 and 21 p.i. We also saw an overall trend in increased frequencies in T cell subsets with the majority of these subsets peaking within the spinal cords of infected mice at day 21 p.i. Infiltrating B cells within the CNS remained relatively constant yet plasma cells peaked at day 21 p.i.

Genetic signatures of immune cells subsets within the CNS of JHMV-infected mice.

We were able to identify distinct subtypes of immune cells based upon unique genetic signatures associated with both defense and disease within the CNS of JHMV-infected mice. We identified four DC effector subtypes including $Cd209^{+}$ DCs, $Xcr1^{+}$ DCs, $Ccr7^{+}$ DCs and plasmacytoid DCs (pDCs) that express a network of genes associated with effective anti-viral responses (**Figure 3A**). We identified one population of $CD4^{+}$ T cells expressing transcripts encoding activation markers including *Tnfrsf4* and *Icos* (**Figure 3B**). We identified three different $CD8^{+}$ T cell [memory (Mem.) CD8, effector (Eff.) CD8 and effector cycling (Eff. Cyc.) CD8], each with unique expression profiles (**Figure 3B**). Similarly, we identified two monocyte clusters, four macrophage clusters (**Figure 3C**) and four microglia subsets (**Figure 3D**) with unique genetic profiles. With regards to the single cluster of CD4+ T cells compared to the three clusters of CD8+ T cells, we were surprised we didn't see regulatory CD4+ T cells as previous studies have demonstrated the presence of these cells within the brains of JHMV-infected mice at day 7 p.i. (33). Subsequent analysis revealed that ~8% of cells within the CD4+ T cell cluster expressed FoxP3 transcripts (**Figure 3E-F**).

Monocyte subtypes expressed *F13a1*, *Hp*, *Gsr*, and *Cd300a,* and while Mono2 appears to overlap with Mac1, Mono1 seems to be representative of a steady-state immune surveilling population of monocytes, having elevated expression of *S100a8* (**Figure 3C**) (34). The four

different macrophage populations expressed common macrophage marker, *Ms4a6d,* and display a transitional gradient from early to later defense against viral infection with Mac1 having the highest expression of *Cybb* and lowest *Tgfb1* and *Slamf7* and Mac4 showing the highest expression of *Slamf7* and *Tgfbi* and the lowest *Cybb* (**Figure 2B**). Mac1 and Mac2 both show elevated expression of *Smox and Isg20* (**Figure 2B**) and when compared with only monocyte and macrophage subpopulations, Mac1 uniquely expresses *Cmpk2, Rsad2, Cxcl10, Crem, and Ccl4*, while Mac2 is characterized by increased IFN-related transcripts including *Irf7*, *Isg20*, and *Ifitm1* (**Figure 3C**). Interestingly, Mac3 and Mac4 present a more phagocytic effecter phenotype, both expressing *Apoe* and *Ms4a7* (**Figure 3C**). When compared with the other monocyte and macrophage subpopulations, Mac3 additionally expresses transcripts encoding MHC class II molecules and F4/80 (*Adgre1*), while Mac4 uniquely expresses *Gpnmb*, *Fabp5*, *Spp1*, *Arg1*, and *Ccl8* (**Figure 3C**). As for the microglia subpopulations, MG1 and MG2 appear to be more "homeostatic", having higher expression of *Tmem119*, *P2ry12, and Slc2a5* (**Figure 4C**) (35). In contrast, MG3 and cycling (Cyc.) MG appear to be more disease-associated, with higher levels of *Ccl2* and *Ccl7* (**Figure 2B**) (13, 36). There was only one minor NK cell cluster, represented by expression of transcripts *Ncr1*, *Klrb1c*, *Klre1*, *Xcl1, and Bcl2* (**Figure 2B**). B cells were subdivided into one minor cluster along with a cluster of plasma cells. B cells were characterized by expression of *Cd79a, Iglc3*, *Ms4a1*, *Cd19*, whereas plasma cells displayed high expression of *Cd79a* as well as *Jchain* and immunoglobulin transcripts, indicative of antibody secretion (37, 38) (**Figure 2B**).

Select immune cells are present in the uninfected brain.

We next assessed the immunological landscape of the uninfected brain through the use of scRNAseq on flow-sorted $CD45^+$ cells. This approach revealed that microglia subtypes MG2 and MG1, which respectively make up 27.61% and 16.14% of the total $CD45^+$ cells sequenced from the control sample, are a predominant immune cell subtype within the brains of uninfected mice (**Figure 4B**). MG1 and MG2 trend towards a more homeostatic microglia subtype with higher expression levels of *Tmem119*, *P2ry12* and *Slc2a5* (**Figure 4C**) (35). The Mono1 subpopulation of monocytes is also enriched within uninfected brains, contributing 16.41% of the total sample population (**Figure 4B**). Neutrophils (9.55%), B cells (5.98%), and effector cycling $CD8^+$ T cells (5.56%) were also among the other prevalent immune cell types present in the uninfected brains of mice (**Figure 4B**). With regards to neutrophil population within the brains of uninfected mice, when evaluating expression of transcripts encoding common activated neutrophil genes C-X-C Motif Chemokine Receptor 2 and 4 (CXCR2/4; *Cxcr2*, *Cxcr4*), Matrix Metalloproteinase (MMP) 8 and 9 (*Mmp8*, *Mmp9*), and L-Selectin (CD62L; *Sell*), there is little-to-no expression of these activation transcripts in uninfected control mice yet expression levels are increased at day 3 p.i. as well as subsequent time points p.i. (14, 39-41) (**Figure 4D**). These findings support the notion of low-level immune surveillance of the uninfected CNS (42-45) and emphasize the rapid mobilization of innate and adaptive immune responses following infection.

Heterogeneous antiviral mechanisms are elicited in innate cell subsets within the CNS following JHMV infection.

Examining the immune responses at day 3 p.i. revealed increased subpopulations of monocytes (Mono2), macrophages (Mac1, Mac2, and Mac3), microglia (MG1, MG2, MG3 and

Cyc. MG) and DCs ($Cd209a^+$ DCs) (**Figure 5A-B**). The most prominent of these populations included Mac2 (19.83%), MG3 (14.65%), and MG1 (13.28%) (**Figure 5B**). Gene set enrichment analysis (GSEA) revealed increased interferon alpha (IFN-α) responses in microglia, macrophages and dendritic cells (**Figure 5C**). Specifically, we found increased expression of transcripts encoding anti-viral response factors including *Myd88*, *Rsad2* (Viperin), and *Tmem173* (STING) that were enriched in distinct subpopulations of monocyte/macrophages (**Figure 5D**), microglia (**Figure 5E**) and DCs (**Figure 5F**). For all three cell populations, there was an increase in expression of *Myd88* and *Rsad2* in the brains at days 3 and 7 p.i. compared to controls, yet these genes were expressed at a lower level in spinal cords by day 21 p.i. (**Figures 5D-F**). Expression of *Tmem173* was elevated in both monocyte/macrophages and DCs within brains at days 3 and 7 p.i. and an opposite trend was observed within spinal cords at day 21 p.i. (**Figures 5D-F**). In contrast, *Tmem173* is constitutively expressed in microglia and expression is only slightly modified at days 3, 7, and 21 p.i. (**Figure 5E**). Unlike microglia, both monocyte/macrophages and DCs express additional anti-viral response factors *Irf1* (Interferon regulatory factor 1) and *RipK1* that are increased in brains at days 3 and 7 p.i. but are comparatively lower within spinal cords at day 21 p.i. (46, 47) (**Figure 5D-F**). Finally, monocyte/macrophages also expressed *Irg1* (Immune-responsive gene 1) that was increased in brains at days 3 and 7 p.i. and lower in spinal cords at day 21 p.i. (**Figure 5D**).

IFN-γ pathways are enriched and associated with T cell-mediated control of JHMV replication by day 7 p.i.

By day 7 p.i., JHMV titers start declining within the brain and this coincides with entry of virus-specific T cells into the CNS that control viral replication. Consistent with this, infiltration

of effector $CD8^+$ T cells and effector cycling $CD8^+$ T cells was increased in greater proportion compared to $CD4^+$ T cells and memory $CD8^+$ T cells (**Figures 6A-B**). We also detected an increase in Mac1, Mac2, Mac3, and Mac4 subpopulations as well as a selective increase in $Cd209a^+$ DCs (**Figures 6A-B**). GSEA revealed an increase in IFN-γ response genes in microglia, macrophages, and dendritic cells (**Figure 6C**). Infiltrating $CD4^+$ and $CD8^+$ T cells expressed IFN-γ at all time points, with day 21 p.i. showing the highest level of expression (**Figure 6D**). Overall, effector $CD8^+$ T cells exhibited the overall highest levels of IFN-γ compared to other T cell subset populations (**Figure 6D**). We and others have demonstrated an important role for CXCL9 and CXCL10 in contributing to host defense in response to JHMV infection of the CNS by attracting virus-specific T cells and plasma cells into the CNS (15-17, 24, 48, 49). CXCR3 is the key signaling receptor for CXCL9 and CXCL10 that promotes migration of lymphocytes to the CNS in response to JHMV infection (50). *Cxcr3* transcripts were detected in both $CD4^+$ and $CD8^+$ T cell populations and gradually increased from day 3 p.i. through day 21 p.i., reflecting the accumulation of T cells within the CNS of infected mice (**Figure 6D**). Our earlier studies indicated that activated astrocytes were the primary cellular source for both CXCL9 and CXCL10 in response to JHMV infection (5, 15). Through scRNAseq, we were able to expand on these findings and show that subsets of microglia (**Figure 6E**) as well as monocytes/macrophage (**Figure 6F**) and DCs (**Figure 6G**) were capable of expression both *Cxcl9* and *Cxcl10* transcripts although expression was largely confined to days 3 and 7 p.i. within the brain and not at day 21 p.i within spinal cords.

Differential expression of MHC transcripts within the CNS in response to JHMV infection.

We next explored the transcript levels of MHC class I and II molecules in antigen-presenting cells (APCs) to evaluate population and temporal dynamics of antigen presentation to $CD8^+$ and $CD4^+$ T cells following viral infection with JHMV. We found that subsets of microglia, monocytes/macrophages and dendritic cells express MHC class I-associated transcripts *H2-K1* and *H2-Q7* (**Figures 7A-C, Cluster Dynamics**). Transcripts *H2-K1* are constitutively expressed in microglia, monocytes/macrophages, and dendritic cells in uninfected mice and subsequently increase following JHMV infection, showing the highest expression at day 7 p.i. (**Figures 7A-C, Temporal Dynamics**). In contrast, transcripts for *H2-Q7* are expressed at almost undetectable levels in uninfected mice yet increase after JHMV infection, also peaking at day 7 p.i. (**Figures 7A-C, Temporal Dynamics**). We observed an increase in transcripts encoding MHC class II-associated proteins including *H2-Aa* and *H2-Eb1* in sub-populations of microglia (**Figure 7D, Cluster Dynamics**), monocytes/macrophages (**Figure 7E, Cluster Dynamics**), and DCs (**Figure 7F, Cluster Dynamics**). Temporal analysis of these transcripts in microglia show very low expression in uninfected mice that gradually increases by day 3 p.i. and is dramatically elevated by days 7 and 21 p.i. (**Figure 7D, Temporal Dynamics**). In monocytes and macrophages, expression of MHC class II-associated transcripts is low in uninfected mice and remains so until increasing considerably at days 7 and 21 p.i. (**Figure 7E, Temporal Dynamics**). In DCs, there is constitutive expression of MHC class II-associated transcripts in uninfected mice that subsequently increases by days 3 and 7 p.i and is highest at day 21 p.i. (**Figure 7F, Temporal Dynamics**). To further investigate the functional dynamics of APC populations following JHMV infection, we investigated the expression of transcripts encoding common T cell checkpoint inhibitory ligands, programmed death-ligand 1 (PD-L1,

Cd274) and Galectin-9 (*Lgals9*) to disclose any dampening of T cell function. Expression of PD-L1 transcripts is elevated in specific monocyte/macrophage and DC subsets, but appears negligible in microglia populations (**Figure 8A-C, Cluster Dynamics**). PD-L1 expression in these populations is also highest at days 3 and 7 p.i. (**Figure 8A-C, Temporal Dynamics**). Galectin-9 (Lgals9) expression appears to range across a larger array of APC cell subsets (**Figure 8A-C, Cluster Dynamics**). Temporal analysis in microglia and monocytes/macrophages shows expression in uninfected mice that increases following JHMV infection, appearing highest at days 3 and 7 p.i. (**Figure 8A-B, Temporal Dynamics**). In DCs, Galectin-9 expression is also low in uninfected mice and increases at days 3 and 7 p.i., though expression drops by day 21 p.i. (**Figure 8C, Temporal Dynamics**). When looking at expression of transcripts encoding PD-L1 and Galectin-9 receptors PD-1 (*Pdcd1*) and TIM-3 (*Havcr2*) in T cells, we find that *Pdcd1* is primarily expressed in $CD4^+$ and effector $CD8^+$ T cell subsets (**Figure 8D**). *Havcr2* (TIM-3) appears to be expressed in effector $CD8^+$ T cells, but at much lower levels than *Pdcd1* (**Figure 8D**). In $CD4^+$ T cells, *Pdcd1* expression is elevated at all defined times post-infection (**Figure 8E**). In $CD8^+$ T cells, expression of both *Havcr2* and *Pdcd1* is highest at days 7 and 21 p.i. (**Figure 8F**).

JHMV persistence is characterized with expression of molecules associated with disease and repair.

By day 21 p.i., JHMV persists within the spinal cords of surviving mice and this is associated with ongoing neuroinflammation and demyelination in which inflammatory T cells and monocyte/macrophages contribute to white matter damage (11, 13, 17, 25, 51-53). scRNAseq performed on $CD45^+$ cells isolated from spinal cords of infected mice at day 21 p.i.

indicated that the prominent inflammatory cells consisted of T cell subsets including $CD4^+$ T cells, memory $CD8^+$ T cells and effector $CD8^+$ T cells (**Figures 9A-B**). In addition, the macrophage subset Mac3 and microglia subset MG3 were increased (**Figures 9A-B**). Plasma cells were also identified, which is consistent with earlier studies demonstrating the importance of these cells in suppressing viral recrudescence (**Figures 9A-B**) (24). We detected expression of transcripts encoding genes associated with demyelination including Apolipoprotein E (*Apoe*), Transmembrane glycoprotein NMB (*Gpnmb*), Osteopontin (*Spp1*), and Triggering receptor expressed on myeloid cells 2 (*Trem2*) in various subsets of monocyte/macrophages and microglia (**Figure 9C**) (54-56). While all microglia subsets expressed *Apoe* and *Trem2* transcripts, only MG3 expressed robust levels of *Spp1*; we did not detect *Gpnmb* transcripts in any microglia subpopulation (**Figure 9C)**. Monocyte/macrophage subpopulations all expressed *Apoe*, while *Gpnmb* was only enriched in the Mac4 subsets, *Spp1* in Mac2 and Mac4 and *Trem2* in Mono1 along with Mac3 and Mac4 subsets (**Figure 9C**). All DC subsets expressed *Apoe* while only the $Xcr1^+$ DC (also expressing the chemokine receptor for XCL1 and XCL2) expressed appreciable levels of *Trem2* transcripts (Data not shown). When combining expression of specific transcripts from individual subsets, i.e. microglia and monocyte/macrophage, we observed an increase in transcript levels throughout the infection with the highest levels being detected within spinal cords at day 21 p.i. (**Figure 9C**). A notable exception to this was that expression of *Trem2* transcripts in microglia subsets which gradually declined following JHMV infection when compared to transcript levels in control mice (**Figure 9C**). Microglia subpopulations MG3 and Cyc. MG expressed transcripts encoding markers associated with remyelination, including Cystatin F (*Cst7*) (57, 58), Insulin-like growth factor 1 (*Igf1*) (59, 60), and Lipoprotein lipase (*Lpl*) (**Figure 9D**) (61). Expression of *Cst7*, *Igf1*, and *Lpl* was the highest

in the MG3 population of microglia, followed by Cyc. MG (**Figure 9D**). The highest levels of expression for *Cst7*, *Igf1* and *Lpl* occurred within the spinal cord at day 21 p.i. and these findings support the notion that microglia may either directly or indirectly influence remyelination within the spinal cord by contributing to controlling expression of genes encoding proteins that regulate oligodendrocyte precursor cell (OPC) maturation (**Figure 9D**) (62, 63). In further support, GSEA analysis demonstrated the enrichment of genes associated with oligodendrocyte differentiation by MG3 and Cyc. MG subpopulations compared to MG1 and MG2 subpopulations (**Figure 9E**).

DISCUSSION

Following i.c. inoculation of susceptible mice with JHMV, there is a rapid innate immune response that helps control viral replication until virus-specific T cells are able to expand and infiltrate into the CNS. Virus-specific T cells control viral replication through IFN-γ secretion and cytolytic activity; however, virus is able to persist within the CNS primarily in white matter tracts resulting in chronic neuroinflammation and demyelination, mediated primarily by T cells and macrophages. Significant strides have been made in understanding the mechanisms associated with both host defense and disease following JHMV infection of the CNS using bulk immune cells isolated from infected tissues. Given the complexity of the immune response to CNS viral infection, we employed scRNAseq as a powerful and high-resolution method to assess the molecular and cellular responses that aid in host defense, disease progression, and CNS repair. To accomplish this, we wanted to capture key events associated with the evolution of the immune response within the CNS during the innate, adaptive and chronic stages of disease following JHMV infection. For innate and adaptive responses, we examined brains at days 3 and 7 p.i., respectively as virus is beginning to replicate and expand within the brain at these times with relative sparing of the spinal cord. By day 21 p.i., virus has spread into the spinal cord and animals have established immune-mediated demyelination and we chose this time to represent chronic disease. We used only uninfected brains to provide a baseline for subsequent comparison of immune responses within JHMV-infected brains and spinal cords via scRNAseq. While the brain and spinal cord are both within the CNS, we recognize these are not identical tissues and using our approach did not capture events occurring within the spinal cord either prior to infection or at days 3 and 7 p.i. Nonetheless, we believe our findings provide reveal the heterogeneity and complexity of immune response within the CNS following JHMV infection as

the virus replicates and spreads within brains and spinal cords and uncovered new pathways that may be contributing to demyelination as well as remyelination.

In the uninfected control brain, the microglia subpopulation MG2 (27.61%) was the dominant $CD45^+$ cell type present, followed closely by MG1 (16.41%) and the monocyte cluster Mono1 (16.41%) (**Figure 4B**). All three of these clusters presented as a homeostatic counterpart to their overall defining cell types (34, 35). Microglia are considered the immune cell of the CNS and are expected to be the primary $CD45^+$ cells in the uninfected brain. The additional cell types present in the control brain included neutrophils (9.55%), B cells (5.95%), and Eff. Cyc. CD8 T cells (5.56%) (**Figure 4B**). Our opinion is that these cells are present as a result of routine immune surveillance (42-45). We were surprised by the drop in neutrophils present within the brains from uninfected mice compared to infected mice as we've previously reported increased levels of neutrophils within the brains at day 3 p.i. with JHMV and then this subsequently declines as determined by flow cytometry (14). However, immature myeloid cells generally have overlapping gene expression signatures with neutrophils and do not always neatly separate from one another, especially considering the lack of differentiation occurring in the uninfected CNS and we believe this may contribute to the surprisingly larger frequency of neutrophils found in the control group. By day 3 p.i., the most prominent cell types present within the brains included monocyte/macrophage and microglia subtypes with the Mac2 subpopulation being the dominant cell type at this time. When compared to the other macrophage and monocyte sub types, Mac2 is unique in that it has increased expression of type I interferon response genes including *Irf7*, *Srgn*, *Isg20*, and *Ifitm1* (**Figure 3C**). This is consistent with GSEA analysis showing an increase in IFN-α responses at day 3 p.i. in macrophages, microglia, and dendritic cells (**Figure 5C**). It is also important to note that in conjunction with Mac2, the presence of unique subpopulations such

as Mono2 (8.1%), Mac1 (9.0%), and Mac3 (5.9%) at this time point suggests potential roles in host defense (**Figure 5B**). Mac1 uniquely expressed transcripts for the chemokines *Cxcl10* and *Ccl4* that attract NK cells, lymphocytes and macrophages, respectively as well as *Rsad2* that encodes the antiviral host protein, Viperin (**Figure 5C**). Mac3 is the dominant antigen presenting macrophage population, expressing MHC class II transcripts (*H2-Eb1*, *H2-Aa*, *H2-Ab1)* and *Cd74* (**Figure 3C**). In addition to the macrophage subpopulations at this time point, microglia clusters MG1 (13.3%) and MG3 (14.7%) make up a large percentage of the day 3 time point, followed by MG2 (8.5%) and Cycling (Cyc.) MG (6.7%) (**Figure 5B**). Of the two top microglia subpopulations, MG3 expresses proinflammatory chemoattractants *Ccl3*, *Ccl4*, *Cxcl10*, similar to that of Mac1, as well as Osteopontin (*Spp1*) and Cholesterol 25-hydroxylase (*Ch25h*), while MG1 retains a homeostatic phenotype with higher expression of *P2ry12*, *Slc2a5*, and *Gpr34* (**Figure 3D**). In summation, the immune landscape of the CNS during the innate response to viral infection of the CNS with JHMV consists largely of microglia and macrophages that assume varying roles involved in Type I IFN response and secretion of immune cell chemo-attractants, while also reserving some cells for homeostatic maintenance.

At day 7 p.i., we found that the most prominent clusters were Mac3 (14.8%), Mac2 (10.4%), and Cd209a+ DCs (9.5%) (**Figure 6B**). By this time, virus-specific T cells have expanded within the cervical lymph nodes and commenced trafficking into the CNS. Through scRNAseq analysis, we have determined that CNS infiltrating T cells at day 7 p.i. are quite diverse and include cytolytic Effector (Eff.) $CD8^+$ T cells, Eff. Cyc. $CD8^+$ T cells, and $CD4^+$ T cells. A limitation of the current study is that astrocytes were not examined, and they provide additional sources of chemokines. We have previously reported that astrocytes were prominent cellular sources for CXCL9 and CXCL10 (15-17, 64). In the present study, we were able to

determine that subpopulations of MG, monocytes, macrophages, and DCs expressed *Cxcl10* transcripts at days 3 and 7 p.i. This is in contrast to astrocyte-derived CXCL10 which was expressed at days 3 and 7 p.i. in the brain, but also at day 21 p.i. in the spinal cord (17, 64). Expression of *Cxcl9* transcripts was primarily restricted to macrophage and DC subpopulations with very little expression detected in either microglia or monocytes. Our earlier studies emphasized an important role for both CXCL9 and CXCL10 in attracting activated T cells and NK cells bearing the signaling receptor CXCR3 into the CNS of JHMV-infected mice during acute disease (15-17, 49, 50). Consistent with these earlier studies is the demonstration in this report that CNS infiltrating subpopulations of T cells express *Cxcr3* transcripts. Infiltrating virus-specific T cells express IFN-γ upon recognition of cognate antigens expressed by activated antigen-presenting cells (APCs) and this aids in controlling JHMV replication as well as enhancing expression of proinflammatory cytokines/chemokines that subsequently amplify neuroinflammation. Findings in this report demonstrate via GSEA analysis an increase in IFN-γ-responsive genes in microglia, macrophages, and dendritic cells, which correlated with increased expression of MHC class I and II transcripts within subpopulations of these cells (**Figures 6C and 7A-F**). For MHC class I-associated transcripts, there was an increase in expression within the brain at day 3 p.i. compared to uninfected mice in all examined cell populations and this gradually increased by day 7 p.i. and sustained out to day 21 p.i. in the spinal cord (**Figure 7A-C**). For microglia and monocytes/macrophages, expression of MHC class II-associated transcripts was relatively low in the brains of both uninfected mice and at day 3 p.i., yet dramatically increased at day 7 p.i. coinciding with the infiltration of virus-specific T cells expressing IFN-γ (**Figure 7D-E**). Expression of MHC class II transcripts in these APC populations remained elevated in the spinal cords out to day 21 p.i. (**Figure 7D-E**). Within

activated DC subpopulations, we detected higher basal levels of MHC class II-associated transcripts from uninfected mice that gradually increased following JHMV infection out to day 21 p.i., supporting earlier studies that JHMV exhibits preferential infection of mature DCs (**Figure 7F**) (65). The unique temporal expression profiles of MHC molecules between APC populations suggests an intricately orchestrated system of anti-viral defense in which different cell populations employ the same function consecutively and not simultaneously, with dendritic cells and monocyte/macrophage populations presenting antigen more acutely and microglia subtypes later in disease. Similarly, when we surveyed expression of transcripts encoding two common T cell checkpoint inhibitory ligands, Programmed death-ligand-1 (PD-L1, *Cd274*) and Galectin-9 (*Lgals9*), we found that DCs had a more limited role later on in disease with reduced expression at day 21 p.i. (**Figure 8C**). Microglia and monocytes/macrophages express *Lgals9* (Galectin-9) in uninfected mice, but expression is higher following infection with JHMV and persists out to day 21 p.i. in spinal cords (**Figure 8A-B**). *Cd274* (PD-L1) is expressed in primarily in Mac1, Mac2, and Mac4 macrophage populations and the $Ccr7^{+}$ DC population, with nearly no expression in microglia (**Figure 8A-C**). Programmed cell death-1 (PD-1) and T-cell immunoglobulin and mucin-domain containing-3 (TIM-3) are inhibitory receptors that are present on activated T cells, where binding to respective ligands, PD-L1 and Galectin-9, transmits an inhibitory signal on T cell effector function (66, 67). Furthermore, the presence of these receptors and ligands suggest T cell exhaustion (67, 68). To determine if T cells show similar temporal expression of the corresponding inhibitory receptors, we evaluated expression of transcripts encoding PD-1 (*Pdcd1*) and TIM-3 (*Havcr2*) in T cells. We found that *Pdcd1* (PD-1) is primarily expressed in $CD4^{+}$ T cells and effector $CD8^{+}$ T cell subsets, while *Havcr2* (TIM-3) is expressed mostly by effector $CD8^{+}$ T cells and at much lower levels (**Figure 8D**). *Pdcd1*

(PD-1) expression is elevated at all defined times post-infection in $CD4^+$ T cells, but expression is highest at days 7 and 21 p.i. in effector $CD8^+$ T cells (**Figure 8E-F**). Similarly, expression of transcripts encoding TIM-3 (*Havcr2*) are also elevated at days 7 and 21 p.i. in effector $CD8^+$ T cells (**Figure 8F**). These findings argue that effector $CD4^+$ and $CD8^+$ T cells exhibit an exhausted phenotype at later stages of disease that may impact control viral replication (23) .

Following the acute phase of infection, virus begins to spread into the spinal cord and this is associated with immune-mediated demyelination. By day 21 p.i., peak inflammation has subsided and infected mice are left with a chronic, demyelinating spinal cord lesion. Inflammatory T cells and macrophages are known to contribute to this demyelination (8, 11, 26, 69-73), although mechanisms by which this occurs remain weakly characterized. To contribute further insight into the physiological players that enhance or control white matter damage during the chronic stage of infection, we conducted scRNAseq analysis of $CD45^+$ cells present within the spinal cord at day 21 p.i. We found enriched populations of $CD4^+$ T cells, effector $CD8^+$ T cells, memory $CD8^+$ T cells, and plasma cells (**Figure 9A-B**). Of the macrophage and microglia populations found in the spinal cord at day 21 p.i., Mac3 and MG3 appear to be dominant (**Figure 9A-B**). When evaluating expression of demyelination-associated transcripts encoding proteins APOE (*Apoe*), transmembrane glycoprotein NMB (*Gpnmb*), osteopontin (*Spp1*), and TREM2 (*Trem2*) in microglia and macrophage subpopulations (54-56), we found that MG3, Mac3, and Mac4 have the highest expression compared to other subpopulations (**Figure 9C**). Furthermore, expression of these transcripts in microglia and macrophages is elevated at day 21 p.i. (**Figure 9C**). These findings are consistent with our previous work showing elevated transcripts *Apoe*, *Spp1*, and *Trem2* in spinal cords at an earlier stage of demyelination (28) and further support the notion these cells tailor the spinal cord microenvironment to regulate ongoing

disease. Defining potential roles for these factors in augmenting demyelination is the focus of ongoing studies. As microglia are known to assume a myriad of functional roles, we sought to determine if any subpopulations present in chronically demyelinated lesions have the potential to ameliorate white matter pathology, we evaluated expression of transcripts *Cst7* (Cystatin F) (57, 58), *Igf1* (Insulin-like growth factor-1, IGF-1) (59, 60), and *Lpl* (lipoprotein lipase) (61) that are associated with promoting remyelination and found that transcripts are highest in the MG3 subpopulation of microglia, with expression also elevated in Cyc. MG (**Figure 9D**). Expression of remyelination-associated transcripts were also found to be the highest in spinal cords at day 21 p.i. (**Figure 9D**). However, when compared to our previous findings examining an earlier stage of demyelination in spinal cords (28), expression of *Cst7*, *Igf1*, and *Lpl* appear to be more relevant to the later stages of spinal cord demyelination seen at day 21 p.i. Furthermore, using GSEA analysis to compare overall transcripts associated with promoting oligodendrocyte differentiation between MG3/Cyc. MG and MG1/MG2, we found that MG3/Cyc. MG showed a drastic increase in comparison at day 21 p.i. (**Figure 9E**). Collectively, these findings enforce the concept that different populations of microglia and macrophages exist within the inflamed CNS during neuroinflammatory disease that can both affect disease progression and repair damage and may offer targets for interventional therapy (28, 55, 74-77).

MATERIALS AND METHODS

Mice and viral infection. Five-week old C57BL/6 male mice were purchased from The Jackson Laboratory. Mice were infected intracranially (i.c.) with 1,500 plaque forming units (PFU) of JHMV strain J2.2v-1 in 30 μL of sterile Hanks balanced sterile solution (HBSS) and animals were euthanized using isoflurane and were perfused with phosphate-buffered saline at days 0 (uninfected control), 3, 7, and 21 post-infection (p.i). Clinical disease in JHMV-infected mice was evaluated using a previously described scale (71). One half each brain was used for determining viral titers and the other halves used for scRNAseq. Spinal cords at day 21 p.i. were used for either determining viral titer or scRNAseq. Isolated brains and spinal cords were homogenized and plaque assays were performed on the DBT astrocytoma cell line as described previously (78). All animal studies were reviewed and approved by the University of Utah Animal Care and Use Committee.

Cell isolation and single cell RNA sequencing (scRNAseq). To isolate immune cells from brains (uninfected controls, day 3 and day 7 p.i) and spinal cords (day 21 p.i), mice were anesthetized using isoflurane and were perfused with phosphate-buffered saline (PBS). Brains and/or spinal cords were removed and single cell suspensions were generated from tissue samples by grinding with frosted microscope slides in 5 mL of RPMI as described previously (71). Immune cells were then enriched via a 2-step Percoll cushion (90% and 63%) and cells were collected at the interface of the two Percoll layers (79, 80). Cells were stained with DAPI and APC conjugated anti-CD45 for 20 minutes on ice in 1X PBS containing 0.5% bovine serum albumin (BSA). Live $CD45^+$ cells were enriched through the use of BD FACS Aria flow sorter (University of Utah Health Science Center) and washed once with 0.04% BSA. Samples were

then processed for single cell RNA sequencing via the 10X Genomics platform performed at the Huntsman Cancer Institute High Throughput Genomics Shared Resource Core Facility (https://uofuhealth.utah.edu/huntsman/shared-resources/gba/). Agilent Hiseq next-generation sequencer was used to perform RNA sequencing (125 cycles) and sequencing reads were processed using the 10X Genomics CellRanger pipeline. Using the Seurat R package, unwanted cells were filtered out based upon mitochondrial gene representation and variances in unique gene counts. Downstream analysis was performed using the Seurat following principal correlation analysis (PCA) and uniform manifold approximation and projection (UMAP) dimensional reduction (29, 30). Gene expression signatures of cells from brains (uninfected controls, day 3 and day 7 p.i.) and spinal cords (day 21 p.i.) of JHMV-infected mice were scrutinized and cells from the aggregated dataset were clustered into corresponding immune cell populations by a shared nearest neighbor (SNN) modularity optimization-based clustering algorithm via the FindClusters function in the Seurat analysis package in R. The resulting clusters were defined using an immune-cell scoring algorithm (https://aekiz.shinyapps.io/CIPR/) (31,32) that compares the gene signatures of each cluster in the experimental dataset with the microarray data available in the Immunological Genome (ImmGen) Project Database (31,32). Expression levels and distribution of population-specific immune cell markers were then analyzed to further identify subpopulations. Once the clusters were established and identified, plots were generated using Seurat and ggpubr R packages and GSEA plots were generated as previously mentioned using the fgsea R package (32).

Histology. Mice were euthanized at defined times points according to IACUC-approved guidelines and the length of spinal cord extending from thoracic vertebrate 6-10 was

cryoprotected in 30% sucrose, cut into 1-mm transverse blocks and processed so as to preserve the craniocaudal orientation and subsequently embedded in O.C.T. (VWR, Radnor, PA, USA). Eight micron (mm)-thick coronal sections were cut and sections were stained with hematoxylin/eosin (H&E) in combination with luxol fast blue (LFB) (81-83).

Statistical analysis. GraphPad Prism was used to perform statistical analyses. Data for each experiment is presented as mean±standard error of mean (SEM). Wilcoxon test was used for analyzing gene expression in scRNAseq clusters and the resulting *p* values were corrected for multiple comparisons by Holm-Sidak method and a *p* value of ≤ 0.05 was considered statistically significant (*$p \leq 0.05$; ** $p \leq 0.01$; ***$p \leq 0.001$; ****$p \leq 0.0001$).

Author contributions

ARS helped design and perform experiments, analyzed and interpreted the data, prepared figures and assisted in writing the manuscript. DDS helped perform experiments and in writing the manuscript; CS helped perform experiments and manuscript preparation; HAE and RMO contributed in scRNAseq data analysis and interpretation and writing the manuscript; TEL designed experiments, participated in data analysis and interpretation and writing the manuscript.

Acknowledgements.

TEL was supported by funding from the National Institutes of Health (NIH) grants R01NS041249 and R35NS116835 and The Ray and Tye Noorda Foundation. TEL and RMO were supported by National Multiple Sclerosis Society (NMSS) Collaborative Research Center Grant CA-1607-25040. RMO was supported by NIH R01AG047956.

REFERENCES

1. Hosking MP, Lane TE. 2009. The Biology of Persistent Infection: Inflammation and Demyelination following Murine Coronavirus Infection of the Central Nervous System. Curr Immunol Rev 5:267-276.

2. Lane TE, Buchmeier MJ. 1997. Murine coronavirus infection: a paradigm for virus-induced demyelinating disease. Trends Microbiol 5:9-14.

3. Coronaviridae Study Group of the International Committee on Taxonomy of V. 2020. The species Severe acute respiratory syndrome-related coronavirus: classifying 2019-nCoV and naming it SARS-CoV-2. Nat Microbiol 5:536-544.

4. Fleming JO, Trousdale MD, el-Zaatari FA, Stohlman SA, Weiner LP. 1986. Pathogenicity of antigenic variants of murine coronavirus JHM selected with monoclonal antibodies. J Virol 58:869-75.

5. Lane TE, Asensio VC, Yu N, Paoletti AD, Campbell IL, Buchmeier MJ. 1998. Dynamic Regulation of {alpha}- and {beta}-Chemokine Expression in the Central Nervous System During Mouse Hepatitis Virus-Induced Demyelinating Disease. J Immunol 160:970-978.

6. Pearce BD, Hobbs MV, McGraw TS, Buchmeier MJ. 1994. Cytokine induction during T-cell-mediated clearance of mouse hepatitis virus from neurons in vivo. J Virol 68:5483-95.

7. Sun N, Grzybicki D, Castro RF, Murphy S, Perlman S. 1995. Activation of astrocytes in the spinal cord of mice chronically infected with a neurotropic coronavirus. Virology 213:482-93.

8. Glass WG, Hickey MJ, Hardison JL, Liu MT, Manning JE, Lane TE. 2004. Antibody Targeting of the CC Chemokine Ligand 5 Results in Diminished Leukocyte Infiltration into the Central Nervous System and Reduced Neurologic Disease in a Viral Model of Multiple Sclerosis. The Journal of Immunology 172:4018-4025.

9. Glass WG, Lane TE. 2003. Functional analysis of the CC chemokine receptor 5 (CCR5) on virus-specific CD8+ T cells following coronavirus infection of the central nervous system. Virology 312:407-14.

10. Glass WG, Lane TE. 2003. Functional expression of chemokine receptor CCR5 on CD4(+) T cells during virus-induced central nervous system disease. J Virol 77:191-8.

11. Glass WG, Liu MT, Kuziel WA, Lane TE. 2001. Reduced macrophage infiltration and demyelination in mice lacking the chemokine receptor CCR5 following infection with a neurotropic coronavirus. Virology 288:8-17.

12. Grist JJ, Marro BS, Skinner DD, Syage AR, Worne C, Doty DJ, Fujinami RS, Lane TE. 2018. Induced CNS expression of CXCL1 augments neurologic disease in a murine

model of multiple sclerosis via enhanced neutrophil recruitment. European Journal of Immunology 48:1199-1210.

13. Held KS, Chen BP, Kuziel WA, Rollins BJ, Lane TE. 2004. Differential roles of CCL2 and CCR2 in host defense to coronavirus infection. Virology 329:251-60.

14. Hosking MP, Liu L, Ransohoff RM, Lane TE. 2009. A protective role for ELR+ chemokines during acute viral encephalomyelitis. PLoS Pathog 5:e1000648.

15. Liu MT, Armstrong D, Hamilton TA, Lane TE. 2001. Expression of Mig (Monokine Induced by Interferon-) Is Important in T Lymphocyte Recruitment and Host Defense Following Viral Infection of the Central Nervous System. The Journal of Immunology 166:1790-1795.

16. Liu MT, Chen BP, Oertel P, Buchmeier MJ, Armstrong D, Hamilton TA, Lane TE. 2000. Cutting Edge: The T Cell Chemoattractant IFN-Inducible Protein 10 Is Essential in Host Defense Against Viral-Induced Neurologic Disease. The Journal of Immunology 165:2327-2330.

17. Liu MT, Keirstead HS, Lane TE. 2001. Neutralization of the chemokine CXCL10 reduces inflammatory cell invasion and demyelination and improves neurological function in a viral model of multiple sclerosis. J Immunol 167:4091-7.

18. Marro BS, Grist JJ, Lane TE. 2016. Inducible Expression of CXCL1 within the Central Nervous System Amplifies Viral-Induced Demyelination. J Immunol doi:10.4049/jimmunol.1501802.

19. Phares TW, Stohlman SA, Hinton DR, Bergmann CC. 2013. Astrocyte-derived CXCL10 drives accumulation of antibody-secreting cells in the central nervous system during viral encephalomyelitis. Journal of virology 87:3382-3392.

20. Trujillo JA, Fleming EL, Perlman S. 2013. Transgenic CCL2 expression in the central nervous system results in a dysregulated immune response and enhanced lethality after coronavirus infection. J Virol 87:2376-89.

21. Lin MT, Stohlman SA, Hinton DR. 1997. Mouse hepatitis virus is cleared from the central nervous systems of mice lacking perforin-mediated cytolysis. J Virol 71:383-91.

22. Parra B, Hinton DR, Marten NW, Bergmann CC, Lin MT, Yang CS, Stohlman SA. 1999. IFN-gamma is required for viral clearance from central nervous system oligodendroglia. J Immunol 162:1641-7.

23. Bergmann CC, Lane TE, Stohlman SA. 2006. Coronavirus infection of the central nervous system: host-virus stand-off. Nat Rev Microbiol 4:121-32.

24. Lin MT, Hinton DR, Marten NW, Bergmann CC, Stohlman SA. 1999. Antibody prevents virus reactivation within the central nervous system. Journal of immunology (Baltimore, Md : 1950) 162:7358-7368.

25. Glass WG, Hickey MJ, Hardison JL, Liu MT, Manning JE, Lane TE. 2004. Antibody targeting of the CC chemokine ligand 5 results in diminished leukocyte infiltration into the central nervous system and reduced neurologic disease in a viral model of multiple sclerosis. J Immunol 172:4018-25.

26. Liu MT, Keirstead HS, Lane TE. 2001. Neutralization of the chemokine CXCL10 reduces inflammatory cell invasion and demyelination and improves neurological function in a viral model of multiple sclerosis. Journal of immunology (Baltimore, Md : 1950) 167:4091-4097.

27. Stohlman SA, Weiner LP. 1981. Chronic central nervous system demyelination in mice after JHM virus infection. Neurology 31:38-44.

28. Mangale V, Syage AR, Ekiz HA, Skinner DD, Cheng Y, Stone CL, Brown RM, O'Connell RM, Green KN, Lane TE. 2020. Microglia influence host defense, disease, and repair following murine coronavirus infection of the central nervous system. Glia doi:10.1002/glia.23844.

29. Butler A, Hoffman P, Smibert P, Papalexi E, Satija R. 2018. Integrating single-cell transcriptomic data across different conditions, technologies, and species. Nat Biotechnol 36:411-420.

30. Stuart T, Butler A, Hoffman P, Hafemeister C, Papalexi E, Mauck WM, 3rd, Hao Y, Stoeckius M, Smibert P, Satija R. 2019. Comprehensive Integration of Single-Cell Data. Cell 177:1888-1902 e21.

31. Ekiz HA, Conley CJ, Stephens WZ, O'Connell RM. 2020. CIPR: a web-based R/shiny app and R package to annotate cell clusters in single cell RNA sequencing experiments. BMC Bioinformatics 21:191.

32. Ekiz HA, Huffaker TB, Grossmann AH, Stephens WZ, Williams MA, Round JL, O'Connell RM. 2019. MicroRNA-155 coordinates the immunological landscape within murine melanoma and correlates with immunity in human cancers. JCI Insight 4.

33. Anghelina D, Zhao J, Trandem K, Perlman S. 2009. Role of regulatory T cells in coronavirus-induced acute encephalitis. Virology 385:358-67.

34. Yang J, Anholts J, Kolbe U, Stegehuis-Kamp JA, Claas FHJ, Eikmans M. 2018. Calcium-Binding Proteins S100A8 and S100A9: Investigation of Their Immune Regulatory Effect in Myeloid Cells. Int J Mol Sci 19.

35. Li Q, Cheng Z, Zhou L, Darmanis S, Neff NF, Okamoto J, Gulati G, Bennett ML, Sun LO, Clarke LE, Marschallinger J, Yu G, Quake SR, Wyss-Coray T, Barres BA. 2019. Developmental Heterogeneity of Microglia and Brain Myeloid Cells Revealed by Deep Single-Cell RNA Sequencing. Neuron 101:207-223 e10.

36. Banisor I, Leist TP, Kalman B. 2005. Involvement of beta-chemokines in the development of inflammatory demyelination. J Neuroinflammation 2:7.

37. Castro CD, Flajnik MF. 2014. Putting J chain back on the map: how might its expression define plasma cell development? J Immunol 193:3248-55.

38. Erlandsson L, Akerblad P, Vingsbo-Lundberg C, Kallberg E, Lycke N, Leanderson T. 2001. Joining chain-expressing and -nonexpressing B cell populations in the mouse. J Exp Med 194:557-70.

39. van Pelt LJ, Huisman MV, Weening RS, von dem Borne AE, Roos D, van Oers RH. 1996. A single dose of granulocyte-macrophage colony-stimulating factor induces systemic interleukin-8 release and neutrophil activation in healthy volunteers. Blood 87:5305-13.

40. Zhou J, Stohlman SA, Atkinson R, Hinton DR, Marten NW. 2002. Matrix metalloproteinase expression correlates with virulence following neurotropic mouse hepatitis virus infection. J Virol 76:7374-84.

41. Zhou J, Stohlman SA, Hinton DR, Marten NW. 2003. Neutrophils promote mononuclear cell infiltration during viral-induced encephalitis. J Immunol 170:3331-6.

42. Kivisakk P, Imitola J, Rasmussen S, Elyaman W, Zhu B, Ransohoff RM, Khoury SJ. 2009. Localizing central nervous system immune surveillance: meningeal antigen-presenting cells activate T cells during experimental autoimmune encephalomyelitis. Ann Neurol 65:457-69.

43. Ransohoff RM, Engelhardt B. 2012. The anatomical and cellular basis of immune surveillance in the central nervous system. Nat Rev Immunol 12:623-35.

44. Mrdjen D, Pavlovic A, Hartmann FJ, Schreiner B, Utz SG, Leung BP, Lelios I, Heppner FL, Kipnis J, Merkler D, Greter M, Becher B. 2018. High-Dimensional Single-Cell Mapping of Central Nervous System Immune Cells Reveals Distinct Myeloid Subsets in Health, Aging, and Disease. Immunity 48:599.

45. Negi N, Das BK. 2018. CNS: Not an immunoprivilaged site anymore but a virtual secondary lymphoid organ. Int Rev Immunol 37:57-68.

46. Christofferson DE, Li Y, Hitomi J, Zhou W, Upperman C, Zhu H, Gerber SA, Gygi S, Yuan J. 2012. A novel role for RIP1 kinase in mediating TNFalpha production. Cell Death Dis 3:e320.

47. Kung HC, Evensen O, Hong JR, Kuo CY, Tso CH, Ngou FH, Lu MW, Wu JL. 2014. Interferon regulatory factor-1 (IRF-1) is involved in the induction of phosphatidylserine receptor (PSR) in response to dsRNA virus infection and contributes to apoptotic cell clearance in CHSE-214 cell. Int J Mol Sci 15:19281-306.

48. Stiles LN, Hardison JL, Schaumburg CS, Whitman LM, Lane TE. 2006. T cell antiviral effector function is not dependent on CXCL10 following murine coronavirus infection. J Immunol 177:8372-80.

49. Stiles LN, Liu MT, Kane JAC, Lane TE. 2009. CXCL10 and trafficking of virus-specific T cells during coronavirus demyelination. Autoimmunity In Press.

50. Stiles LN, Hosking MP, Edwards RA, Strieter RM, Lane TE. 2006. Differential roles for CXCR3 in CD4+ and CD8+ T cell trafficking following viral infection of the CNS. Eur J Immunol 36:613-22.

51. Lane TE, Hosking MP. 2010. The pathogenesis of murine coronavirus infection of the central nervous system. Crit Rev Immunol 30:119-30.

52. Marro BS, Blanc CA, Loring JF, Cahalan MD, Lane TE. 2014. Promoting remyelination: utilizing a viral model of demyelination to assess cell-based therapies. Expert Rev Neurother 14:1169-79.

53. Wu GF, Perlman S. 1999. Macrophage infiltration, but not apoptosis, is correlated with immune-mediated demyelination following murine infection with a neurotropic coronavirus. Journal of virology 73:8771-8780.

54. Chabas D, Baranzini SE, Mitchell D, Bernard CC, Rittling SR, Denhardt DT, Sobel RA, Lock C, Karpuj M, Pedotti R, Heller R, Oksenberg JR, Steinman L. 2001. The influence of the proinflammatory cytokine, osteopontin, on autoimmune demyelinating disease. Science 294:1731-5.

55. Krasemann S, Madore C, Cialic R, Baufeld C, Calcagno N, El Fatimy R, Beckers L, O'Loughlin E, Xu Y, Fanek Z, Greco DJ, Smith ST, Tweet G, Humulock Z, Zrzavy T, Conde-Sanroman P, Gacias M, Weng Z, Chen H, Tjon E, Mazaheri F, Hartmann K, Madi A, Ulrich JD, Glatzel M, Worthmann A, Heeren J, Budnik B, Lemere C, Ikezu T, Heppner FL, Litvak V, Holtzman DM, Lassmann H, Weiner HL, Ochando J, Haass C, Butovsky O. 2017. The TREM2-APOE Pathway Drives the Transcriptional Phenotype of Dysfunctional Microglia in Neurodegenerative Diseases. Immunity 47:566-581 e9.

56. Ulrich JD, Holtzman DM. 2016. TREM2 Function in Alzheimer's Disease and Neurodegeneration. ACS Chem Neurosci 7:420-7.

57. Ma J, Tanaka KF, Shimizu T, Bernard CC, Kakita A, Takahashi H, Pfeiffer SE, Ikenaka K. 2011. Microglial cystatin F expression is a sensitive indicator for ongoing demyelination with concurrent remyelination. J Neurosci Res 89:639-49.

58. Shimizu T, Wisessmith W, Li J, Abe M, Sakimura K, Chetsawang B, Sahara Y, Tohyama K, Tanaka KF, Ikenaka K. 2017. The balance between cathepsin C and cystatin F controls remyelination in the brain of Plp1-overexpressing mouse, a chronic demyelinating disease model. Glia 65:917-930.

59. Wlodarczyk A, Holtman IR, Krueger M, Yogev N, Bruttger J, Khorooshi R, Benmamar-Badel A, de Boer-Bergsma JJ, Martin NA, Karram K, Kramer I, Boddeke EW, Waisman A, Eggen BJ, Owens T. 2017. A novel microglial subset plays a key role in myelinogenesis in developing brain. EMBO J 36:3292-3308.

60. Ye P, Li L, Richards RG, DiAugustine RP, D'Ercole AJ. 2002. Myelination is altered in insulin-like growth factor-I null mutant mice. J Neurosci 22:6041-51.

61. Bruce KD, Gorkhali S, Given K, Coates AM, Boyle KE, Macklin WB, Eckel RH. 2018. Lipoprotein Lipase Is a Feature of Alternatively-Activated Microglia and May Facilitate Lipid Uptake in the CNS During Demyelination. Front Mol Neurosci 11:57.

62. Lloyd AF, Davies CL, Holloway RK, Labrak Y, Ireland G, Carradori D, Dillenburg A, Borger E, Soong D, Richardson JC, Kuhlmann T, Williams A, Pollard JW, des Rieux A, Priller J, Miron VE. 2019. Central nervous system regeneration is driven by microglia necroptosis and repopulation. Nat Neurosci 22:1046-1052.

63. Lloyd AF, Miron VE. 2019. The pro-remyelination properties of microglia in the central nervous system. Nat Rev Neurol 15:447-458.

64. Lane TE, Asensio VC, Yu N, Paoletti AD, Campbell IL, Buchmeier MJ. 1998. Dynamic regulation of alpha- and beta-chemokine expression in the central nervous system during mouse hepatitis virus-induced demyelinating disease. J Immunol 160:970-8.

65. Zhou H, Perlman S. 2006. Preferential infection of mature dendritic cells by mouse hepatitis virus strain JHM. J Virol 80:2506-14.

66. Butte MJ, Keir ME, Phamduy TB, Sharpe AH, Freeman GJ. 2007. Programmed death-1 ligand 1 interacts specifically with the B7-1 costimulatory molecule to inhibit T cell responses. Immunity 27:111-22.

67. Wherry EJ. 2011. T cell exhaustion. Nat Immunol 12:492-9.

68. Taghiloo S, Allahmoradi E, Tehrani M, Hossein-Nataj H, Shekarriz R, Janbabaei G, Abediankenari S, Asgarian-Omran H. 2017. Frequency and functional characterization of exhausted CD8(+) T cells in chronic lymphocytic leukemia. Eur J Haematol 98:622-631.

69. Dandekar AA, Perlman S. 2002. Virus-induced demyelination in nude mice is mediated by gamma delta T cells. Am J Pathol 161:1255-63.

70. Kim TS, Perlman S. 2005. Viral expression of CCL2 is sufficient to induce demyelination in RAG1-/- mice infected with a neurotropic coronavirus. J Virol 79:7113-20.

71. Lane TE, Liu MT, Chen BP, Asensio VC, Samawi RM, Paoletti AD, Campbell IL, Kunkel SL, Fox HS, Buchmeier MJ. 2000. A central role for CD4(+) T cells and RANTES in virus-induced central nervous system inflammation and demyelination. J Virol 74:1415-24.

72. Templeton SP, Perlman S. 2007. Pathogenesis of acute and chronic central nervous system infection with variants of mouse hepatitis virus, strain JHM. Immunol Res 39:160-72.

73. Templeton SP, Perlman S. 2008. Role of IFN-gamma responsiveness in CD8 T-cell-mediated viral clearance and demyelination in coronavirus-infected mice. J Neuroimmunol 194:18-26.

74. Hammond TR, Dufort C, Dissing-Olesen L, Giera S, Young A, Wysoker A, Walker AJ, Gergits F, Segel M, Nemesh J, Marsh SE, Saunders A, Macosko E, Ginhoux F, Chen J, Franklin RJM, Piao X, McCarroll SA, Stevens B. 2019. Single-Cell RNA Sequencing of Microglia throughout the Mouse Lifespan and in the Injured Brain Reveals Complex Cell-State Changes. Immunity 50:253-271 e6.

75. Masuda T, Sankowski R, Staszewski O, Bottcher C, Amann L, Sagar, Scheiwe C, Nessler S, Kunz P, van Loo G, Coenen VA, Reinacher PC, Michel A, Sure U, Gold R, Grun D, Priller J, Stadelmann C, Prinz M. 2019. Spatial and temporal heterogeneity of mouse and human microglia at single-cell resolution. Nature 566:388-392.

76. Masuda T, Sankowski R, Staszewski O, Prinz M. 2020. Microglia Heterogeneity in the Single-Cell Era. Cell Rep 30:1271-1281.

77. Priller J, Prinz M. 2019. Targeting microglia in brain disorders. Science 365:32-33.

78. Hirano N, Murakami T, Fujiwara K, Matsumoto M. 1978. Utility of mouse cell line DBT for propagation and assay of mouse hepatitis virus. Jpn J Exp Med 48:71-5.

79. Blanc CA, Rosen H, Lane TE. 2014. FTY720 (fingolimod) modulates the severity of viral-induced encephalomyelitis and demyelination. J Neuroinflammation 11:138.

80. Chen L, Coleman R, Leang R, Tran H, Kopf A, Walsh CM, Sears-Kraxberger I, Steward O, Macklin WB, Loring JF, Lane TE. 2014. Human neural precursor cells promote neurologic recovery in a viral model of multiple sclerosis. Stem Cell Reports 2:825-37.

81. Blanc CA, Grist JJ, Rosen H, Sears-Kraxberger I, Steward O, Lane TE. 2015. Sphingosine-1-phosphate receptor antagonism enhances proliferation and migration of engrafted neural progenitor cells in a model of viral-induced demyelination. Am J Pathol 185:2819-32.

82. Dickey LL, Worne CL, Glover JL, Lane TE, O'Connell RM. 2016. MicroRNA-155 enhances T cell trafficking and antiviral effector function in a model of coronavirus-induced neurologic disease. J Neuroinflammation 13:240.

83. Marro BS, Grist JJ, Lane TE. 2016. Inducible Expression of CXCL1 within the Central Nervous System Amplifies Viral-Induced Demyelination. J Immunol 196:1855-64.

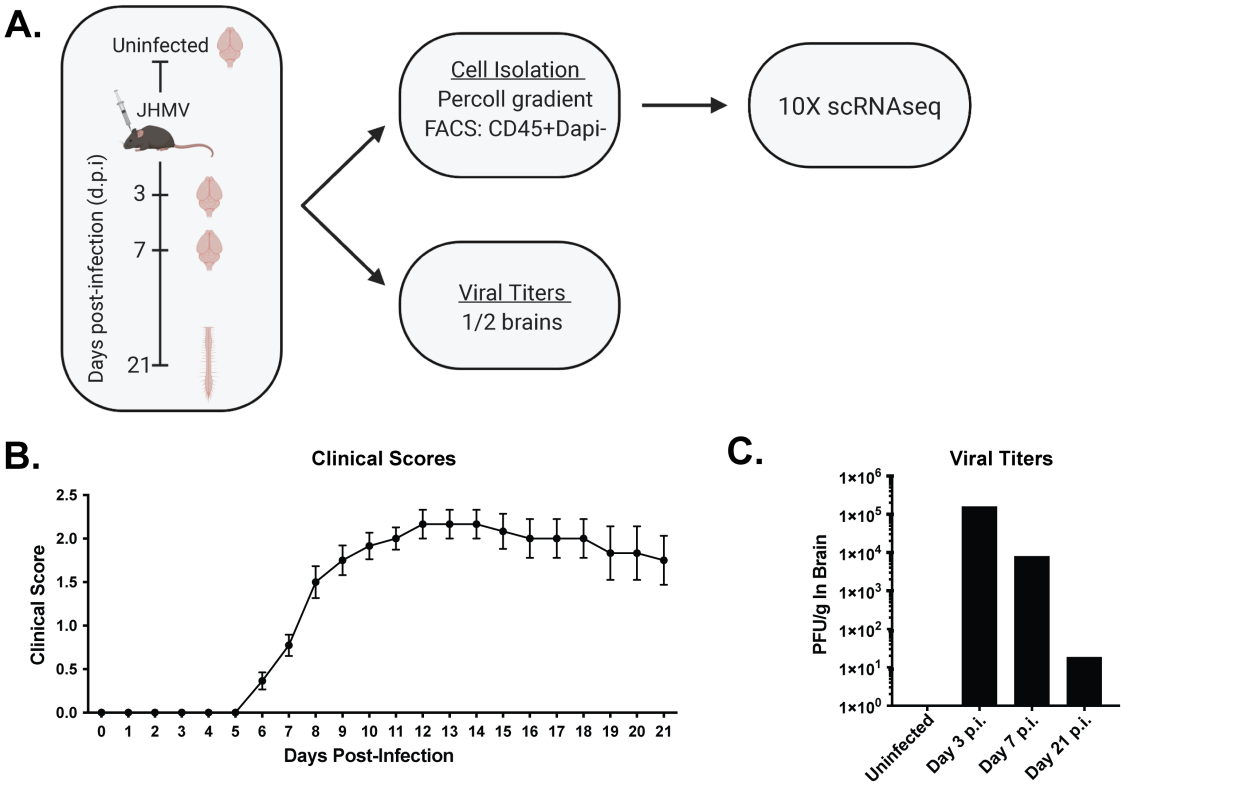

E.

Sample	Uninfected Brain	Day 3 p.i. Brain	Day 7 p.i. Brain	Day 21 p.i. Spinal Cord
Pooled N	6	5	5	6
Cell Number	1,456	3,863	2,573	1,423
Reads/Cell	36,399	40,055	41,717	52,751

Figure 1: JHMV infection of the CNS. (**A**) Schematic outline of experimental design indicating times post-infection (p.i.) for sacrifice, tissue isolation and experimental procedures performed. (**B**) Clinical disease in C57BL/6 mice (*n*=22) following intracranial (i.c.) inoculation with 1500 PFU of JHMV. (**C**) Viral titers within the brains from uninfected mice and infected animals at days 3, 7, and 21 days p.i. (*n*=5-6 per group) (**D**) Representative spinal cords stained with hematoxylin and eosin (H&E) and luxol fast blue (LFB) from uninfected Control mice and infected mice at day 21 p.i. revealing demyelination within the ventral funiculus and lateral white matter columns. (**E**) Data table summarizing the number of $CD45^{+}$ cells isolated from either brain (control and days 3 and 7 p.i.) or spinal cord (day 21 p.i.) tissue used in downstream analysis as well as the number of reads/cell following scRNAseq analysis (5-6 mice pooled/ group).

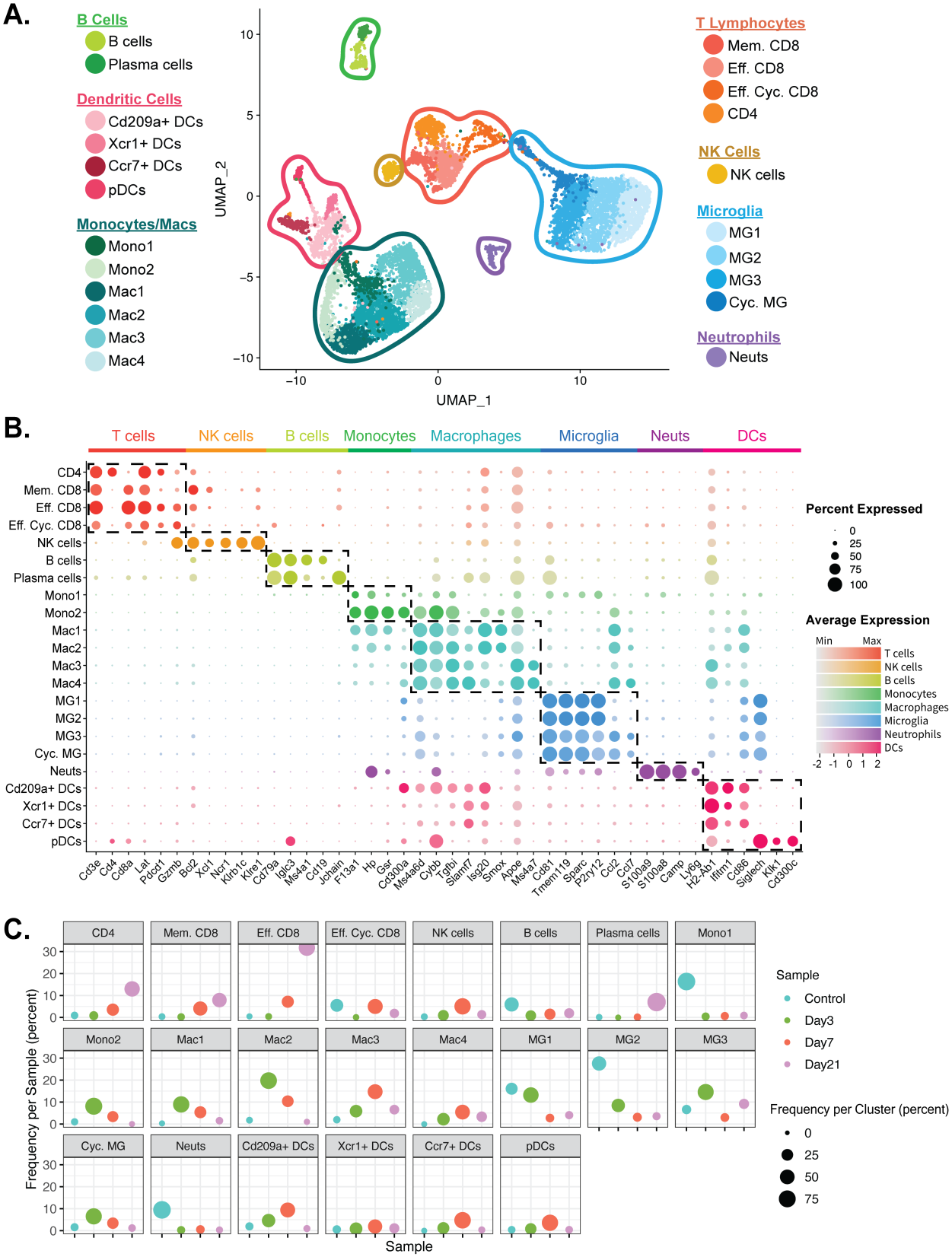
A.
B Cells
B cells
Plasma cells
Dendritic Cells
Cd209a+ DCs
Xcr1+ DCs
Ccr7+ DCs
pDCs
Monocytes/Macs
Mono1
Mono2
Mac1
Mac2
Mac3
Mac4
UMAP_2
UMAP_1
T Lymphocytes
Mem. CD8
Eff. CD8
Eff. Cyc. CD8
CD4
NK Cells
NK cells
Microglia
MG1
MG2
MG3
Cyc. MG
Neutrophils
Neuts
B.
T cells
NK cells
B cells
Monocytes
Macrophages
Microglia
Neuts
DCs
Percent Expressed
Average Expression
Min
Max
C.
Frequency per Sample (percent)
Sample
Control
Day3
Day7
Day21
Frequency per Cluster (percent)

Figure 2: scRNAseq analysis of CD45^{+} cells within the CNS at defined times p.i. (**A**) UMAP plot showing aggregate data of the immune landscape in brains and spinal cords of uninfected (Control) and infected mice at 3, 7, and 21 days p.i. with JHMV revealing 22 distinct cell clusters (5-6 mice pooled per group). (**B**) Dot plot presenting expression of selected genes within the 22 cell clusters. Size of the dot is representative of the frequency of cells within a cluster expressing the gene of interest, while the degree of color intensity is indicative of the level of expression of the gene. The dashed boxes highlight commonly and uniquely expressed genes of clusters within overarching cell types. (**C**) Dot plot showing the frequency in percent of cells for each cluster. The y-axis shows the overall frequency of cells from a cluster per sample, while the size of the dot represents the frequency of cells from control (teal), day 3 p.i. (green), day 7 p.i. (red), and day 21 p.i. (purple) within a cell cluster.

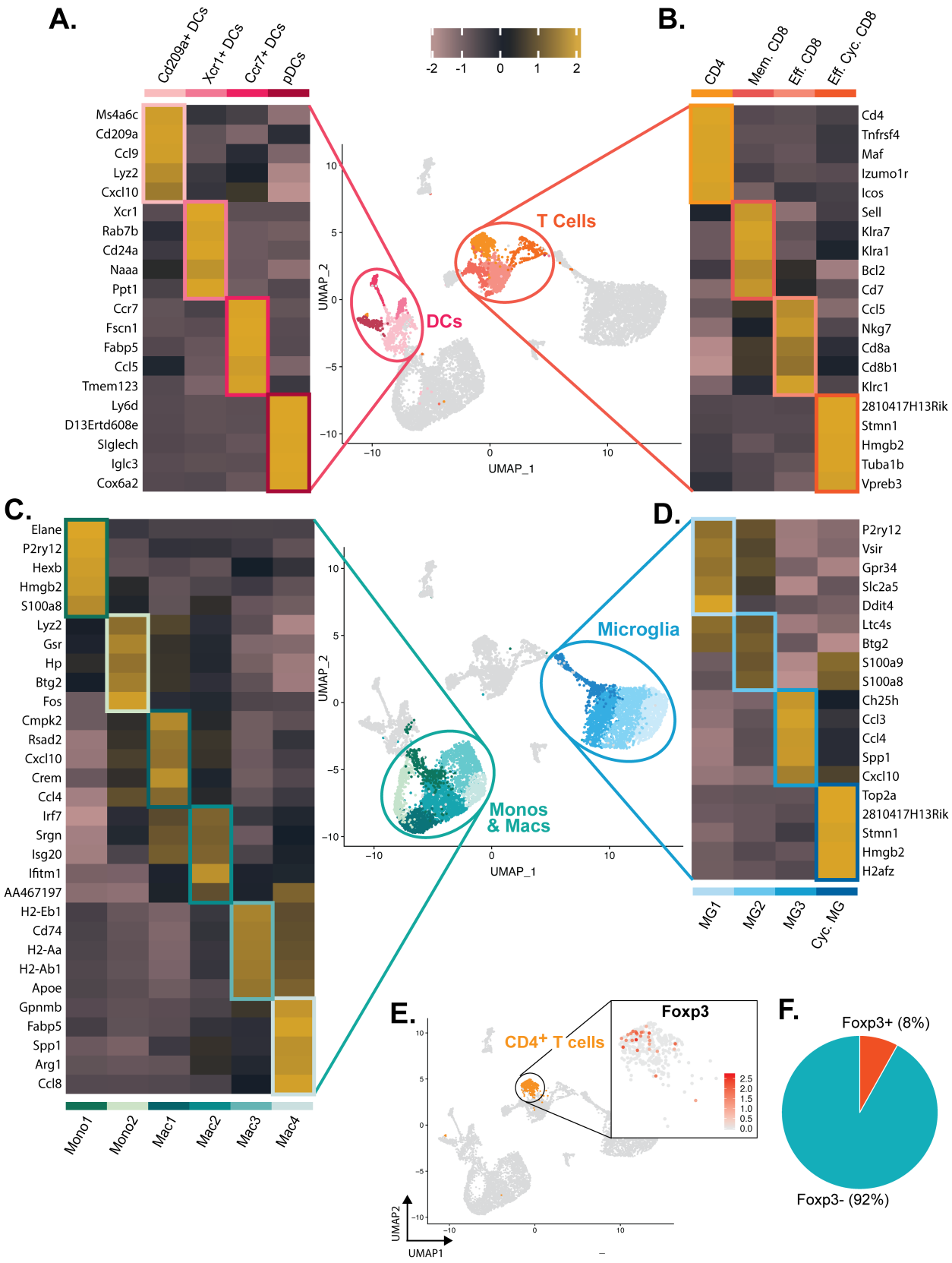
A.
Cd209a+ DCs
Xcr1+ DCs
Ccr7+ DCs
pDCs
-2 -1 0 1 2
Ms4a6c
Cd209a
Ccl9
Lyz2
Cxcl10
Xcr1
Rab7b
Cd24a
Naaa
Ppt1
Ccr7
Fscn1
Fabp5
Ccl5
Tmem123
Ly6d
D13Ertd608e
Slglech
Iglc3
Cox6a2
DCs
T Cells
UMAP_1
UMAP_2
B.
CD4
Mem. CD8
Eff. CD8
Eff. Cyc. CD8
Cd4
Tnfrsf4
Maf
Izumo1r
Icos
Sell
Klra7
Klra1
Bcl2
Cd7
Ccl5
Nkg7
Cd8a
Cd8b1
Klrc1
2810417H13Rik
Stmn1
Hmgb2
Tuba1b
Vpreb3
C.
Elane
P2ry12
Hexb
Hmgb2
S100a8
Lyz2
Gsr
Hp
Btg2
Fos
Cmpk2
Rsad2
Cxcl10
Crem
Ccl4
Irf7
Srgn
Isg20
Ifitm1
AA467197
H2-Eb1
Cd74
H2-Aa
H2-Ab1
Apoe
Gpnmb
Fabp5
Spp1
Arg1
Ccl8
Mono1
Mono2
Mac1
Mac2
Mac3
Mac4
Microglia
Monos & Macs
D.
P2ry12
Vsir
Gpr34
Slc2a5
Ddit4
Ltc4s
Btg2
S100a9
S100a8
Ch25h
Ccl3
Ccl4
Spp1
Cxcl10
Top2a
2810417H13Rik
Stmn1
Hmgb2
H2afz
MG1
MG2
MG3
Cyc. MG
E.
CD4+ T cells
Foxp3
2.5
2.0
1.5
1.0
0.5
0.0
UMAP2
UMAP1
F.
Foxp3+ (8%)
Foxp3- (92%)

Figure 3: Genetic signatures of immune cells subsets within the CNS of JHMV-infected mice. Heatmap showing top 5 differentially expressed transcripts between heterogeneous subpopulations for subsets of (**A**) dendritic cells, (**B**) T cells, (**C**) monocytes/macrophages and (**D**) microglia. Each heatmap is generated with subset data from (**A**) dendritic cells, (**B**) T cells, (**C**) monocytes/macrophages and (**D**) microglia populations and isolated from all other clusters outside of what is shown in each individual map. (**A**-**D**) Data are aggregated from uninfected (Control) and infected at days 3, 7, and 21 p.i. Columns represent the different clusters and rows represent expression of transcripts. (**E**) UMAP plot showing scaled expression of transcripts encoding FOXP3 (*Foxp3*) in $CD4^+$ T cells. (**F**) Pie chart showing the percentage of $Foxp3^+$ cells (red) versus $Foxp3^-$ cells (blue) within the $CD4^+$ T cell cluster.

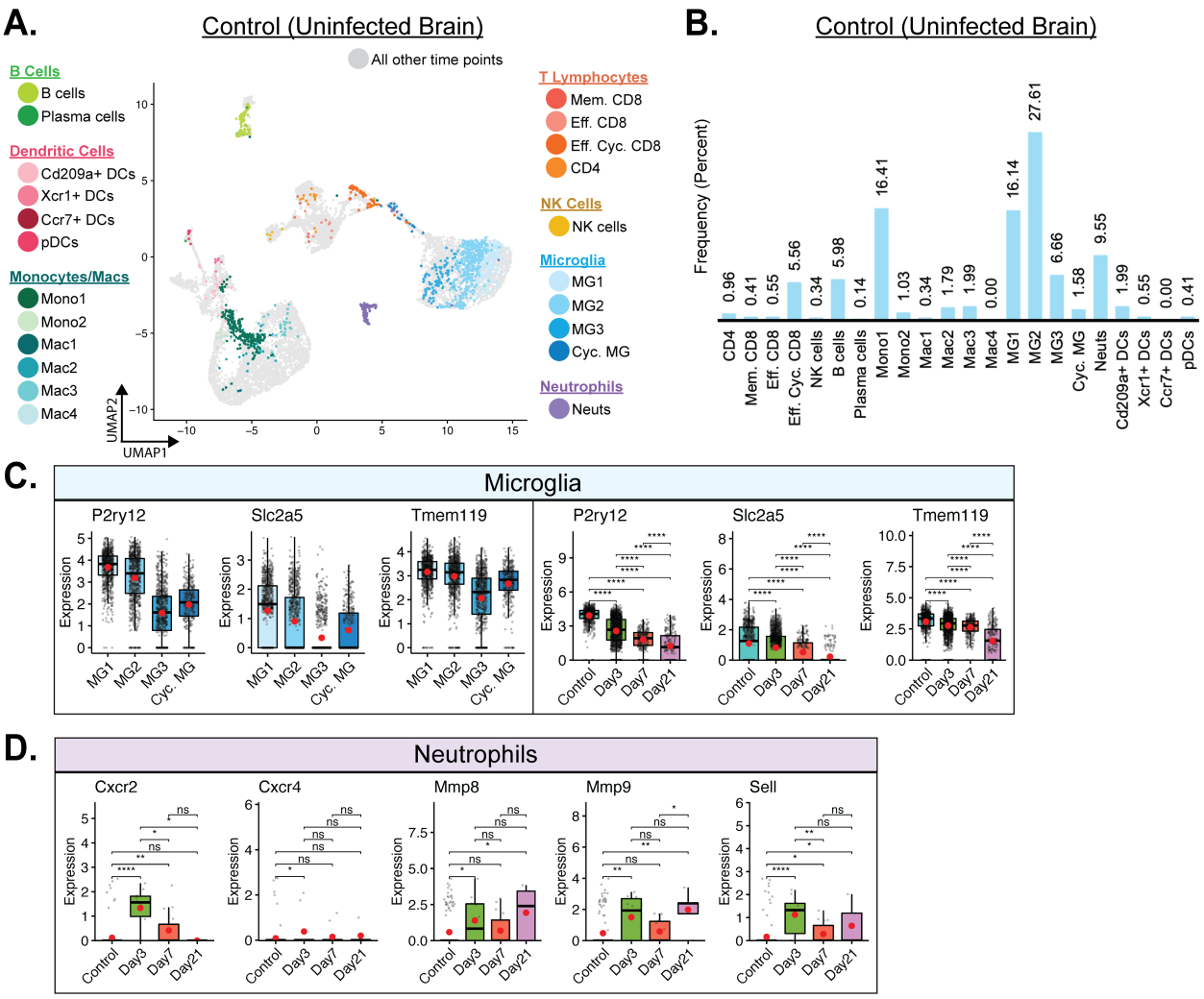

Figure 4: Immune landscape in the uninfected CNS. (**A**) UMAP cells within clusters exclusively from uninfected control brains. (**B**) Bar graph showing frequency of cell clusters within the brains of uninfected mice. Microglia are the dominant cell types enriched within uninfected brains, followed by the monocyte subpopulation Mono1 and neutrophils. (**C**) Expression of *P2ry12*, *Slc2a5*, and *Tmem119* transcripts by microglia (MG). Temporal analysis represents aggregate data from subsets. (**D**) Temporal analysis of expression of transcripts encoding CXCR2/4 (*Cxcr2/Cxcr4*), MMP-8/9 (*Mmp8*, *Mmp9*), and L-Selectin (CD62L, *Sell*) that are indicative of neutrophil activation. Transcript levels are elevated in defined times post-infection with JHMV. For data in ***C-D***, normalized expression values were used and random noise was added to show the distribution of data points. The box plots show interquartile range and the median value (bold horizontal bar). Average expression value per sample is indicated by the red dots. Wilcoxon's test was used for statistical analysis. ns, not significant; *p≤ 0.05; ** p≤ 0.01; ****p≤ 0.0001

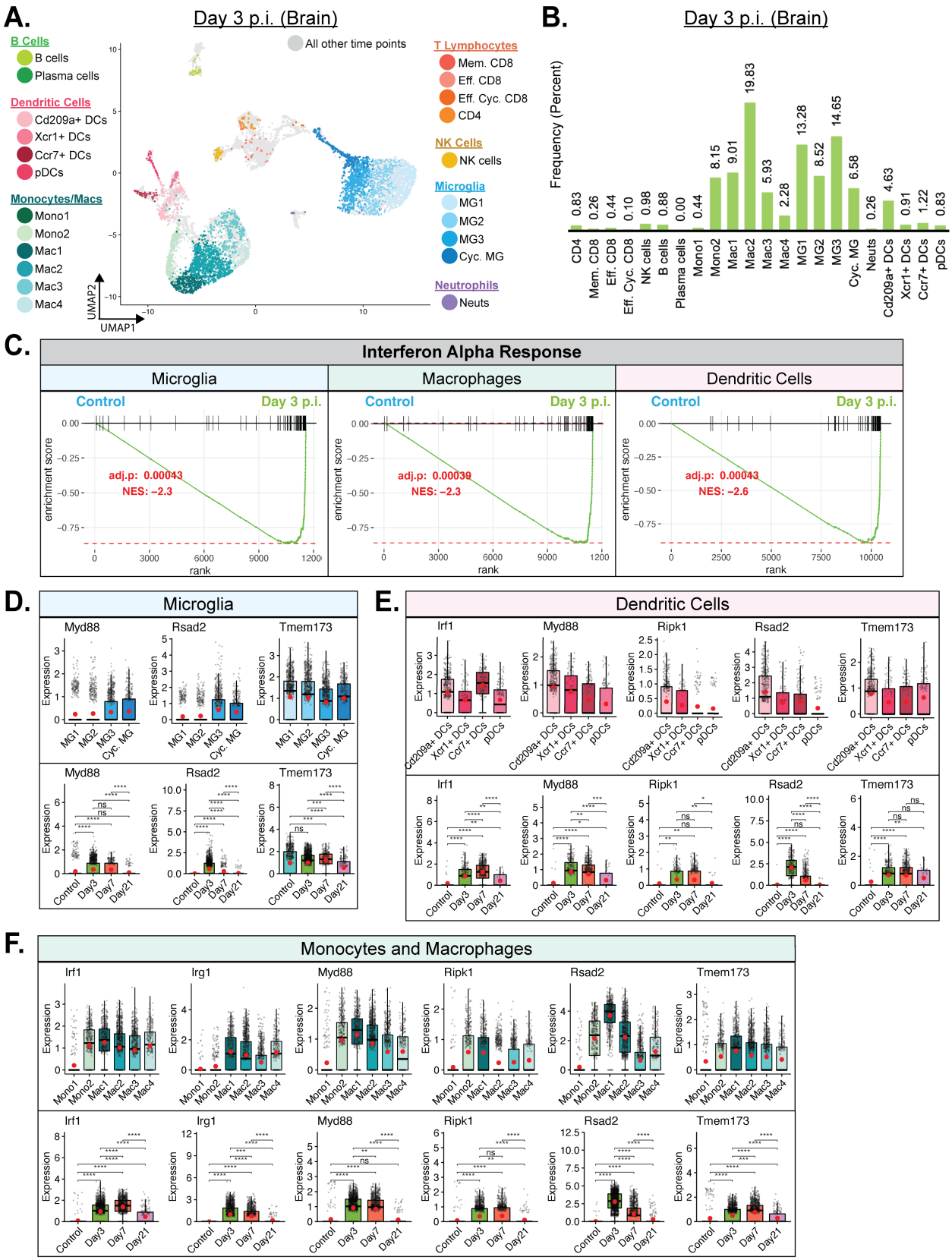
A.
Day 3 p.i. (Brain)
All other time points
B Cells
B cells
Plasma cells
Dendritic Cells
Cd209a+ DCs
Xcr1+ DCs
Ccr7+ DCs
pDCs
Monocytes/Macs
Mono1
Mono2
Mac1
Mac2
Mac3
Mac4
T Lymphocytes
Mem. CD8
Eff. CD8
Eff. Cyc. CD8
CD4
NK Cells
NK cells
Microglia
MG1
MG2
MG3
Cyc. MG
Neutrophils
Neuts
UMAP1
UMAP2
B.
Day 3 p.i. (Brain)
Frequency (Percent)
0.83
0.26
0.44
0.10
0.98
0.88
0.00
0.44
8.15
9.01
19.83
5.93
2.28
13.28
8.52
14.65
6.58
0.26
4.63
0.91
1.22
0.83
CD4
Mem. CD8
Eff. CD8
Eff. Cyc. CD8
NK cells
B cells
Plasma cells
Mono1
Mono2
Mac1
Mac2
Mac3
Mac4
MG1
MG2
MG3
Cyc. MG
Neuts
Cd209a+ DCs
Xcr1+ DCs
Ccr7+ DCs
pDCs
C.
Interferon Alpha Response
Microglia
Macrophages
Dendritic Cells
Control
Day 3 p.i.
enrichment score
adj.p: 0.00043
NES: −2.3
adj.p: 0.00039
NES: −2.3
adj.p: 0.00043
NES: −2.6
rank
D.
Microglia
Myd88
Rsad2
Tmem173
Expression
MG1
MG2
MG3
Cyc. MG
Control
Day3
Day7
Day21
E.
Dendritic Cells
Irf1
Myd88
Ripk1
Rsad2
Tmem173
Cd209a+ DCs
Xcr1+ DCs
Ccr7+ DCs
pDCs
F.
Monocytes and Macrophages
Irf1
Irg1
Myd88
Ripk1
Rsad2
Tmem173
Mono1
Mono2
Mac1
Mac2
Mac3
Mac4

Figure 5: Innate immune response following JHMV infection of the CNS. (**A**) UMAP cells within clusters exclusively from brains at day 3 p.i. with JHMV. (**B**) Bar graph showing frequency of cells from a cluster within the brains of mice 3 days post-infection (p.i.) with JHMV. Both macrophages and microglia are the main cell types enriched at day 3 p.i. (**C**) Gene set enrichment analysis (GSEA) for IFN-α responses in microglia, macrophages, and dendritic cells at day 3 p.i. from brains of JHMV-infected mice. Area under the curve represents enrichment of response genes. Normalized enrichment scores and *p* values shown. (**D**) Data showing expression of *Myd88*, *Rsad2*, and *Tmem173* transcripts in microglia subpopulations as well as overall temporal expression at defined times p.i. with JHMV (**E**) Expression of *Irf1*, *Irg1*, *Myd88*, *Ripk1*, *Rsad2* and *Tmem173* transcripts in monocyte (monos) and macrophage (macs) subpopulations in response to JHMV infection. (**F**) Dendritic cell (DC) subpopulations expression of *Irf1*, *Myd88*, *Ripk1*, *Rsad2*, and *Tmem173* following JHMV infection. Normalized expression values were used and random noise was added. Box plots show interquartile range, median value (bold horizontal bar) and average expression value per sample (red dots). Wilcoxon's test was used for statistical analysis. ns, not significant; *p≤ 0.05; ** p≤ 0.01; ***p≤ 0.001; ****p≤ 0.0001

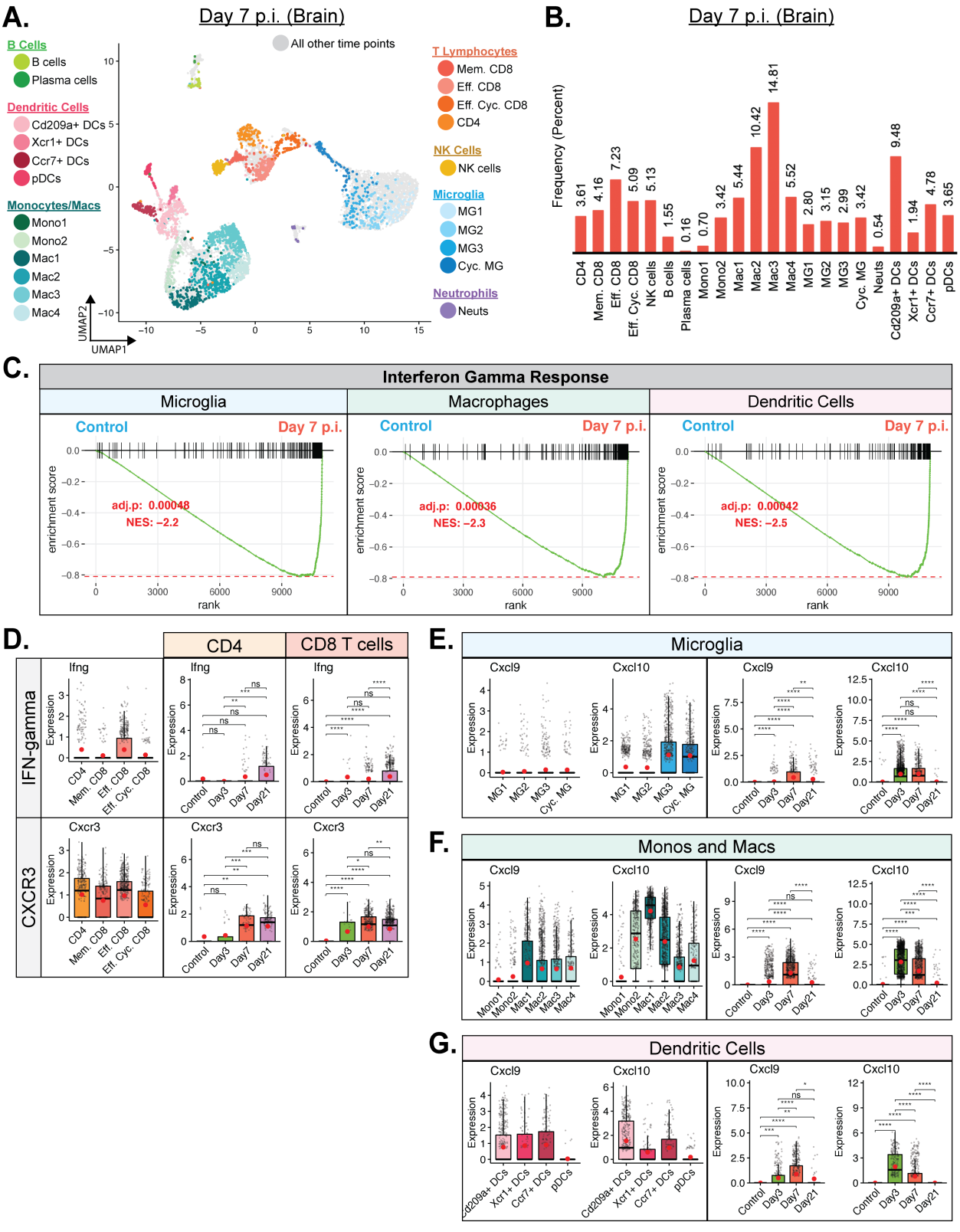
A.
Day 7 p.i. (Brain)
All other time points
B Cells
B cells
Plasma cells
Dendritic Cells
Cd209a+ DCs
Xcr1+ DCs
Ccr7+ DCs
pDCs
Monocytes/Macs
Mono1
Mono2
Mac1
Mac2
Mac3
Mac4
T Lymphocytes
Mem. CD8
Eff. CD8
Eff. Cyc. CD8
CD4
NK Cells
NK cells
Microglia
MG1
MG2
MG3
Cyc. MG
Neutrophils
Neuts
UMAP1
UMAP2
B.
Day 7 p.i. (Brain)
Frequency (Percent)
3.61
4.16
7.23
5.09
5.13
1.55
0.16
0.70
3.42
5.44
10.42
14.81
5.52
2.80
3.15
2.99
3.42
0.54
9.48
1.94
4.78
3.65
CD4
Mem. CD8
Eff. CD8
Eff. Cyc. CD8
NK cells
B cells
Plasma cells
Mono1
Mono2
Mac1
Mac2
Mac3
Mac4
MG1
MG2
MG3
Cyc. MG
Neuts
Cd209a+ DCs
Xcr1+ DCs
Ccr7+ DCs
pDCs
C.
Interferon Gamma Response
Microglia
Macrophages
Dendritic Cells
Control
Day 7 p.i.
enrichment score
adj.p: 0.00048
NES: −2.2
adj.p: 0.00036
NES: −2.3
adj.p: 0.00042
NES: −2.5
rank
D.
CD4
CD8 T cells
IFN-gamma
CXCR3
Ifng
Cxcr3
Expression
CD4
Mem. CD8
Eff. CD8
Eff. Cyc. CD8
Control
Day3
Day7
Day21
E.
Microglia
Cxcl9
Cxcl10
MG1
MG2
MG3
Cyc. MG
F.
Monos and Macs
Mono1
Mono2
Mac1
Mac2
Mac3
Mac4
G.
Dendritic Cells
Cd209a+ DCs
Xcr1+ DCs
Ccr7+ DCs
pDCs

Figure 6: T cell infiltration into CNS correlates with enriched IFN-γ response. (**A**) UMAP showing cells within clusters exclusively from brains at day 7 p.i. with JHMV. (**B**) Bar graph showing frequency of cells from a cluster within the brains of mice 7 days post-infection (p.i.) with JHMV. By day 7 p.i., there is an increase in T cell populations as well as macrophage and dendritic cell (DC) subsets. (**C**) Gene set enrichment analysis (GSEA) for IFN-γ responses in microglia, macrophages, and dendritic cells at day 7 p.i. from brains of JHMV-infected mice. Area under the curve represents enrichment of response genes. Normalized enrichment scores and *p* values shown. (**D**) Expression of *Ifng* and *Cxcr3* transcripts by infiltrating T cell populations. Expression of *Cxcl9* and *Cxcl10* transcripts in (**E**) microglia (MG), (**F**) monocytes (Mono) and macrophage (Mac) subsets, and (**G**) DC subsets. Temporal analysis represents aggregate data from corresponding cell subsets. For data ***D-G***, normalized expression values were used and random noise was added. Box plots show interquartile range, median value (bold horizontal bar) and average expression value per sample (red dots). Wilcoxon's test was used for statistical analysis. ns, not significant; *p≤ 0.05; ** p≤ 0.01; ***p≤ 0.001; ****p≤ 0.0001

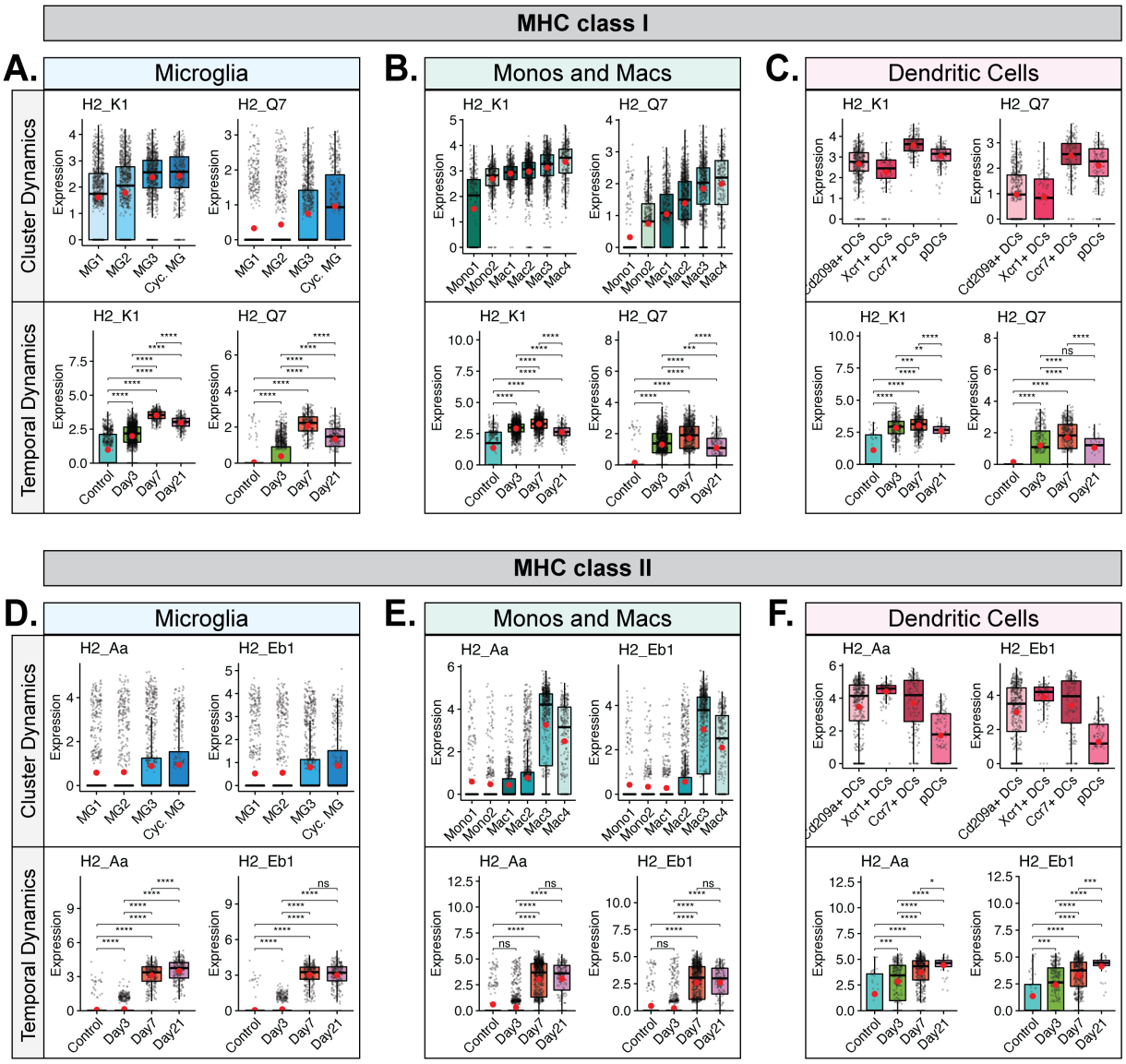

Figure 7: MHC and T cell inhibitor expression in microglia, monocytes/macrophages and dendritic cells. Box plots showing expression of MHC class I-associated genes *H2-K1* and *H2-Q7* in subpopulations of (**A**) microglia, (**B**) monocyte and macrophage, and (**C**) dendritic cells. Expression of MHC class II-associated genes *H2-Aa* and *H2-Eb1* in subpopulations of (**D**) microglia, (**E**) monocyte and macrophage, and (**F**) dendritic cell subpopulations. In ***A-F***, the top row demonstrates Cluster Dynamics and displays the aggregate data from all times points with regards to expression in subpopulations of cells, while the bottom row demonstrates Temporal Dynamics and shows overall expression of transcripts from the combined corresponding cell subtypes at defined times post-infection. Normalized expression values were used and random noise was added. Box plots show interquartile range, median value (bold horizontal bar) and average expression value per sample (red dots). Wilcoxon test was used for statistical analysis. ns, not significant; *p≤ 0.05; ** p≤ 0.01; ***p≤ 0.001; ****p≤ 0.0001

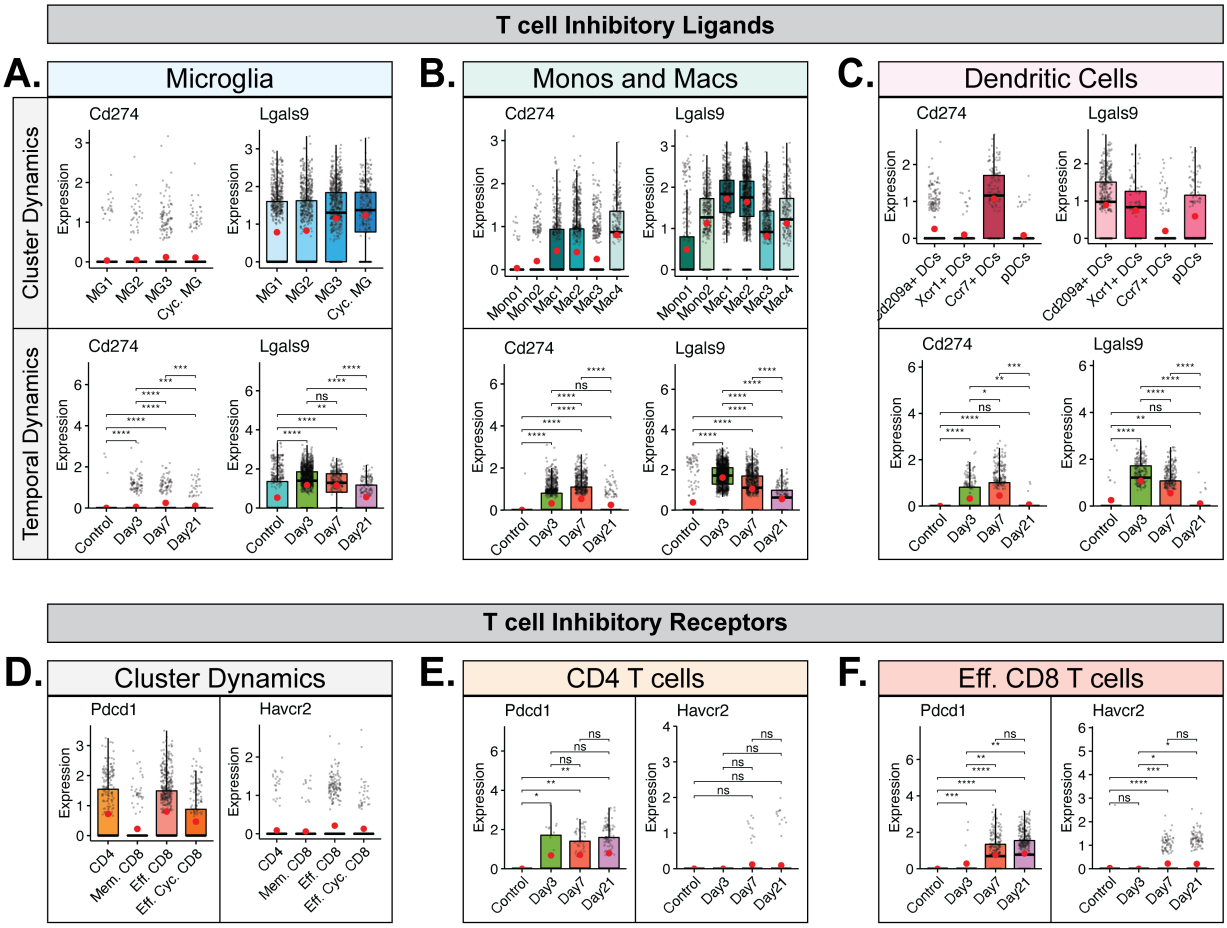

Figure 8: Expression of checkpoint inhibitor receptors and ligands in T cell populations and antigen presenting cells. Box plots showing expression of transcripts *Cd274* and *Lgals9* encoding T cell inhibitory ligands PD-L1 and Galectin-9 in subpopulations of (**A**) microglia, (**B**) monocyte and macrophage, and (**C**) dendritic cells. In ***A-C***, the top row demonstrates Cluster Dynamics and display the aggregate data from all times points with regards to expression in subpopulations of cells, while the bottom row demonstrates Temporal Dynamics and shows overall expression of transcripts from the combined corresponding cell subtypes at defined times post-infection. ***D-F*** shows expression of transcripts encoding T cell inhibitory receptors PD-1 (*Pdcd1*) and TIM-3 (*Havcr2*) in subpopulations of T cells. (**D**) Cluster Dynamics of PD-1 and TIM-3 expression show the aggregate data from all times points with regards to expression in subpopulations of T cells. Temporal analysis of PD-1 and TIM-3 transcript expression are shown in (**E**) $CD4^+$ T cells and (**F**) effector $CD8^+$ T cells (includes Eff. CD8 and Eff. Cyc. CD8 clusters). Normalized expression values were used and random noise was added. Box plots show interquartile range, median value (bold horizontal bar) and average expression value per sample (red dots). Wilcoxon test was used for statistical analysis. ns, not significant; *p≤ 0.05; ** p≤ 0.01; ***p≤ 0.001; ****p≤ 0.0001

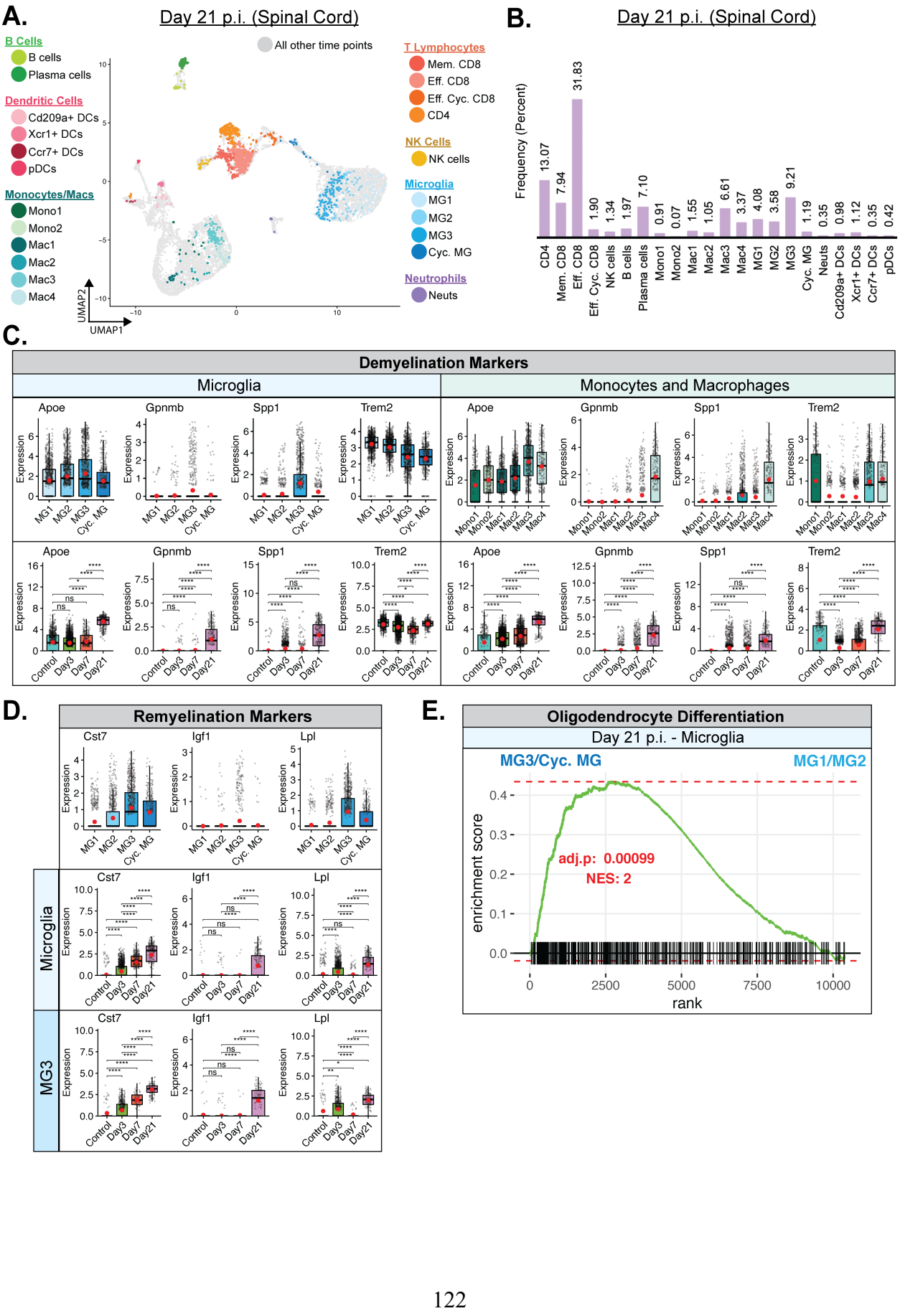
A.
Day 21 p.i. (Spinal Cord)
All other time points
B Cells
B cells
Plasma cells
Dendritic Cells
Cd209a+ DCs
Xcr1+ DCs
Ccr7+ DCs
pDCs
Monocytes/Macs
Mono1
Mono2
Mac1
Mac2
Mac3
Mac4
T Lymphocytes
Mem. CD8
Eff. CD8
Eff. Cyc. CD8
CD4
NK Cells
NK cells
Microglia
MG1
MG2
MG3
Cyc. MG
Neutrophils
Neuts
UMAP1
UMAP2
B.
Day 21 p.i. (Spinal Cord)
Frequency (Percent)
13.07
7.94
31.83
1.90
1.34
1.97
7.10
0.91
0.07
1.55
1.05
6.61
3.37
4.08
3.58
9.21
1.19
0.35
0.98
1.12
0.35
0.42
CD4
Mem. CD8
Eff. CD8
Eff. Cyc. CD8
NK cells
B cells
Plasma cells
Mono1
Mono2
Mac1
Mac2
Mac3
Mac4
MG1
MG2
MG3
Cyc. MG
Neuts
Cd209a+ DCs
Xcr1+ DCs
Ccr7+ DCs
pDCs
C.
Demyelination Markers
Microglia
Monocytes and Macrophages
Apoe
Gpnmb
Spp1
Trem2
Expression
MG1
MG2
MG3
Cyc. MG
Mono1
Mono2
Mac1
Mac2
Mac3
Mac4
Control
Day3
Day7
Day21
D.
Remyelination Markers
Cst7
Igf1
Lpl
Microglia
MG3
E.
Oligodendrocyte Differentiation
Day 21 p.i. - Microglia
MG3/Cyc. MG
MG1/MG2
adj.p: 0.00099
NES: 2
enrichment score
rank

Figure 9: Microglia contribute to T cell and macrophage-mediated chronic demyelination and promote remyelination. (**A**) UMAP showing cells within clusters exclusively from spinal cords at day 21 p.i. with JHMV. (**B**) Bar graph showing frequency of cells from a cluster within the spinal cords of mice at day 21 post-infection (p.i.) with JHMV. By day 21 p.i., there is an increase in T cell and populations and plasma cells as well as specific macrophage and microglia subsets. (**C**) Expression of transcripts *Apoe*, *Gpnmb*, *Spp1* and *Trem2* that are associated with demyelination are elevated in spinal cords at day 21 p.i. in specific subpopulations of microglia and macrophages. (**D**) Expression of remyelination markers *Cst7*, *Igf1* and *Lpl* are also increased in specific subpopulations of microglia in spinal cords at day 21 p.i. with JHMV. For data *C-D*, temporal analysis represents aggregate data from subsets. Normalized expression values were used and random noise was added. Box plots show interquartile range, median value (bold horizontal bar) and average expression value per sample (red dots). Wilcoxon's test was used for statistical analysis. (**E**) Gene set enrichment analysis (GSEA) for genes involved in promoting Oligodendrocyte Differentiation, comparing aggregated microglia subpopulations MG3 and Cycling MG with MG1 and MG2 at day 21 p.i. from spinal cords of JHMV-infected mice. Area under the curve represents enrichment of involved genes. Normalized enrichment scores and *p* values are shown. ns, not significant; *$p \leq 0.05$; ** $p \leq 0.01$; ****$p \leq 0.0001$

Chapter 3

MAC2 IS A LONG-LASTING MARKER OF PERIPHERAL CELL INFILTRATES INTO THE MOUSE CNS AFTER BONE MARROW TRANSPLANTATION AND CORONAVIRUS INFECTION

Glia, 2022: 1-17

MAC2 is a long-lasting marker of peripheral cell infiltrates into the mouse CNS after bone marrow transplantation and coronavirus infection

Lindsay A. Hohsfield[1], Kate Inman Tsourmas[1], Yasamine Ghorbanian[2,3], Amber R. Syage[1], Sung Jin Kim[1], Yuting Cheng[1], Susana Furman[1], Matthew A. Inlay[2,3], Thomas E. Lane[1]* and Kim N. Green[1]*

[1]Department of Neurobiology and Behavior, University of California, Irvine, CA 92697, USA

[2]Sue and Bill Gross Stem Cell Research Center, University of California, Irvine, CA 92697, USA

[3]Department of Molecular Biology and Biochemistry, University of California, Irvine, CA 92697, USA

Correspondence

Kim N. Green, Ph.D.

3208 Biological Sciences III, University of California, Irvine, CA 92697-4545, USA.

Email: kngreen@uci.edu

Thomas E. Lane, Ph.D.

Department of Neurobiology & Behavior, School of Biological Sciences, University of California, Irvine, CA 92697-4545, USA.

Email: tlane@uci.edu

Funding information

K.N.G was supported by the National Institutes of Health (NIH) under awards: R01NS083801 (NINDS), R01AG056768 (NIA), and P50AG016573 (NIA). L.A.H. was supported by the Alzheimer's Association Research Fellowship (AARF-16-442762). T.E.L. was supported by the National Institutes of Health (NIH) under awards: R01NS041249 (NINDS) and R35NS116835 (NINDS), the National Multiple Sclerosis Society (NMSS) Collaborative Research Center grant CA-1607-25040 and The Ray and Tye Noorda Foundation. Y.G. was supported by NIH T32 training grant (NS082174).

ABSTRACT

Microglia are the primary resident myeloid cells of the brain responsible for maintaining homeostasis and protecting the central nervous system (CNS) from damage and infection. Monocytes and monocyte-derived macrophages arising from the periphery have also been implicated in CNS pathologies, however, distinguishing between different myeloid cell populations in the CNS has been difficult. Here, we set out to develop a reliable histological marker that can assess distinct myeloid cell heterogeneity and functional contributions, particularly in the context of disease and/or neuroinflammation. scRNAseq from brains of mice infected with the neurotropic JHM strain of the mouse hepatitis virus (JHMV), a mouse coronavirus, revealed that *Lgals3* is highly upregulated in monocyte and macrophage populations, but not in microglia. Subsequent immunostaining for galectin-3 (encoded by *Lgals3*), also referred to as MAC2, highlighted the high expression levels of MAC2 protein in infiltrating myeloid cells in JHMV-infected and bone marrow (BM) chimeric mice, in stark contrast to microglia, which expressed little to no staining in these models. Expression of MAC2 was found even 6-10 months following BM-derived cell infiltration into the CNS. We also demonstrate that MAC2 is not a specific label for plaque-associated microglia in the 5xFAD mouse model, but only appears in a distinct subset of these cells in the presence of JHMV infection or during aging. Our data suggest that MAC2 can serve as a reliable and long-lasting histological marker for monocyte/macrophages in the brain, identifying an accessible approach to distinguishing resident microglia from infiltrating cells in the CNS under certain conditions.

Keywords

Alzheimer's disease, brain, Lgals3, MAC2, microglia, monocytes, mouse coronavirus

INTRODUCTION

Myeloid cells of the innate immune system are comprised of two distinct populations: tissue-resident and monocyte-derived macrophages. In the central nervous system (CNS), the macrophage compartment consists of parenchymal macrophages, known as microglia, and non-parenchymal macrophages, known as CNS (or border)-associated macrophages (CAMs or BAMs) (Katrin Kierdorf, Masuda, Jordão, & Prinz, 2019; Mrdjen et al., 2018). Microglia reside in the brain parenchyma spatially arranged in discrete non-overlapping territories, while BAMs reside within specialized CNS border interfaces that separate the CNS from the periphery, including the choroid plexus, meninges, and perivascular spaces. Recent studies indicate that microglia and non-parenchymal macrophages represent ontologically, phenotypically, and functionally distinct cell populations (Jordao et al., 2019; Masuda et al., 2019; Mrdjen et al., 2018; Munro et al., 2020; Anat Shemer et al., 2018; Utz et al., 2020; Van Hove et al., 2019); however, inflammation-induced phenotypic changes in these cells have made distinguishing and assessing different myeloid cell populations and their diverse functions during disease difficult.

In mice, studies have shown that microglia derive from erythromyeloid precursors in the yolk sac, entering the brain as primitive or pre-macrophages to colonize the CNS during embryonic development (Ginhoux et al., 2010; K. Kierdorf et al., 2013). Once the blood-brain barrier (BBB) is formed, myeloid cell infiltration into the CNS is restricted and microglial population maintenance relies on local self-proliferation without contributions from peripheral monocytes (A. Shemer, Erny, Jung, & Prinz, 2015). While studies have shown that specific BAM subsets (e.g. perivascular and leptomeningeal macrophages) also derive from the yolk sac (Gomez Perdiguero et al., 2015; Utz et al., 2020), it appears that choroid plexus and dural macrophage populations can also be replenished by bone marrow (BM)-derived monocytes under steady-state conditions (Goldmann et al., 2016; Van Hove et al., 2019). Under inflammatory or disease conditions (e.g.

facial nerve axotomy, amyotrophic lateral sclerosis, experimental autoimmune encephalomyelitis), studies have shown that peripheral-derived monocytes enter the brain, but do not contribute significantly to the microglial pool unless under defined experimental circumstances (e.g. irradiation, myeloablative chemotherapy, BBB disruption) (B. Ajami, Bennett, Krieger, McNagny, & Rossi, 2011; B. Ajami, Bennett, Krieger, Tetzlaff, & Rossi, 2007; Cronk et al., 2018; Ginhoux et al., 2010; Hohsfield et al., 2020; Jordao et al., 2019; Lund et al., 2018; Mildner et al., 2007; Reed-Geaghan, Croxford, Becher, & Landreth, 2020).

Despite their distinct origins and functions, assessing the individual contributions of infiltrated myeloid cells and activated microglia remains one of the major challenges in neuroimmunology, particularly within the context of neuroinflammatory diseases (Herz, Filiano, Smith, Yogev, & Kipnis, 2017; Honarpisheh et al., 2020; Prinz & Priller, 2014). Monocytes and microglia share substantial transcriptional and phenotypic overlap. Several of the genes and proteins used to separate these two populations are not exclusively expressed but instead only relatively enriched in one population (e.g. CD45, CX3CR1, CCR2) (Haage et al., 2019; Honarpisheh et al., 2020; Ransohoff & Cardona, 2010; A. Shemer et al., 2015). Microglial-specific genes and proteins have been identified; however, microglia downregulate their homeostatic signature (e.g. *P2ry12*, *Tmem119, Sall1, Siglech*) and upregulate monocyte/macrophage-associated (e.g. *Apoe*, *Itgax*, *Lyz2*) markers during disease (M. L. Bennett et al., 2016; Butovsky et al., 2014; Buttgereit et al., 2016; Keren-Shaul et al., 2017; Konishi et al., 2017). Studies have also identified genes and proteins that are highly expressed in BM-derived myeloid cells, including brain engrafted macrophages (e.g. *Ms4a7*, *Clec12a*, *Ccr2*, *Apoe*, *CD38*, *Mrc1, Cd11a*), but many of these genes are also found in other CNS myeloid subsets or fail to label cells during immunohistochemical investigations on fixed brain sections (F. C. Bennett et al., 2018; Mrdjen et

al., 2018; Anat Shemer et al., 2018; Shukla et al., 2019). As such, there is no histological marker that can reliably identify peripheral myeloid cell infiltrates vs. activated microglia in the CNS to date.

Researchers currently utilize a number of experimental approaches to identify peripheral myeloid cells in the CNS. However, many of these paradigms pose concerning caveats. The generation of GFP BM chimeras provides labeling of BM-derived cells, but this approach involves irradiation, which can induce BBB damage and non-homeostatic peripheral contributions to the microglial niche (B. Ajami et al., 2007; Mildner et al., 2007). Parabiosis avoids these irradiation-induced effects but can involve complicated surgery and result in host-graft rejection. Despite the usefulness of mice genetically labeled for monocyte markers (e.g. *Ccr2*^{RFP} mice), studies have shown that these cells may downregulate CCR2 as they mature/differentiate and enter the brain (Gschwandtner, Derler, & Midwood, 2019; Saederup et al., 2010). Furthermore, these mice are haploinsufficient for CCR2, a critical factor for monocyte migration and entry into the CNS (Chu et al., 2014). Fate mapping techniques have allowed for unprecedented exploration and manipulation of monocytes, but again these techniques are not without their limitations (H.-R. Chen et al., 2020; Liu et al., 2019). The use of lineage tracing from BM-expressed drivers involves the use of tamoxifen, which has recently been identified as a neutral agonist in macrophage lineage tracing studies. A recent study has shown that tamoxifen treatment of pregnant mice induces a significant expansion of the embryonic macrophage population (Rojo, Sauter, Lefevre, Hume, & Pridans, 2018).

Given the lack of reliable markers that can distinguish between monocyte-derived cells and activated microglia, we set out to develop a new histological tool for peripheral myeloid cell studies in the mouse CNS. To accomplish this, we employed infection of C57BL/6 mice with the

neuroadapted JHM strain of mouse hepatitis virus (JHMV), a mouse coronavirus and a robust mouse model for monocyte infiltration in the CNS. Studies indicate that JHMV-infected mice exhibit substantial infiltration by monocytes along with other peripheral immune cells (Held, Chen, Kuziel, Rollins, & Lane, 2004; Savarin, Stohlman, Atkinson, Ransohoff, & Bergmann, 2010). We recently employed single-cell RNA sequencing (scRNAseq) on flow-sorted CD45+ cells infiltrating into the CNS of JHMV-infected mice to better understand the immunological landscape at defined times following infection with a neurotropic virus (Syage et al., 2020). Using this approach, we identified *Lgals3* as a highly enriched gene for monocytes. We then validated the expression of this marker at the protein level via galectin-3/MAC2 staining in BM-derived myeloid cells, and its utility in distinguishing between monocyte and microglia populations in response to JHMV infection as well as in young transgenic mouse models of Alzheimer's disease (AD). This approach not only provides a reliable marker for peripheral-derived cells, but also eliminates the necessity of complex transgenic mouse lines to discern myeloid cell populations, broadening the study of myeloid cell spatial and phenotypic profiles during disease and neuroinflammation.

MATERIALS AND METHODS

Compounds. Pexidartinib (PLX3397) was provided by Plexxikon Inc. and formulated in AIN-76A standard chow at a dose of 600 ppm by Research Diets Inc.

Mice. All mice were obtained from The Jackson Laboratory. For transplant studies, bone marrow cells were isolated from CAG-EGFP mice (Stock No. 006567). Male and female 5xFAD mice were obtained from MMRRC-JAX (Stock No. 34848) and have been previously described in detail (Oakley et al., 2006). For 5xFAD genotyping, the primer sequences used were PS1 Forward 5′ - AAT AGA GAA CGG CAG GAG CA – 3′ and PS1 Reverse 5′ - GCC ATG AGG GCA CTA ATC AT – 3′. All other mice were male C57BL/6 (000664) mice. Animals were housed with open access to food and water under 12h/12h light-dark cycles.

Animal Treatments. All rodent experiments were performed in accordance with animal protocols approved by the Institutional Animal Care and Use Committee at the University of California, Irvine (UCI). *JHMV infection*: Six-week-old C57BL/6 mice (males and females) and four-month-old 5xFAD mice (males and females) were infected intracranially (i.c.) with 200-250 PFU of JHMV in 30 μl of sterile Hanks balanced sterile solution (HBSS); control mice received an i.c. injection of HBSS. JHMV-infected C57BL/6 mice were sacrificed at 7, 14, and 21 days post-infection (d.p.i.) and brains and spinal cords isolated to assess viral titers and perform immunohistochemical staining to assess monocyte infiltration. JHMV-infected 5xFAD mice were sacrificed at 10 d.p.i. and brains removed to determine viral titers, evaluate β-amyloid (Aβ) burden and perform immunohistochemical staining to assess monocyte infiltration. scRNAseq was conducted on male animals. *Microglial depletion:* Mice were administered ad libitum with

PLX3397 at a dosage of 600 ppm (to eliminate microglia) or vehicle (control) for 14d. *Bone marrow transplant:* Tissue from a previous study by Hohsfield et. al were employed for analyses performed in the present report (Hohsfield et al., 2020). In brief, C57BL/6 mice were anesthetized with isoflurane and then irradiated with 1000 cGy (whole body) and reconstituted via retroorbital injection with 2 x 10^6 whole BM cells from CAG-EGFP mice. Blood was measured at 4, 8, and/or 12 weeks post transplantation to track granulocyte chimerism. At time of sacrifice, mice were euthanized, and BM was harvested and analyzed by flow cytometry for HSC chimerism. This established an average percent chimerism of >95% in whole body irradiated mice as previously reported (Hohsfield et al., 2020). *Tissue collection:* Following treatments, adult mice were sacrificed via carbon dioxide inhalation and perfused transcardially with 1X PBS. Brains were extracted and dissected down the midline, with one half flash-frozen for subsequent RNA and protein analyses, and the other half drop-fixed in 4% paraformaldehyde. Fixed brains were cryopreserved in PBS + 0.05% sodium azide + 30% sucrose, frozen, and sectioned at 40 □m on a Leica SM2000 R sliding microtome for subsequent immunohistochemical analyses. For brains and spinal cords from JHMV-infected mice, half brains dissected down the midline and the length of spinal cord extending from thoracic vertebrate 6-10 was cryoprotected in 30% sucrose, cut into 1-mm transverse blocks and processed to preserve the craniocaudal orientation and subsequently embedded in O.C.T. (VWR, Radnor, PA, USA). For spinal cords, eight micron (mm)-thick coronal sections were cut and sections were stained following standard immunofluorescence protocols; for brains, eight micron sagittal sections were cut(Blanc et al., 2015; Dickey, Worne, Glover, Lane, & O'Connell, 2016; Marro, Grist, & Lane, 2016).

Histology and confocal microscopy. Fluorescent immunolabeling followed a standard indirect technique as described previously (Elmore et al., 2014). Brain sections were stained with antibodies against the following defined antigens: ionized calcium binding adaptor molecule 1 (IBA1; 1:1000; 019-19741, Wako and ab5076, Abcam) and MAC2/Galectin-3 (1:500; CL8942AP Cedarlane). For DAPI staining, mounted brain sections were cover-slipped using Fluoromount-G with DAPI (00-4959-52, Invitrogen). Amylo-Glo (TR-300-AG; Biosensis) staining was performed according to the manufacturer's instructions. High resolution fluorescent images were obtained using a Leica TCS SPE-II confocal microscope and LAS-X software. For confocal imaging, one field of view (FOV) per brain region was captured per mouse unless otherwise indicated. For whole brain stitches, automated slide scanning was performed using a Zeiss AxioScan.Z1 equipped with a Colibri camera and Zen AxioScan 2.3 software. Microglial morphology was determined using the filaments module in Bitplane Imaris 7.5, as described previously (Elmore, Lee, West, & Green, 2015). Cell quantities were determined using the spots module in Imaris. MAC1+ IBA1+ staining was quantified by using a standardized algorithm in the Surfaces module in Imaris. Total IBA1+ and MAC2+IBA1+ surface area in the field of view was categorized as plaque-associated or non-plaque-associated based on proximity to plaques (plaque-associated = < 5.8 μm). Percentage of MAC2+ IBA1+ coverage was calculated by dividing MAC2+IBA1+ / total IBA1+ surface area.

Data analysis and statistics. Statistical analysis was performed with Prism Graph Pad (v.8.0.1). To compare two groups, the unpaired Student's t-test was used. To compare multiple groups, a one-way ANOVA with Tukey's posthoc test was performed. For all analyses, statistical significance was accepted at $p < 0.05$. All bar graphs are represented as means +/- SEM and

significance expressed as follows: *$p < 0.05$, **$p < 0.01$, ***$p < 0.001$. n is given as the number of mice within each group, unless otherwise indicated.

RESULTS

*Lgals3/*MAC2 distinguishes infiltrating cells from microglia in the adult CNS.

We and others have previously identified distinct transcriptional and phenotypic profiles of brain-engrafted peripherally derived myeloid cells from resident microglia in the adult mouse brain; however, these findings have yet to translate into reliable histological markers that distinguish peripheral infiltrates from their microglial counterparts in the CNS (F. C. Bennett et al., 2018; Cronk et al., 2018; Hohsfield et al., 2020; Anat Shemer et al., 2018). In this study, we explored a previously described scRNAseq data set to identify transcripts that distinguish between resident microglia and infiltrating myeloid cells (Syage et al., 2020). scRNAseq data was obtained from the JHMV mouse model which recapitulates many characteristics of human diseases associated with encephalomyelitis and demyelination (Bergmann, Lane, & Stohlman, 2006; Lampert, Sims, & Kniazeff, 1973; Lane & Buchmeier, 1997; Savarin et al., 2010; Weiner, 1973). In brief, intracranial inoculation of susceptible C57BL/6 mice with the neuroadapted JHMV, a member of the Coronaviridae family, results in an acute encephalomyelitis characterized by wide-spread viral replication in astrocytes, microglia, and oligodendroglia with relative sparing of neurons (Bergmann et al., 2006; Lane & Hosking, 2010). In response to JHMV infection, proinflammatory cytokines and chemokines are expressed by activated microglia and astrocytes, resulting in an orchestrated inflammatory response consisting of neutrophils, monocytes/macrophages, and activated virus-specific CD4+ and CD8+ T cells (Bergmann et al., 2006; Hosking & Lane, 2010; Lane & Hosking, 2010).

We recently performed a detailed analysis of immune cell infiltration into the CNS of JHMV-infected mice through scRNAseq, which highlighted the heterogeneity of the immune response following infection with a neurotropic virus, in addition to confirming that monocytes

and neutrophils are the prominent cells entering the CNS (Syage et al., 2020). Here, we employed the scRNAseq data set to identify differentially expressed genes between monocyte/macrophage cells compared to microglia. *Lgals3* transcripts were enriched in infiltrating monocytes and macrophages, and lowly expressed in microglia (specifically in MG3 and Cyc. MG clusters) even under JHMV/inflammatory conditions (**Figure 1a-d**). *Lgals3* encodes galectin-3 (also known as MAC2), which is a member of the lectin family involved in monocyte/macrophage chemoattraction and activation (MacKinnon et al., 2008). Since low levels of *Lgals3* transcripts were detected in some microglia clusters, we next evaluated whether galectin-3/MAC2 expression was present in both monocyte/macrophage and distinct microglial populations. To assess this, we subsequently infected a separate cohort of C57BL/6 mice with JHMV and evaluated the ability of galectin-3/MAC2 to distinguish distinct myeloid cell populations. Histological analyses for MAC2 in non-infected brain sections revealed no MAC2 staining in IBA1+ cells, except in areas associated with ventricles and choroid plexus (**Figure 1e-f**). Analysis of JHMV-infected brain and spinal cord sections showed a clear population of IBA1+/MAC2+ cells that were not present in uninfected animals. IBA1+/MAC2+ cells appear spatially and morphologically distinct from IBA1+/MAC2- cells, which resemble microglia and reside in parenchymal areas (**Figure 1e, f, i**). In the brain, IBA1+/MAC2+ cells accumulated in the brainstem (medulla, pons, midbrain, thalamus, and hypothalamus), cerebellum (near the fourth ventricle), and in white matter tracts (corpus callosum), whereas little to no deposition was observed in the cerebrum at any timepoint (hippocampus, cortex, striatum) with the exception of sites near the lateral ventricle and/or white matter tracts (**Figure 1e, f, h**). Many areas of high MAC2+ cell accumulation appear to be in or near white matter areas (**Figure 1f**). IBA1+/MAC2+ cells appear less ramified with retracted/thickened processes and enlarged cell somas compared to IBA1+/MAC2- cells (**Figure**

1f). IBA1+/MAC2+ cell infiltration in the brain appears to peak around 14 d.p.i (**Figure 1e, g, h**); however, the brainstem still shows prominent accumulation at 21 d.p.i. In the spinal cord, IBA1+/MAC2+ cell infiltration peaked at 14 d.p.i. and declined by 21 d.p.i. with cells enriched in white matter tracts within ventral funiculus (**Figure 1i, j**).

MAC2 is a specific and long-lasting marker for bone marrow-derived infiltrating cells.

Beyond acute CNS infiltration, current monocyte markers make it difficult to distinguish between peripheral and resident myeloid cells. CCR2 and CD14 are downregulated following monocyte differentiation into macrophages (Fantuzzi et al., 1999; Steinbach & Thiele, 1994; Wong et al., 1997) and studies using $CCR2^{RFP}$ knock-in mice report that $CCR2^{RFP}$+ cells are not detected in the CNS, even under inflammatory conditions (Saederup et al., 2010), meaning that these markers fail to label monocyte-derived cells past a few days following engraftment in the CNS. Given these difficulties, we next sought to examine whether MAC2 could serve as 1) a marker for BM-derived cells and 2) a long-lasting marker for these cells once engrafted in the brain.

To accomplish this, we utilized BM GFP chimeric mice to assess the ability of this monocyte/macrophage marker candidate to label infiltrating BM-derived cells. CAG-GFP donor BM was administered (via retro-orbital injection) to whole body (WB, with >95% chimerism) irradiated mice and allowed to recover for ~10 months, resulting in long-term GFP chimeric mice. In this model, GFP+ expression indicates that cells derive from the BM. Following recovery, we explored co-localization of MAC2 expression in GFP+ cells in the adult mouse brains of long-term GFP BM chimeric mice and long-term GFP BM chimeric mice that underwent colony-stimulating factor 1 receptor inhibitor (CSF1Ri)-induced myeloid cell depletion and repopulation (~6 months following CSF1Ri treatment and CNS engraftment) (**Figure 2a**). In a previous study,

we demonstrated that irradiation/BM transplant followed by CSF1Ri treatment results in substantial replacement of the microglial compartment with BM-derived monocytes (Hohsfield et al., 2020), providing a model to evaluate long-term and brain-wide BM-derived monocyte/macrophage engraftment.

Ten-month WB irradiated mice exhibited ~20% infiltration of GFP+ cells, with prominent deposition observed in areas near the lateral ventricle/subventricular zone (SVZ), medial habenula (MHb), internal capsule (IC), and meninges (**Figure 2a, b**). In accordance with our prior data, we observed that these infiltrating GFP+ cells express little to no levels of P2RY12 and TMEM119, two canonical microglial markers (data not shown). Ten-month WB irradiated mice treated with CSF1Ri exhibited 79-96% (mean = 86%) engraftment of GFP+ cells, seen throughout the brain parenchyma (**Figure 2a, d, h-j**). In aged-matched controls, no GFP+ cell deposition is visible (**Figure 2b, h-j**). Notably, we found that MAC2+ staining was still apparent in GFP+/IBA1+ cells, even 6 and 10 months after CNS infiltration was stimulated, while no MAC2 expression was seen in control animals or in GFP-/IBA1+ cells (**Figure 2b-g, h-j**). In 10 mo WB irradiated mice, an average of 89-96% of GFP+ cells express MAC2 near the lateral ventricle/SVZ, MHb, and IC (**Figure 2k-m**). In 10 mo WB irradiated + CSF1Ri treated mice, an average of 85-93% of GFP+ cells express of MAC2 near the lateral ventricle/SVZ, MHb, and IC (**Figure 2k-m**). It should be noted that there are lower and higher levels of MAC2+ staining in GFP+ cells in mice, which likely reflects the more recent infiltration of BM-derived cells into the parenchyma, indicating that MAC2 expression may gradually decrease over time as cells become more CNS parenchymal macrophage- or microglia-like to fill the tissue niche. Some MAC2 expression is seen in the nuclei of resident microglia, but clearly fills the cell body and processes of GFP+/IBA+ cells. Given the high level of co-expression of MAC2 in GFP BM-derived myeloid cells, these results indicate that

MAC2 can serve as a histological marker of BM-derived infiltrating cells and utilized as a potential long-lasting marker to distinguish between peripherally derived monocytes/macrophages and resident microglia.

MAC2 is not a ubiquitous marker for plaque-associated microglia during the early stages of disease in 5xFAD mice.

While we identified MAC2 as a marker for peripheral infiltrates, Lgals3 has also been reported in specific myeloid cell populations under certain conditions. For example, *Lgals3* was identified as an upregulated gene in amyloid-β (Aβ) plaque-associated microglia, also known as disease-associated microglia (DAM) or microglial neurodegenerative (MGnD) phenotype (Butovsky & Weiner, 2018; Krasemann et al., 2017), and in isolated amyloid plaque-containing microglia (Grubman et al., 2021). Moreover, galectin-3/MAC2 staining has been found in microglia in close contact with Aβ plaques in both human and mice (Boza-Serrano et al., 2019). However, it is often difficult to distinguish between monocytes/macrophages and activated microglia, as they share many morphological and gene expression similarities (M. L. Bennett et al., 2016; Butovsky et al., 2014; Buttgereit et al., 2016; Keren-Shaul et al., 2017; Konishi et al., 2017). To directly test *Lgals3*/Galectin-3 expression in the AD brain, we stained for MAC2 in 5xFAD mice, and then used JHMV infection to trigger peripheral infiltration, evaluating whether MAC2 expression is specific to plaque-associated microglia.

5xFAD mice, which express five human APP and PSEN1 transgenes with familial Alzheimer's disease mutations, display extensive extracellular plaque deposition and microgliosis (Oakley et al., 2006). In these mice, amyloid plaques begin to form around 3 months of age and exhibit significant plaque deposition and microglial activation in the cerebral cortex and brain

stem, including the thalamus, midbrain, and hindbrain, by 4 months of age (**Figure 3a**). Here, we i.c. infected 4-month-old 5xFAD mice with JHMV to stimulate monocyte infiltration into the CNS. Brain sections of uninfected and JHMV-infected mice were stained for amyloid plaques (Amylo-Glo), myeloid cells (IBA1), and MAC2. Evaluation of whole brain sagittal sections showed profound MAC2 staining in JHMV-infected 5xFAD **(Figure 3b**), but not uninfected mice (**Figure 3a**). Similar to WT JHMV-infected mice, MAC2+ cell deposition is apparent in areas near ventricles (in the cerebellum near the fourth ventricle, in tissue near the lateral ventricle) and white matter tracts (the corpus callosum, middle longitudinal fasciculus), whereas little to no MAC2 staining is present in 5xFAD controls (**Figure 3a-e**). MAC2+ cells are seen in the choroid plexus of 5xFAD controls, but they do not infiltrate into the parenchyma (**Figure 3c,e**). High resolution images show little to no MAC2+ staining in plaque-associated microglia (1.6% of MAC2 staining in plaque-associated IBA1+ cells) in uninfected 5xFAD mice (**Figure 3f-g**), and an average of 16.4% of MAC2 staining in IBA1+ cells surrounding amyloid plaques in JHMV-infected 5xFAD mice (**Figure 3h-i**). It also appears that not all plaque-associated microglia are MAC2+ nor is there an abundance of MAC2+IBA1+ in plaque-associated regions. MAC2+ staining is also present in non-plaque-associated regions in IBA1+ cells (8.7% MAC2+IBA1+ staining) in JHMV-infected mice (**Figure 3d,h-i**). These findings provide evidence that MAC2 is not a specific marker for plaque-associated microglia and is not expressed by microglia in the young non-infected 5xFAD mouse model, indicating that *Lgals3*/MAC2 expression may reflect peripheral infiltrates honing to plaques.

The effects of aging on MAC2 staining in WT and 5xFAD mice.

Transcriptional profile analysis has revealed an upregulation of *Lgals3* in microglia isolated from mouse models of neurodegenerative disease, including Alzheimer's disease and amyotrophic lateral sclerosis as well as aging, and identified *Lgals3* as a hub gene for primed microglia (Holtman et al., 2015). Safaiyan et al. recently identified white matter-associated microglia (WAM), which accumulate in white matter tracts during aging. *Lgals3* was one of 39 transcripts of the WAM signature that was identified when comparing aged white matter compared to young matter or aged gray matter myeloid cells; and the authors report expression of galectin-3 in IBA1+ cells in old but not young white matter (Safaiyan et al., 2021).

To address whether MAC2 staining also increases with aging under steady-state and diseased conditions, we next stained brain sections from 4, 8, 12, and 18 mo WT and 5xFAD mice with MAC2, IBA1, and Amylo-Glo. Again, we observe that MAC2+IBA1+ cells and staining is most apparent in the choroid plexus of WT and 5xFAD mice, regardless of age (**Figure 4 a-b**). In line with previous studies, our data shows an age-dependent increase in MAC2+IBA1+ cell accumulation in 5xFAD mice in the hippocampus, cortex, and in white matter areas (e.g. fimbria, corpus callosum) within close proximity to the lateral ventricle (**Figure 4b, c, e**). In gray matter regions, the majority of MAC2+ cells are IBA1+ plaque-associated microglia (**Figure 4b, c**). However, there appears to be a lag in the appearance of MAC2 expression and microglial/DAM activation around plaques. For example, prominent MAC2 expression in plaque-associated IBA1+ cells appear at 18 mo of age in the cortex despite the accumulation of these plaque-associated microglia at 4 mo of age (**Figure 4c**). Furthermore, the majority of IBA1+ plaque-associated cells do not express MAC2 (<20% of IBA1+ cells are MAC2+; **Figure 4e**), meaning MAC2 does not account for a significant proportion of plaque-associated cells. MAC2+IBA1+ cell deposition does

not occur in gray matter areas in the aged WT mice (**Figure 4a, d, f**); however, interestingly we do observe MAC2+IBA1+ cells present in white matter areas at 18 mo of age (**Figure 4d**). This is also true for 5xFAD mice (**Figure 4c**). Thus, it appears that MAC2 expression is not a specific response to plaques. Given the proximity of these brain regions to the lateral ventricles and the lack of MAC2 expression in the majority of plaque-associated microglia, we postulate two scenarios: 1) a specific subpopulation of activated microglia (subset of DAM and/or WAM) switch on *Lgals3* and galectin-3/MAC2 expression over time or 2) that MAC2+ cells derive from a different cell source, such as from the periphery. Since microglia and macrophages undergo rapid morphological and transcriptional transformations upon activation, reflective of the highly plastic nature of myeloid cells, defining MAC2 expression as an indicator of cell activation or peripheral infiltration remains difficult. However, given the findings in this study, specifically the spatial and temporal expression of MAC2+IBA1+ cells in areas that are closely associated with peripheral immune cell infiltration in CNS disorders, most prominently in white matter areas in multiple sclerosis, we hypothesize that MAC2 expression labels a subset of peripheral immune cells in the young adult brain that can infiltrate and engraft the brain.

DISCUSSION

Microglia and BM-derived monocytes are implicated in a number of neurological disorders (Herz et al., 2017). In AD, several genome-wide association studies have identified variants associated with myeloid cells that increase disease risk, highlighting the importance of myeloid cells and the growing need to decipher their phenotype and function during disease (Bradshaw et al., 2013; Guerreiro et al., 2013; Jonsson et al., 2013; Lambert et al., 2013). However, myeloid cells are highly dynamic cells which can be influenced at both the transcriptional and protein level by specific diseases during disease induction and progression, thus complicating the use of reliable and stable cell-specific markers and posing challenges to the functional exploration and contributions of these distinct cells. For instance, the presence of peripheral-derived myeloid cells around amyloid plaques and their contribution in AD pathology has been a long-standing question in the field with contrasting results (El Khoury et al., 2007; Hawkes & McLaurin, 2009; Jay et al., 2015; Reed-Geaghan et al., 2020; Simard, Soulet, Gowing, Julien, & Rivest, 2006).

Under steady state conditions, microglia and monocyte/macrophages populations express several overlapping surface markers, including Cd11b, F4/80, CD115 (CSF1R), and IBA1 (Gautier et al., 2012; Prinz, Priller, Sisodia, & Ransohoff, 2011). Recent gene expression studies have identified surface markers and transcription factors unique to resident microglia (e.g., P2RY12, TMEM119, SIGLEC-H, *Sall1*), but several of these markers lose their distinct homeostatic expression levels during disease/cell activation (M. L. Bennett et al., 2016; Butovsky et al., 2014; Buttgereit et al., 2016; Chen & Colonna, 2021; Keren-Shaul et al., 2017; Konishi et al., 2017). Despite the utility of previous approaches (e.g., BM chimeras, parabiosis, and mouse models of fluorescent protein expression or tamoxifen-inducible Cre-recombinase under monocyte/microglia promoters) in providing myeloid cell-specific labeling/targeting and

unprecedented opportunities to study microglia and monocytes (B. Ajami et al., 2007; Jung et al., 2000; Mildner et al., 2007; Wang et al., 2016), the field has lacked a commercially available histological marker for monocyte-derived populations in the CNS.

In this study, our main goal was to identify a marker that can discern between murine microglial and monocyte-derived cell populations during inflammation and disease in the CNS. Given the plasticity of myeloid cells, we recognize that the identification of cell lineage based on a single marker is not ideal (M. L. Bennett et al., 2016; Butovsky et al., 2014); however, previous studies have identified unique single genes and markers for microglia, such as P2ry12 and Tmem119, that have aided investigations and added to the repertoire of tools utilized by CNS myeloid cell researchers (M. L. Bennett et al., 2016; Butovsky et al., 2014). These markers have been indispensable to identifying endogenous and homeostatic microglia in the CNS. Here, we show that *Lgals3* is highly expressed in monocyte/macrophages in the healthy and JHMV-infected brain, and that galectin-3/MAC2 can be used as a histological marker to distinguish peripherally derived myeloid cells from microglia under both steady state and neuroinflammatory conditions. Galectin-3/MAC2 is a β-galactoside-binding lectin that is highly expressed in and secreted by monocytes/macrophages; it is associated with many macrophage functions, including cell adhesion, migration, proliferation, and apoptosis (MacKinnon et al., 2008). However, galectin-3 expression has also been reported in other cell populations, including fibroblasts, osteoblasts, endothelial cells, neuronal cells, and immune cells (neutrophils, eosinophils, basophils, mast cells) (Thomas & Pasquini, 2018). Here, we show that *Lgals3* is not highly expressed in other Cd11b+ cell populations via scRNAseq, including T cells, B cells, NK cells, neutrophils, and microglia, but is highly expressed in several monocyte and macrophage cell clusters. Although we do not observe significant MAC2+ staining in non-IBA1+ cells in the CNS, careful consideration here is

also warranted and IBA1 (or other myeloid cell markers) should be employed in combination with MAC2 to distinguish these myeloid populations.

In line with our study, recent work by Ochocka et al. using scRNAseq and flow cytometry of CD11b+ myeloid cells in naïve and glioma-bearing mice showed that *Lgals3* and galectin-3 are highly expressed by infiltrating monocyte/macrophages at RNA and protein levels, respectively (Ochocka et al., 2021). These authors propose the use of TMEM119 and galectin-3 for efficient and distinguishable separation of microglia and monocyte/macrophages in glioma models and highlighted their ability to achieve distinct spatial distribution of these cells within tumor tissue (Ochocka et al., 2021). Moreover, recent studies in mouse models of diabetes and spinal cord injury have identified unique populations of infiltrating and phagocytic macrophages, distinct from resident microglia, that express *Lgals3*/galectin-3/MAC2. In diabetes, galactin-3 expressing macrophages infiltrate and aggregate near injury sites, implicating these cells in the response to cerebrovascular insults (Mehina et al., 2021). In spinal cord injury, injury-activated macrophages maintain a transcriptionally distinct identify to activated microglia, expressing higher levels of *Lgals3*, *Apoe*, and *Cxcr4*, among other genes (Wahane et al., 2021). In the present study, we also observed distinct spatial distribution of MAC2+ cells in the JHMV-infected brain; cells were sequestered in the brain stem, white matter areas, and regions surrounding the ventricles. Further study is needed to evaluate the distinct contributions of MAC2+ myeloid cells and MAC2- myeloid cells in pathogenesis, but given the role of BM-derived myeloid cells in demyelination (Yamasaki et al., 2014), it is not surprising to find their selective recruitment in these areas. In GFP BM chimeras, MAC2+ cells were observed in the choroid plexus and perivascular spaces in whole body-irradiated mice, respectively, consistent with their partial cell turnover from BM sources (Goldmann et al., 2016; Van Hove et al., 2019). Identifying MAC2 as a distinct histological marker

for monocytes provides investigators with the ability to explore the spatial distribution and dynamics of these peripheral cells without the side effects of irradiation or other experimental caveats (e.g., tamoxifen).

In mice, monocytes express CD11b and CD45, and are divided into two main subpopulations: classical/inflammatory monocytes (Ly6C^{hi}CCR2+CX3CR1^{lo}) and non-classical/patrolling monocytes (Ly6C^{lo}CCR2^{lo} CX3CR1^{hi}) (Geissmann, Jung, & Littman, 2003; Geissmann et al., 2010). Of interest, studies have shown that *Lgals3* is enriched in a population of Ly6C+ monocytes located in the BM and blood (Mildner et al., 2017). Although transcriptional profile analyses of microglia and monocytes have generated several proposed monocyte-specific markers based off of an identified monocyte signature, including *Apoe*, *Ccr2*, *Ms4a7*, and *Clec12a* (F. C. Bennett et al., 2018; Cronk et al., 2018; Hohsfield et al., 2020; Lund et al., 2018; Anat Shemer et al., 2018) these markers have presented a number of limitations: upregulation during disease, downregulation upon macrophage differentiation, or lack of success in staining fixed adult brain tissue. For example, though Cd11a (*Itgal*) is expressed on all peripheral circulating immune cells and not microglia, it could only be detected on infiltrating cells in fixed brain sections using a tedious tyramide amplification strategy, limiting its practical use (Shuka et al., 2019). In addition, Bennett et al. identified MS4A7 as a unique marker for HSC-derived cells, but MS4A7 staining was only shown in blood, fetal brain, and primary human microglia, and RNA *in situ* hybridization was required to show staining in postmortem AD brain samples (F. C. Bennett et al., 2018). CD44 was a marker identified for distinguishing CNS infiltrating from CNS resident cells by Korin et al., however, later found by Mrdjen et al. to be upregulated in microglia during disease or aging (Korin et al., 2017; Mrdjen et al., 2018). Given that monocytes and macrophages exist as heterogenous populations with varying expression profiles (reflecting functional diversity,

differential origins, differentiation status, tissue of residence) and dynamic adaption of their transcription regulatory networks to changing environments (Gosselin et al., 2014; Lavin et al., 2014), it has been challenging for researchers to develop a marker for monocyte-derived cells that remains intact following differentiation and tissue engraftment. Here, we show that MAC2 staining is retained in BM-derived cells 6-10 months following CNS recruitment in the brain, indicating that MAC2 may be a marker that is conserved across several monocyte and macrophages subpopulations, or at least the subsets recruited to the CNS/sites of inflammation.

Transcriptional profile analysis of isolated microglia from mouse models of AD, amyotrophic lateral sclerosis, and aging identified *Lgals3* as a central hub gene in primed microglia, along with *Apoe*, *Axl*, *Clec7a*, and *Itgax* (Holtman et al., 2015). Further comprehensive scRNAseq analysis of microglia in neurodegenerative diseases discovered a unique microglial subset, termed disease-associated microglia (DAM) or microglial neurodegenerative phenotype (MGnD) microglia. These cells exhibit a downregulation in homeostatic microglia genes (e.g., *P2ry12*, *Tmem119*) and upregulation in genes involved in phagocytic, lysosomal, and lipid metabolism pathways (e.g., *Apoe*, *Axl*, *Clec7a*, *Cst7*, *Itgax*, *Lilrb4*) (Keren-Shaul et al., 2017), including *Lgals3* (Butovsky & Weiner, 2018; Krasemann et al., 2017), which is upregulated during later stages of neurodegeneration (Chen & Colonna, 2021). However, a recent study has shown that enzymatic dissociation methods can induce aberrant gene expression signatures in microglia (Marsh et al., 2020), indicating that some scRNAseq findings may be confounded and an artefact of isolation methods, analysis, or sequencing platform. A recent investigation utilizing scRNAseq, snRNAseq and scATACseq identified distinct microglia subpopulations in 3xTgAD and 5xFAD mice, including a DAM cluster containing *Cst7*, but lacking *Lgals3*; instead, *Lgals3* was found in a small cluster containing *Cd14* and *Itgal* (Balderrama-Gutierrez et al., 2021). Galectin-3 was also

shown to be significantly elevated in human AD patients, exhibit preferential expression in microglia in contact with plaques, and serve as a ligand for TREM2 (Boza-Serrano et al., 2019). In contrast, Sobue et al. showed that gene expression levels of *LGALS3*, *AIF1*, and *CD68*, were unchanged in human AD precuneus samples (Sobue et al., 2021). In line with this, using bulk-tissue RNAseq analysis, our lab has shown that while *Lgals3* is upregulated in 5xFAD mice in the hippocampus and thalamus compared to wild types, expression levels do not change following sustained microglial depletion, unlike several homeostatic (e.g., *Csf1r*, *Cx4cr1*, *Hexb*, *Siglech*) and DAM genes (e.g., *Clec7a*, *Cst7*, *Itgax*) which are significantly downregulated by microglial depletion (Spangenberg et al., 2019). These data provide evidence that elevated *Lgals3* in 5xFAD brains may not be specific to microglia. Consistent with spatial transcriptomics and *in situ* sequencing data in $APP^{NL\text{-}G\text{-}F}$ mice, *Lgals3* was not identified in plaque-induced genes (PIGs), consisting of 57 genes that overlap with several DAM genes (W. T. Chen et al., 2020). The current study shows that MAC2 staining is not present in plaque-associated microglia in the young 5xFAD mice, and only appears in plaque-associated IBA1+ cells during JHMV infection or in aged animals (albeit at modest numbers). A recent study - showing clonal hematopoiesis of indeterminate potential (CHIP) is associated with protection against AD – detected mutated marrow-derived cells in the brains of patients which appear indistinguishable from microglia (Bouzid et al., 2021), highlighting the potential role for peripheral infiltrates in replacing defective microglia during aging or disease. Thus, the presence of MAC2+ cells in disease and experimental models should be considered a potential sign of peripheral infiltrates, and subsequently followed up with BM chimeric models, parabiosis, or BM lineage tracing transgenics. It is possible that microglia may upregulate *Lgals3* under certain conditions, including infection or inflammatory stimulus, or that upregulated mRNA does not effectively translate to protein expression. Likewise,

we cannot discount the possibility that microglia in other conditions (stroke, injury, and chronic neurodegenerative disease) may also upregulate *Lgals3*, or that these MAC2+ cells may derive from BM sources. Other explanations for the disparity between *Lgals3* transcript levels and MAC2 staining in plaque-associated microglia could be a result of: 1) microglia and infiltrating peripheral myeloid cells expressing different isoforms of *Lgals3*/galectin-3, in which one isoform is detectible by the MAC2 antibody while the other is not, or 2) different secretion and/or cellular retention rates of *Lgals3*/galectin-3 within these two myeloid cell populations. Moreover, *Lgals3* may also be expressed by discrete microglial populations in the brain–for example, in specialized axon tract-associated microglia (ATM) or P7/early postnatal microglia (termed proliferative region-associated microglia (PAM), which appear as amoeboid cells that transiently reside in axon tracts of the corpus callosum and cerebellum (Hammond et al., 2019; Li et al., 2019), as well as in white matter-associated microglia (WAM), found specifically in white matter areas that increase with aging (Safaiyan et al., 2021). Furthermore, surviving microglia following CSF1Ri-induced depletion have been described as MAC2+ (Zhan, Sohn, Zhou, Li, & Gan, 2019). Given these findings and the data from this current study, we would implore researchers to consider *Lgals3*/MAC2 expression as a potential indicator of peripheral origins, but encourage further validation with other important tools, such as fate-mapping techniques. For example, lineage tracing from *Ms4a3* or *Cxcr4* could be utilized, as it has recently been shown as a specific gene expressed by BM-derived granulocyte-monocyte progenitors (GMPs) or HSC-derived monocytes, respectively, to efficiently trace monocyte-derived cells (Liu et al., 2019; Werner et al., 2020). Other markers include Cd49d, also expressed by T cells and DCs, and Cd49e, which were identified in peripheral monocyte populations, but not in CNS resident myeloid cell populations utilizing CyTOF (Bahareh Ajami et al., 2018).

In sum, we identify galectin-3/MAC2 as a potential monocyte marker that can be utilized in inflamed CNS tissue. Unlike other markers, BM-derived myeloid cells retain MAC2 expression even as they leave perivascular areas and occupy the parenchymal niche for prolonged periods of time. The ability to discern peripherally derived cells from resident microglia is critical to exploring their distinct roles in health and disease. Growing attention has been placed on understanding CNS myeloid cells and the environmental cues that sculpt their transcriptional and phenotypic profiles, particularly during disease. Detailed knowledge of these distinct myeloid cell populations and our ability to distinguish microglia and monocytes will prove essential in targeting these cells for improved therapeutic strategies.

Acknowledgments

We thank Edna Hingco for her excellent technical assistance. WT and 5xFAD time course tissue was provided by U54 AG054349 (NIA Model Organism Development and Evaluation for Late onset Alzheimer's Disease (MODEL-AD)). K.N.G was supported by the National Institutes of Health (NIH) under awards: R01NS083801 (NINDS), RF1AG056768 (NIA), and RF1AG065329 (NIA). L.A.H. was supported by the Alzheimer's Association Research Fellowship (AARF-16-442762). T.E.L. was supported by the National Institutes of Health (NIH) under awards: R01NS041249 (NINDS) and R35NS116835 (NINDS), the National Multiple Sclerosis Society (NMSS) Collaborative Research Center grant CA-1607-25040 and The Ray and Tye Noorda Foundation. Y.G. was supported by NIH T32 training grant (NS082174).

Conflict of interest

The authors declare that they have no conflicts of interest.

Author contributions

L.A.H. developed experimental protocols, designed, performed, and analyzed experiments and wrote the manuscript. K.I.T. and Y.G. performed and analyzed experiments. A.R.S. performed experiments and bioinformatic analysis. S.J.K., Y.C., and S.F. performed experiments. M.A.I. contributed to project design. T.E.L. and K.N.G. directed the project, designed the experiments, interpreted the results and wrote the manuscript.

Data availability statement

The data that support the findings of this study are available from TEL and KNG upon reasonable request.

ORCID

Matthew A. Inlay http://orcid.org/0000-0002-0451-2076

Thomas E. Lane http://orcid.org/0000-0003-0392-0825

Kim N. Green http://orcid.org/0000-0002-6049-6744

REFERENCES

1. Ajami, B., Bennett, J. L., Krieger, C., McNagny, K. M., & Rossi, F. M. (2011). Infiltrating monocytes trigger EAE progression, but do not contribute to the resident microglia pool. *Nat Neurosci, 14*(9), 1142-1149. doi:10.1038/nn.2887

2. Ajami, B., Bennett, J. L., Krieger, C., Tetzlaff, W., & Rossi, F. M. (2007). Local self-renewal can sustain CNS microglia maintenance and function throughout adult life. *Nat Neurosci, 10*(12), 1538-1543. doi:10.1038/nn2014

3. Ajami, B., Samusik, N., Wieghofer, P., Ho, P. P., Crotti, A., Bjornson, Z., . . . Steinman, L. (2018). Single-cell mass cytometry reveals distinct populations of brain myeloid cells in mouse neuroinflammation and neurodegeneration models. *Nat Neurosci, 21*(4), 541-551. doi:10.1038/s41593-018-0100-x

4. Balderrama-Gutierrez, G., Liang, H., Rezaie, N., Carvalho, K., Forner, S., Matheos, D., . . . Mortazavi, A. (2021). Single-cell and nucleus RNA-seq in a mouse model of AD reveal activation of distinct glial subpopulations in the presence of plaques and tangles. *bioRxiv*, 2021.2009.2029.462436. doi:10.1101/2021.09.29.462436

5. Bennett, F. C., Bennett, M. L., Yaqoob, F., Mulinyawe, S. B., Grant, G. A., Hayden Gephart, M., . . . Barres, B. A. (2018). A Combination of Ontogeny and CNS Environment Establishes Microglial Identity. *Neuron, 98*(6), 1170-1183.e1178. doi:10.1016/j.neuron.2018.05.014

6. Bennett, M. L., Bennett, F. C., Liddelow, S. A., Ajami, B., Zamanian, J. L., Fernhoff, N. B., . . . Barres, B. A. (2016). New tools for studying microglia in the mouse and human CNS. *Proc Natl Acad Sci U S A, 113*(12), E1738-1746. doi:10.1073/pnas.1525528113

7. Bergmann, C. C., Lane, T. E., & Stohlman, S. A. (2006). Coronavirus infection of the central nervous system: host-virus stand-off. *Nat Rev Microbiol, 4*(2), 121-132. doi:10.1038/nrmicro1343

8. Blanc, C. A., Grist, J. J., Rosen, H., Sears-Kraxberger, I., Steward, O., & Lane, T. E. (2015). Sphingosine-1-phosphate receptor antagonism enhances proliferation and migration of engrafted neural progenitor cells in a model of viral-induced demyelination. *Am J Pathol, 185*(10), 2819-2832. doi:10.1016/j.ajpath.2015.06.009

9. Bouzid, H., Belk, J. A., Jan, M., Qi, Y., Sarnowski, C., Wirth, S., . . . Jaiswal, S. (2021). Clonal hematopoiesis is associated with protection from Alzheimer's disease. *medRxiv*, 2021.2012.2010.21267552. doi:10.1101/2021.12.10.21267552

10. Boza-Serrano, A., Ruiz, R., Sanchez-Varo, R., García-Revilla, J., Yang, Y., Jimenez-Ferrer, I., . . . Deierborg, T. (2019). Galectin-3, a novel endogenous TREM2 ligand, detrimentally regulates inflammatory response in Alzheimer's disease. *Acta neuropathologica, 138*(2), 251-273. doi:10.1007/s00401-019-02013-z

11. Bradshaw, E. M., Chibnik, L. B., Keenan, B. T., Ottoboni, L., Raj, T., Tang, A., . . . De Jager, P. L. (2013). CD33 Alzheimer's disease locus: altered monocyte function and amyloid biology. *Nat Neurosci, 16*(7), 848-850. doi:10.1038/nn.3435

12. Butovsky, O., Jedrychowski, M. P., Moore, C. S., Cialic, R., Lanser, A. J., Gabriely, G., . . . Weiner, H. L. (2014). Identification of a unique TGF-beta-dependent molecular and functional signature in microglia. *Nat Neurosci, 17*(1), 131-143. doi:10.1038/nn.3599

13. Butovsky, O., & Weiner, H. L. (2018). Microglial signatures and their role in health and disease. *Nat Rev Neurosci, 19*(10), 622-635. doi:10.1038/s41583-018-0057-5

14. Buttgereit, A., Lelios, I., Yu, X., Vrohlings, M., Krakoski, N. R., Gautier, E. L., . . . Greter, M. (2016). Sall1 is a transcriptional regulator defining microglia identity and function. *Nat Immunol, 17*(12), 1397-1406. doi:10.1038/ni.3585

15. Chen, H.-R., Sun, Y.-Y., Chen, C.-W., Kuo, Y.-M., Kuan, I. S., Tiger Li, Z.-R., . . . Kuan, C.-Y. (2020). Fate mapping via CCR2-CreER mice reveals monocyte-to-microglia transition in development and neonatal stroke. *Science Advances, 6*(35), eabb2119. doi:10.1126/sciadv.abb2119

16. Chen, W. T., Lu, A., Craessaerts, K., Pavie, B., Sala Frigerio, C., Corthout, N., . . . De Strooper, B. (2020). Spatial Transcriptomics and In Situ Sequencing to Study Alzheimer's Disease. *Cell, 182*(4), 976-991.e919. doi:10.1016/j.cell.2020.06.038

17. Chen, Y., & Colonna, M. (2021). Microglia in Alzheimer's disease at single-cell level. Are there common patterns in humans and mice? *Journal of Experimental Medicine, 218*(9). doi:10.1084/jem.20202717

18. Chu, H. X., Arumugam, T. V., Gelderblom, M., Magnus, T., Drummond, G. R., & Sobey, C. G. (2014). Role of CCR2 in inflammatory conditions of the central nervous system. *J Cereb Blood Flow Metab, 34*(9), 1425-1429. doi:10.1038/jcbfm.2014.120

19. Cronk, J. C., Filiano, A. J., Louveau, A., Marin, I., Marsh, R., Ji, E., . . . Kipnis, J. (2018). Peripherally derived macrophages can engraft the brain independent of irradiation and maintain an identity distinct from microglia. *J Exp Med, 215*(6), 1627-1647. doi:10.1084/jem.20180247

20. Dickey, L. L., Worne, C. L., Glover, J. L., Lane, T. E., & O'Connell, R. M. (2016). MicroRNA-155 enhances T cell trafficking and antiviral effector function in a model of coronavirus-induced neurologic disease. *J Neuroinflammation, 13*(1), 240. doi:10.1186/s12974-016-0699-z

21. El Khoury, J., Toft, M., Hickman, S. E., Means, T. K., Terada, K., Geula, C., & Luster, A. D. (2007). Ccr2 deficiency impairs microglial accumulation and accelerates progression of Alzheimer-like disease. *Nat Med, 13*(4), 432-438. doi:10.1038/nm1555

22. Elmore, M. R., Lee, R. J., West, B. L., & Green, K. N. (2015). Characterizing newly repopulated microglia in the adult mouse: impacts on animal behavior, cell morphology, and neuroinflammation. *PLoS One, 10*(4), e0122912. doi:10.1371/journal.pone.0122912

23. Elmore, M. R., Najafi, A. R., Koike, M. A., Dagher, N. N., Spangenberg, E. E., Rice, R. A., . . . Green, K. N. (2014). Colony-stimulating factor 1 receptor signaling is necessary for microglia viability, unmasking a microglia progenitor cell in the adult brain. *Neuron, 82*(2), 380-397. doi:10.1016/j.neuron.2014.02.040

24. Fantuzzi, L., Borghi, P., Ciolli, V., Pavlakis, G., Belardelli, F., & Gessani, S. (1999). Loss of CCR2 expression and functional response to monocyte chemotactic protein (MCP-1) during the differentiation of human monocytes: role of secreted MCP-1 in the regulation of the chemotactic response. *Blood, 94*(3), 875-883.

25. Gautier, E. L., Shay, T., Miller, J., Greter, M., Jakubzick, C., Ivanov, S., . . . Randolph, G. J. (2012). Gene-expression profiles and transcriptional regulatory pathways that underlie the identity and diversity of mouse tissue macrophages. *Nat Immunol, 13*(11), 1118-1128. doi:10.1038/ni.2419

26. Geissmann, F., Jung, S., & Littman, D. R. (2003). Blood monocytes consist of two principal subsets with distinct migratory properties. *Immunity, 19*(1), 71-82. doi:10.1016/s1074-7613(03)00174-2

27. Geissmann, F., Manz, M. G., Jung, S., Sieweke, M. H., Merad, M., & Ley, K. (2010). Development of monocytes, macrophages, and dendritic cells. *Science, 327*(5966), 656-661. doi:10.1126/science.1178331

28. Ginhoux, F., Greter, M., Leboeuf, M., Nandi, S., See, P., Gokhan, S., . . . Merad, M. (2010). Fate mapping analysis reveals that adult microglia derive from primitive macrophages. *Science, 330*(6005), 841-845. doi:10.1126/science.1194637

29. Goldmann, T., Wieghofer, P., Jordao, M. J., Prutek, F., Hagemeyer, N., Frenzel, K., . . . Prinz, M. (2016). Origin, fate and dynamics of macrophages at central nervous system interfaces. *Nat Immunol, 17*(7), 797-805. doi:10.1038/ni.3423

30. Gomez Perdiguero, E., Klapproth, K., Schulz, C., Busch, K., Azzoni, E., Crozet, L., . . . Rodewald, H.-R. (2015). Tissue-resident macrophages originate from yolk-sac-derived erythro-myeloid progenitors. *Nature, 518*(7540), 547-551. doi:10.1038/nature13989

31. Gosselin, D., Link, V. M., Romanoski, C. E., Fonseca, G. J., Eichenfield, D. Z., Spann, N. J., . . . Glass, C. K. (2014). Environment drives selection and function of enhancers controlling tissue-specific macrophage identities. *Cell, 159*(6), 1327-1340. doi:10.1016/j.cell.2014.11.023

32. Grubman, A., Choo, X. Y., Chew, G., Ouyang, J. F., Sun, G., Croft, N. P., . . . Polo, J. M. (2021). Transcriptional signature in microglia associated with Aβ plaque phagocytosis. *Nat Commun, 12*(1), 3015. doi:10.1038/s41467-021-23111-1

33. Gschwandtner, M., Derler, R., & Midwood, K. S. (2019). More Than Just Attractive: How CCL2 Influences Myeloid Cell Behavior Beyond Chemotaxis. *Front Immunol, 10*(2759). doi:10.3389/fimmu.2019.02759

34. Guerreiro, R., Wojtas, A., Bras, J., Carrasquillo, M., Rogaeva, E., Majounie, E., . . . Hardy, J. (2013). TREM2 variants in Alzheimer's disease. *N Engl J Med, 368*(2), 117-127. doi:10.1056/NEJMoa1211851

35. Haage, V., Semtner, M., Vidal, R. O., Hernandez, D. P., Pong, W. W., Chen, Z., . . . Gutmann, D. H. (2019). Comprehensive gene expression meta-analysis identifies signature genes that distinguish microglia from peripheral monocytes/macrophages in health and glioma. *Acta Neuropathol Commun, 7*(1), 20. doi:10.1186/s40478-019-0665-y

36. Hammond, T. R., Dufort, C., Dissing-Olesen, L., Giera, S., Young, A., Wysoker, A., . . . Stevens, B. (2019). Single-Cell RNA Sequencing of Microglia throughout the Mouse Lifespan and in the Injured Brain Reveals Complex Cell-State Changes. *Immunity, 50*(1), 253-271.e256. doi:10.1016/j.immuni.2018.11.004

37. Hawkes, C. A., & McLaurin, J. (2009). Selective targeting of perivascular macrophages for clearance of beta-amyloid in cerebral amyloid angiopathy. *Proc Natl Acad Sci U S A, 106*(4), 1261-1266. doi:10.1073/pnas.0805453106

38. Held, K. S., Chen, B. P., Kuziel, W. A., Rollins, B. J., & Lane, T. E. (2004). Differential roles of CCL2 and CCR2 in host defense to coronavirus infection. *Virology, 329*(2), 251-260. doi:10.1016/j.virol.2004.09.006

39. Herz, J., Filiano, A. J., Smith, A., Yogev, N., & Kipnis, J. (2017). Myeloid Cells in the Central Nervous System. *Immunity, 46*(6), 943-956. doi:10.1016/j.immuni.2017.06.007

40. Hohsfield, L. A., Najafi, A. R., Ghorbanian, Y., Soni, N., Hingco, E. E., Kim, S. J., . . . Green, K. N. (2020). Effects of long-term and brain-wide colonization of peripheral bone marrow-derived myeloid cells in the CNS. *J Neuroinflammation, 17*(1), 279. doi:10.1186/s12974-020-01931-0

41. Holtman, I. R., Raj, D. D., Miller, J. A., Schaafsma, W., Yin, Z., Brouwer, N., . . . Eggen, B. J. (2015). Induction of a common microglia gene expression signature by aging and neurodegenerative conditions: a co-expression meta-analysis. *Acta Neuropathol Commun, 3*, 31. doi:10.1186/s40478-015-0203-5

42. Honarpisheh, P., Lee, J., Banerjee, A., Blasco-Conesa, M. P., Honarpisheh, P., d'Aigle, J., . . . McCullough, L. D. (2020). Potential caveats of putative microglia-specific markers for assessment of age-related cerebrovascular neuroinflammation. *J Neuroinflammation, 17*(1), 366. doi:10.1186/s12974-020-02019-5

43. Hosking, M. P., & Lane, T. E. (2010). The role of chemokines during viral infection of the CNS. *PLoS Pathog, 6*(7), e1000937. doi:10.1371/journal.ppat.1000937

44. Jay, T. R., Miller, C. M., Cheng, P. J., Graham, L. C., Bemiller, S., Broihier, M. L., . . . Lamb, B. T. (2015). TREM2 deficiency eliminates TREM2+ inflammatory macrophages and ameliorates pathology in Alzheimer's disease mouse models. *J Exp Med, 212*(3), 287-295. doi:10.1084/jem.20142322

45. Jonsson, T., Stefansson, H., Steinberg, S., Jonsdottir, I., Jonsson, P. V., Snaedal, J., . . . Stefansson, K. (2013). Variant of TREM2 associated with the risk of Alzheimer's disease. *N Engl J Med, 368*(2), 107-116. doi:10.1056/NEJMoa1211103

46. Jordao, M. J. C., Sankowski, R., Brendecke, S. M., Sagar, Locatelli, G., Tai, Y. H., . . . Prinz, M. (2019). Single-cell profiling identifies myeloid cell subsets with distinct fates during neuroinflammation. *Science, 363*(6425). doi:10.1126/science.aat7554

47. Jung, S., Aliberti, J., Graemmel, P., Sunshine, M. J., Kreutzberg, G. W., Sher, A., & Littman, D. R. (2000). Analysis of fractalkine receptor CX(3)CR1 function by targeted deletion and green fluorescent protein reporter gene insertion. *Mol Cell Biol, 20*(11), 4106-4114. doi:10.1128/mcb.20.11.4106-4114.2000

48. Keren-Shaul, H., Spinrad, A., Weiner, A., Matcovitch-Natan, O., Dvir-Szternfeld, R., Ulland, T. K., . . . Amit, I. (2017). A Unique Microglia Type Associated with Restricting Development of Alzheimer's Disease. *Cell, 169*(7), 1276-1290.e1217. doi:10.1016/j.cell.2017.05.018

49. Kierdorf, K., Erny, D., Goldmann, T., Sander, V., Schulz, C., Perdiguero, E. G., . . . Prinz, M. (2013). Microglia emerge from erythromyeloid precursors via Pu.1- and Irf8-dependent pathways. *Nat Neurosci, 16*(3), 273-280. doi:10.1038/nn.3318

50. Kierdorf, K., Masuda, T., Jordão, M. J. C., & Prinz, M. (2019). Macrophages at CNS interfaces: ontogeny and function in health and disease. *Nature Reviews Neuroscience, 20*(9), 547-562. doi:10.1038/s41583-019-0201-x

51. Konishi, H., Kobayashi, M., Kunisawa, T., Imai, K., Sayo, A., Malissen, B., . . . Kiyama, H. (2017). Siglec-H is a microglia-specific marker that discriminates microglia from CNS-associated macrophages and CNS-infiltrating monocytes. *Glia, 65*(12), 1927-1943. doi:10.1002/glia.23204

52. Korin, B., Ben-Shaanan, T. L., Schiller, M., Dubovik, T., Azulay-Debby, H., Boshnak, N. T., . . . Rolls, A. (2017). High-dimensional, single-cell characterization of the brain's immune compartment. *Nat Neurosci, 20*(9), 1300-1309. doi:10.1038/nn.4610

53. Krasemann, S., Madore, C., Cialic, R., Baufeld, C., Calcagno, N., El Fatimy, R., . . . Butovsky, O. (2017). The TREM2-APOE Pathway Drives the Transcriptional Phenotype of Dysfunctional Microglia in Neurodegenerative Diseases. *Immunity, 47*(3), 566-581.e569. doi:10.1016/j.immuni.2017.08.008

54. Lambert, J. C., Ibrahim-Verbaas, C. A., Harold, D., Naj, A. C., Sims, R., Bellenguez, C., . . . Amouyel, P. (2013). Meta-analysis of 74,046 individuals identifies 11 new susceptibility loci for Alzheimer's disease. *Nat Genet, 45*(12), 1452-1458. doi:10.1038/ng.2802

55. Lampert, P. W., Sims, J. K., & Kniazeff, A. J. (1973). Mechanism of demyelination in JHM virus encephalomyelitis. Electron microscopic studies. *Acta neuropathologica, 24*(1), 76-85. doi:10.1007/bf00691421

56. Lane, T. E., & Buchmeier, M. J. (1997). Murine coronavirus infection: a paradigm for virus-induced demyelinating disease. *Trends Microbiol, 5*(1), 9-14. doi:10.1016/s0966-842x(97)81768-4

57. Lane, T. E., & Hosking, M. P. (2010). The pathogenesis of murine coronavirus infection of the central nervous system. *Crit Rev Immunol, 30*(2), 119-130. doi:10.1615/critrevimmunol.v30.i2.20

58. Lavin, Y., Winter, D., Blecher-Gonen, R., David, E., Keren-Shaul, H., Merad, M., . . . Amit, I. (2014). Tissue-resident macrophage enhancer landscapes are shaped by the local microenvironment. *Cell, 159*(6), 1312-1326. doi:10.1016/j.cell.2014.11.018

59. Li, Q., Cheng, Z., Zhou, L., Darmanis, S., Neff, N. F., Okamoto, J., . . . Barres, B. A. (2019). Developmental Heterogeneity of Microglia and Brain Myeloid Cells Revealed by Deep Single-Cell RNA Sequencing. *Neuron, 101*(2), 207-223.e210. doi:10.1016/j.neuron.2018.12.006

60. Liu, Z., Gu, Y., Chakarov, S., Bleriot, C., Kwok, I., Chen, X., . . . Ginhoux, F. (2019). Fate Mapping via Ms4a3-Expression History Traces Monocyte-Derived Cells. *Cell, 178*(6), 1509-1525.e1519. doi:10.1016/j.cell.2019.08.009

61. Lund, H., Pieber, M., Parsa, R., Han, J., Grommisch, D., Ewing, E., . . . Harris, R. A. (2018). Competitive repopulation of an empty microglial niche yields functionally distinct subsets of microglia-like cells. *Nat Commun, 9*(1), 4845. doi:10.1038/s41467-018-07295-7

62. MacKinnon, A. C., Farnworth, S. L., Hodkinson, P. S., Henderson, N. C., Atkinson, K. M., Leffler, H., . . . Sethi, T. (2008). Regulation of alternative macrophage activation by galectin-3. *Journal of immunology (Baltimore, Md. : 1950), 180*(4), 2650-2658. doi:10.4049/jimmunol.180.4.2650

63. Marro, B. S., Grist, J. J., & Lane, T. E. (2016). Inducible Expression of CXCL1 within the Central Nervous System Amplifies Viral-Induced Demyelination. *J Immunol, 196*(4), 1855-1864. doi:10.4049/jimmunol.1501802

64. Marsh, S. E., Kamath, T., Walker, A. J., Dissing-Olesen, L., Hammond, T. R., Young, A. M. H., . . . Stevens, B. (2020). Single Cell Sequencing Reveals Glial Specific Responses to Tissue Processing & Enzymatic Dissociation in Mice and Humans. *bioRxiv*, 2020.2012.2003.408542. doi:10.1101/2020.12.03.408542

65. Masuda, T., Sankowski, R., Staszewski, O., Bottcher, C., Amann, L., Sagar, . . . Prinz, M. (2019). Spatial and temporal heterogeneity of mouse and human microglia at single-cell resolution. *Nature, 566*(7744), 388-392. doi:10.1038/s41586-019-0924-x

66. Mehina, E. M. F., Taylor, S., Boghozian, R., White, E., Choi, S. E., Cheema, M. S., . . . Brown, C. E. (2021). Invasion of phagocytic Galectin 3 expressing macrophages in the diabetic brain disrupts vascular repair. *Science Advances, 7*(34), eabg2712. doi:doi:10.1126/sciadv.abg2712

67. Mildner, A., Schmidt, H., Nitsche, M., Merkler, D., Hanisch, U. K., Mack, M., . . . Prinz, M. (2007). Microglia in the adult brain arise from Ly-6ChiCCR2+ monocytes only under defined host conditions. *Nat Neurosci, 10*(12), 1544-1553. doi:10.1038/nn2015

68. Mildner, A., Schönheit, J., Giladi, A., David, E., Lara-Astiaso, D., Lorenzo-Vivas, E., . . . Jung, S. (2017). Genomic Characterization of Murine Monocytes Reveals C/EBPβ Transcription Factor Dependence of Ly6C(-) Cells. *Immunity, 46*(5), 849-862.e847. doi:10.1016/j.immuni.2017.04.018

69. Mrdjen, D., Pavlovic, A., Hartmann, F. J., Schreiner, B., Utz, S. G., Leung, B. P., . . . Becher, B. (2018). High-Dimensional Single-Cell Mapping of Central Nervous System Immune Cells Reveals Distinct Myeloid Subsets in Health, Aging, and Disease. *Immunity, 48*(2), 380-395.e386. doi:10.1016/j.immuni.2018.01.011

70. Munro, D. A. D., Bradford, B. M., Mariani, S. A., Hampton, D. W., Vink, C. S., Chandran, S., . . . Priller, J. (2020). CNS macrophages differentially rely on an intronic Csf1r enhancer for their development. *Development, 147*(23). doi:10.1242/dev.194449

71. Oakley, H., Cole, S. L., Logan, S., Maus, E., Shao, P., Craft, J., . . . Vassar, R. (2006). Intraneuronal beta-amyloid aggregates, neurodegeneration, and neuron loss in transgenic mice with five familial Alzheimer's disease mutations: potential factors in amyloid plaque formation. *J Neurosci, 26*(40), 10129-10140. doi:10.1523/jneurosci.1202-06.2006

72. Ochocka, N., Segit, P., Walentynowicz, K. A., Wojnicki, K., Cyranowski, S., Swatler, J., . . . Kaminska, B. (2021). Single-cell RNA sequencing reveals functional heterogeneity of glioma-associated brain macrophages. *Nat Commun, 12*(1), 1151. doi:10.1038/s41467-021-21407-w

73. Prinz, M., & Priller, J. (2014). Microglia and brain macrophages in the molecular age: from origin to neuropsychiatric disease. *Nat Rev Neurosci, 15*(5), 300-312. doi:10.1038/nrn3722

74. Prinz, M., Priller, J., Sisodia, S. S., & Ransohoff, R. M. (2011). Heterogeneity of CNS myeloid cells and their roles in neurodegeneration. *Nat Neurosci, 14*(10), 1227-1235. doi:10.1038/nn.2923

75. Ransohoff, R. M., & Cardona, A. E. (2010). The myeloid cells of the central nervous system parenchyma. *Nature, 468*(7321), 253-262. doi:10.1038/nature09615

76. Reed-Geaghan, E. G., Croxford, A. L., Becher, B., & Landreth, G. E. (2020). Plaque-associated myeloid cells derive from resident microglia in an Alzheimer's disease model. *J Exp Med, 217*(4). doi:10.1084/jem.20191374

77. Rojo, R., Sauter, K. A., Lefevre, L., Hume, D. A., & Pridans, C. (2018). Maternal tamoxifen treatment expands the macrophage population of early mouse embryos. *bioRxiv*, 296749. doi:10.1101/296749

78. Saederup, N., Cardona, A. E., Croft, K., Mizutani, M., Cotleur, A. C., Tsou, C. L., . . . Charo, I. F. (2010). Selective chemokine receptor usage by central nervous system myeloid cells in CCR2-red fluorescent protein knock-in mice. *PLoS One, 5*(10), e13693. doi:10.1371/journal.pone.0013693

79. Safaiyan, S., Besson-Girard, S., Kaya, T., Cantuti-Castelvetri, L., Liu, L., Ji, H., . . . Simons, M. (2021). White matter aging drives microglial diversity. *Neuron, 109*(7), 1100-1117.e1110. doi:10.1016/j.neuron.2021.01.027

80. Savarin, C., Stohlman, S. A., Atkinson, R., Ransohoff, R. M., & Bergmann, C. C. (2010). Monocytes regulate T cell migration through the glia limitans during acute viral encephalitis. *J Virol, 84*(10), 4878-4888. doi:10.1128/jvi.00051-10

81. Shemer, A., Erny, D., Jung, S., & Prinz, M. (2015). Microglia Plasticity During Health and Disease: An Immunological Perspective. *Trends Immunol, 36*(10), 614-624. doi:10.1016/j.it.2015.08.003

82. Shemer, A., Grozovski, J., Tay, T. L., Tao, J., Volaski, A., Süß, P., . . . Jung, S. (2018). Engrafted parenchymal brain macrophages differ from microglia in transcriptome, chromatin landscape and response to challenge. *Nat Commun, 9*(1), 5206. doi:10.1038/s41467-018-07548-5

83. Shukla, A. K., McIntyre, L. L., Marsh, S. E., Schneider, C. A., Hoover, E. M., Walsh, C. M., . . . Inlay, M. A. (2019). CD11a expression distinguishes infiltrating myeloid cells from plaque-associated microglia in Alzheimer's disease. *Glia, 67*(5), 844-856. doi:10.1002/glia.23575

84. Simard, A. R., Soulet, D., Gowing, G., Julien, J. P., & Rivest, S. (2006). Bone marrow-derived microglia play a critical role in restricting senile plaque formation in Alzheimer's disease. *Neuron, 49*(4), 489-502. doi:10.1016/j.neuron.2006.01.022

85. Sobue, A., Komine, O., Hara, Y., Endo, F., Mizoguchi, H., Watanabe, S., . . . Yamanaka, K. (2021). Microglial gene signature reveals loss of homeostatic microglia associated with neurodegeneration of Alzheimer's disease. *Acta Neuropathol Commun, 9*(1), 1. doi:10.1186/s40478-020-01099-x

86. Spangenberg, E., Severson, P. L., Hohsfield, L. A., Crapser, J., Zhang, J., Burton, E. A., . . . Green, K. N. (2019). Sustained microglial depletion with CSF1R inhibitor impairs parenchymal plaque development in an Alzheimer's disease model. *Nat Commun, 10*(1), 3758. doi:10.1038/s41467-019-11674-z

87. Steinbach, F., & Thiele, B. (1994). Phenotypic investigation of mononuclear phagocytes by flow cytometry. *J Immunol Methods, 174*(1-2), 109-122. doi:10.1016/0022-1759(94)90015-9

88. Syage, A. R., Ekiz, H. A., Skinner, D. D., Stone, C., O'Connell, R. M., & Lane, T. E. (2020). Single-Cell RNA Sequencing Reveals the Diversity of the Immunological Landscape following Central Nervous System Infection by a Murine Coronavirus. *J Virol, 94*(24). doi:10.1128/jvi.01295-20

89. Thomas, L., & Pasquini, L. A. (2018). Galectin-3-Mediated Glial Crosstalk Drives Oligodendrocyte Differentiation and (Re)myelination. *Front Cell Neurosci, 12*, 297. doi:10.3389/fncel.2018.00297

90. Utz, S. G., See, P., Mildenberger, W., Thion, M. S., Silvin, A., Lutz, M., . . . Greter, M. (2020). Early Fate Defines Microglia and Non-parenchymal Brain Macrophage Development. *Cell, 181*(3), 557-573.e518. doi:10.1016/j.cell.2020.03.021

91. Van Hove, H., Martens, L., Scheyltjens, I., De Vlaminck, K., Pombo Antunes, A. R., De Prijck, S., . . . Movahedi, K. (2019). A single-cell atlas of mouse brain macrophages reveals unique transcriptional identities shaped by ontogeny and tissue environment. *Nat Neurosci, 22*(6), 1021-1035. doi:10.1038/s41593-019-0393-4

92. Wahane, S., Zhou, X., Zhou, X., Guo, L., Friedl, M.-S., Kluge, M., . . . Zou, H. (2021). Diversified transcriptional responses of myeloid and glial cells in spinal cord injury shaped by HDAC3 activity. *Science Advances, 7*(9), eabd8811. doi:doi:10.1126/sciadv.abd8811

93. Wang, Y., Ulland, T. K., Ulrich, J. D., Song, W., Tzaferis, J. A., Hole, J. T., . . . Colonna, M. (2016). TREM2-mediated early microglial response limits diffusion and toxicity of amyloid plaques. *J Exp Med, 213*(5), 667-675. doi:10.1084/jem.20151948

94. Weiner, L. P. (1973). Pathogenesis of demyelination induced by a mouse hepatitis. *Arch Neurol, 28*(5), 298-303. doi:10.1001/archneur.1973.00490230034003

95. Werner, Y., Mass, E., Ashok Kumar, P., Ulas, T., Händler, K., Horne, A., . . . Stumm, R. (2020). Cxcr4 distinguishes HSC-derived monocytes from microglia and reveals monocyte immune responses to experimental stroke. *Nat Neurosci, 23*(3), 351-362. doi:10.1038/s41593-020-0585-y

96. Wong, L. M., Myers, S. J., Tsou, C. L., Gosling, J., Arai, H., & Charo, I. F. (1997). Organization and differential expression of the human monocyte chemoattractant protein 1 receptor gene. Evidence for the role of the carboxyl-terminal tail in receptor trafficking. *J Biol Chem, 272*(2), 1038-1045. doi:10.1074/jbc.272.2.1038

97. Yamasaki, R., Lu, H., Butovsky, O., Ohno, N., Rietsch, A. M., Cialic, R., . . . Ransohoff, R. M. (2014). Differential roles of microglia and monocytes in the inflamed central nervous system. *J Exp Med, 211*(8), 1533. doi:10.1084/jem.20132477

98. Zhan, L., Sohn, P. D., Zhou, Y., Li, Y., & Gan, L. (2019). A Mac2-positive progenitor-like microglial population survives independent of CSF1R signaling in adult mouse brain. *bioRxiv*, 722090. doi:10.1101/722090

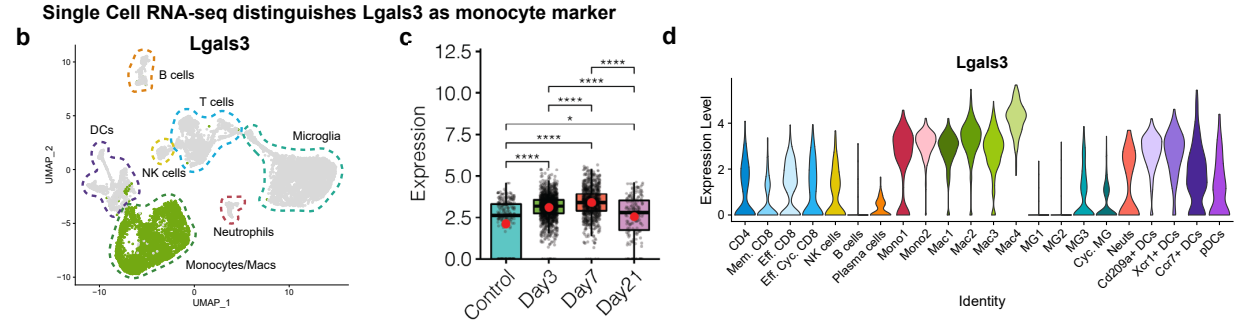

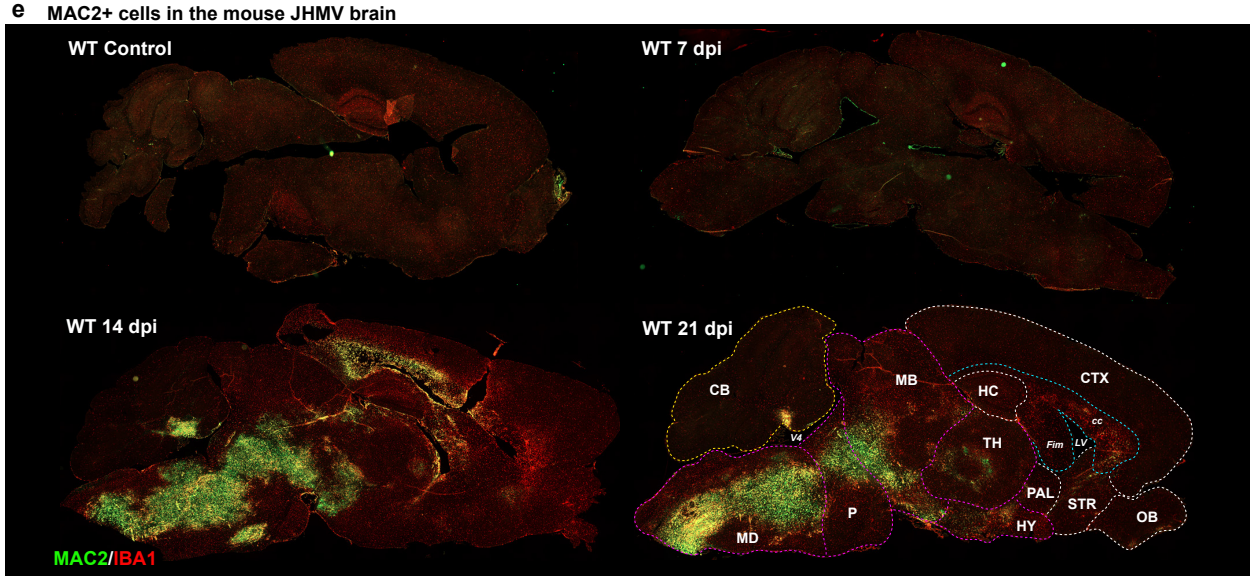

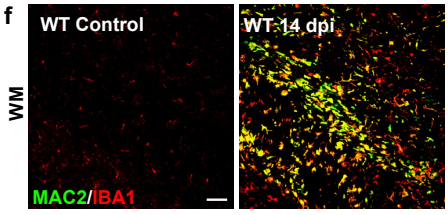

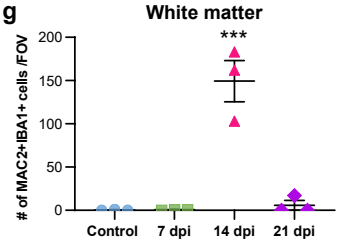

h MAC2+ distribution in JHMV mouse brain

	Animal group			
Brain region	Control	7 dpi	14 dpi	21 dpi
Brainstem	-	-	+++	+++
Cerebellum	-	-	++	+
White matter	-	-	+++	+
Cerebrum	-	-	-	-

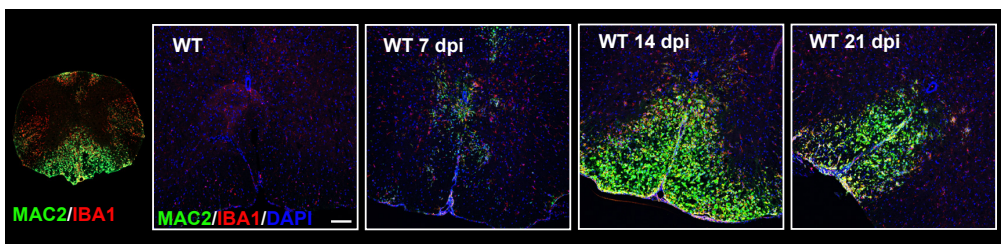

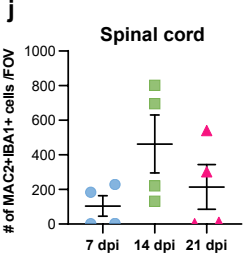

Figure 1. *Lgals3/*MAC2 distinguishes infiltrating cells from microglia in the adult CNS.
(a) Schematic of experimental design of intracranial (i.c.) infection of five to six-week-old C57BL/6 wild type (WT) mice with 250 PFU of the neurotropic JHM-J2.2v-1 strain of mouse hepatitis virus (JHMV). Brains and spinal cords were collected at 7, 14, 21 days post infection (d.p.i.). (b) UMAP plot displays aggregate data of CD45+ cells and shows scaled expression of transcripts encoding *Lgals3* in monocyte/macrophage (Monocytes/Macs) clusters (Syage et al., 2020). (c) Temporal analysis of expression of transcripts encoding *Lgals3*. Transcript levels were elevated at defined timepoints during JHMV infection. Data is presented as normalized expression values, and random noise was added to show data point distribution. Box plots show interquartile range and median value (bold horizontal bar). Red dots indicate the average expression value per sample. Wilcoxon's test was used for statistical analysis. (d) Violin plot shows gene expression of *Lgals3* in all CD45+ cells on the single-cell level and that *Lgals3* is upregulated in monocytes and macrophage clusters. (e) Representative whole sagittal brain sections of MAC2 (green) and IBA1 (red) staining in WT non-infected and JHMV-infected mice at 7, 14, and 21 d.p.i. (f) High resolution 20x confocal images of MAC2+ (green) and IBA1+ (red) cells in the white matter tracts of WT non-infected and JHMV-infected at 14 d.p.i. (g) Quantification of MAC+IBA1+ cells per field of view (FOV) in white matter tracts of brains in WT control and JHMV-infected mice.(h) Table of the relative MAC2+ cell distribution in distinct brain regions. – indicates no accumulation. + indicates low accumulation. ++ indicates moderate accumulation. +++ indicates extensive accumulation. (i) Representative confocal images of MAC2+ (green) and IBA1+ (red) cells in the spinal cords of WT control and JHMV-infected mice at various timepoints post infection. (j) Quantification of (i). Mouse, syringe and virus illustrations were obtained from Servier Medical Art at smart.servier.com. IBA1, ionized calcium adapter molecule 1; CB, cerebellum; cc, corpus callosum; CTX, cortex; Fim, fimbria; HC, hippocampus; HY, hypothalamus; LV, lateral ventricle; MB, midbrain; MD, medulla; OB, olfactory bulb; P, pons; PAL, pallidum; STR, striatum; TH, thalamus; V4, fourth ventricle. Data are represented as mean ± SEM (n=3-4 mice/timepoint). * $p < 0.05$, *** $p < 0.001$, **** $p < 0.0001$, compared to control unless otherwise indicated. Scale bar in (f) ~100 µm; in (i) inserts ~160 µm.

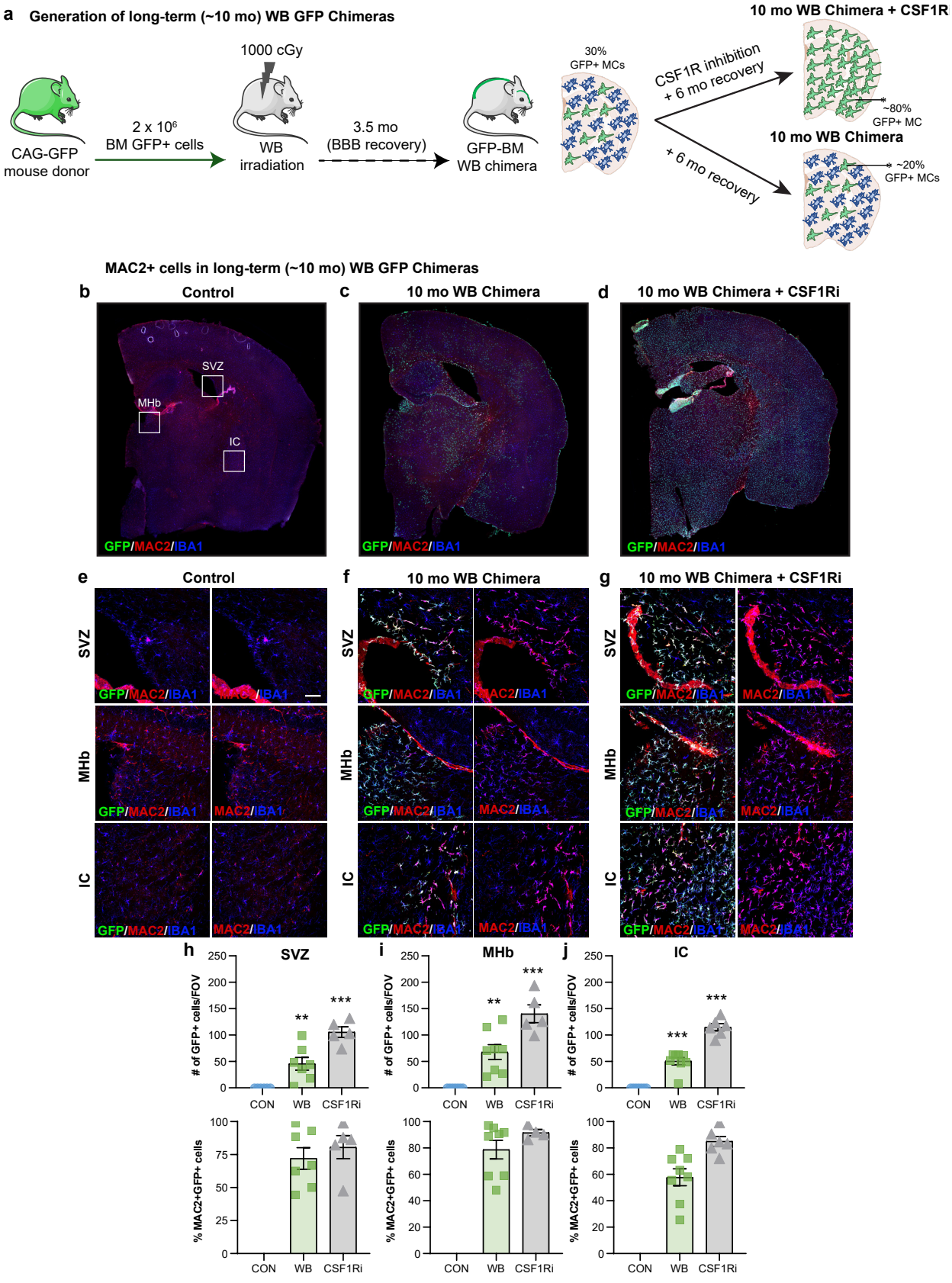
a
Generation of long-term (~10 mo) WB GFP Chimeras
CAG-GFP mouse donor
2 x 10⁶ BM GFP+ cells
1000 cGy
WB irradiation
3.5 mo (BBB recovery)
GFP-BM WB chimera
30% GFP+ MCs
CSF1R inhibition + 6 mo recovery
10 mo WB Chimera + CSF1R
~80% GFP+ MC
+ 6 mo recovery
10 mo WB Chimera
~20% GFP+ MCs
MAC2+ cells in long-term (~10 mo) WB GFP Chimeras
b Control
c 10 mo WB Chimera
d 10 mo WB Chimera + CSF1Ri
SVZ
MHb
IC
GFP/MAC2/IBA1
e Control
f 10 mo WB Chimera
g 10 mo WB Chimera + CSF1Ri
SVZ
MHb
IC
GFP/MAC2/IBA1
MAC2/IBA1
h SVZ
i MHb
j IC
# of GFP+ cells/FOV
% MAC2+GFP+ cells
CON
WB
CSF1Ri
**
***

Figure 2. MAC2 is a specific and long-lasting marker for bone marrow-derived infiltrating cells. (a) Schematic of experimental design for the generation of long-term green fluorescent protein (GFP) bone marrow (BM) chimeras. Treatment of BM chimeras with colony-stimulating factor 1 receptor (CSF1R) inhibitor results in extensive parenchymal engraftment of BM-derived peripheral myeloid cells in the brain (Hohsfield et al., 2020). Four-month-old wild type (WT) mice underwent whole body (WB) irradiation (1000 cGy) and BM transplant via retro-orbital injection of 2 x 10^6 BM cells from age- and sex- matched CAG-GFP mice. Following a 3.5 mo recovery, mice were treated with CSF1R inhibitor PLX3397 (600 ppm) for 14d, and then placed on control diet for 6 mo. (b-g) Representative images of whole coronal brain sections (b-d) and high resolution 20x confocal (e-g) images of GFP+ (green), MAC2+ (red) and IBA1+ (red) cells in control (b, e), ~10 mo WB chimeras (c, f), and ~10 mo WB chimeric mice treated with a CSF1R inhibitor (d, g). White boxes in (b) indicate brain regions of interest shown in (e-g). Images show that MAC2+ cells co-localize with GFP BM-derived cells in the brain parenchyma. (h-j) Quantification of the number of GFP+ cells per field of view (FOV) in the subventricular zone (SVZ) (h), medial habenula (MHb) (i), and internal capsule (IC) (j) in control, ~10 mo WB chimeras, and ~10 mo WB chimeric mice treated with a CSF1R inhibitor. (k-m) Percentage of GFP+ cells that express MAC or MAC2+ cells that express GFP in the subventricular zone (SVZ) (k), medial habenula (MHb) (l), and internal capsule (IC) (m) in control, ~10 mo WB chimeras, and ~10 mo WB chimeric mice treated with a CSF1R inhibitor. Data are represented as mean ± SEM (n=5-9). ** $p < 0.01$, *** $p < 0.001$, compared to control. Scale bar ~60 μm.

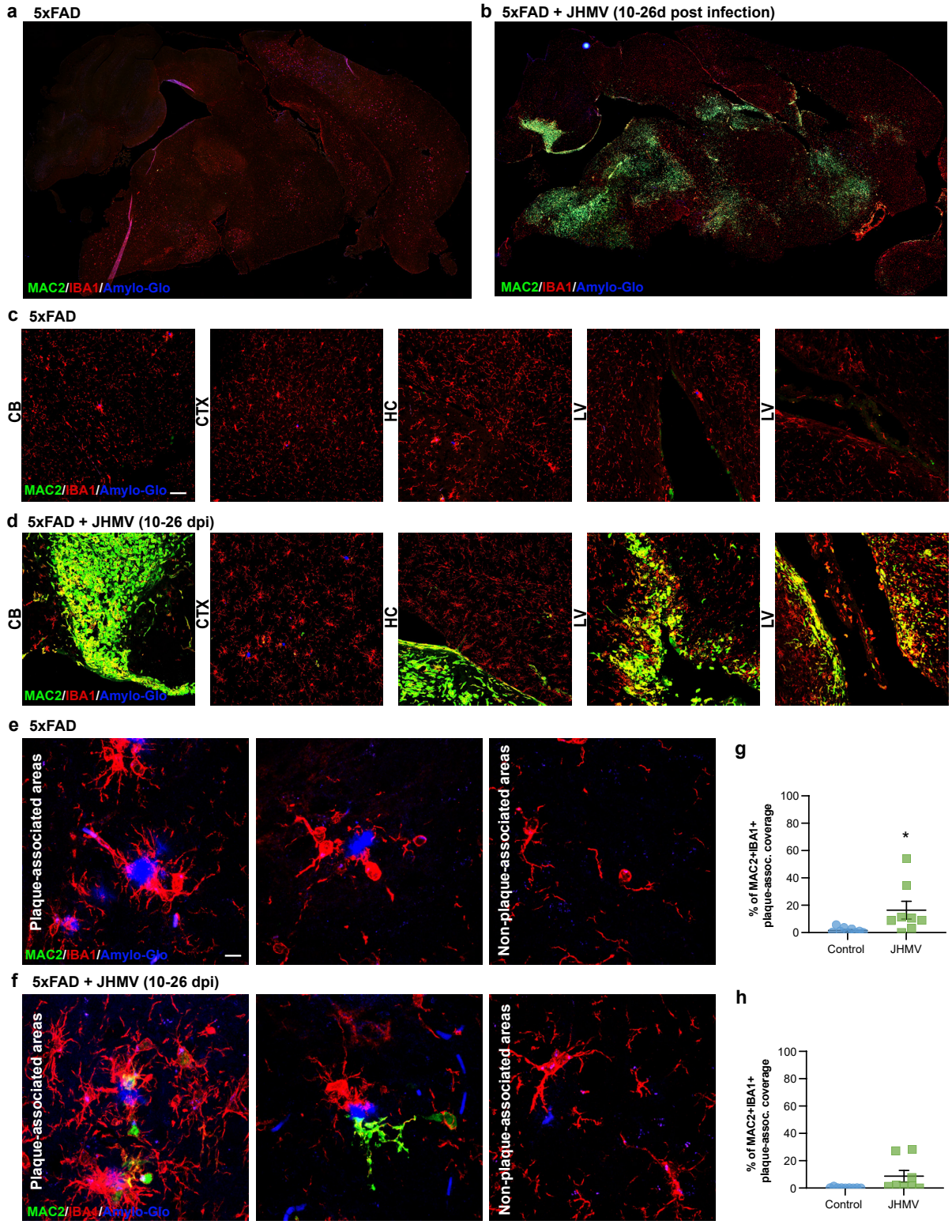
a 5xFAD
b 5xFAD + JHMV (10-26d post infection)
MAC2/IBA1/Amylo-Glo
c 5xFAD
CB
CTX
HC
LV
LV
MAC2/IBA1/Amylo-Glo
d 5xFAD + JHMV (10-26 dpi)
CB
CTX
HC
LV
LV
MAC2/IBA1/Amylo-Glo
e 5xFAD
Plaque-associated areas
Non-plaque-associated areas
MAC2/IBA1/Amylo-Glo
g
% of MAC2+IBA1+ plaque-assoc. coverage
100
80
60
40
20
0
*
Control
JHMV
f 5xFAD + JHMV (10-26 dpi)
Plaque-associated areas
Non-plaque-associated areas
MAC2/IBA1/Amylo-Glo
h
% of MAC2+IBA1+ plaque-assoc. coverage
100
80
60
40
20
0
Control
JHMV

Figure 3. MAC2 is not a ubiquitous marker for plaque-associated microglia during the early stages of disease in 5xFAD mice. Four-month-old 5xFAD mice were infected intracranially with 200 PFU of JHMV strain and brains evaluated at 10-25 d.p.i. (a-d) Representative whole sagittal brain section (a-b) and 20x confocal (c-d) images of Amylo-Glo (amyloid, blue), MAC2 (green), and IBA1 (red) staining in control (a, c) and JHMV-infected (b, d) 5xFAD mice. (e) Quantification of the number of MAC2+IBA1+ cells per field of view (FOV) in the cerebellum (CB), cortex (CTX), hippocampus (HC), and lateral ventricle (LV). (f,h) Representative high resolution 100x confocal images of Amylo-Glo+ plaques (amyloid, blue), MAC2+ (green) cells, and IBA1+ (red) cells in plaque-associated and non-plaque-associated areas in the brains of control (f) and JHMV-infected (h) 5xFAD mice. Images show that MAC2+ cells do not label plaque-associated microglia in non-infected 5xFAD mice. (g,i) Quantification of % MAC2+IBA1+ staining in IBA1+ cells and in plaque-associated (g) and non-plaque-associated (i) areas of the cortex and hippocampus. Multiple field of views in these brain regions were quantified across three animals from each group. Data are represented as mean ± SEM (n=8-9). * $p < 0.05$. Scale bar in (c) ~60 μm; in (e) ~10 μm.

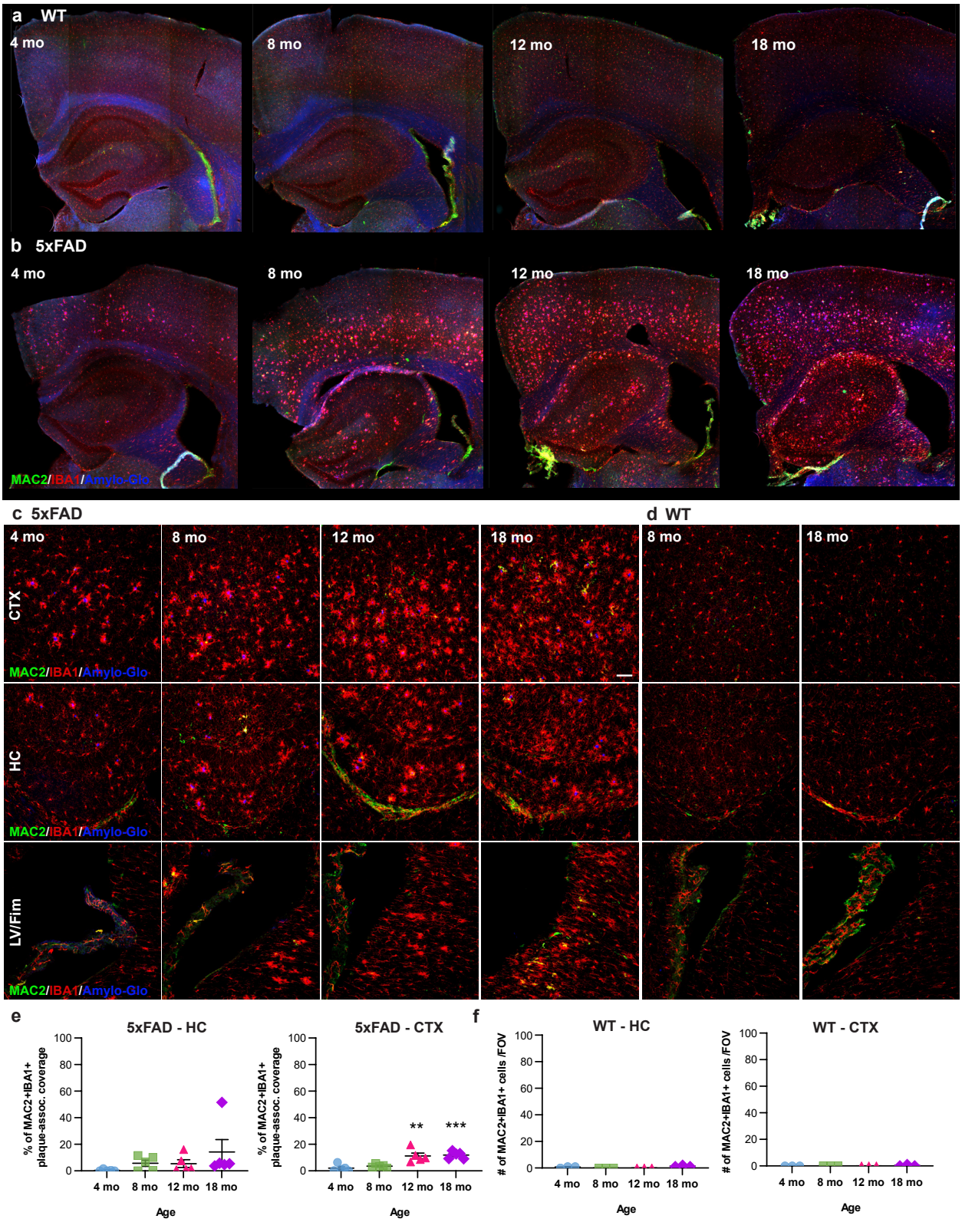
a WT
4 mo
8 mo
12 mo
18 mo
b 5xFAD
4 mo
8 mo
12 mo
18 mo
MAC2/IBA1/Amylo-Glo
c 5xFAD
d WT
4 mo
8 mo
12 mo
18 mo
CTX
HC
LV/Fim
MAC2/IBA1/Amylo-Glo
e
5xFAD - HC
5xFAD - CTX
% of MAC2+IBA1+ plaque-assoc. coverage
100
80
60
40
20
0
4 mo
8 mo
12 mo
18 mo
Age
**
***
f
WT - HC
WT - CTX
# of MAC2+IBA1+ cells /FOV

Figure 4. The effects of aging on MAC2 staining in WT and 5xFAD mice. Brains of wild type (WT) and 5xFAD mice at 4, 8, 12, and 18 months (mo) of age were evaluated for MAC2 staining in plaque-associated microglia. (a-b) Representative images of MAC2 (green), IBA1 (red, myeloid cells), and Amylo-Glo (blue, amyloid plaques) staining in brain sections of WT (a) and 5xFAD (b) mice. (c-d) Representative 20x confocal images of MAC2, IBA1, and Amylo-Glo staining in the cortex (CTX), hippocampus (HC), and lateral ventricle (LV)/fimbria (Fim) of WT (d) and 5xFAD (c) mice shows the age-dependent increase in MAC2 staining in 5xFAD mice. (e-f) Quantification of plaque-associated MAC2+IBA1+ staining and MAC2+IBA1+ cells in 5xFAD and WT mice, respectively. Female (pink) and male (blue) mice are indicated by color scheme. Data are represented as mean ± SEM (n=3-5). ** $p < 0.01$, *** $p < 0.001$, compared to 4 mo. Scale bar in (c) ~60 μm.

Chapter 5

EVALUATING THE ROLE OF CYSTATIN F IN DEMYELINATION AND REMYELINATION FOLLOWING CNS INFECTION WITH A VIRAL MODEL OF MULTIPLE SCLEROSIS

ABSTRACT

Multiple sclerosis (MS) leaves millions of people worldwide with impaired central nervous system (CNS) function. A great deal remains unknown about the physiological landscape of MS pathogenesis and of what factors might exacerbate or ameliorate the severity of disease outcomes. As the resident immune cell of the CNS, microglia are considered active members of this pathogenic landscape, but whether their contributions are more destructive, or protective remains highly debated. Our previous studies using the microglia-depleting drug PLX5622, demonstrated that upon depletion of microglia prior to infection of susceptible mice with the neurotropic JHM strain of the mouse hepatitis virus (JHMV), resulted in an increase in viral load and worsened demyelination associated with impaired remyelination. However, the mechanisms by which microglia reduce the severity of demyelination and enhance remyelination remains unclear. Using 10x single cell RNA sequencing (scRNAseq), we found that depletion of microglia in JHMV infected mice results in reduced expression of *Cst7* transcripts that encodes cystatin F which has been implicated as important in influencing remyelination. Cystatin F is a secreted lysosomal cysteine protease inhibitor that is normally only expressed by immune cells and not in the CNS, but expression increases in acute demyelinating lesions in several models of demyelination, specifically by microglia. Cystatin F expression is commonly found in areas where both demyelination and remyelination are ongoing and expression is induced upon microglia phagocytosis of myelin debris. The effect on demyelination and remyelination by cystatin F are thought to occur through regulation of its main target, cathepsin C, that stimulates expression of immune cell chemoattractants and promotes pro-inflammatory polarization in microglia/macrophages. Cystatin F serves as a promising mediator of demyelination and remyelination, but mechanisms associated with these processes within the context of viral-induced

neurologic disease remain to be characterized. We hypothesized that cystatin F restricts the severity of virus-induced demyelination and promotes subsequent remyelination following JHMV infection of the CNS. Using a Cystatin F knock-out mouse line (*Cst7* KO), we found that following CNS infection with JHMV, *Cst7* KO mice had worsened spinal cord demyelination compared to wild-type littermates at both days 14 and 21 post-infection (p.i.). Flow cytometric analysis of brains of infected mice showed increased infiltration of T cells in *Cst7* KO mice at day 21 p.i., but not at day 7 p.i. Electron microscopic analysis along with g-ratio calculations showed a reduction in spinal cord remyelination at day 21 pi. ScRNAseq of CD45+ cells enriched from spinal cords at day 21 p.i. revealed increased expression of T cell chemoattractant *Cxcl9* and increased expression of CD8+ T cell activation markers. Results from this study highlight a previously unappreciated role of cystatin F in restricting the severity of demyelination and influencing remyelination in a viral model of neurologic disease.

INTRODUCTION

The human demyelinating disease Multiple sclerosis (MS) is a devastating neurodegenerative disease that affects millions of people worldwide. Unfortunately, there is no single known cause of disease and effective treatments are limited in reversing outcomes. A majority of the existing FDA-approved therapies are for patients with the Relapsing-Remitting form of disease and are focused on blocking infiltration of activated immune cells into the central nervous system (CNS) to limit new lesion formation. However, these disease modifying therapies (DMTs) do not target activated resident cells of the CNS which may also contribute to ongoing neurodegeneration. Microglia play an important role in promoting remyelination[1]. This is most likely a result of a multitude of specialized microglial functions, ranging from phagocytosis of myelin debris, of which is known to inhibit OPC differentiation and remyelination[2–6], through recruiting and promoting differentiation of oligodendrocyte progenitor cells (OPCs)[7,8], and by altering the microenvironment to encourage remyelination and survival of oligodendrocytes and OPCs by secreting growth factors and signaling mediators[9–13]. Understanding the specific mechanisms that dictate these restorative functions will provide novel and promising targets for therapeutic intervention.

The ubiquitously expressed cystatin C has gotten more attention in the realm of neurodegenerative diseases including ALZ, ALS, MS, and in aging, for its inhibitory effect on cathepsin b[14–16], but as the role of cystatins and their target cathepsins in CNS disease is a relatively new field of research, not much is known of the potential roles of other cystatins. One of more recent interest is cystatin F, a papain-like lysosomal cysteine protease inhibitor. Unlike cystatin C, cystatin F is only expressed by immune cells and not at all in the CNS, except by microglia when demyelination is occurring[17–20]. Curiously, expression patterns of cystatin F only overlap in

demyelinating regions where remyelination is also occurring in mouse models of demyelinating disease EAE, CPZ, $Plp^{4e/-}$ and in plaques from patients with MS, garnering new interest in the protein for its potential role in demyelinating disease[17,18,20,21]. Unlike cystatin C, cystatin F is secreted and is unique from other secreted cystatins in that it is secreted as an inactive disulfide-linked dimer and only becomes active upon proteolytic cleavage of 15 N-terminal residues when endocytosed by target cells, where it is trafficked to endosomal/lysosomal compartments thus suggesting its primary function is to modulate surrounding cells[22–24]. Cystatin F is more commonly known for its use by cancer cells to immunosuppress granule-mediated cytotoxicity of effector CD8+ T cells and NK cells[25–28]. This is accomplished through secretion of cystatin F by cancer cells and internalization by antigen-specific CD8+ T cells, where the now active cystatin F can inhibit its main target protease cathepsin C, a lysosomal cysteine protease that processes pro-granzymes for release[25–29]. In addition to processing granzymes for release by immune cell populations, cathepsin C has also been found to process cytokines and chemokines for release[27,29–31] promote polarization of microglia and macrophages to more pro-inflammatory states[30,32]. Expression of cystatin F by microglia in the CNS is triggered by phagocytosis of myelin debris[19], eluding that microglia may be secreting cystatin F to prevent further damage inflicted by activated pro-inflammatory cells, similar to its employment by cancer cells to prevent granule-mediated cytotoxicity. With the growing understanding that immune cells play a more prominent role in neurodegenerative diseases than previously recognized, it is important to understand their contributions to disease and endogenous attempts to defend against this damaging effect that immune cells may have on neurons and myelin. Cystatin F is a promising factor for therapeutic use, but a deeper understanding of how this protein functions is crucial before implementing in a complex human disease like MS, to which there is no single identified cause.

We previously determined that ablation of microglia prior to infection with JHMV resulted in increased demyelination and impaired remyelination, which coincided with a reduction in expression of transcripts associated with remyelination in macrophages and remaining microglia, the most greatly reduced being *Cst7*. In this study, we set out to determine if cystatin F is involved in this process of modulating white matter damage and repair in a viral model of demyelinating disease and employed a novel *Cst7* KO mouse to assess response to JHMV infection. Findings from this study indicate increased demyelination and reduced remyelination in addition to increased CNS infiltration of CD8+ and CD4+ T cells in *Cst7* KO mice compared to controls. These results indicate a potential role for cystatin F as a mechanism for microglia in restricting disease severity and promoting recovery. Cystatin F is a promising factor for therapeutic use, but a deeper understanding of how this protein functions is crucial before implementing in a complex human disease like MS, to which there is no single identified cause.

MATERIALS AND METHODS

Mice and viral infection. Cst7$^{-/-}$ transgenic mice (referred to as Cst7 KO) were generated by the University of California, Irvine transgenic mouse facility. Cst7 KO mice have a 168bp deletion of the 3' end of *Cst7* Exon 1 and the 5' end of intron 1. The mutant Exon 1 retains the initiator AUG, but lacks a splice donor sequence at the end of Exon 1. Heterozygous *Cst7* mice (*Cst7*$^{+/-}$) were bred to produce experimental Cst7 KO mice (*Cst7*$^{-/-}$) and wildtype littermate Controls (*Cst7*$^{+/+}$). Five to eight-week-old male and female Cst7 KO mice and Controls were infected intracranially (i.c.) with 750-1200 plaque forming units (PFU) of JHMV strain J2.2v-1 in 30μL of sterile Hanks balanced sterile solution (HBSS) and animals were euthanized at days 7, 14, and 21 post-infection (p.i). Clinical disease in JHMV-infected mice was evaluated using a previously described scale[33]. To determine viral titers within brains, experimental animals were sacrificed at defined times p.i, brains isolated, homogenized and plaque assay were performed on the DBT astrocytoma cell line as described previously[34]. All animal studies were reviewed and approved by the University of California, Irvine Animal Care and Use Committee.

Cell isolation and flow cytometry. Flow cytometry was performed to identify inflammatory cells entering the CNS using established protocols[35,36]. In brief, single cell suspensions were generated from tissue samples by grinding with frosted microscope slides. Immune cells were enriched via a 2-step Percoll cushion (90% and 63%) and cells were collected at the interface of the two Percoll layers. Before staining with fluorescent antibodies, isolated cells were incubated with anti-CD16/32 Fc block (BD Biosciences, San Jose, CA) at a 1:200 dilution. Immunophenotyping was performed using commercially available antibodies specific for the following cell surface markers: CD4 (Invitrogen, 11-0042-82), CD8a (Invitrogen, 17-0081-82),

CD11b (Abcam, ab24874) and CD45 (Biolegend, 103112; 103130). The following flow cytometric gating strategies were employed for inflammatory cells isolated from the CNS: macrophages ($CD45^{hi}CD11b+$) and microglia ($CD45^{lo}$ CD11b+). APC-conjugated rat anti-mouse CD4 and a PE-conjugated tetramer specific for the CD4 immunodominant epitope present within the JHMV matrix (M) glycoprotein spanning amino acids 133-147 (M133-147 tetramer) to determine total and virus-specific $CD4^+$ cells, respectively[36,37]; APC-conjugated rat anti-mouse CD8a and a PE-conjugated tetramer specific for the CD8 immunodominant epitope present in the spike (S) glycoprotein spanning amino acids 510-518 (S510-518) to identify total and virus-specific $CD8^+$ cells, respectively[36,37]. Data were collected using a Novocyte flow cytometer and analyzed with FlowJo software (Tree Star Inc.).

Histology. Mice were euthanized at days 14 and 21 p.i. with isoflurane, and immediately cardiac perfused with 20mL of 1X PBS. Mouse torsos containing spinal cords were isolated and stored in 4% paraformaldehyde for 24-36 hours. The length of spinal cord extending from thoracic vertebrate 6-10 was carefully removed and cryoprotected in 30% sucrose for a minimum of 2 days, then cut into 1-mm transverse blocks and processed so as to preserve the craniocaudal orientation and subsequently embedded in O.C.T. (VWR, Radnor, PA, USA). Eight micron (μm)-thick coronal sections were cryosectioned and sections were stained with hematoxylin/eosin (H&E) in combination with luxol fast blue (LFB) and between 4-8 sections/mouse analyzed. Areas of total white matter and demyelinated white matter were determined with Image J Software and demyelination was scored as a percentage of total white matter from spinal cord sections analyzed[35,37–39].

Electron microscopy and analysis. Mice were euthanized at day 21 p.i. with isoflurane, and immediately underwent cardiac perfusion with 20mL of 1X PBS followed by 20mL of 0.1 M cacodylate buffer containing 2% paraformaldehyde/2% glutaraldehyde. The length of spinal cord extending from thoracic vertebrate 6-10 was carefully removed and stored in 2% paraformaldehyde/2% glutaraldehyde overnight. Serial ultrathin sections of spinal cord embedded in Epon epoxy resin were stained with uranyl acetate-lead citrate and analyzed as previously described[1]. Images were taken at 1200X magnification in demyelinating regions within the spinal cord ventral and lateral funiculus for Cst7 KO mice (n=2, 13-15 images analyzed/mouse, 329-537 axons analyzed/mouse) and wildtype littermates (n=2, 10-15 images analyzed/mouse, 451-453 axons analyzed/mouse) and analyzed using Image J software. G-ratio is calculated as a ratio of axon diameter to total outer fiber diameter[40]. Axons were considered to be remyelinated if myelin thickness was less than 0.5 μm and the g-ratio was greater than 0.65. Absence of myelin sheath was used as the criterion for demyelinated axons. For each sample, between 10-15 images were analyzed, with a minimum of 750 axons analyzed per experimental group.

10X Genomics Chromium Single Cell 3' Single Cell RNA sequencing (scRNASeq). Cells were isolated via homogenization and percoll gradient as previously described, keeping cells in RPMI with 10% FBS and on ice whenever possible. Isolated cells were incubated with anti-CD16/32 Fc block (BD Biosciences, San Jose, CA) at a 1:200 dilution. Cells were stained with DAPI and APC conjugated anti-CD45 (Biolegend, 103112) for 20 minutes on ice in 1X PBS containing 0.5% bovine serum albumin (BSA). Live $CD45^+$ cells were enriched using both BD FACSAria II and BD Fusion cell sorters (UC Irvine Stem Cell Research Center, Flow Cytometry

Core), washed once with 0.04% BSA. Individual samples were then labeled with 100 µl of a unique Cell Multiplexing Oligo (CMO), consisting of a Feature Barcode oligonucleotide conjugated to a lipid (10X Genomics Chromium Single Cell 3' CellPlex Kit) for 5 min at room temperature. Samples were washed twice with 1% BSA in PBS, counted, and pooled. Relatively equal cell numbers were pooled from each sample, with one or two samples containing too low of a cell count to match exactly if the required number of total cells was to be achieved. Pooled samples were reconstituted to a concentration of 1,000 cells/µl and processed by the UC Irvine Genomics High-Throughput Facility (https://ghtf.biochem.uci.edu) for single cell RNA sequencing using the 10X Genomics Chromium Single Cell 3' platform. The NovaSeq 6000 sequencer was used to perform RNA sequencing (200 cycles) and sequencing reads were processed using the 10X Genomics CellRanger pipeline.

scRNAseq analysis. Using Seurat version 4.1.1 experimental groups were filtered, integrated, normalized, and scaled. Genes that were found in less than 10 cells, as well as cells with less than 500 and greater than 3,500 detected genes were removed. Additionally, cells with more than 30,000 UMIs and greater than 5% mitochondrial counts were regressed out. Gene counts per cell were normalized by total expression, multiplied by a scale factor of 10,000, then transformed to log scale. Downstream analysis was performed in Seurat, following principal correlation analysis (PCA) and uniform manifold approximation and projection (UMAP) dimensional reduction[41,42]. Gene expression signatures of $CD45^+$ cells from spinal cords of uninfected and JHMV-infected Cst7 KO and WT mice at day 21 p.i. were scrutinized and cells from the aggregated dataset were clustered into corresponding immune cell populations by a shared nearest neighbor (SNN) modularity optimization-based clustering algorithm via the FindClusters function in the Seurat

analysis package in R. The resulting clusters were defined by analysis of expression levels and distribution of population-specific immune cell markers. Once the clusters were established and identified, plots were generated using Seurat and ggpubr R packages[43].

Statistical analysis. GraphPad Prism was used to perform statistical analyses. Data for each experiment is presented as mean±standard error of mean (SEM). Values from experimental groups were compared using either unpaired (two-tailed) t-test, Mann-Whitney *U* test, or Welch's t-test. Wilcoxon test was used for analyzing gene expression in scRNAseq clusters and the resulting *p* values were corrected for multiple comparisons by Holm-Sidak method and a *p* value of ≤ 0.05 was considered statistically significant (*$p \leq 0.05$; ** $p \leq 0.01$; ***$p \leq 0.001$; ****$p \leq 0.0001$).

RESULTS

Derivation of Cst7 KO mice.

Our experimental goals were to determine the functional role of cystatin F in regulating molecular and cellular events contributing to host defense, disease, and tissue repair following JHMV infection of the CNS. To achieve this, we employed a novel cystatin F knock-out mouse line, *Cst7*$^{-/-}$ (referred to as Cst7 KO) that has a 168bp deletion of the 3' end of *Cst7* Exon 1 and the 5' end of intron 1. The mutant Exon 1 retains the initiator AUG, but lacks a splice donor sequence at the end of Exon 1. Homozygous ablation of *Cst7* was confirmed using PCR primers that generate an amplicon following deletion of the 168bp sequence in Exon 1 (**Supplemental Figure 1**).

JHMV infection and Cst7 expression.

First, to determine the expression profile of cystatin F and its target, cathepsin C, we looked at expression patterns in our previous scRNAseq dataset with adult C57BL/6 mice infected i.c. with 1000 PFU of JHMV at days 3, 7, and 21 p.i.[44]. We found that microglia show the highest expression of *Cst7* and this peak expression level is reached at the chronic disease time point of day 21 p.i. (**Figure 1**), consistent with expression patterns of cystatin F in the context of MS and preclinical demyelinating diseases[17,18,20,21]. Examining the expression patterns of its lysosomal target, cathepsin C (*Ctsc*), and found expression was highest in monocyte and macrophage populations and was highest during innate (day 3p.i.) and adaptive (day 7p.i.) immune response time points (**Supplemental Figure 2**). This pattern is consistent with the idea that cystatin F negatively regulates cathepsin C. Whether this is simply through its known

canonical function of interacting directly with the protein or if it has a noncanonical impact on expression of cathepsin C, is still unclear.

Cystatin F does not impact immune cell infiltration and viral clearance in brains at day 7 p.i.

Cst7 KO and WT mice were infected i.c. with 1200 PFU of virus, brains were removed at day 7 to determine viral burden via plaque assay and immune cell infiltration through flow cytometric analysis, and clinical scores were recorded daily out to day 21 p.i. (**Figure 2a**). Infection of Cst7 KO mice results in increased clinical disease severity from day 16 to 21 p.i. compared to WT littermates (**Figure 2b**). Quantification of plaques from brains of infected mice showed no significant difference in viral titers between Cst7 KO mice and WT mice at day 7 p.i. ($p = 0.3590$) (**Figure 2c**) indicating that cystatin F was not involved in controlling virus replication during acute disease.

Cystatin F has been suggested to play a role in suppressing target cells from secreting immune cell chemoattractants[21,29]. We next conducted flow cytometric analysis on brains at day 7p.i. to examine a role for cystatin F in influencing immune cell recruitment into the CNS at peak adaptive response to JHMV infection. We quantified numbers of CD4+ (CD45+CD4+) and CD8+ (CD45+CD8a+) T cells, CD4+ (CD45+CD4+M133tet+) and CD8+ (CD45+CD8a+S510tet+) virus-specific T cells, macrophages (CD11b+CD45^{hi}), and microglia (CD11b+CD45^{lo}) and found no significant differences in cell numbers of macrophages (**Figure 2d**), microglia (**Figure 2e**) nor either of CD4+ or CD8+ T cells as well as virus-specific CD4+ and CD8+ T cells (**Figures 2f-i**) between Cst7 KO mice and WT controls.

Genetic ablation of cystatin F increases immune cell recruitment into CNS at day 21 p.i.

We next wanted to determine if silencing cystatin F impacted immune cell infiltration into the CNS at day 21 p.i., as this correlated with the timepoint maintaining the highest expression of cystatin F (**Figure 3a**). Brains were isolated from Cst7 KO and WT littermates at day 21 p.i. to evaluate differences in number of infiltrating immune cells. Flow cytometric analysis revealed no difference in numbers of either macrophages (**Figure 3b**), microglia (**Figure 3c**) or virus-specific CD8+ T cells (**Figure 3e**) between Cst7 KO and WT mice. However, infiltration of CD8+ T cells (**Figure 3d**), CD4+ T cells (**Figure 3f**) and virus-specific CD4+ T cells (**Figure 3g**) was increased in Cst7 KO mice compared to WT controls.

Genetic ablation of cystatin F increases the severity of spinal cord demyelination following JHMV infection.

We next assessed how genetic ablation of cystatin F affected spinal cord demyelination during acute and chronic demyelinating time points in JHMV-infected mice. Spinal cords were removed at days 14 and 21 p.i. to evaluate differences in severity of demyelination (**Figure 3a**). The severity of spinal cord demyelination was significantly increased in Cst7 ko mice at days 14 ($p = 0.0275$) and 21 ($p = 0.0103$) p.i. as compared to infected WT mice (**Figures 3h-j**).

Absence of Cystatin F results in impaired remyelination in spinal cords in JHMV-infected mice.

To determine whether remyelination was impacted by the absence of cystatin F, electron microscopic (EM) analysis of spinal cord sections was performed (**Figure 4a**). High

magnification (1200X) images of demyelinating regions in the spinal cord ventral and lateral funiculus of Cst7 KO mice (n=2, 13-15 images analyzed/mouse, 329-537 axons analyzed/mouse) compared to wildtype littermates (n=2, 10-15 images analyzed/mouse, 451-453 axons analyzed/mouse) were used to assess remyelination (**Figure 4b**). Measurement of *g*-ratio, the ratio of the inner axonal diameter to the total outer fiber diameter, is commonly employed as a structural index of remyelination, with lower ratios indicating more extensive myelination[40]. From analysis of axons in these electron micrographs, we found that when compared with wildtype littermates, Cst7 KO mice had increased g-ratios (WT:0.847; KO: 0.902) (**Figure 4c**), reduced myelin thickness (**Figure 4d**), an increased ratio of demyelinated axons (**Figure 4e**), and a reduced ratio of remyelinated axons (**Figure 4f**), suggesting an impaired capacity to remyelinate in the absence of cystatin F.

10X scRNAseq reveals immune cell diversity between Cst7 KO and WT controls following JHMV infection.

To better understand the molecular mechanisms by which cystatin F impacted neuroinflammation and demyelination, we elected to perform 10X Chromium 3' scRNAseq on spinal cords of JHMV infected Cst7 KO mice and WT littermate controls at day 21 p.i. (KO-Day21pi, WT-Day21pi) as well as noninfected Cst7 KO (KO-Uninfected) and WT mice (WT-Uninfected) (**Figure 5a**). Spinal cords were removed from experimental mice; infiltrating immune cells and microglia were FACS sorted on a CD45+DAPI- gate, filtering out dead cells and potential doublets, and enriched CD45+DAPI- cells were subsequently Cell Multiplexing Oligo (CMO) labeled and pooled before undergoing scRNAseq (**Figure 5a**). Any remaining unhealthy or dead cells and doublets were regressed out using the Seurat R package and final cell

numbers used in downstream analysis were reported [WT-uninfected: 2,788 cells (n = 4), KO-uninfected: 3,175 cells (n = 5), WT-Day21pi: 4,982 cells (n = 6), KO-Day21pi: 5,901 cells (n = 6)]. Unbiased clustering analysis revealed 19 unique cell clusters (**Figure 5b**). *Cst7* expression was evaluated and found to be exclusively expressed in WT-Day21pi mice, confirming that *Cst7* was effectively ablated in Cst7 KO mice and that expression of *Cst7* is not present in uninfected, healthy controls, consistent previous findings (**Figures 5c and d**)[44]. To corroborate the algorithm-assisted identification of clusters, we assessed expression of known cellular markers in our dataset and found that expression of these markers corresponded with respective cell cluster identities (**Figures 5e**).

We next analyzed differences in population dynamics of CD45+ cells between experimental groups, finding that CD45+ cells from spinal cords of uninfected experimental mice (WT-Uninfected, KO-Uninfected) are primarily comprised of microglia subpopulations MG1 and MG2 (**Figures 6a and b**). Interestingly, a relatively large number of neutrophils were present in uninfected groups (**Figures 6a and b**). However, these neutrophils do not appear to express transcripts defining activated neutrophils and may be an artifact of poor perfusion, as without more CD45+ cells present, these artifacts may be overrepresented (data not shown). Infected Cst7 KO and WT controls (KO-Day21pi, WT-Day21pi) appear to be largely comprised of CD4+ and CD8+ T cells, proliferating or cycling CD8+ T cells (Cyc. CD8+), regulatory T cells (Tregs), antibody secreting cells (ASCs), NK cells, dendritic cells (DCs), macrophages (Macs), and microglia subpopulations MG3 and MG4 (**Figures 6a and b**). Infected Cst7 KO mice reveal increased frequencies of CD4+, CD8+, and Cycling CD8+ T cells, as well as antibody secreting cells (ASCs), macrophages (Macs), and dendritic cells (DCs) compared to infected WT controls, with few of these cells found in the uninfected groups, consistent with

flow cytometric data (**Figures 6a and b**). Of the four different microglia subpopulations, MG1 and MG2 presented more of a homeostatic gene expression signature (*P2ry12*, *Tmem119*, *Cx3cr1*)[45,46], while MG3 and MG4 showed elevated expression of transcripts associated with damage (*Apoe*, *Spp1*, *Trem2*)[45–47] and repair (*Cst7*, *Lpl*, *Igf1*)[48–50] (**Figure 6c-e**).

Ablation of Cst7 leads to increased activation of surrounding cells in JHMV infection.

We next evaluated if absence of cystatin F impacted differential activation states in specific cell populations of infected mice (**Figures 7 and 8**). When comparing expression of markers associated with demyelination and remyelination, we found an increase in expression of *Apoe* and *Trem2* in microglia and macrophages of infected Cst7 KO mice compared to WT controls, but no difference in expression of *Spp1* (osteopontin) (**Figures 7c and d**) or transcripts associated with remyelination *Igf1* (Insulin-like growth factor-1) or *Lpl* (lipoprotein lipase) (**Figures 7e and f**)[45,48–50]. Additionally, we found that expression of homeostatic microglia markers *Cx3cr1*, *P2ry12*, and *Tmem119*, were reduced in infected Cst7 KO mice compared to infected WT controls (**Figure 7g**)[45].

When comparing expression of markers associated with T cell activation in infected Cst7 KO and WT controls, we found an increase in expression of *Gzmb* (granzyme B), *Prf1* (perforin), and *Ifng* (IFN-gamma) by CD8+ T cells and Cyc. CD8+ T cells in Cst7 KO mice (**Figures 8b and c**). Similarly, we found an increase in expression of activation markers including *Tnfrsf4* and *Icos* (Inducible T cell co-stimulator) in CD4+ T cells clusters by Cst7 KO mice compared to WT controls (**Figure 8e**)[51,52]. We next assessed if ablation of *Cst7* impacted expression of T cell chemoattractants and found an increase in expression of transcripts encoding CXCL9 in both microglia and monocyte/macrophage populations (**Figures 8f and g**).

DISCUSSION

Microglia have been found to play a role in restricting the severity of spinal cord demyelination and promoting remyelination following intracranial infection with JHMV, a viral pre-clinical model of MS, though the mechanism of how remains unclear[1]. Though microglia are important for launching an effective immune response to control of virus replication[1], further work by Yuting Cheng *et.al.* has shown that a delayed microglia depletion after viral infection has been controlled still results in increased demyelination and impaired remyelination (data not shown). This further upholds the idea that microglia contribute a more direct role in repair during chronic disease in JHMV infection. Microglia-derived cystatin F has been found to play a role in modulating disease severity in other mouse models of demyelination, including EAE, CPZ, and $Plp^{4e/-}$, and MS and is found at the leading edges of plaques in postmortem tissue from MS patients suggesting a role in demyelination and remyelination[17,18,20,21]. However, its exact role is not well characterized and has never been examined in the context of viral induced demyelinating disease; an environment that can be resemble to both a relapse triggered by viral infection in MS patients (acute JHMV infection) as well as chronic disease in progressive MS (chronic JHMV infection). Therefore, we sought to determine if cystatin F is a mechanism for how microglia restrict the severity of demyelination and promote remyelination in chronic disease, but also assessed any potential roles in acute disease.

We first wanted to evaluate the expression profile of cystatin F throughout infection and found that its highest expression was by microglia at day 21 p.i., which is a chronic timepoint where demyelination and remyelination is ongoing, consistent with the expression profile found in other pre-clinical models of demyelination and in MS (**Figures 1a-c**)[17,18,20,21]. Following infection with 1200 PFU of JHMV, Cst7 KO mice show significantly higher clinical scores than

WT littermates from day 16 p.i. out to day 21 p.i.; demonstrating that without cystatin F, mice not only experience worse clinical disease, but show an impaired ability to recover. Cystatin F acts through inhibiting its main target protease, cathepsin C. Cathepsin C is known to cleave pro-enzymes into their active forms and have been found to do so with granzymes in immune cell populations[25–29], as well as with cytokines and chemokines[27,29–31]. Therefore, we wanted to know if perhaps this worsened clinical disease demonstrated by Cst7 KO mice was an artifact of elevated or sustained immune cell infiltration, resulting from uninhibited cathepsin C-mediated chemokine secretion and/or granzyme release. We wanted to see if there were any changes at day 21 p.i., where we have the highest Cst7 expression (**Figure 1c**), but also at day 7 p.i. to determine if the low levels of *Cst7* expressed by T cells and microglia during acute disease could impact early immune response as well (**Figures 1a and b**). We infected Cst7 KO and WT controls and isolated brains at days 7 and 21 p.i., conducting viral titers at day 7 p.i. and flow cytometric analysis of immune cell populations at both days 7 and 21 p.i. (**Figures 2 and 3**). At day 7 p.i., there was no significant difference in viral burden between Cst7 KO and WT controls (**Figure 2c**), as well as no change in CNS infiltration by T cells, virus-specific T cells, and macrophages (**Figures 2d-i**). This indicates that cystatin F does not play a prominent role in acute disease following JHMV infection and that these low levels of *Cst7* expression by T cells and microglia during early infection may be negligible. However, at day 21 p.i. we found a significant increase in CD8+ and CD4+ T cells as well as virus-specific CD4+ T cells in brains of Cst7 KO mice compared to WT controls (**Figures 3b-g**). This sustained infiltration by CD4+ and CD8+ T cells at day 21 p.i. correlated with amplified spinal cord demyelination in Cst7 KO mice at both days 14 and 21 p.i. when compared to WT controls (**Figures 3i-k**), demonstrating that outcomes resulting from cystatin F in response to JHMV infection arise at later time points.

We next analyzed spinal cords via EM analysis at day 21 p.i. to determine if there was a potential role for cystatin F in promoting remyelination in disease and found an increase in g-ratios in Cst7 KO mice, indicating impaired remyelination in comparison to WT controls (**Figure 4c**). Additionally, measured variables including myelin thickness and ratios of remyelinated axons were lower in the Cst7 KO mice compared to controls, while ratios of demyelinated axons were higher in Cst7 KO mice (**Figures 4d-f**). Together, results signify that cystatin F plays a role in restricting the severity of JHMV-induced demyelination and promoting subsequent remyelination during chronic disease, possibly by inhibiting recruitment of potentially damaging immune cells.

Cystatin F has also been found to limit polarization to pro-inflammatory states in microglia and macrophages by inhibiting cathepsin C in other models of demyelination[30]. Therefore, we examined activation states in CD45+ (immune cell infiltrates and microglia) cells from spinal cords of uninfected and infected Cst7 KO and WT littermates at day 21 p.i. through 10X scRNAseq. Population dynamics were consistent with our flow cytometry findings in brains, showing an increase in CD4+ and CD8+ T cells in spinal cords of infected Cst7 KO mice (KO-Day21pi) compared to WT infected controls (WT-Day21pi), as well as an increase in antibody secreting cells (ASCs), dendritic cells (DCs), and macrophages (**Figures 5a and b**). Furthermore, spinal cords of infected Cst7 KO (KO-day21pi) appear to have fewer cells from the homeostatic microglia populations (MG1, MG2) then infected controls; similarly, expression of homeostatic transcripts *Cx3cr1*, *Tmem119*, and *P2ry12* was reduced in microglia from KO-day21pi (**Figure 7g**). When microglia are depleted prior to JHMV infection, expression of transcripts encoding APOE (*Apoe*), osteopontin (*Spp1*), and TREM-2 (*Trem2*) that are associated with demyelination were increased, and expression of transcripts encoding insulin-like growth

factor-1 (IGF-1, *Igf1*) *Igf1* and lipoprotein lipase (*Lpl*) that are associated with remyelination, were reduced [1,48–50]. Therefore, we compared expression of these demyelination and remyelination markers in microglia and monocyte/macrophage populations between infected Cst7 KO (KO-Day21pi) mice and infected WT controls (WT-Day21pi) in our scRNASeq dataset and found an increase in expression of *Apoe* and *Trem2* in both microglia and monos/macs from spinal cords of infected Cst7 KO mice (**Figures 7c and d**). However, we found no change in expression of *Igf1* or *Lpl* between infected Cst7 KO and WT groups (**Figures 7e and f**). We next wanted to see if there was a change in expression of transcripts encoding markers for T cell activation and found an increase in expression of *Gzmb* (granzyme b), *Prf1* (perforin), and *Ifng* (IFN-gamma) in CD8+ and Cyc. CD8+ T cells, and an increase in expression of *Icos* (Inducible T cell co-stimulator) and *Tnfrsf4* (TNF receptor superfamily member 4) in CD4+ T cells (**Figure 8**). Additionally, we looked at changes in expression of T cell chemoattractants between infected Cst7 KO and WT controls and found elevated levels of *Cxcl9* expression in microglia and macrophage populations from spinal cords of infected Cst7 KO mice (**Figures 8f and g**). Together, these findings indicated that not only does cystatin F reduce immune cell recruitment and T cell-mediated cytolytic activity through inhibition of cathepsin C-mediated processing and release of granzymes and chemokines, but also modulates the expression of these proteins as well.

In summary, cystatin F plays a role in restricting the severity of demyelination and promoting remyelination and could be potential mechanism for microglia in repair. Cystatin F has a modulatory effect on immune cell recruitment into the CNS and this effect during chronic disease (i.e. day 21p.i.) in JHMV infection with no impact on immune response an recruitment during acute disease (i.e. day 7 p.i.), further advocating a relevant role for cystatin F in chronic

MS. Cystatin F influenced activation of CD4+ and CD8+ T cells as well as expression of disease-associated markers *Apoe* and *Trem2*, but did not impact expression of remyelination associated markers. There is currently no data showing a direct role for cystatin F in modulating gene expression, but these changes in expression may be indirect and resulting from downstream processes. Additionally, promotion of remyelination may also be a result of limiting inflammation surrounding damaged myelin sheaths, allowing for regeneration to efficiently presume. Future research will be conducted to identify a more direct link between microglia and cystatin F, but results from this study shed light on a very novel area of research.

REFERENCES

1. Mangale, V. *et al.* Microglia influence host defense, disease, and repair following murine coronavirus infection of the central nervous system. *Glia* 1–16 (2020). doi:10.1002/glia.23844

2. Syed, Y. A. *et al.* Inhibition of oligodendrocyte precursor cell differentiation by myelin-associated proteins. *Neurosurg. Focus* **24**, E5 (2008).

3. Plemel, J. R., Manesh, S. B., Sparling, J. S. & Tetzlaff, W. Myelin inhibits oligodendroglial maturation and regulates oligodendrocytic transcription factor expression. *Glia* **61**, 1471–1487 (2013).

4. Kotter, M. R., Li, W. W., Zhao, C. & Franklin, R. J. M. Myelin impairs CNS remyelination by inhibiting oligodendrocyte precursor cell differentiation. *J. Neurosci.* **26**, 328–332 (2006).

5. Sosa, R. A., Murphey, C., Ji, N., Cardona, A. E. & Forsthuber, T. G. The kinetics of myelin antigen uptake by myeloid cells in the central nervous system during experimental autoimmune encephalomyelitis. *J. Immunol.* **191**, 5848–5857 (2013).

6. Rawji, K. S. *et al.* Deficient Surveillance and Phagocytic Activity of Myeloid Cells Within Demyelinated Lesions in Aging Mice Visualized by Ex Vivo Live Multiphoton Imaging. *J. Neurosci. Off. J. Soc. Neurosci.* **38**, 1973–1988 (2018).

7. Arnett, H. A. *et al.* TNF alpha promotes proliferation of oligodendrocyte progenitors and remyelination. *Nat. Neurosci.* **4**, 1116–1122 (2001).

8. Voss, E. V. *et al.* Characterisation of microglia during de- and remyelination: can they create a repair promoting environment? *Neurobiol. Dis.* **45**, 519–528 (2012).

9. Mason, J. L., Ye, P., Suzuki, K., D'Ercole, A. J. & Matsushima, G. K. Insulin-like growth factor-1 inhibits mature oligodendrocyte apoptosis during primary demyelination. *J. Neurosci.* **20**, 5703–5708 (2000).

10. Giera, S. *et al.* Microglial transglutaminase-2 drives myelination and myelin repair via GPR56/ADGRG1 in oligodendrocyte precursor cells. *Elife* **7**, (2018).

11. Miron, V. E. *et al.* M2 microglia and macrophages drive oligodendrocyte differentiation during CNS remyelination. *Nat. Neurosci.* **16**, 1211–1218 (2013).

12. Dillenburg, A. *et al.* Activin receptors regulate the oligodendrocyte lineage in health and disease. *Acta Neuropathol.* **135**, 887–906 (2018).

13. Mason, J. L., Suzuki, K., Chaplin, D. D. & Matsushima, G. K. Interleukin-1beta promotes repair of the CNS. *J. Neurosci. Off. J. Soc. Neurosci.* **21**, 7046–7052 (2001).

14. Gauthier, S., Kaur, G., Mi, W., Tizon, B. & Levy, E. Protective mechanisms by cystatin C

in neurodegenerative diseases. *Front. Biosci. (Schol. Ed).* **3**, 541–554 (2011).

15. Nakanishi, H. Microglial cathepsin B as a key driver of inflammatory brain diseases and brain aging. *Neural Regen. Res.* **15**, 25–29 (2020).

16. Sun, B. *et al.* Cystatin C-Cathepsin B Axis Regulates Amyloid Beta Levels and Associated Neuronal Deficits in an Animal Model of Alzheimer's Disease. *Neuron* **60**, 247–257 (2008).

17. Shimizu, T. *et al.* The balance between cathepsin C and cystatin F controls remyelination in the brain of Plp1-overexpressing mouse, a chronic demyelinating disease model. *Glia* **65**, 917–930 (2017).

18. Ma, J., Tanaka, K. F., Yamada, G. & Ikenaka, K. Induced expression of cathepsins and cystatin C in a murine model of demyelination. *Neurochem. Res.* **32**, 311–320 (2007).

19. Ma, J. *et al.* Microglial cystatin F expression is a sensitive indicator for ongoing demyelination with concurrent remyelination. *J. Neurosci. Res.* **89**, 639–649 (2011).

20. Ma, J. *et al.* Microglial cystatin F expression is a sensitive indicator for ongoing demyelination with concurrent remyelination. *J. Neurosci. Res.* **89**, 639–649 (2011).

21. Liang, J. *et al.* Disinhibition of cathepsin C caused by cystatin F deficiency aggravates the demyelination in a cuprizone model. *Front. Mol. Neurosci.* **9**, 1–12 (2016).

22. Colbert, J. D., Plechanovová, A. & Watts, C. Glycosylation directs targeting and activation of cystatin F from intracellular and extracellular sources. *Traffic* **10**, 425–437 (2009).

23. Nathanson, C. M., Wassélius, J., Wallin, H. & Abrahamson, M. Regulated expression and intracellular localization of cystatin F in human U937 cells. *Eur. J. Biochem.* **269**, 5502–5511 (2002).

24. Ni, J. *et al.* Cystatin F is a glycosylated human low molecular weight cysteine proteinase inhibitor. *J. Biol. Chem.* **273**, 24797–24804 (1998).

25. Perišić Nanut, M., Sabotič, J., Švajger, U., Jewett, A. & Kos, J. Cystatin F Affects Natural Killer Cell Cytotoxicity. *Front. Immunol.* **8**, 1459 (2017).

26. Prunk, M. *et al.* Extracellular Cystatin F Is Internalised by Cytotoxic T Lymphocytes and Decreases Their Cytotoxicity. *Cancers (Basel).* **12**, (2020).

27. Prunk, M., Nanut, M. P., Sabotic, J., Svajger, U. & Kos, J. Increased cystatin F levels correlate with decreased cytotoxicity of cytotoxic T cells. *Radiol. Oncol.* **53**, 57–68 (2019).

28. Nanut, M. P., Sabotič, J., Jewett, A. & Kos, J. Cysteine cathepsins as regulators of the cytotoxicity of nk and t cells. *Front. Immunol.* **5**, 7–9 (2014).

29. Fan, K. *et al.* Up-regulation of microglial cathepsin C expression and activity in lipopolysaccharide-induced neuroinflammation. *J. Neuroinflammation* **9**, 1–13 (2012).

30. Liu, Q. *et al.* Cathepsin C promotes microglia M1 polarization and aggravates neuroinflammation via activation of Ca 2+ -dependent PKC/p38MAPK/NF-κB pathway. *J. Neuroinflammation* **16**, 1–18 (2019).

31. Nakanishi, H. Cathepsin regulation on microglial function. *Biochim. Biophys. Acta - Proteins Proteomics* **1868**, 140465 (2020).

32. Tejera, D. *et al.* Systemic inflammation impairs microglial Aβ clearance through NLRP 3 inflammasome . *EMBO J.* **38**, (2019).

33. Lane, T. E. *et al.* A Central Role for CD4+ T Cells and RANTES in Virus-Induced Central Nervous System Inflammation and Demyelination. *J. Virol.* **74**, 1415–1424 (2000).

34. Hirano, N., Murakami, T., Fujiwara, K. & Matsumoto, M. Utility of mouse cell line DBT for propagation and assay of mouse hepatitis virus. *Jpn. J. Exp. Med.* **48**, 71–75 (1978).

35. Blanc, C. A., Rosen, H. & Lane, T. E. FTY720 (fingolimod) modulates the severity of viral-induced encephalomyelitis and demyelination. *J. Neuroinflammation* **11**, 138 (2014).

36. Chen, L. *et al.* Human neural precursor cells promote neurologic recovery in a viral model of multiple sclerosis. *Stem cell reports* **2**, 825–837 (2014).

37. Marro, B. S., Grist, J. J. & Lane, T. E. Inducible Expression of CXCL1 within the Central Nervous System Amplifies Viral-Induced Demyelination. *J. Immunol.* **196**, 1855–1864 (2016).

38. Blanc, C. A. *et al.* Sphingosine-1-phosphate receptor antagonism enhances proliferation and migration of engrafted neural progenitor cells in a model of viral-induced demyelination. *Am. J. Pathol.* **185**, 2819–2832 (2015).

39. Dickey, L. L., Worne, C. L., Glover, J. L., Lane, T. E. & O'Connell, R. M. MicroRNA-155 enhances T cell trafficking and antiviral effector function in a model of coronavirus-induced neurologic disease. *J. Neuroinflammation* **13**, 240 (2016).

40. Smith, K. J., Bostock, H. & Hall, S. M. Saltatory conduction precedes remyelination in axons demyelinated with lysophosphatidyl choline. *J. Neurol. Sci.* **54**, 13–31 (1982).

41. Butler, A., Hoffman, P., Smibert, P., Papalexi, E. & Satija, R. Integrating single-cell transcriptomic data across different conditions, technologies, and species. *Nat. Biotechnol.* **36**, 411–420 (2018).

42. Stuart, T. *et al.* Comprehensive Integration of Single-Cell Data. *Cell* **177**, 1888-1902.e21 (2019).

43. Ekiz, H. A. *et al.* MicroRNA-155 coordinates the immunological landscape within murine melanoma and correlates with immunity in human cancers. *JCI Insight* (2019). doi:10.1172/jci.insight.126543

44. Syage, A. R. *et al.* Single-Cell RNA Sequencing Reveals the Diversity of the Immunological Landscape following Central Nervous System Infection by a Murine Coronavirus. *J. Virol.* **94**, 1–21 (2020).

45. Krasemann, S. *et al.* The TREM2-APOE Pathway Drives the Transcriptional Phenotype of Dysfunctional Microglia in Neurodegenerative Diseases Article The TREM2-APOE Pathway Drives the Transcriptional Phenotype of Dysfunctional Microglia in Neurodegenerative Diseases. 566–581 (2017). doi:10.1016/j.immuni.2017.08.008

46. Masuda, T. *et al.* Spatial and temporal heterogeneity of mouse and human microglia at single-cell resolution. *Nature* **566**, 388–392 (2019).

47. Deczkowska, A. *et al.* Disease-Associated Microglia: A Universal Immune Sensor of Neurodegeneration. *Cell* **173**, 1073–1081 (2018).

48. Wlodarczyk, A. *et al.* CSF1R Stimulation Promotes Increased Neuroprotection by CD11c+ Microglia in EAE. *Front. Cell. Neurosci.* **12**, (2019).

49. Ye, P., Li, L., Richards, R. G., DiAugustine, R. P. & D'Ercole, A. J. Myelination is altered in insulin-like growth factor-I null mutant mice. *J. Neurosci.* **22**, 6041–6051 (2002).

50. Bruce, K. D. *et al.* Lipoprotein lipase is a feature of alternatively-activated microglia and may facilitate lipid uptake in the CNS during demyelination. *Front. Mol. Neurosci.* **11**, 1–13 (2018).

51. Dong, C. *et al.* ICOS co-stimulatory receptor is essential for T-cell activation and function . *Nature* **409**, 97–101 (2001).

52. Croft, M. Control of immunity by the TNFR-related molecule OX40 (CD134). *Annu. Rev. Immunol.* **28**, 57–78 (2010).

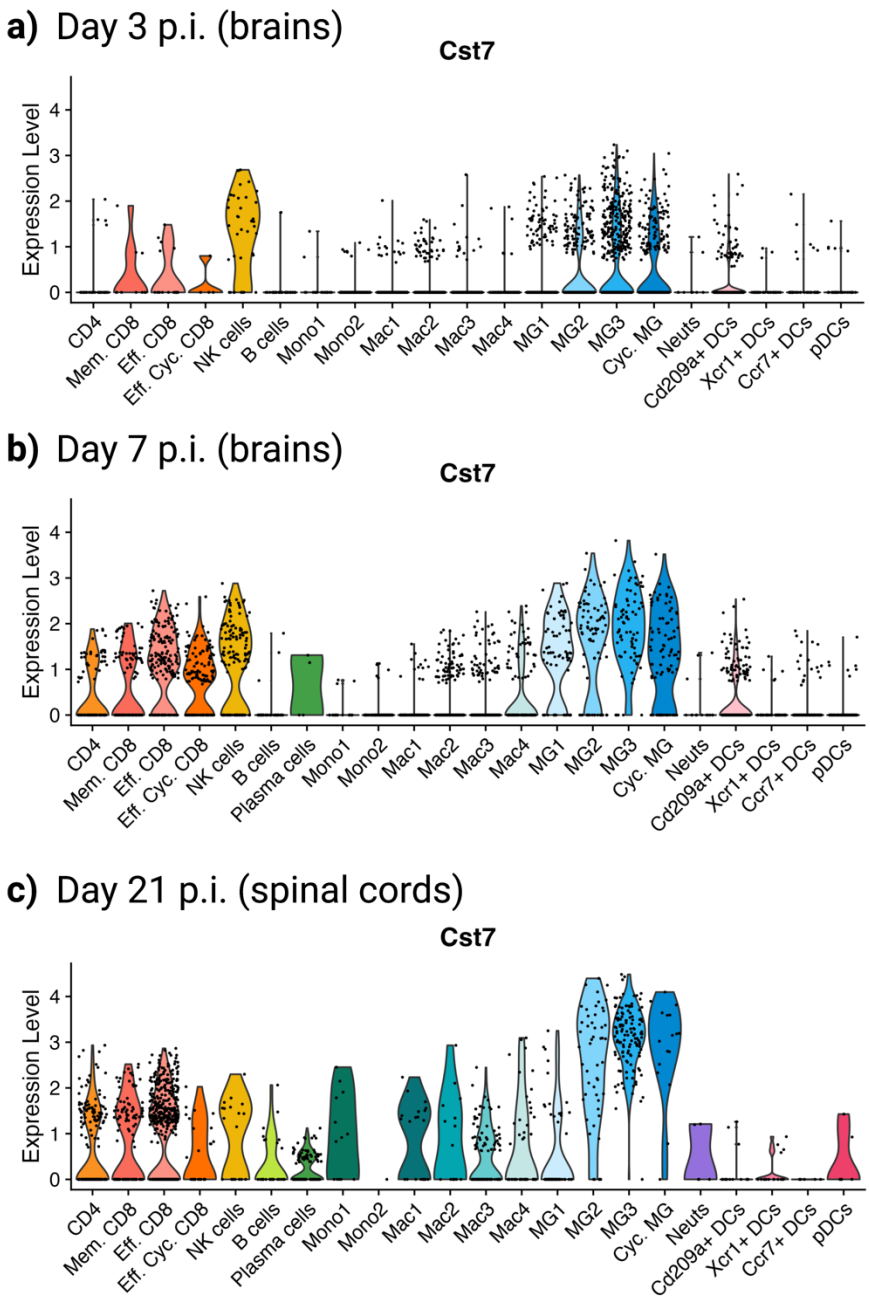

Figure 1. Expression profile of *Cst7* in CD45+ cells at defined times post-infection. Violin plots showing expression levels of cystatin F (Cst7) within each cell cluster from a previous scRNAseq study on CD45+ cells from brains or spinal cords of JHMV infected mice at (a) Day 3 p.i. (brains), (b) Day 7 p.i. (brains), and (c) Day 21 p.i. (spinal cords). Dots shown in plots represent individual cells.

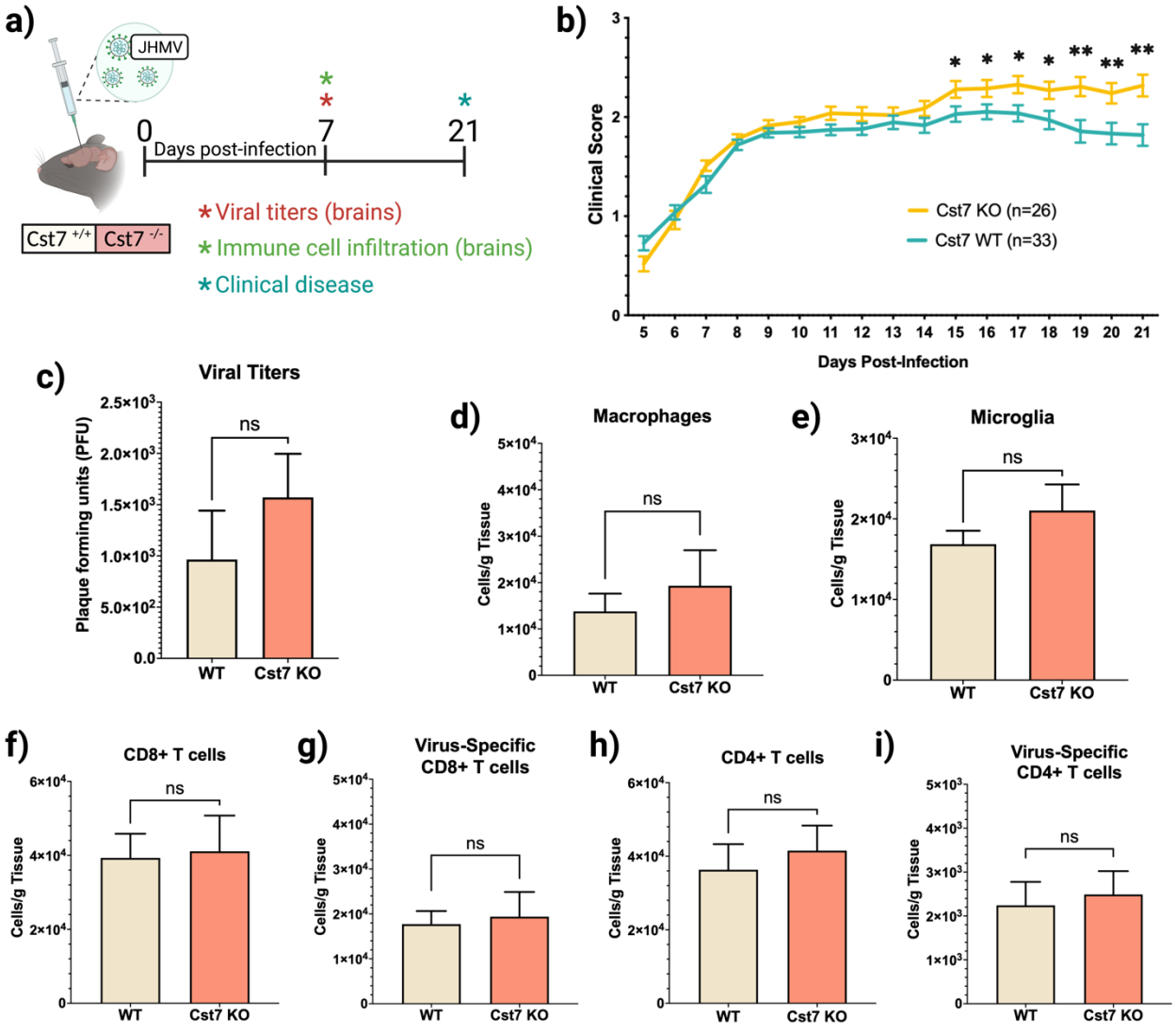

Figure 2. Absence of cystatin F does lead to changes during acute disease following CNS infection with JHMV. (a) Schematic outline of experimental design demonstrating that Cst7 KO mice and WT littermates were infected with JHMV and brains were isolated at day 7 p.i. for flow cytometric analysis and viral titers. (b) Cst7 KO mice and wildtype littermates (Cst7 WT) were i.c. infected with JHMV and clinical disease was recorded daily starting at day 5 p.i. until day 21 p.i., revealing a significant increase in clinical disease determined by more severe hind-limb paralysis in Cst7 KO mice compared to Cst7 WT controls. (c) Viral titers on brains at day 7 p.i. showed no significant difference ($p = 0.0712$) in viral load between Cst7 KO ($n = 9$) and Cst7 WT ($n = 7$) mice. Quantification of flow cytometric analysis in brains at day 7 p.i. showing no difference in cells/gram tissue in (d) macrophages (Cd11b+Cd45hi, $p = 0.6620$), (e) microglia (Cd11b+Cd45lo, $p = 0.4136$), (f) CD8+ T cells (Cd8a+, $p > 0.9999$), (g) virus-specific CD8+ T cells (Cd8a+S510tet+, $p = 0.9497$), (h) CD4+ T cells (Cd4+, $p = 0.6620$), and (j) virus-specific CD4+ T cells (Cd4+M133tet+, $p = 0.9497$) between Cst7 KO mice ($n = 6$) and WT controls ($n = 8$). Data represent the mean ± SEM, ns means no significance, *$p<0.05$, **$p<0.01$ by Mann Whitney *U* test.

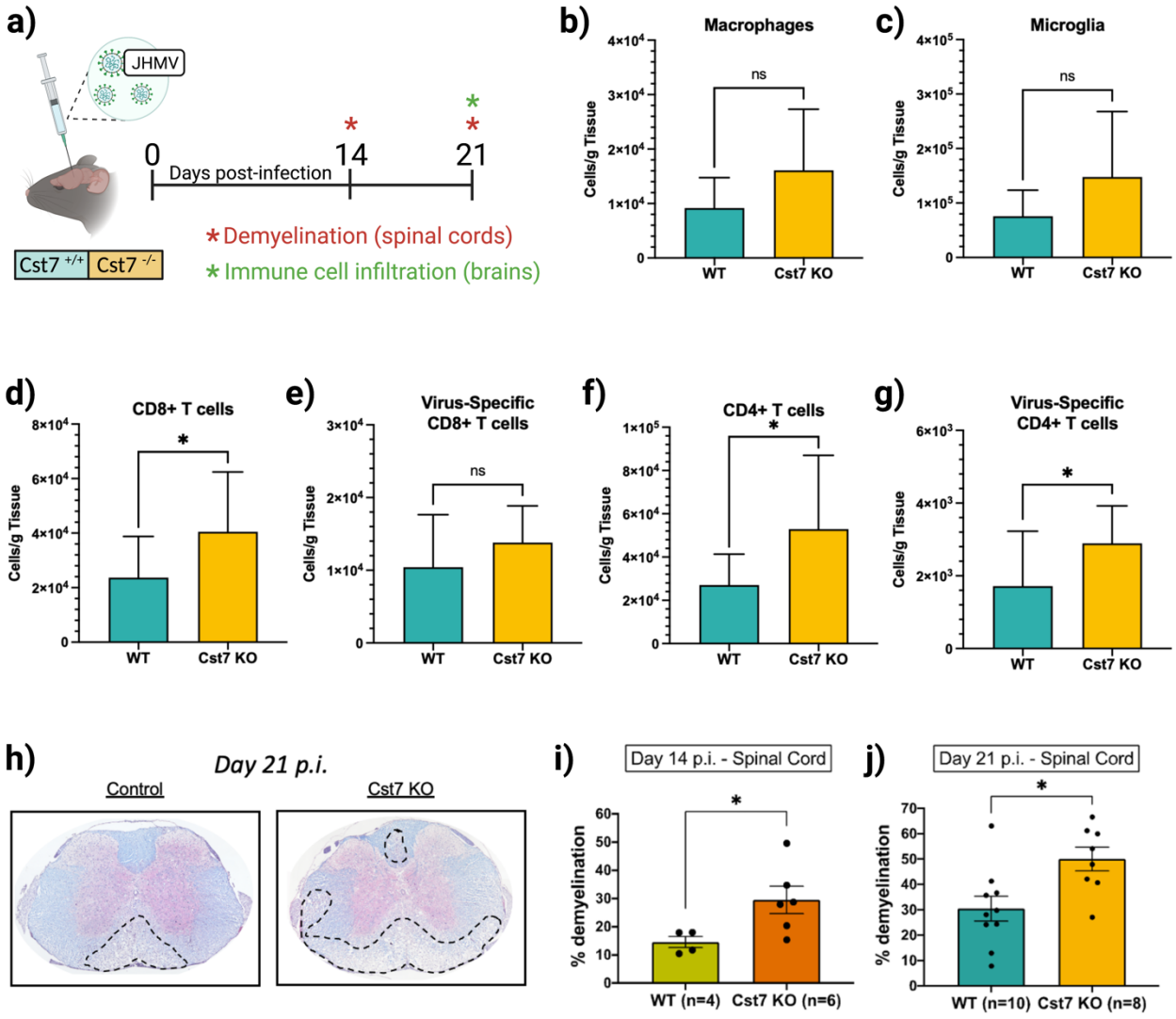

Figure 3. Genetic ablation of cystatin F results in increased demyelination and infiltration of immune cells in chronic disease following JHMV infection of the CNS. (a) Schematic outline showing experimental design for data shown in *b-j* – Cst7 KO mice (Cst7-/-) and wildtype littermates (Cst7 WT, Cst7+/+) were i.c. infected with JHMV and spinal cords were isolated at days 14 and 21 p.i. and brains at day 21 p.i. Flow cytometric analysis showing cells/gram tissue in brains of Cst7 KO mice (n = 9) and WT controls (n = 10) at day 21 p.i. for (b) macrophages (Cd11b+Cd45hi, p = 0.1128), (c) microglia (Cd11b+Cd45lo, p = 0.1333), (d) CD8+ T cells (Cd8a+, p = 0.0435), (e) virus-specific CD8+ T cells (Cd8a+S510tet+, p = 0.1823), (f) CD4+ T cells (Cd4+, p = 0.0172), and (g) virus-specific CD4+ T cells (Cd4+M133tet+, p = 0.0279). Mann-Whitney *U* test was used to compare data between groups in *b-g*. (h) Representative spinal cords stained with hematoxylin and eosin (H&E) and luxol fast blue (LFB) from infected Cst7 KO and Cst7 WT mice at day 21 p.i. revealing demyelination within the ventral funiculus and lateral white matter columns (outlined by black dashed line) and quantification of percentage of white matter that is demyelinated at (i) day 14p.i. (p=0.0275) and (j) day 21 p.i. (p=0.0103) by Welch's t-test. Data represent the mean ± SEM, ns means no significance, *p<0.05, **p<0.01.

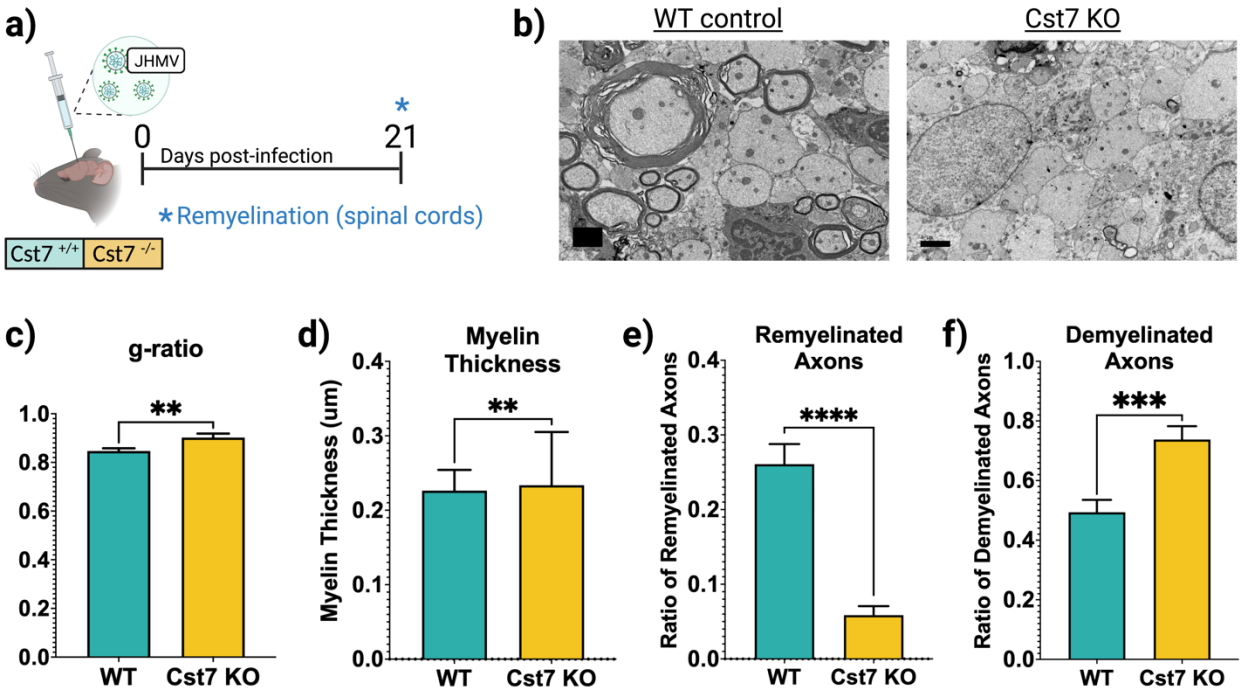

Figure 4. Cystatin F is necessary for remyelination following JHMV-induced demyelination. (a) Experimental schematic Cst7 KO mice (Cst7-/-) and wildtype littermates (Cst7 WT, Cst7+/+) were i.c. infected with JHMV and spinal cords were isolated at day 21 p.i. (b) Electron micrographs showing ultrathin spinal cord sections from Cst7 WT and Cst7 KO mice at day 21 p.i. Histological comparisons in the ventral funiculus and lateral white matter columns between Cst7 KO mice and controls were made from electron micrographs, including calculations of (c) g-ratio (axon diameter/total fiber diameter), (d) average myelin thickness, and ratio of (e) demyelinated axons and (f) remyelinated axons. Scale bar for ***b*** is 2 μm. Data represent the mean ± SEM, ns means no significance, *p<0.05, **p<0.01, ***p<0.001, p<0.0001 by Mann Whitney *U* test. For ***c-f***, n=2 and analysis compared between 10-15 images/experimental group, with 330-550 axons analyzed/image.

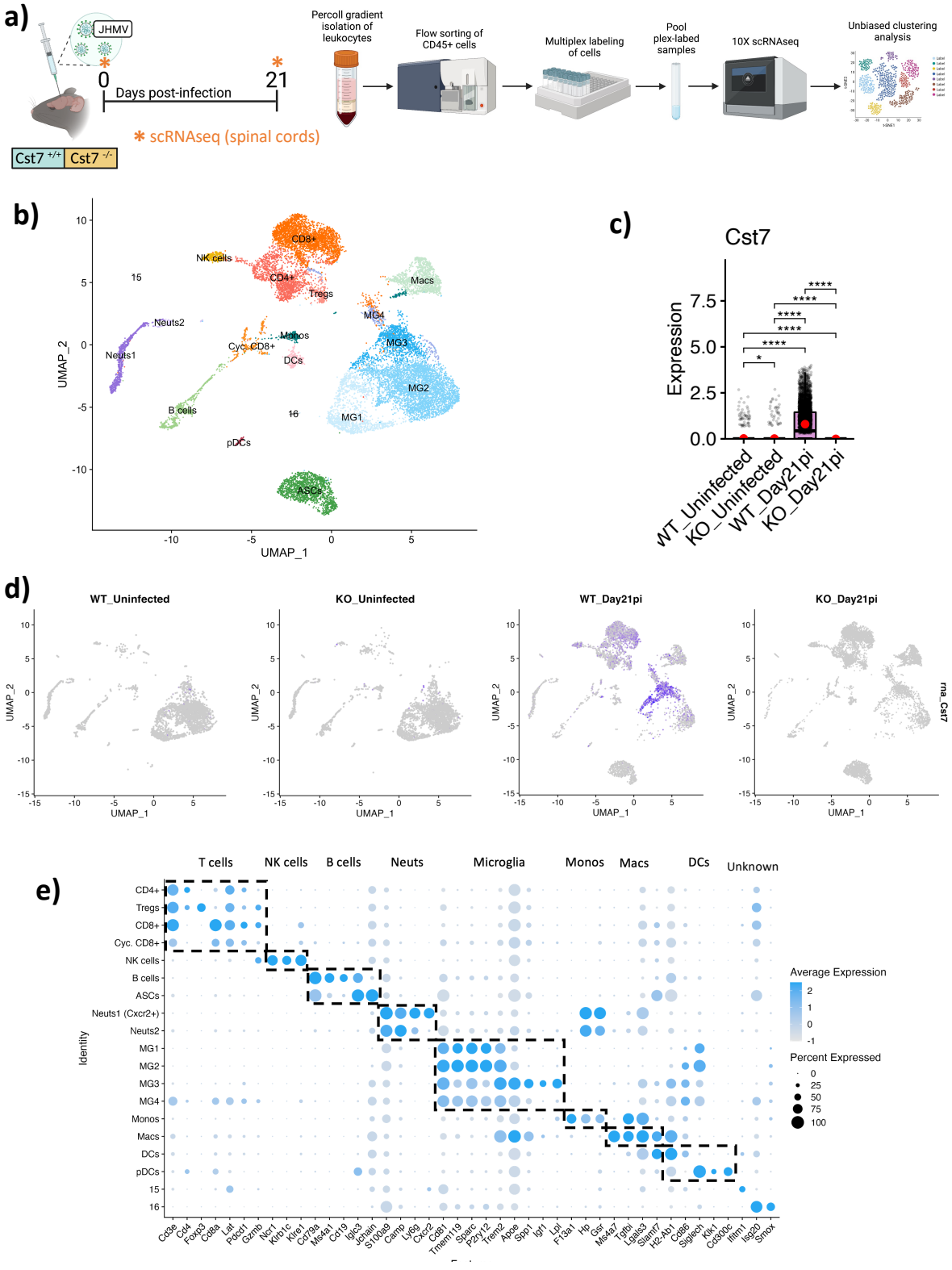
a)
JHMV
0
Days post-infection
21
* scRNAseq (spinal cords)
Cst7 +/+
Cst7 -/-
Percoll gradient isolation of leukocytes
Flow sorting of CD45+ cells
Multiplex labeling of cells
Pool plex-labed samples
10X scRNAseq
Unbiased clustering analysis
b)
CD8+
NK cells
CD4+
Tregs
Macs
MG4
Neuts2
Monos
MG3
Neuts1
Cyc. CD8+
DCs
MG2
B cells
16
MG1
pDCs
ASCs
UMAP_2
UMAP_1
c)
Cst7
Expression
7.5
5.0
2.5
0.0
****
*
WT_Uninfected
KO_Uninfected
WT_Day21pi
KO_Day21pi
d)
WT_Uninfected
KO_Uninfected
WT_Day21pi
KO_Day21pi
UMAP_2
UMAP_1
rna_Cst7
e)
T cells
NK cells
B cells
Neuts
Microglia
Monos
Macs
DCs
Unknown
CD4+
Tregs
CD8+
Cyc. CD8+
NK cells
B cells
ASCs
Neuts1 (Cxcr2+)
Neuts2
MG1
MG2
MG3
MG4
Monos
Macs
DCs
pDCs
15
16
Identity
Cd3e Cd4 Foxp3 Cd8a Lat Pdcd1 Gzmb Ncr1 Klrb1c Klre1 Cd79a Ms4a1 Cd19 Igfc3 Jchain S100a9 Camp Ly6g Cxcr2 Cd61 Tmem119 Sparc P2ry12 Trem2 Apoe Spp1 Igf1 Lpl F13a1 Hp Gsr Ms4a7 Tgfbi Lgals3 Slamf7 H2-Ab1 Cd86 Siglech Klk1 Cd300c Ifitm1 Isg20 Smox
Average Expression
2
1
0
-1
Percent Expressed
0
25
50
75
100

Figure 5. scRNAseq analysis of CD45^{+} cells from spinal cords of uninfected and infected Cst7 KO and Control mice at day 21 p.i. (a) Schematic outline of experimental design indicating times post-infection (p.i.) for sacrifice, tissue isolation and experimental procedures performed. Spinal cords were isolated from uninfected and JHMV infected Cst7 KO mice (Cst7-/-) and wildtype littermates (Cst7 WT, Cst7+/+) at day 21 p.i. Lymphocytes were isolated, live Cd45+ cells were FACS sorted out, samples were multiplex labeled, pooled and underwent 10X 3' single cell RNA sequencing (scRNASeq). (b) UMAP of aggregated cells from each sample showing 19 unique cell clusters. (c) Box plot comparing levels of expression of *Cst7* (cystatin F) between experimental groups and (d) feature heatmap showing *Cst7* expression across each experimental group. (e) SplitDotPlot showing expression of cell type specific markers, where dot size represents the percentage of cells from the cluster that express the gene and the degree of color represents the average expression level of the gene. Dots shown in plots *b-d* represent individual cells. For data in ***c,*** normalized expression values were used and random noise was added to show the distribution of data points. The box plots show interquartile range and the median value (bold horizontal bar). Average expression value per sample is indicated by the red dots. Wilcoxon's test was used for statistical analysis. ns, not significant; *p≤ 0.05; ****p≤ 0.0001.

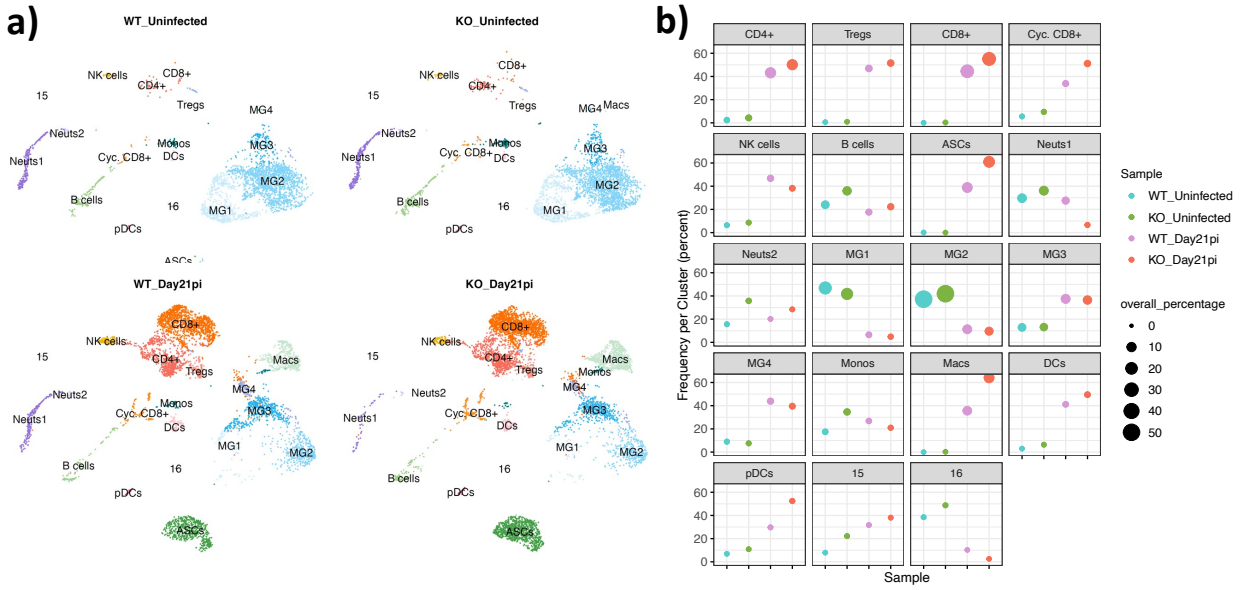
a)
WT_Uninfected
KO_Uninfected
WT_Day21pi
KO_Day21pi
NK cells
CD8+
CD4+
Tregs
Neuts2
Neuts1
Cyc. CD8+
Monos
DCs
Macs
B cells
pDCs
ASCs
MG1
MG2
MG3
MG4
15
16
b)
CD4+
Tregs
CD8+
Cyc. CD8+
NK cells
B cells
ASCs
Neuts1
Neuts2
MG1
MG2
MG3
MG4
Monos
Macs
DCs
pDCs
15
16
Frequency per Cluster (percent)
Sample
Sample
WT_Uninfected
KO_Uninfected
WT_Day21pi
KO_Day21pi
overall_percentage
0
10
20
30
40
50

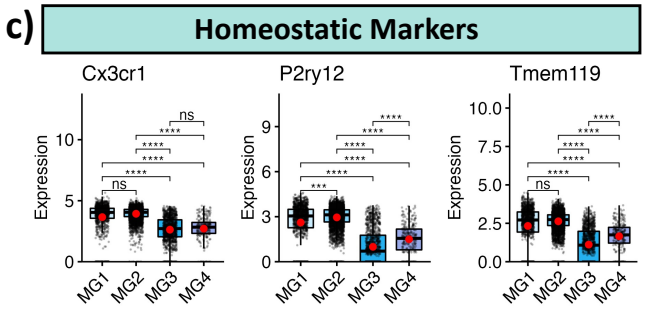
c)
Homeostatic Markers
Cx3cr1
P2ry12
Tmem119
Expression
MG1
MG2
MG3
MG4
ns
****
***

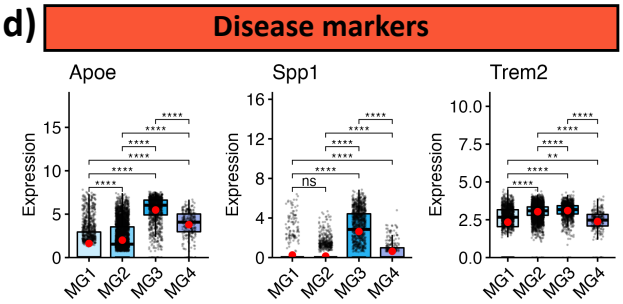
d)
Disease markers
Apoe
Spp1
Trem2
Expression
MG1
MG2
MG3
MG4
ns
****
**

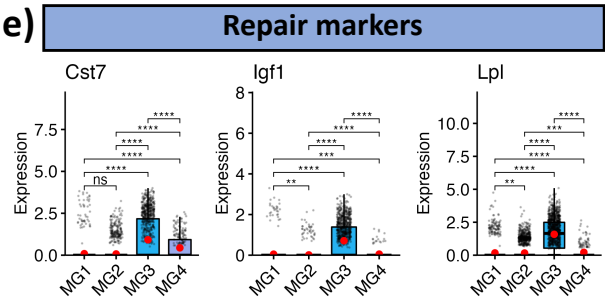
e)
Repair markers
Cst7
Igf1
Lpl
Expression
MG1
MG2
MG3
MG4
ns
****
***
**

Figure 6. Immune landscape of uninfected and infected Cst7 KO and Control mice at day 21 p.i. (a) UMAP color-coded and labeled by cluster and split by sample condition. (b) Dot Plot showing cell percentages for each cluster, where the y-axis shows the percentage of cells from each Sample per Cluster and dot size represents the percentage of cells from each Cluster per Sample. Box plots showing expression levels of transcripts encoding microglia markers associated with (c) homeostatic function [Cx3cr1 (fractalkine receptor), *P2ry12*, and *Tmem119*), (d) disease [Apolipoprotein-E (*Apoe*), and osteopontin (*Spp1*), and TREM-2 (*Trem2*)], and (e) repair [cystatin F (*Cst7*), insulin-like growth factor-1 (*Igf1*), and lipoprotein lipase (*Lpl*)]. Dots shown in plots *a* and *c-e* represent individual cells. For data in ***c-e***, normalized expression values were used and random noise was added to show the distribution of data points. The box plots show interquartile range and the median value (bold horizontal bar). Average expression value per sample is indicated by the red dots. Wilcoxon's test was used for statistical analysis. ns, not significant; *p≤ 0.05; ** p≤ 0.01; ***p≤0.001; ****p≤ 0.0001.

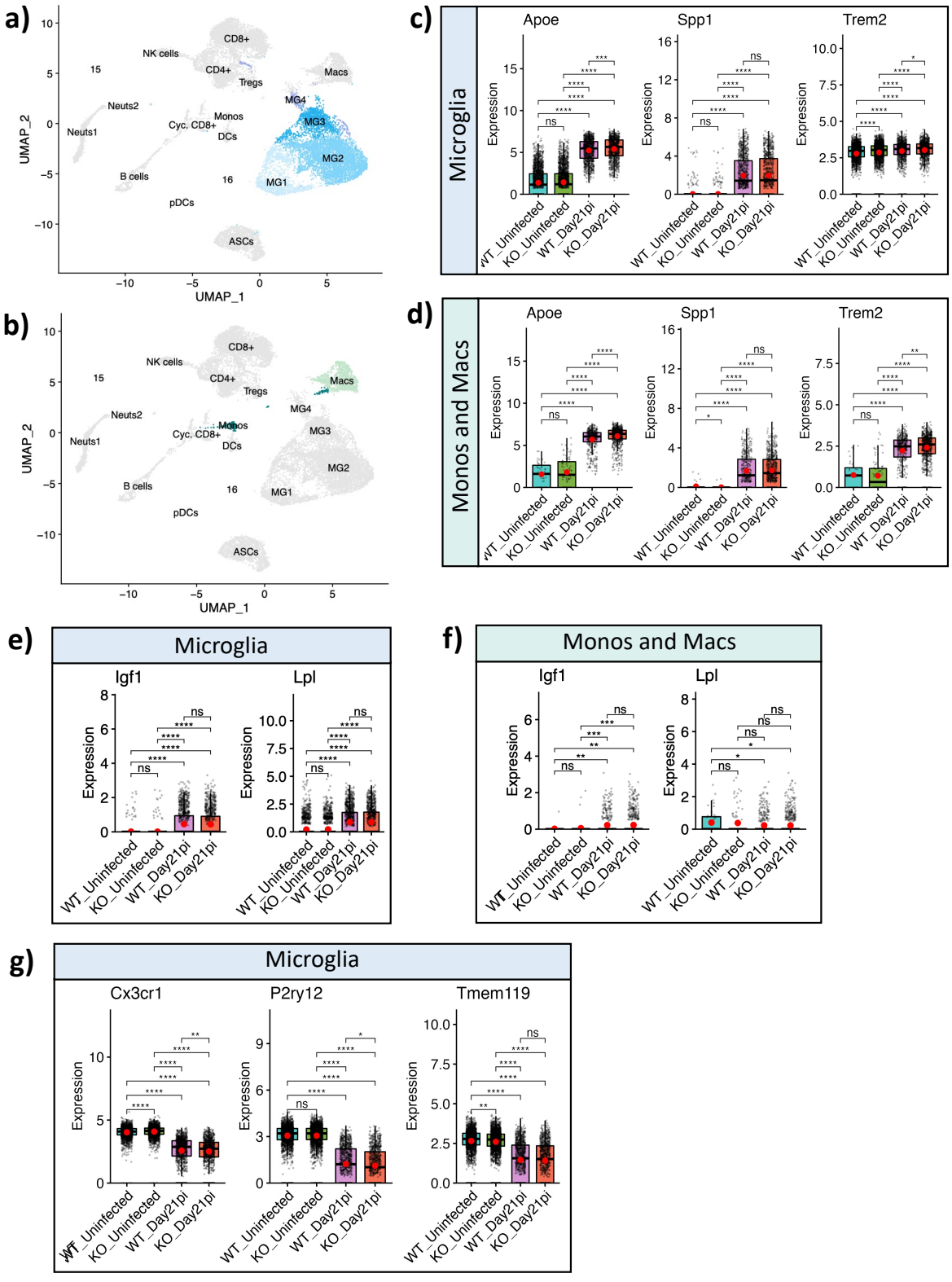
a)
b)
c)
d)
e)
f)
g)
UMAP_1
UMAP_2
CD8+
NK cells
CD4+
Tregs
Macs
MG4
MG3
MG2
MG1
Monos
Cyc. CD8+
DCs
Neuts1
Neuts2
B cells
pDCs
ASCs
15
16
Microglia
Monos and Macs
Apoe
Spp1
Trem2
Igf1
Lpl
Cx3cr1
P2ry12
Tmem119
Expression
WT_Uninfected
KO_Uninfected
WT_Day21pi
KO_Day21pi

Figure 7. Absence of Cystatin F in chronic JHMV infection leads to increased expression of disease associated transcripts in microglia and macrophages. (a) UMAPs highlighting microglia populations MG1, MG2, MG3, and MG4 and (b) monocyte/macrophage populations and corresponding box plots showing expression levels of disease-associated transcripts *Apoe* (Apolipoprotein-E), *Spp1* (Osteopontin), and *Trem2* (TREM-2) in (c) microglia and (d) monocytes/macrophages. Box plots comparing expression levels of remyelination-associated transcripts *Igf1* (Insulin-like growth factor-1) and *Lpl* (Lipoprotein lipase) in (e) microglia and (f) monocytes/macrophages. (g) Box plots showing expression levels of homeostatic microglia markers *Cx3cr1*, *P2ry12*, and *Tmem119* Dots shown in plots represent individual cells. For data in ***c-g***, normalized expression values were used and random noise was added to show the distribution of data points. The box plots show interquartile range and the median value (bold horizontal bar). Average expression value per sample is indicated by the red dots. Wilcoxon's test was used for statistical analysis. ns, not significant; *p≤ 0.05; ** p≤ 0.01; ***p≤0.001; ****p≤ 0.0001.

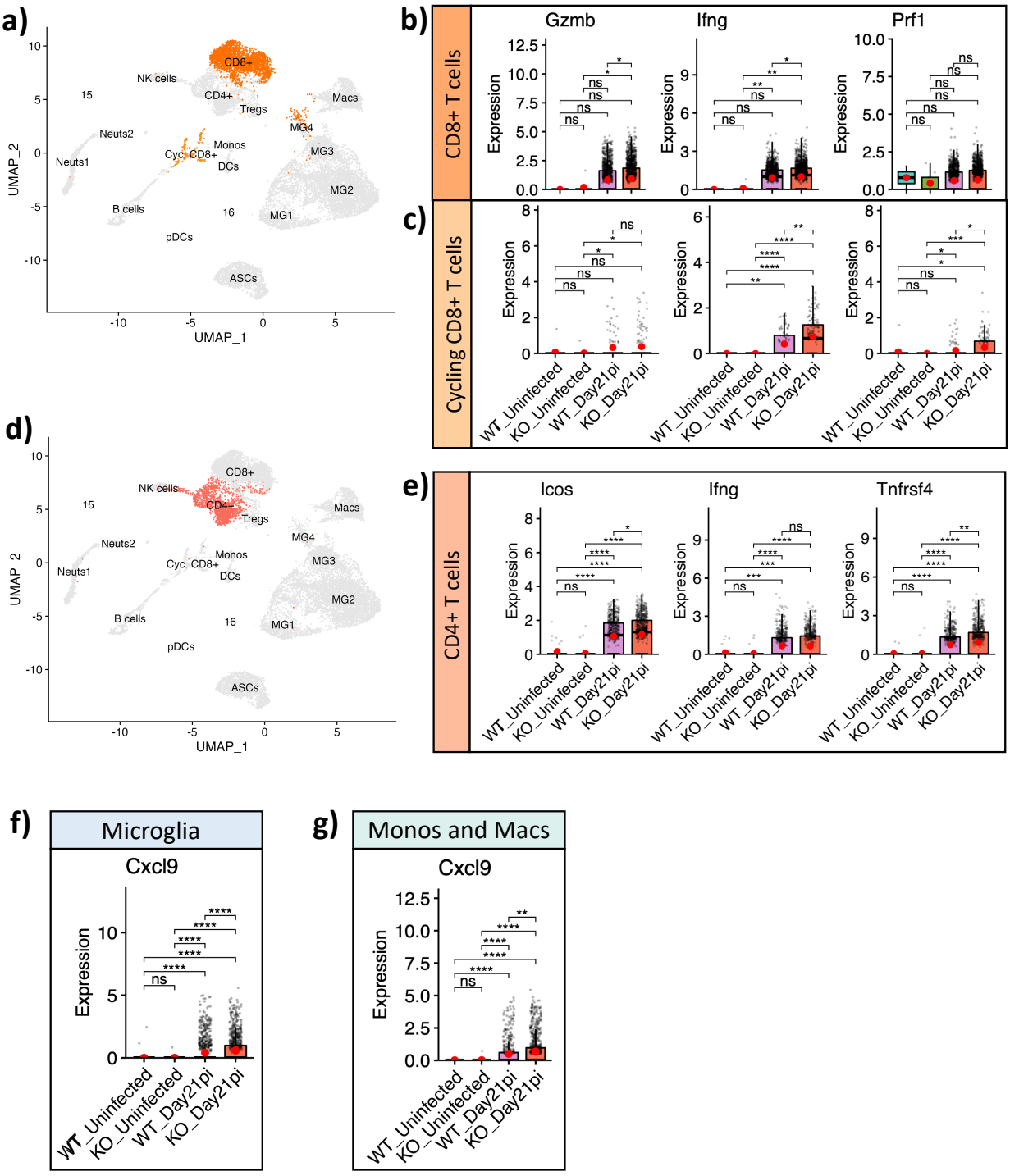

Figure 8. Ablation of *Cst7* leads to increased activation of T cells in chronic JHMV infection. (a) UMAP highlighting CD8+ T cells and proliferating CD8+ T cells (Cyc CD8+) and corresponding box plots showing expression levels of transcripts encoding CD8+ T cell activation markers [granzyme b (*Gzmb*), perforin (*Prf1*), interferon-gamma (*Ifng*)] in (b) CD8+ T cells and (c) Cyc.CD8+ T cell populations. (d) UMAP highlighting CD4+ T cells and (e) corresponding box plots showing expression levels of transcripts encoding CD4+ T cell

activation markers [inducible T cell co-stimulator (*Icos*), interferon-gamma (*Ifng*), and tumor necrosis factor receptor superfamily member 4 (*Tnfrsf4*)] in CD4+ T cells. (e) UMAP highlighting microglia populations MG1, MG2, MG3, and MG4 and (f) corresponding Box plots showing expression levels of transcripts encoding T cell chemoattractant *Cxcl9* in (f) microglia populations and (g) monocyte/macrophage populations. Dots shown in plots represent individual cells. For data in ***b-g,*** normalized expression values were used and random noise was added to show the distribution of data points. The box plots show interquartile range and the median value (bold horizontal bar). Average expression value per sample is indicated by the red dots. Wilcoxon's test was used for statistical analysis. ns, not significant; *$p \leq 0.05$; ** $p \leq 0.01$; ***$p \leq 0.001$; ****$p \leq 0.0001$.

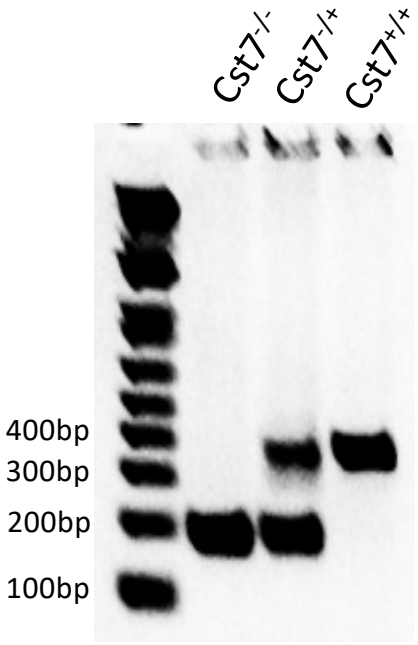

Supplemental Figure 1. PCR confirmation of *Cst7* ablation. Homozygous ablation of *Cst7* was confirmed using PCR primers that generate an amplicon following deletion of the 168bp sequence in Exon 1. Image of gel showing bands for Cst7 KO (*Cst7*$^{-/-}$), heterozygous (*Cst7*$^{-/+}$), and Wildtype littermates (*Cst7*$^{+/+}$).

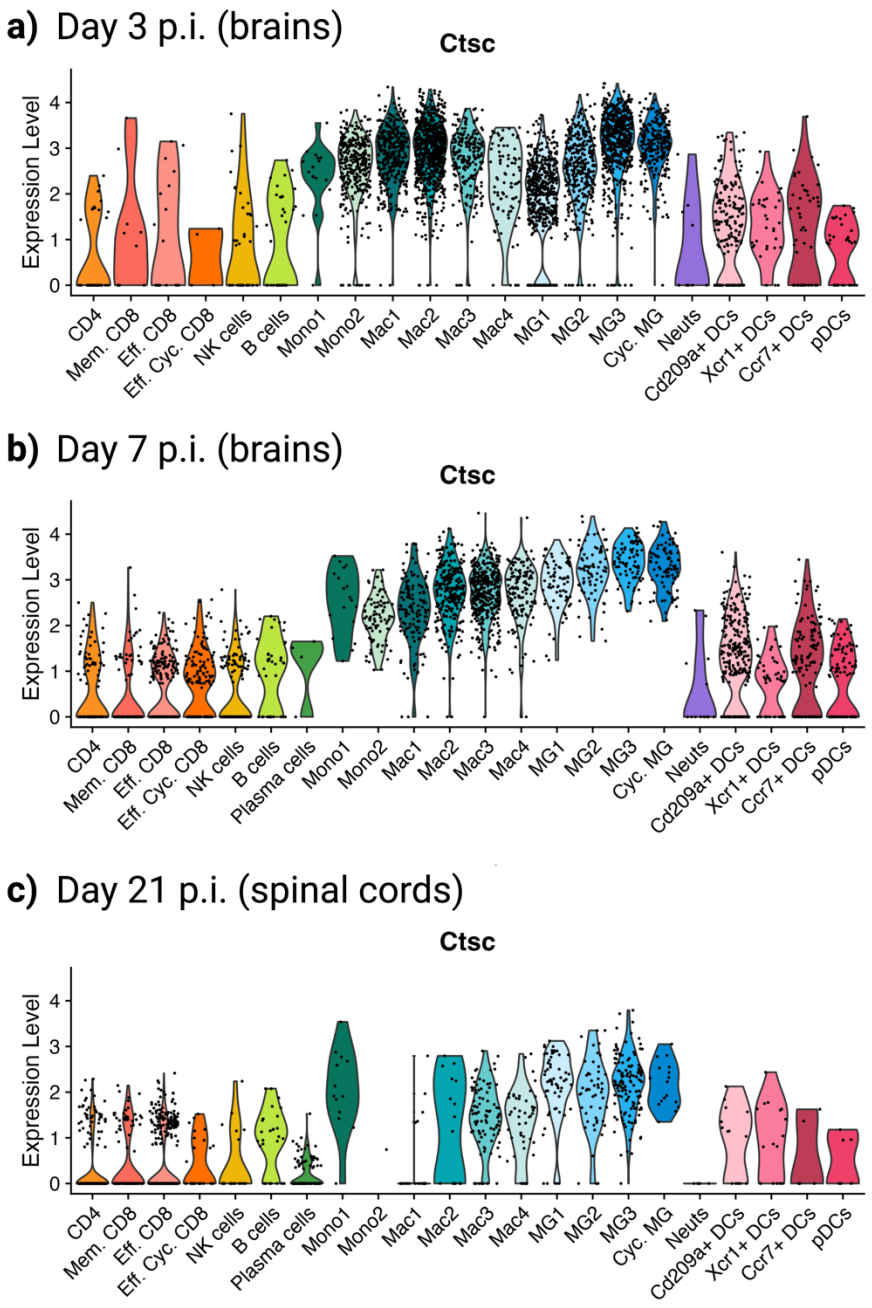

Supplemental Figure 2. Expression profile of *Ctsc* in CD45+ cells at defined times post-infection. Violin plots showing expression levels of cathepsin C (*Ctsc*) within each cell cluster from a previous scRNAseq study on CD45+ cells from brains or spinal cords of JHMV infected mice at (a) Day 3 p.i. (brains), (b) Day 7 p.i. (brains), and (c) Day 21 p.i. (spinal cords). Dots shown in plots represent individual cells.

Chapter 6

SUMMARY

SUMMARY AND SIGNIFICANCE

Microglia influence host defense, disease, and repair following murine coronavirus infection of the central nervous system.

Multiple sclerosis is an incredibly devastating and debilitating disease and much remains unclear about the physiological landscape found in chronic MS. As a result, there are no current treatments available for those who have advanced to progressive forms of the disease. Our research objective was to further investigate and understand the characteristics of chronic disease with the goal of discovering promising targets for therapeutic intervention that can prevent new lesion formation and promote sustained remyelination. Microglia are the resident immune cells of the CNS and are capable of assuming a diverse range of functions, that can be both homeostatic and reparative or inflammatory and damaging[1–8]. We aimed to understand the role of microglia in host defense and repair in JHMV-mediated neurologic disease. We showed that pharmacological depletion of microglia with CSF1R inhibitor PLX5622 prior to JHMV infection, results in increased mortality of mice and an impaired ability to control viral replication in comparison to controls. Additionally, microglia depletion results in increased infiltration of CD4+ and CD8+ T cells and virus-specific T cells into brains at days 7 and 14 p.i. ScRNAseq on CD45+ cells revealed that mice treated with PLX5622 have increased MHC class I expression on antigen presenting cells (APCs) within the CNS associated with activation of CD8+ T cells, but reduced MHC class II expression on macrophages and muted activation of CD4+ T cells as well as reduced expression of transcription factor T-bet required for an effective TH1 response, suggesting an important role for microglia in tailoring an effective antiviral immune response following JHMV infection of the CNS. Furthermore, depletion of microglia prior to infection leads to increased severity of spinal cord demyelination and impaired

remyelination. Similarly, scRNAseq data revealed increased expression of transcripts *Apoe*, *Trem2*, and *Spp1* in spinal cord macrophages that have previously been associated with disease and demyelination[9–11] as well as a reduction in expression of transcripts associated with remyelination *Cst7*, *Igf1*, and *Lpl*[12–14] in the spinal cords. Results from this study led us to question whether increased demyelination and impaired remyelination in the absence of microglia is merely due to sustained T cell activation and neuroinflammation resulting in response to an inability to control JHMV replication, or if microglia have a unique role in promoting repair in chronic disease, independent of their role in host response. To address this question, we ablated microglia following acute disease, which represented a time in which persistent infection and demyelination was established. Using this approach, we found that depletion of microglia after demyelination was established resulted in increased demyelination and impaired remyelination, indicating that microglia have an important role in influencing both white matter damage and repair (Cheng et al., unpublished observations).

Single-Cell RNA Sequencing Reveals the Diversity of the Immunological Landscape following Central Nervous System Infection by a Murine Coronavirus

To understand more about the different subpopulations of microglia and infiltrating immune cells throughout JHMV infection, we conducted scRNAseq on sorted CD45+ cells isolated from brains during the innate as well as adaptive immune responses and from spinal cords during a chronic demyelinating time point when remyelination efforts are also occurring. We found that there is a subpopulation of microglia that are uniquely present in spinal cords at chronic disease time points that expressed transcripts associated with remyelination, including

Cst7, *Igf1*, and *Lpl*[12–14]. Data from this study further support the notion that microglia play a specific role in repair and regeneration following JHMV-induced demyelination.

Evaluating the Role of Cystatin F in Demyelination and Remyelination Following CNS Infection with a Viral Model of Multiple Sclerosis

Cystatin F, a papain-like lysosomal cysteine protease inhibitor, has garnered increasing interest as a potential target for therapeutic intervention in treating MS patients[15,16]. Cystatin F is normally only expressed by immune cells and functional studies have been mostly performed within the context of cancer cells, which employ cystatin F to suppress targeted attacks by T cells[17–20]. Cystatin F is not expressed in the CNS in healthy individuals, yet under conditions of acute demyelination in MS patients as well as pre-clinical mouse models of MS including EAE, CPZ, and *Plp*$^{4e/-}$, a drastic increase in expression of cystatin F is found in microglia, exclusively in regions where remyelination is also occurring [15,21,22]. In chronic phases of demyelination when remyelination has ceased, cystatin F is no longer expressed by microglia [15,21]. Cystatin F is unique from other cystatins in that it is secreted as an inactive form and is only activated upon a cleavage event when internalized by its target cell, where it is transported to the lysosome[23–25]. Interestingly, microglia expression of cystatin F was found to be induced upon phagocytosis of myelin debris[16]. This implies that the function of microglia-derived cystatin F is utilized once damage has been inflicted on myelin. Microglia expression of cystatin F in areas of remyelination argues that cystatin F is an endogenous neuroprotective tool used by microglia to prevent further damage and potentially signal to induce repair mechanisms.

We have demonstrated JHMV infection of a novel germline *Cst7* knock-out (Cst7 KO) mouse model resulted in increased severity of clinical disease and spinal cord demyelination at

day 14 and day 21 p.i. when compared to infected WT mice. Cystatin F does not play any obvious roles in acute disease, as Cst7 KO mice infected with JHMV showed no change in viral load at day 7 p.i. when compared to WT littermates and there was no difference in T cell or monocyte/macrophage infiltration into the CNS of experimental mice. However, by 21 days p.i. there were increased numbers of CD4+ and CD8+ T cells as well as virus-specific CD4+ T cells in the spinal cords of JHMV-infected Cst7 KO mice when compared to WT mice and this correlated with increased demyelination. Interestingly, Cst7 KO mice infected with JHMV also showed impaired remyelination compared to WT littermates. scRNAseq analysis revealed increased expression of transcripts associated with disease in microglia and monocytes/macrophages as well as CD4+ and CD8+ T cell activation in spinal cords of infected Cst7 KO mice; no change in expression of remyelination associated markers was found in microglia and macrophage/monocyte populations. Together, cystatin F may provide a neuroprotective effect by negatively regulating recruitment and activation of damaging immune cells, though further studies are required to confirm that this increase in T cell infiltration and neuroinflammation is not an artifact of increased viral burden in *Cst7* KO mice during chronic disease. Though cystatin F does not appear to have an impact on influencing expression of pro-regenerative markers in microglia and monocyte/macrophage populations, we cannot conclude whether cystatin F maintains a potential for directly promoting remyelination through regulation of phagocytosis of myelin debris and recycling of proteins or through inhibition of an unidentified function of cathepsin C in oligodendrocyte progenitor cells (OPCs), as expression of cathepsin C is expressed in OPCs.

The potential for microglia to either worsen disease outcomes or reduce, and even reverse, them in pre-clinical models of MS is becoming more evident and an understanding of

how microglia carry out these functions and of what regulates their ability to do so is necessary for development of effective treatments for patients with progressive forms of MS. Our research has demonstrated a potential for cystatin F as a mechanism for how microglia may be hampering disease severity and promoting remyelination. This mechanism may be through dampening signals that lead to recruitment of immune cells and neuroinflammation. With the emerging realization that immune cells contribute to various neurodegenerative diseases and not just those with an auto-immune component like MS, the value of understanding how immune cell activation states within the CNS are regulated, only increases. Altogether, arguing for cystatin F as a promising target for further consideration in MS drug development.

REFERENCES

1. Miron, V. E. *et al.* M2 microglia and macrophages drive oligodendrocyte differentiation during CNS remyelination. *Nat. Neurosci.* **16**, 1211–1218 (2013).

2. Salter, M. W. & Stevens, B. Microglia emerge as central players in brain disease. *Nat. Med.* **23**, 1018–1027 (2017).

3. Cash, E., Zhang, Y. & Rott, O. Microglia present myelin antigens to t cells after phagocytosis of oligodendrocytes. *Cellular Immunology* **147**, 129–138 (1993).

4. Edwards, J. P., Zhang, X., Frauwirth, K. A. & Mosser, D. M. Biochemical and functional characterization of three activated macrophage populations. *J. Leukoc. Biol.* **80**, 1298–1307 (2006).

5. Hammond, T. R., Robinton, D. & Stevens, B. Microglia and the Brain: Complementary Partners in Development and Disease. *Annu. Rev. Cell Dev. Biol.* **34**, 523–544 (2018).

6. Tejera, D. *et al.* Systemic inflammation impairs microglial Aβ clearance through NLRP 3 inflammasome . *EMBO J.* **38**, (2019).

7. Wolf, S. A., Boddeke, H. W. G. M. & Kettenmann, H. Microglia in Physiology and Disease. *Annu. Rev. Physiol.* **79**, 619–643 (2017).

8. Banati, R. B., Gehrmann, J., Schubert, P. & Kreutzberg, G. W. Cytotoxicity of microglia. *Glia* **7**, 111–118 (1993).

9. Krasemann, S. *et al.* The TREM2-APOE Pathway Drives the Transcriptional Phenotype of Dysfunctional Microglia in Neurodegenerative Diseases Article The TREM2-APOE Pathway Drives the Transcriptional Phenotype of Dysfunctional Microglia in Neurodegenerative Diseases. 566–581 (2017). doi:10.1016/j.immuni.2017.08.008

10. Masuda, T. *et al.* Spatial and temporal heterogeneity of mouse and human microglia at single-cell resolution. *Nature* **566**, 388–392 (2019).

11. Deczkowska, A. *et al.* Disease-Associated Microglia: A Universal Immune Sensor of Neurodegeneration. *Cell* **173**, 1073–1081 (2018).

12. Wlodarczyk, A. *et al.* CSF1R Stimulation Promotes Increased Neuroprotection by CD11c+ Microglia in EAE. *Front. Cell. Neurosci.* **12**, (2019).

13. Ye, P., Li, L., Richards, R. G., DiAugustine, R. P. & D'Ercole, A. J. Myelination is altered in insulin-like growth factor-I null mutant mice. *J. Neurosci.* **22**, 6041–6051 (2002).

14. Bruce, K. D. *et al.* Lipoprotein lipase is a feature of alternatively-activated microglia and may facilitate lipid uptake in the CNS during demyelination. *Front. Mol. Neurosci.* **11**, 1–13 (2018).

15. Shimizu, T. *et al.* The balance between cathepsin C and cystatin F controls remyelination in the brain of Plp1-overexpressing mouse, a chronic demyelinating disease model. *Glia* **65**, 917–930 (2017).

16. Ma, J. *et al.* Microglial cystatin F expression is a sensitive indicator for ongoing demyelination with concurrent remyelination. *J. Neurosci. Res.* **89**, 639–649 (2011).

17. Prunk, M., Nanut, M. P., Sabotic, J., Svajger, U. & Kos, J. Increased cystatin F levels correlate with decreased cytotoxicity of cytotoxic T cells. *Radiol. Oncol.* **53**, 57–68 (2019).

18. Prunk, M. *et al.* Extracellular Cystatin F Is Internalised by Cytotoxic T Lymphocytes and Decreases Their Cytotoxicity. *Cancers (Basel).* **12**, (2020).

19. Nanut, M. P., Sabotič, J., Jewett, A. & Kos, J. Cysteine cathepsins as regulators of the cytotoxicity of nk and t cells. *Front. Immunol.* **5**, 7–9 (2014).

20. Perišić Nanut, M., Sabotič, J., Švajger, U., Jewett, A. & Kos, J. Cystatin F Affects Natural Killer Cell Cytotoxicity. *Front. Immunol.* **8**, 1459 (2017).

21. Ma, J. *et al.* Microglial cystatin F expression is a sensitive indicator for ongoing demyelination with concurrent remyelination. *J. Neurosci. Res.* **89**, 639–649 (2011).

22. Liang, J. *et al.* Disinhibition of cathepsin C caused by cystatin F deficiency aggravates the demyelination in a cuprizone model. *Front. Mol. Neurosci.* **9**, 1–12 (2016).

23. Colbert, J. D., Plechanovová, A. & Watts, C. Glycosylation directs targeting and activation of cystatin F from intracellular and extracellular sources. *Traffic* **10**, 425–437 (2009).

24. Nathanson, C. M., Wassélius, J., Wallin, H. & Abrahamson, M. Regulated expression and intracellular localization of cystatin F in human U937 cells. *Eur. J. Biochem.* **269**, 5502–5511 (2002).

25. Ni, J. *et al.* Cystatin F is a glycosylated human low molecular weight cysteine proteinase inhibitor. *J. Biol. Chem.* **273**, 24797–24804 (1998).